Tuning the Properties of Isoindigo-Based Organic Semiconductors Through Structural Engineering

A Thesis Submitted to the College of Graduate and Postdoctoral Studies

In Partial Fulfillment of the Requirements for the Degree of

Doctor of Philosophy

In the Department of Chemistry

University of Saskatchewan

Saskatoon

By

Nicholas M. Randell

Permission to Use

In presenting this thesis in partial fulfillment of the requirements for a Postgraduate degree from the University of Saskatchewan, I agree that the Libraries of this University may make it freely available for inspection. I further agree that permission for copying of this thesis/dissertation in any manner, in whole or in part, for scholarly purposes may be granted by the professor or professors who supervised my thesis/dissertation work or, in their absence, by the Head of the Department or the Dean of the College in which my thesis work was done. It is understood that any copying or publication or use of this thesis/dissertation or parts thereof for financial gain shall not be allowed without my written permission. It is also understood that due recognition shall be given to me and to the University of Saskatchewan in any scholarly use which may be made of any material in my thesis/dissertation.

Requests for permission to copy or to make other uses of materials in this thesis/dissertation in whole or part should be addressed to:

Head of the Department of Chemistry
University of Saskatchewan
Saskatoon, Saskatchewan
S7N 5C9, Canada

OR

Dean
College of Graduate Studies and Research
University of Saskatchewan
107 Administration Place
Saskatoon, Saskatchewan S7N 5A2
Canada

Abstract

Solar power is one of the most prominent renewable energy technologies vying to replace fossil fuels. Traditionally, this field has been dominated by silicon solar cells; recent innovations, such as organic photovoltaic devices (OPVs), offer the possibility of lightweight, flexible solar power generation with a wide range of applications, from building façades to textiles. Unfortunately, organic solar cells suffer from low power conversion efficiencies. To overcome this problem, the design of new organic semiconductors has become an area of intense research. In engineering these materials, it is essential to develop strong links between molecular structure and the optoelectronic properties of the resulting semiconductors, such as optical band gap, extinction coefficient, frontier orbital energies, and charge carrier mobility. This thesis explores the relationship between structural differences in isoindigo derivatives, such as increasing electron deficiency, or increased molecular planarity, and differences in the resulting material's optoelectronic properties.

The first two sections of this thesis investigate the effects of heteroatom substitution on isoindigo-based semiconductors. Four target compounds were synthesized, each containing either electron-withdrawing nitrogen atoms, or electron rich alkoxy groups. The semiconductors were incorporated into the active layer of organic solar cells. Alkoxy substitution was shown to improve device efficiency; conversely, nitrogen substitution led to lowered device efficiency. In a follow-up study, it was shown that the azaisoindigo groups were capable of coordinating to a Lewis acid; this coordination caused a red-shift in the molecule's $S_0 \rightarrow S_1$ transition. The Lewis adduct was identified using UV/vis spectroscopy, NMR spectroscopy, and (TD)DFT calculations. It was then demonstrated that the coordination reaction could be performed with vapor phase Lewis acids.

The third project in this thesis focuses on the synthesis of two isoindigo dimers. The first, bisisoindigo, is a ring-fused dimer of isoindigo. This was chosen to study the effects of increased planarity and conjugation length on the optoelectronic properties of isoindigo. Initially, both bisisoindigo and a donor-acceptor molecular semiconductor based on bisisoindigo were synthesized, characterized, and used in OPVs. Poor active layer morphology, due to aggregation of the bisisoindigo, led to low efficiencies in the OPVs.

Following work on the ring-fused isoindigo structure, a second dimer was synthesized in which two isoindigo units were joined by a single bond; this design provides free rotation between isoindigo units. Both dimers, as well as isoindigo, were used as electron acceptors in a study of the effects of acceptor number and planarity in donor-acceptor copolymers. The acceptors were copolymerized with thiophene and terthiophene to yield a total of six polymers. Both the optoelectronic properties of these polymers, and their performance in OPVs, were compared to discover trends in donor-acceptor semiconductor properties with increasing acceptor content.

Over the course of four major projects it has been demonstrated that altering the structure of the conjugated building block isoindigo has major effects on the optical band gap, orbital energies, and charge transport characteristics of the resulting organic semiconductors. The final chapter of this thesis will serve to link these projects in a general discussion of how the design of isoindigo-based organic semiconductors can be used to produce desired optoelectronic properties in the resulting materials. The thesis will conclude with a brief look towards the prospects of this area of research, including establishing the general applicability of these design strategies to organic semiconductors beyond those based on isoindigo.

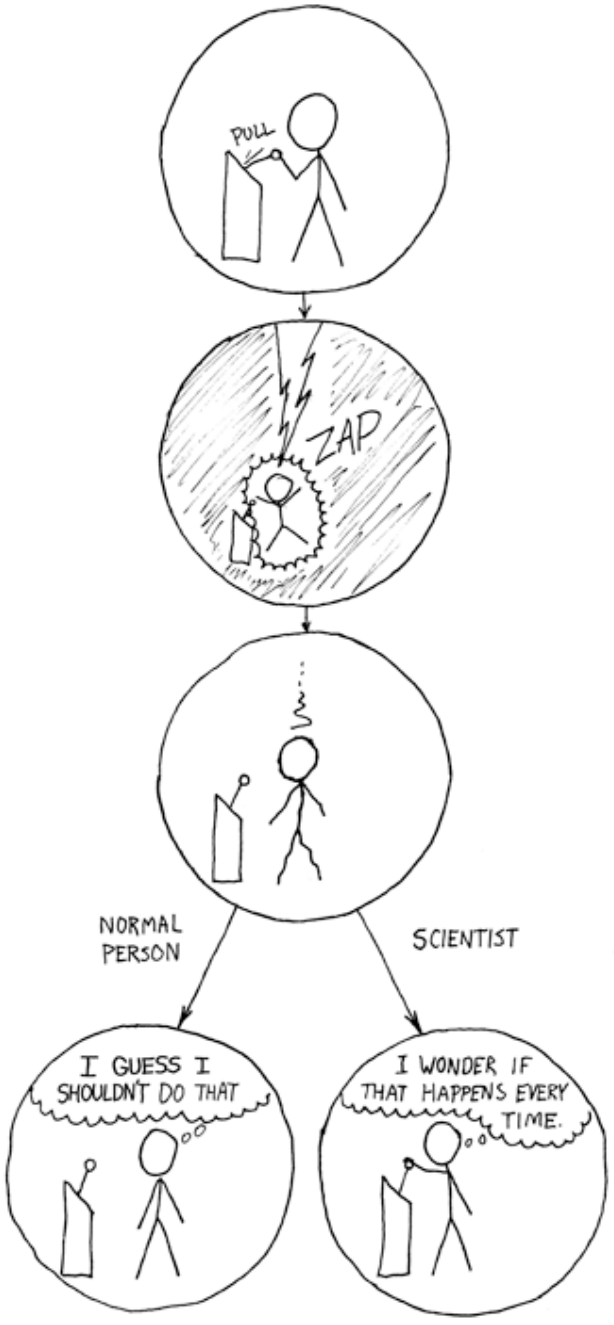

Reproduced with permission from https://xkcd.com/242/
Attributed to Randall Munroe

Acknowledgements

First, I must thank my supervisor Prof. Tim Kelly; his insight when I needed firm guidance and when I needed to be told “I don’t know, try it!” has helped me not only to finish the work in this thesis, but to become a more confident scientist. He has also taught me many important non-scientific lessons. Without him, I would not have properly used the semicolon in the first line.

The members of the Kelly group past and present are acknowledged for their support, and helpful suggestions during my time here. In particular, Phil Boutin for exchanging four years of physics education for my in-depth training in how to draw a hexagon.

I also thank the members of my advisory committee, particularly Prof. Ron Steer. I know that in attaining emeritus status he had the option of removing himself from advisory committees, and I would like to thank him for remaining to see my PhD to its conclusion.

Next, I have to thank the friends that have made Saskatoon feel like home for half a decade. I moved here expecting graduate school would be a process that was endured, not necessarily enjoyed, and they have proved me wrong time and again. Whether it was knowing when I needed to kill an afternoon at the pub, or introducing me to a sport I will be thoroughly addicted to for the rest of my days I am thankful.

I would not be here (literally) without the lifelong support of my parents. Twenty-seven years of guidance from them, my sister and my brother-in-law shaped me into a passionately curious person.

Finally, and most importantly, I must acknowledge the unending support of my wife, April Woods. This thesis might have gotten submitted without you, but I don’t know if I would have liked the person that submitted it.

Table of Contents

List of Figures

List of Charts

List of Schemes

List of Tables

List of Abbreviations

AFM	Atomic force microscopy
BDOPV	Benzodifuran-based oligo-*p*-phenylenevinylene
BHJ	Bulk heterojunction
Bis-iI	Bisisoindigo
BTD	5,5′-Dioctyl-1,1′-4H-bithieno[3,4-c]pyrrole-4,4′,6,6′(5H,5′H)-tetrone
BTI	Bithiopheneimide
DA	Donor-acceptor
DAA	Donor-acceptor-acceptor
DFT	Density functional theory
DIO	1,8-Diiodooctane
Di-iI	Diisoindigo
DMA	Dimethylacetamide
DMF	*N,N*-Dimethylformamide
DMSO	Dimethylsulfoxide
DPP	Diketopyrrolopyrrole
EA	Electron affinity
$E_{g,opt}$	Optical band gap
$E_{g,elec}$	Electronic band gap
$E_{g,calc}$	Calculated electronic band gap
ETL	Electron transport layer
EtOH	Ethanol
EtOAc	Ethyl acetate
FF	Fill factor
EQE	External quantum efficiency
GIWAXS	Grazing incidence wide angle x-ray scattering
HOMO	Highest occupied molecular orbital
iI	Isoindigo
ITO	Indium doped tin oxide
IP	Ionization potential

J_{ph}	Photocurrent density
J_{SC}	Short circuit current density
J-V	Current-voltage
LUMO	Lowest unoccupied molecular orbital
MALDI-TOF	Matrix assisted laser desorption ionization time-of-flight
MDMO-PPV	Poly[2-methoxy-5-(3′,7′-dimethyloctyloxy)-1,4-phenylenevinylene]
MEH-PPV	Poly[2-methoxy-5-(2-ethylhexyloxy)-1,4-phenylenevinylene]
M_n	Number average molecular weight
MO	Molecular orbital
M_w	Weight average molecular weights
NBS	*N*-bromosuccinimide
NMR	Nuclear magnetic resonance
OFET	Organic Field effect transistor
OLED	Organic light emitting diode
OPV	Organic Photovoltaic
OTFT	Organic thin film transistor
P3HT	Poly(3-heyxlthiophene)
$PC_{61}BM$	Phenyl-C_{61}-butyric acid methyl ester
$PC_{71}BM$	Phenyl-C_{71}-butyric acid methyl ester
PCDTBT	Poly[*N*-9′-heptadecanyl-2,7-carbazole-*alt*-5,5-(4′,7′-di-2-thienyl-2′,1′,3′-benzothiadiazole)]
PCE	Power conversion efficiency
PDI	perylene diimide
PDMS	Poly(dimethylsiloxane)
PEDOT:PSS	Poly(3,4-ethylenedioxythiophene):poly(styrenesulfonate)
P_{out}	Power output
PPV	Poly(paraphenylenevinylene)
PTFE	Poly(trifluoroethylene)
R_S	Series resistance
R_{Sh}	Shunt resistance
R_q	Root-mean-squared roughness

TCB	1,3,5-trichlorobenzene
TDDFT	Time dependent density functional theory
TEM	Transmission electron microscopy
THF	Tetrahydrofuran
TPD	Thieno[3,4-c]pyrrole-4,6-dione
UV/vis	Ultra violet and visible light
V_{OC}	Open circuit voltage

Chapter 1

Introduction

1.1 Climate change and the case for solar energy

It is an undeniable fact that global temperatures are rising; the overwhelming consensus amongst the scientific community is that this climate change is caused by human action.[1] The primary driving force for this increase in average temperature is a dramatic rise in greenhouse gas levels.[1] Since the industrial revolution heralded the mass burning of fossil fuels in the 1800's, atmospheric CO_2 levels have risen from 278 ppm to >400 ppm in 2016.[2] Today, 85% of energy used by humans is still generated by the burning of fossil fuels, and the development of cleaner renewable energy technologies is one of humanity's greatest modern scientific challenges.[2] Many energy sources are being explored as fossil fuel replacements, and it will require a variety of technologies to end humanity's dependence on fossil fuels.

One of the fastest growing areas of renewable energy generation is solar energy. For many decades solar cells were thought of as an expensive technology, primarily useful for satellites and space stations; however, the threat of anthropogenic climate change has accelerated the development of solar energy.[3] Advances in the production of multicrystalline silicon, as well as increases in its production rate, have pushed costs steadily lower. In 2006, the global average cost per module for multicrystalline silicon solar cells was US\$4 W^{-1}; by 2016, the cost had been driven down by an order of magnitude, to US\$0.4 W^{-1}.[4] This decrease in manufacturing cost has driven a massive boom in solar installations, from 7 GW of electrical power capacity worldwide in 2006 to ~300 GW in 2016.[4] With production costs at an all-time low, government agencies have begun to set solar energy research and development goals, such as the US Department of Energy's

SunShot2030 program, which aims to lower the levelized cost of solar electricity to US$0.05 kW h^{-1} for residential installation by 2030.[2] Such low manufacturing costs mean silicon solar cells will likely dominate residential and commercial solar energy for the foreseeable future.[2] However, the exponential growth of solar energy in the last two decades has made room for emerging photovoltaic technologies to have a significant place in the market. Many new solar cell technologies promise more versatility than traditional silicon and are quickly becoming used in applications such as portable and wearable electronics.

Organic photovoltaics (OPVs) are an emerging solar cell technology that use organic semiconductors to generate photocurrent. OPVs have several advantages which make them more useful than traditional silicon solar cells in a variety of applications.[5] OPVs are light weight and mechanically flexible, allowing them to be incorporated into such technologies as wearable electronics without the heavy weight, and rigidity of silicon solar cells. Unlike silicon, organic semiconductors have a tuneable band gap, allowing them to be synthesized in a variety of colors; this optical band gap can be pushed beyond the visible spectrum, producing transparent devices which absorb near-infrared light. These OPVs could be used to generate colorful building facades or solar energy harvesting windows.[6] As an emerging technology, there is much to be learned about organic solar cells; the stability and efficiency of the devices must be improved before they can achieve widespread commercial success. It is important to develop a deeper understanding of how the structure of new organic solar cell materials affects their optoelectronic properties, and in turn, device stability and performance. The focus of this thesis is on the design and synthesis of new organic semiconductors for use in OPVs.

1.2 Introduction to organic semiconductors

1.2.1 From molecular orbitals to semiconductor band structure

Semiconducting behavior in organic molecules and polymers results from the delocalization of electrons in structures with extended π conjugation. Figure 1.1 depicts the extension of conjugation in the simplest π-bonded system, a linear alkene, as repeat units are added. In ethene, the highest occupied molecular orbital (HOMO) and lowest unoccupied molecular orbital (LUMO) are the π bonding and π* antibonding orbitals. When a second double bond is added in 1,3-butadiene, the p-orbitals of the carbon atoms can be aligned four ways, forming two bonding and two antibonding orbitals. Each time the system is extended by another ethene unit, two more π electrons and two more orbitals are added. Eventually, as the chain extends to *n* ethene units there are enough π orbitals with very small energy spacing between them that an effective continuum of energy states exists. There is now a continuous valence band (π bonding orbitals), separated from a continuous conduction band (π* antibonding orbitals) by a discrete band gap, *i.e.* an organic semiconductor.

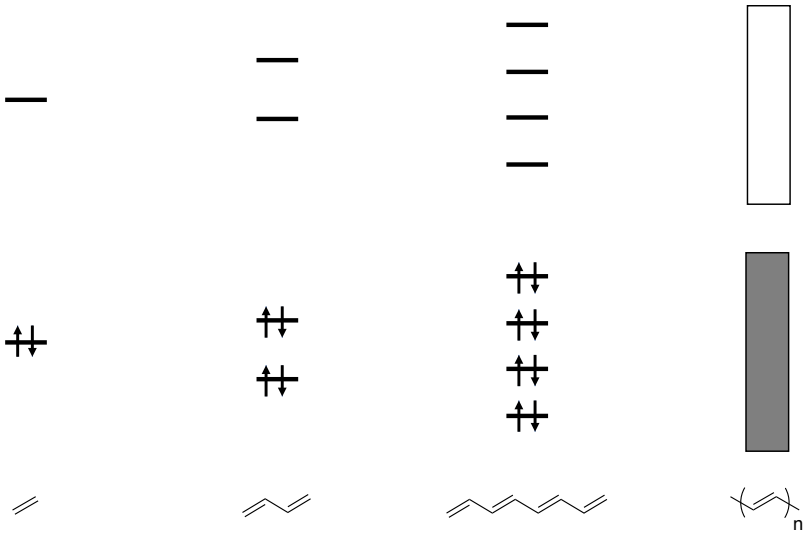

Figure 1.1 Molecular orbital (MO) diagrams of linear alkenes increasing in length, and the band diagram of poly(acetylene).

Organic semiconductors are not limited to polymeric materials; in their solid state, conjugated small molecules can also function as semiconductors.[7] Semiconducting behavior has long been known in crystalline solids of linear acenes such as pentacene; Figure 1.2 illustrates the extension of conjugation in a series of linear acenes from benzene to pentacene, the longest stable linear acene.[8-10] Even in pentacene, with five fused benzene rings, the electronic structure of the molecule is still best described in discrete molecular orbitals. To generate a band structure in a molecular semiconductor, the interactions between molecules in the solid state must be considered. The strongest electronic coupling in pentacene comes from the interactions of π orbitals between molecules, π-π stacking.[10] This electronic coupling causes a small splitting in the energy levels of the two stacked molecules (Figure 1.2). When this interaction is expanded to a macroscopic solid the number of electronic states is large enough to be best described by a narrow band structure.

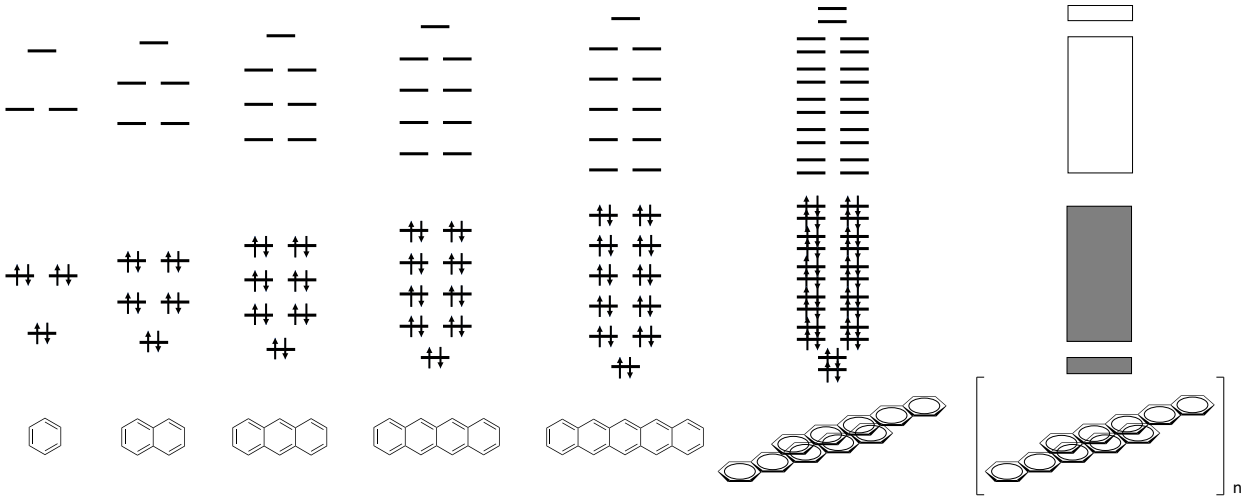

Figure 1.2 MO diagrams of a series of linear acenes, and the band structure of pentacene in the solid state.

A density of states plot for an organic semiconductor reveals narrow bands of states centered around the HOMO and LUMO energies (Figure 1.3); the full width at half maximum of these bands is much smaller than what is expected in an inorganic semiconductor. Due to the narrow nature of these bands, and the fact that discrete orbitals better describe the electronic structure in solution, HOMO and LUMO and often used instead of valence and conduction band when describing organic semiconductors.

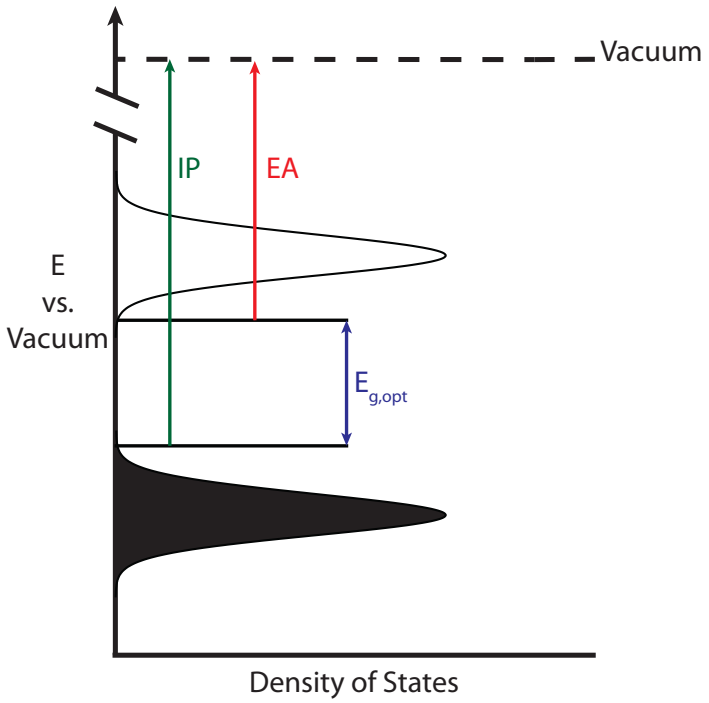

Figure 1.3 Density of states approximation of an organic semiconductor. Adapted from Ref. 11.

1.2.2 Optoelectronic properties of organic semiconductors

The important optoelectronic properties of organic semiconductors are largely the same as those of traditional inorganic semiconductors; these properties include the optical band gap ($E_{g,opt}$), the energy of the HOMO (E_{HOMO}), the energy of the LUMO (E_{LUMO}), and the charge carrier mobility (hole mobility μ_h and electron mobility μ_e). The optical band gap of a semiconductor is defined as the minimum energy required to promote an electron from the HOMO to the LUMO; this is analogous to promotion of an electron from the valence to conduction band in an inorganic semiconductor. Optical band gaps are typically measured by ultra-violet and visible light (UV/vis) absorption spectroscopy.

While the optical band gap of an organic semiconductor is the energy difference between the HOMO and the LUMO, it gives no indication of the absolute energy of these orbitals. Knowing the absolute energies of the HOMO and LUMO of a new organic semiconductor is essential when

determining its potential use in devices such as OPVs. The E_{HOMO} of a semiconductor is the electronic energy of the highest lying occupied orbital. The ionization potential (IP) of an organic semiconductor is the minimum energy required to remove an electron (*vs*. vacuum); this is a useful approximation of E_{HOMO} and is often written as ($E_{HOMO\ elec}$). The IP is typically measured by either cyclic voltammetry (the onset of semiconductor oxidation is equal to the IP), or photoelectron spectroscopy. The E_{LUMO} is the energy of the LUMO. The electron affinity (EA) of a semiconductor is often used to approximate E_{LUMO} (*vs*. vacuum); this is the energy released by placing an electron from vacuum into the LUMO of a molecule, and is often denoted ($E_{LUMO\ elec}$). EA is typically determined by measuring the onset of reduction of a semiconductor in a cyclic voltammetry experiment, or by adding E_{HOMO} and $E_{g,opt}$. Both E_{HOMO} and E_{LUMO} are also frequently calculated using density functional theory (DFT).[12]

It is important to note that the methods discussed above for determining E_{HOMO} and E_{LUMO} are approximations with significant limitations. Calculation of these energy levels by DFT makes two assumptions. First, simple DFT calculations do not account for electron-electron interactions; this can lead to large discrepancies between calculated and experimental frontier orbital levels. Secondly, in DFT calculations, Koopman's theorem and the frozen orbital approximation are assumed to be true; that is, the energies of the orbitals are not affected by removal of an electron from the HOMO, or placement of an electron in the LUMO. In reality, the orbital energy can change significantly with the removal (or addition) of an electron.[12] Similarly, estimations of E_{HOMO} and E_{LUMO} from voltammetry also have shortcomings. In a voltammetry experiment the semiconductor has time for nuclear reorganization after oxidation or reduction, unlike spectroscopic transitions, which are vertical transitions on a timescale too fast for nuclear movement (the Born-Oppenheimer approximation). Therefore, there can be large differences in

the HOMO-LUMO gap measured by voltammetry and the spectroscopic optical band gap. Additionally, equating the EA and E_{LUMO} of a semiconductor assumes that Koopman's theorem holds and that the energy of the orbital does not change when an electron is placed in it; experimentally this is not valid, and E_{LUMO} values taken from the EA must be viewed as relatively crude approximations.[12]

The final optoelectronic property that is evaluated in most novel organic semiconductors is charge carrier mobility. The charge carriers in semiconductors are electrons in the conduction band/LUMO, and holes in the valence band/HOMO. Holes are quasiparticles used to represent a vacancy in the otherwise filled valence band. The mobility of holes (μ_h) and electrons (μ_e) is a measure of how easily the charge carrier can move through a semiconductor. In an inorganic semiconductor charge carrier mobility is a function of its mean scattering time and effective mass, as described by the Drude model of drift mobility. Charge carrier mobility in organic semiconductors is often more complex, as these materials lack the continuous solid lattice of inorganic semiconductors; it is best conceptualized by the hopping of a charge carrier from molecule to molecule, or down a polymer chain. Organic semiconductors can be either p-type or n-type depending on whether the material conducts holes or electrons more easily. Semiconductors with a higher μ_h are p-type, while those with a higher μ_e are n-type; organic semiconductors in which $\mu_h \approx \mu_e$ are termed ambipolar. There are a variety of methods for measuring the charge carrier mobility of organic semiconductors; in this thesis charge carrier mobilities are primarily determined by incorporating the semiconductor into the active layer of an organic field effect transistor. By measuring the current density between source and drain electrodes as a function of voltage applied between the source electrode and a gate electrode the charge carrier mobilities can be calculated.

1.2.3 Organic semiconductors with historical relevance to OPVs

Conducting polymers such as doped poly(acetylene) were discovered by Shirakawa *et al.* in the late 1970s.[13] For their work with conductive poly(acetylene), Shirakawa, Heeger, and MacDiarmid were awarded the 2000 Nobel prize in chemistry. While poly(acetylene) has not found a wide range of utility, the discovery of its electronic properties launched the field of organic electronics. Since the work of Heeger, Shirakawa, and MacDiarmid, the field of semiconducting polymers has grown exponentially.[14-16] Two families of polymers that have been integral to progress in OPVs are poly(*p*-phenylenevinylene) (PPV) derivatives and poly(thiophene)-based polymers.

PPV-based polymers feature repeating phenyl units joined by a vinylene spacer; the function of the vinylene unit is to increase the planarity of the polymer by decreasing the steric repulsion between hydrogens that would be present if the phenyl rings were directly bonded to one another, as in poly(phenylene). The parent polymer PPV has low solubility in common organic solvents, and is typically functionalized with solubilizing substituents such as alkoxy groups. Two common PPVs featuring alkoxy solubilizing groups are poly[2-methoxy-5-(2-ethylhexyloxy)-1,4-phenylenevinylene] (MEH-PPV), and poly[2-methoxy-5-(3′,7′-dimethyloctyloxy)-1,4-phenylenevinylene] (MDMO-PPV) (Chart 1.1). PPVs were first synthesized in the late 1960s, and were a very important class of early semiconducting polymers.[17] PPVs were first used as the emitting layer in an organic light emitting diode (OLED) in the early 1990s.[18,19] The first evidence of polymer to fullerene charge transfer, as well as the first polymer-fullerene photodiodes and photovoltaics all relied on PPV derivatives.[20,21] While PPVs were instrumental in the early days of organic semiconductor-based devices, their relatively low μ_h, and high optical band gap limited

their performance in OPVs.[22,23] Both drawbacks were improved upon in the next group of polymers that were essential in the growth of OPVs, poly(thiophene)s.

MEH-PPV $R_1 = R_2$ = 2-ethylhexyl
MDMO-PPV R_1 = Methyl, R_2 = 3,7-dimethyloctyl

P3HT

Chart 1.1 Structures of common PPV and poly(thiophene) polymers.

Poly(thiophene)s are a class of polymers containing the heterocycle thiophene as their repeat unit. Poly(thiophene)s have been known since the 1950s, but only came into major research focus in the 1980s during the initial boom of conductive polymer synthesis.[24] In 1993 McCullough *et al.* developed the first synthesis of regioregular poly(3-hexylthiophene) (P3HT); the regioregularity of this polymer made it highly crystalline in the solid state.[25] The crystallinity of this polymer, as well as its high hole mobility, and lower optical band gap made it a better p-type semiconductor for OPV applications. Early OPVs that used P3HT as the primary light absorbing semiconductor performed poorly. However, after it was discovered that thermal annealing improved the crystallinity and μ_h of P3HT based devices, the polymer became a mainstay of OPV research for almost a decade, and was essential to much of the early success in the field.[15,17,22,26] In the last decade design rules for organic semiconductor synthesis have evolved such that modern organic semiconductors far outperform either PPVs or P3HT. The design and synthesis of modern organic semiconductors with a focus on OPV applications will be discussed in Section 1.4.

1.3 Organic photovoltaic devices

1.3.1 Photovoltaic devices: the Shockley equation and equivalent circuit models

Like all photovoltaic devices, OPVs are photodiodes and can be modelled mathematically, using a modified version of the Shockley diode equation (Equation 1 and 2), or with a circuit diagram, using an equivalent circuit model (Figure 1.5). [3,27]

$$J(V) = J_{ph} - J_0\left(\exp\left(\frac{eV}{k_bT}\right) - 1\right) \quad \text{(Eq. 1)}$$

$$J(V) = J_{ph} - J_0\left(\exp\left(\frac{e(V+JR_s)}{nk_bT}\right) - 1\right) - \frac{V+JR_s}{R_{sh}} \quad \text{(Eq. 2)}$$

The Shockley equation models the current density (J) in a diode, as a function of voltage (V); to modify the equation for a solar cell, the photocurrent (J_{ph}) is added. The photocurrent flows in opposition to the diode current. At $V = 0$, the current flowing is the short circuit current density (J_{SC}); according to Equation 1, $J(0) = J_{SC} = J_{ph}$. The term J_0 is the reverse saturation current density; in an inorganic semiconductor, this current is very small (e.g., $J_0 \approx 10^{-8}$ - 10^{-12} A cm^{-2} near 298 K).[27] The other terms in Equation 1 are elementary charge (e), Boltzmann's constant (k_b), and the temperature (T). By convention, in photovoltaics, the direction of photocurrent flow is taken as positive, and the diode current is negative. [3,27]

Figure 1.4 depicts the current-voltage (J-V) characteristics of an ideal solar cell according to Equation 1, both in the dark and under illumination. In the absence of light, normal diode behavior is observed; current only flows when a positive voltage is applied, in accordance with the rectifying properties of a diode. Only the small J_0 flows when $V < V_{turn\text{-}on}$ in the absence of light (the turn-on voltage ($V_{turn\text{-}on}$) is the voltage beyond which there is a substantial increase in current).[27] When the cell is illuminated, the curve is shifted upward by an amount corresponding to J_{ph}, as photocurrent flows. As the voltage is increased, the positive current decreases until it

reaches zero. The point at which the $J(V) = 0$ is the open circuit voltage (V_{OC}); at this point, the diode current is exactly balanced by the photocurrent.

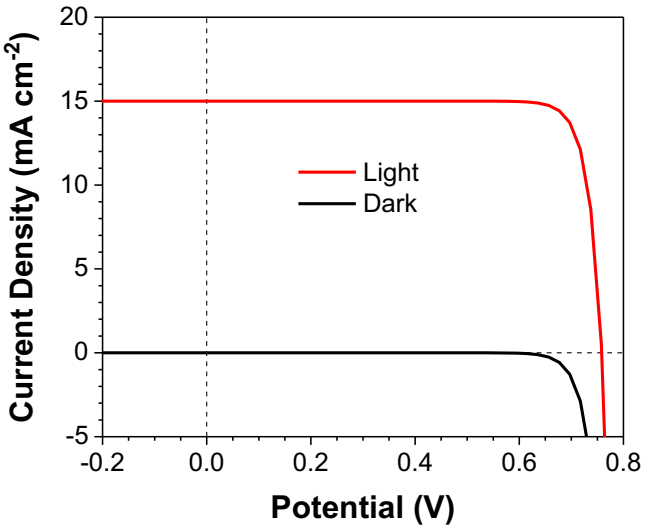

Figure 1.4 The *J-V* characteristic curve of an ideal photovoltaic device according to the Shockley equation, in the dark (black), and under illumination (red).

The equivalent circuit diagram (Figure 1.5) models a solar cell as a constant current generator (constant J_{ph}) in parallel with a diode, with the J_{ph} flowing in opposition to the diode current. Under short circuit conditions, the positive and negative terminals are shorted together; here $J = J_{SC} = J_{ph}$ and the device current is at a maximum, but there is no voltage, and the device has zero power output. If a load is placed between the terminals, a potential difference is created and the cell is now producing power. V_{OC} is reached when a sufficient load (*i.e.,* an extremely high resistance) is placed on the system such that no current is flowing.

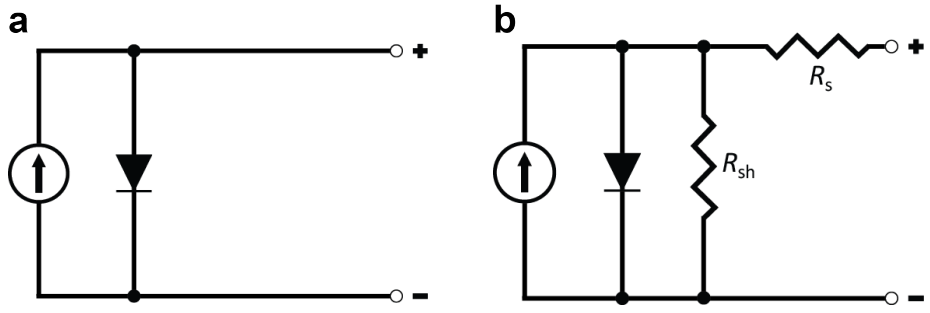

Figure 1.5 Equivalent circuit models of (a) ideal, and (b) non-ideal photovoltaic devices.

Both Equation 1 and Figure 1.5a depict ideal solar cells. More complex models add parasitic resistances to account for non-ideal behavior; these resistances are called the series (R_S) and shunt resistance (R_{Sh}). Series resistance is the resistance to the flow of current through the diode in the forward direction.[3,28] Series resistance impedes current flow by the desired pathway, and an ideal series resistance is 0. Many factors can contribute to a high R_S including Ohmic resistances between the layers of an OPV and poor charge carrier mobility. The other resistance incorporated into the model of a non-ideal solar cell is the shunt resistance. This is the resistance to current flowing in the undesired direction. Unlike series resistance, an ideal R_{Sh} value is infinitely large, forcing the current density to flow along the desired pathway. Problems in a device which cause low R_{Sh} include leakage current, and non-geminate recombination of charge carriers.[3,28] Equation 2 and Figure 1.5b expand the Shockley equation and equivalent circuit model to incorporate R_S and R_{Sh}. The n term in the expanded Shockley equation (Equation 2) is an empirical ideality factor to account for recombination in the device; n has a value between 1 and 2, and is a property of the semiconductor in use.[27]

To experimentally measure the *J-V* characteristics of a cell a source-measure unit is used. Rather than test the cell with a series of loads, the diode potential is swept linearly and the output current is measured. Figure 1.6 is an output *J-V* curve for a P3HT/PC_{61}BM-based OPV under 1

sun illumination. This *J-V* characteristic curve gives the information necessary to calculate the power conversion (PCE) efficiency of an OPV. The maximum power output (P_{out}) of the cell is the point at which the power output, $J \cdot V$, is highest; the J and V values at max power are referred to as J_{max} and V_{max} respectively. The fill factor (FF), a measure of the ideality of the diode, is calculated by dividing the maximum power output ($J_{max} \cdot V_{max}$) by the product of the J_{SC} and V_{OC} (Equation 3). The PCE is calculated using Equation 4, where the input power density (P_{in}) is that of the illumination source.[29]

$$FF = \frac{J_{\max P} \cdot V_{\max P}}{J_{SC} \cdot V_{OC}} \quad \text{(Eq. 3)}$$

$$PCE(\%) = \frac{P_{out}}{P_{in}} \cdot 100\% = \frac{J_{SC} \cdot V_{OC} \cdot FF}{P_{in}} \cdot 100\% \quad \text{(Eq. 4)}$$

By approximating the behavior of the device near V_{OC} and J_{SC} as a linear Ohmic resistor, the series and shunt resistances of a cell can also be calculated using the J·V curve. The series resistance of a cell is the inverse of the slope of this line as it passes through V_{OC}, and the shunt resistance is the inverse of the slope at J_{SC}.

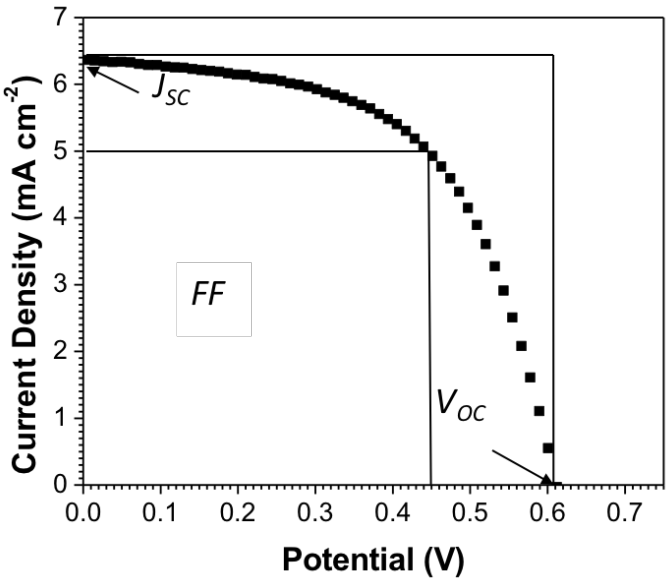

Figure 1.6 A *J-V* curve generated by a source-measure unit.

1.3.2 A band diagram approach to organic photovoltaic devices

OPVs use an active layer made up of two organic semiconductors (one p-type and one n-type) sandwiched between two electrodes to harness solar energy to do work. Figure 1.7 features an energy level diagram of an OPV consisting of a p-type semiconductor, an n-type semiconductor, a metal electrode and a transparent indium doped tin oxide (ITO) electrode (Figure 1.7a).

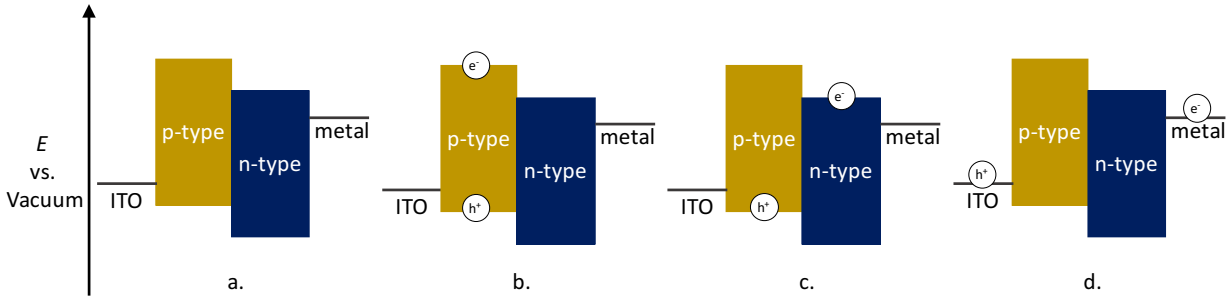

Figure 1.7 Energy level diagram of a simple organic photovoltaic device.

When the p-type semiconductor absorbs light an electron is promoted from the HOMO to the LUMO, forming a quasiparticle, made up of a bound electron hole pair, called an exciton (Figure 1.7b). Once an exciton has been generated, it can migrate to the interface between the p-type and n-type semiconductors and dissociate into two independent charge carriers, a hole, and an electron (Figure 1.7c). Excitons in organic semiconductors have a high binding energy, owing to the large coulombic attraction between the hole and the electron and the low dielectric constant of organic semiconductors.[30] Therefore, it is necessary that the LUMO of the n-type semiconductor be lower in energy than that of the p-type semiconductor, as illustrated in Figure 1.7.[30] This energy difference creates an energetic driving force for charge transfer between the p-type and n-type semiconductors; typically, this energy difference must be >300 meV for efficient exciton dissociation to occur.[31] Once the exciton has dissociated, the hole and electron must move through the p-type and n-type semiconductors respectively (Figure 1.7d); the movement of holes and electrons is governed by the charge carrier mobilities of the semiconductors. The electric field generated by the different work functions of the two electrodes help the hole and electron overcome their coulombic attraction and move to the anode and cathode respectively.

The first two component active layer in an OPV was reported by Tang *et al.* in 1986; it consisted of p-type copper phthalocyanine (CuPC) and n-type perylene diimide (PDI) based semiconductors.[32] In this device, the active layer consisted of a planar junction between the CuPC and PDI; they achieved a maximum PCE of 0.95%. However, these OPVs suffered from low J_{SC} (~2 mA cm^{-2}); this was caused by a low driving force for charge separation, poorly absorbing active layers, and a high probability of electron-hole recombination.

The discovery of the carbon allotrope fullerene (C_{60}), and its n-type semiconductor properties, led to major advances in OPV research. In 1992, Saricifitci *et al.* first demonstrated the

photoinduced transfer of electrons from the p-type semiconductor MEH-PPV to fullerene.[20] In this work, it was demonstrated that MEH-PPV luminescence was efficiently quenched by fullerene. In addition to this, at low temperature, electron paramagnetic resonance signals for both the radical cation of MEH-PPV and the radical anion of C_{60} were observed.

Building upon this discovery, a year later Saricifitci *et al.* demonstrated that a MEH-PPV:C_{60} planar heterojunction could function as the active layer in photodiodes, and photovoltaic cells.[21] These early photovoltaic cells had an architecture consisting of an ITO coated glass substrate, onto which was spin cast a 100 nm film of MEH-PPV. Onto this polymer layer 100 nm of C_{60} was deposited by thermal evaporation, followed by a gold electrode. These devices achieved a maximum PCE of just 0.04%. Despite the efficient electron transfer between MEH-PPV and fullerene, these early OPVs suffered from very poor PCEs, primarily due to low photocurrent densities. It was shown that the wavelength of maximum light absorbance in MEH-PPV corresponded to a minimum in the amount of photocurrent produced by their OPVs. This was attributed to the fact that, due to the thickness of the MEH-PPV layer, insufficient light was reaching the heterojunction between MEH-PPV and fullerene at this wavelength. Excitons in organic semiconductors have very limited diffusion lengths, on the order of 10 nm; this means that only excitons generated within 10 nm of the heterojunction can be effectively dissociated into holes and electrons.[33] Since the layers of MEH-PPV and C_{60} in these early devices were ~100 nm thick, excitons generated in most of the active layer could not reach the interface and dissociate. This is one of the fundamental problems in OPV research, balancing sufficient light absorption with efficiently extracting charge. The innovation that most helped to solve this problem was the invention of the bulk heterojunction active layer.

1.3.3 The bulk heterojunction active layer

One of the largest advances in OPV research was the use of the bulk heterojunction active layer (BHJ) (Figure 1.8b). Early OPVs relied on a planar heterojunction of two organic semiconductors (Figure 1.8a). As seen in Section 1.3.2, excitons generated in these thick planar layers cannot be efficiently transported to an interface to be dissociated; however, if the layer thickness were on the order of an exciton diffusion length (10 nm), the device would not absorb sufficient light to generate an appreciable photocurrent.

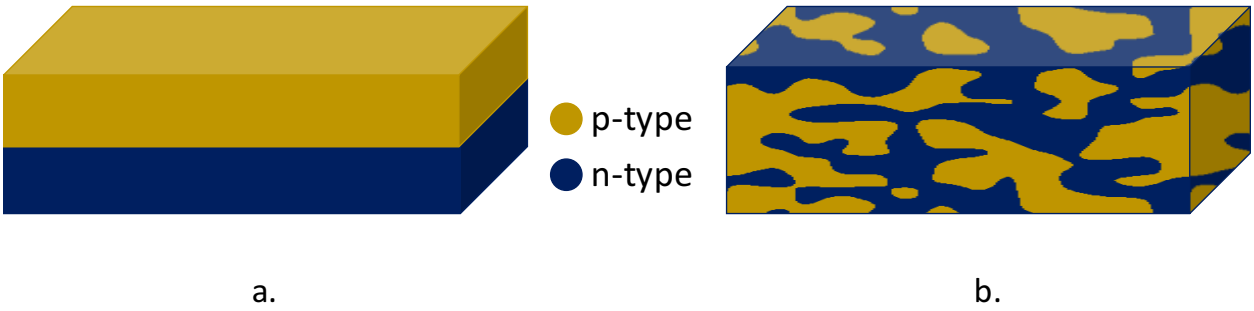

Figure 1.8 (a) Planar and (b) bulk heterojunction active layers containing p-type and n-type semiconductors.

In 1995, Yu *et al.* introduced the concept of the bulk heterojunction active layer (Figure 1.8b).[34] To overcome the insolubility of C_{60} and its tendency to overcrystallize in solid state blends, a derivatized version of fullerene, phenyl-C_{61}-butyric acid methyl ester ($PC_{61}BM$), was used. Thin films cast from concentrated solutions containing both $PC_{61}BM$ and MEH-PPV spontaneously segregated into nanoscale domains, yielding an active layer with a bulk heterojunction morphology. These first BHJ devices were two orders of magnitude more efficient than their planar heterojunction counterparts, achieving a maximum PCE of 2.9%.

Since exciton diffusion lengths are small in organic semiconductors, the ideal size of p and n-type semiconductor domains in a bulk heterojunction is ~10 nm.[33] Its characteristic small, interpenetrated domains gives the bulk heterojunction a much larger interfacial area than the traditional planar heterojunction, making it much more likely that an exciton makes it to an interfacial boundary before geminate recombination can occur. Thanks to the mixing of components throughout the active layer, the entirety of a BHJ can be used to generate photocurrent. Because of this, active layers of BHJ OPVs can be upwards of 100 nm thick without loss of efficiency due to poor charge extraction.[35] While BHJs offer many advantages over planar heterojunctions, their use makes optimizing film morphology an important factor in OPV performance. Achieving nanoscale domain separation is crucial for achieving high efficiencies in BHJ OPVs. This is often done using processing additives in the active layer solution, or through thermal/solvent annealing of the thin films. Thermal or solvent annealing can increase the crystalline packing of active layer components, improving charge carrier mobilities; however, sometimes this can also lead to domains which are too large for efficient exciton migration.[36] Another strategy for optimizing film morphology is the use of blend additives; these are compounds added to the active layer solution, in small amounts, to influence the morphology of the active layer blend. Common blend additives include 1,8-octanedithiol, chloronaphthalene, and the most common additive, 1,8-diiodooctane (DIO). [16,37,38] Most often, these are high boiling point compounds that allow the active layer components to crystallize more slowly than would be possible with the casting solvent alone. The optimization of solvent additive use, and annealing treatments, can have a dramatic effect on OPV efficiency.[26,39,40] Despite the challenges of optimizing blend morphology, the bulk heterojunction architecture has largely persisted until

today. Although vacuum deposited planar heterojunction OPVs are still an active area of research, the work presented in this thesis has been performed using this bulk heterojunction architecture.

1.3.4 Interlayers, electrodes, and inverted *vs.* normal architecture

Early OPVs typically consisted of an active layer simply sandwiched between a transparent ITO electrode and a thermally evaporated metal electrode. This basic architecture suffered from two principal problems.[30] First, the boundary between the active layer and a metal can often create a non-Ohmic contact with a large barrier to charge injection due to poor matching of the work function of the electrode with either the HOMO or LUMO of the semiconductor. Secondly, most common electrode materials, such as ITO or Al, are not selective for a specific charge carrier, and recombination at the electrode surface can dramatically decrease an OPV's shunt resistance. This problem is especially apparent in BHJ devices, since both holes and electrons are generated uniformly throughout the active layer. To combat these two problems, modern OPVs incorporate interlayers between the electrode and active layer.[41]

Interlayers are materials which are designed to aid in the collection of the desired charge carrier at the appropriate electrode; they are often semiconductors with frontier orbitals tailored to permit passage of a single charge carrier.[30] Interfacial layers are characterized based on which charge carrier they are selective for. Hole transport layers are selective for the transport of holes; they typically have a HOMO aligned with the HOMO of the p-type semiconductor in the active layer, and a LUMO level that is poorly aligned with that of the n-type semiconductor, preventing electron transport. Electron transport layers (ETLs) are selective for the passage of electrons and usually have a LUMO level aligned with that of the n-type semiconductor in the active layer, while the HOMO is too low in energy to transfer holes from the active layer effectively. In addition to

having a properly matched HOMO or LUMO to collect the desired charge carrier, it is important that interlayers have a high mobility of the desired charge carrier. Figure 1.9 depicts the band structure of a number of common interlayer materials, along with typical electrode work functions, and frontier orbital energies of active layer materials.[42] The use of interlayers make electrodes far more selective for a single charge carrier than would otherwise be the case; for instance, ITO can be used to collect either holes, or electrons, depending on whether a HTL or ETL is placed on top of it. This increased charge carrier selectivity has given rise to two distinct architectures of OPVs, the normal architecture, and the inverted architecture.

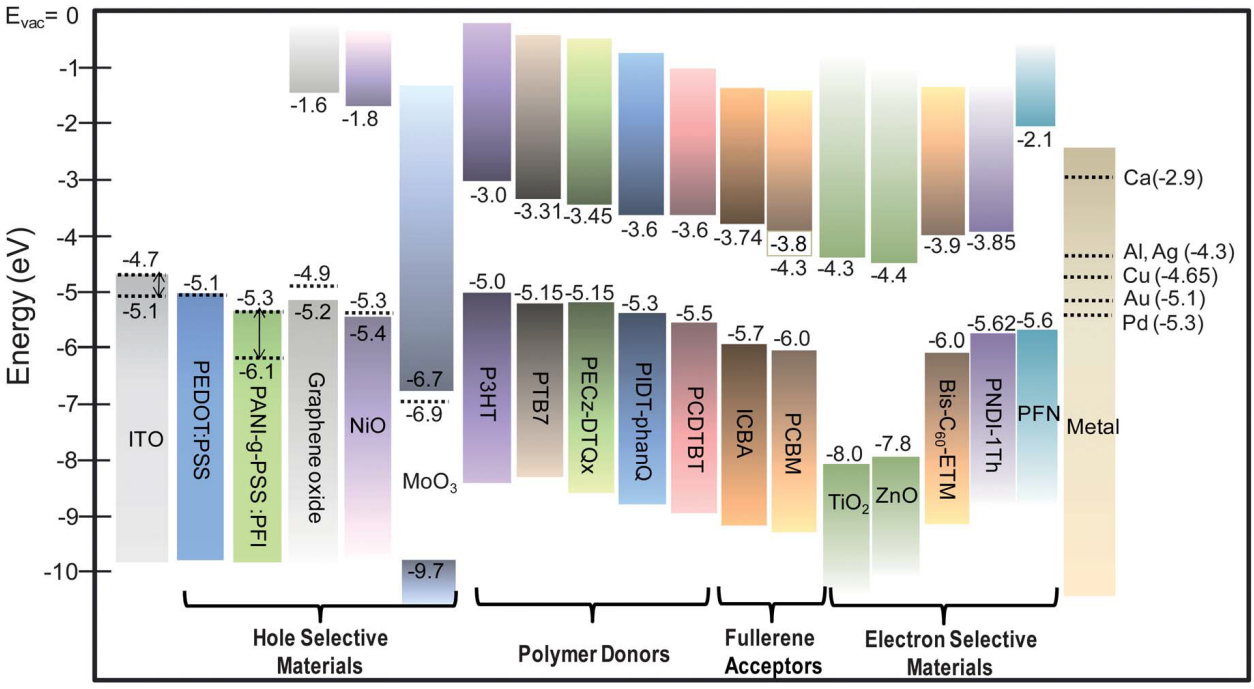

Figure 1.9 Frontier orbital energies of common interlayer materials with respect to vacuum. Reproduced from Ref 42 with permission of the Royal Society of Chemistry.

In a normal architecture device (Figure 1.10), the ITO acts as the anode, and collects holes. To make the ITO hole selective, a HTL is used. The most common HTL in normal architecture OPVs is the p-type organic semiconductor poly(3,4-ethylenedioxythiophene)-poly(styrenesulfonate) (PEDOT:PSS). This blend is typically used as a dispersion in H_2O. The active layer is typically cast on top of this PEDOT:PSS layer. To increase the cathode's selectivity for electrons, an ETL is deposited between the active layer and the metal electrode; an example of this is a thin layer (<1 nm) of LiF, typically deposited by thermal evaporation. Unlike the semiconductor ETLs in Figure 1.9, LiF is an insulator that helps block the passage of holes and aid in electron transport by creating a dipole at the active layer/electrode interface. Since LiF is a dielectric, it has a poor electron mobility and care must be taken to keep the layer thickness low, so electron flow is not impeded. Finally, the cathode is added on top of the hole blocking layer; in the case of a normal architecture device, this is a metal with a small work function such as Ca or Al.[41]

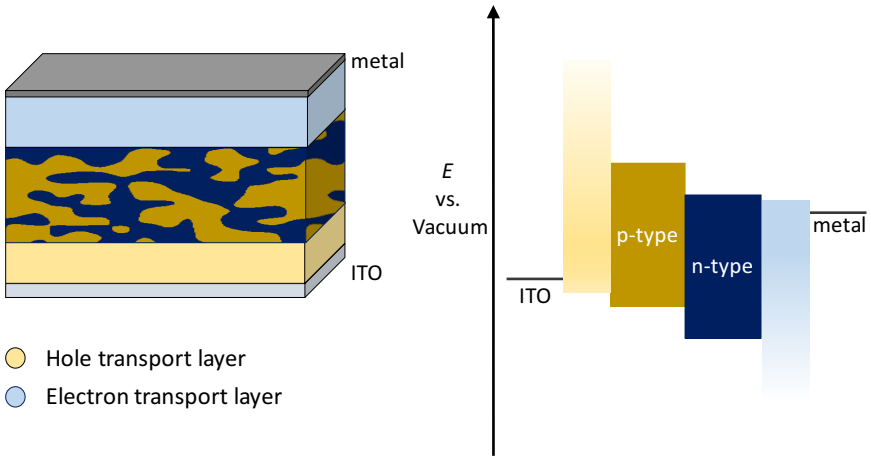

Figure 1.10 Normal architecture bulk heterojunction OPV.

Inverted architecture OPVs use the opposite arrangement of anode and cathode (Figure 1.11). In this case, the ITO electrode acts as the cathode, and is rendered electron selective using an ETL, a common example of which is ZnO. ZnO is often spin coated onto the ITO substrate from either a sol-gel precursor solution, or as a colloidal suspension of nanoparticles.[43,44] The active layer is deposited on top of the ETL. A hole transport layer such as MoO_3 is then added on top of the active layer, often by thermal evaporation. This is followed by a high work function metal, such as Ag, as the anode.[41]

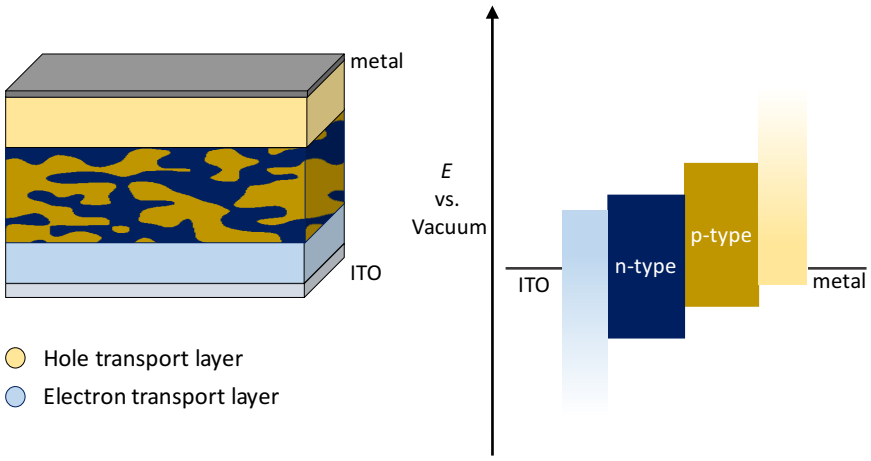

Figure 1.11 Inverted architecture bulk heterojunction OPV.

Early OPVs were primarily fabricated using the normal architecture; in recent years the inverted architecture OPV has increased in popularity due to its increased stability.[45] The PEDOT:PSS layer common to normal architecture OPVs is highly hygroscopic and very acidic. This leads to infiltration of H_2O into the device, as well as leaching of indium ions from the ITO layer, leading to device degradation.[30] Secondly, normal architecture devices use metals such as Al and Ca as the top electrode, which are prone to oxidation in ambient atmosphere; inverted devices typically use more stable Ag top electrodes as the anode.

1.4 The donor-acceptor organic semiconductor

The design and synthesis of new semiconductors for use in OPV active layers is one of the largest areas of organic solar cells research. In Section 1.2.3, PPV and P3HT were introduced as two historically significant organic semiconductors used in OPVs. While P3HT performed better in OPVs than PPV-based polymers, it still had two significant drawbacks. P3HT has a relatively large optical band gap, making it incapable of efficiently harvesting near-infrared solar energy; secondly, OPVs with P3HT:fullerene active layers have relatively low V_{OC}.[15,22] To develop semiconductors with better OPV performance than P3HT, both properties must be improved. First, new materials should have a lower band gap than P3HT, allowing them to harvest the near-infrared portion of the solar spectrum.[15,22,46] Additionally, new semiconductors require a lower HOMO level than P3HT. In OPVs, the V_{OC} of a device is proportional to the energy difference between the HOMO of the p-type semiconductor and the LUMO of the n-type one; for a new semiconductor to improve on the V_{OC} of P3HT devices, it must have a lower HOMO level to increase this energy difference.[22] To meet these requirements, many new organic semiconductors have adopted a donor-acceptor design.[15]

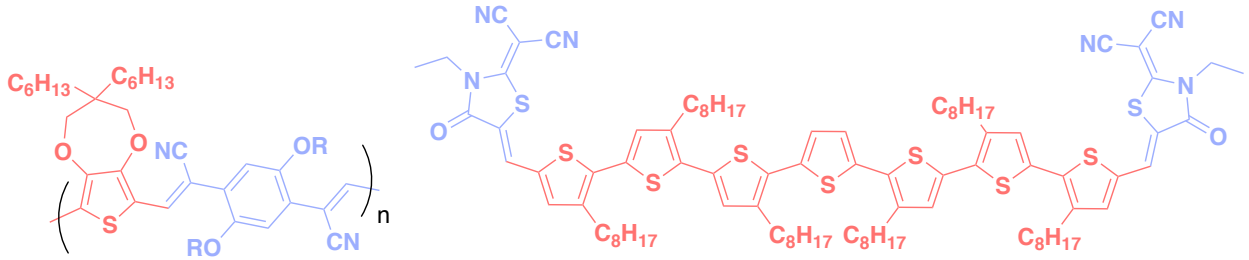

Chart 1.2 Donor-acceptor polymer and molecular semiconductors.[31,47]

Donor-acceptor, or "push-pull", semiconductors are composed of alternating electron-rich (donor) and electron-deficient (acceptor) sub-units (Chart 1.2).[31,48] The HOMO and LUMO of the donor group are relatively high energy compared to the low energy frontier orbitals of the acceptor; this limits the amount of orbital mixing that occurs when the two units are combined in a donor-acceptor semiconductor, as seen in a molecular orbital diagram (Figure 1.12).

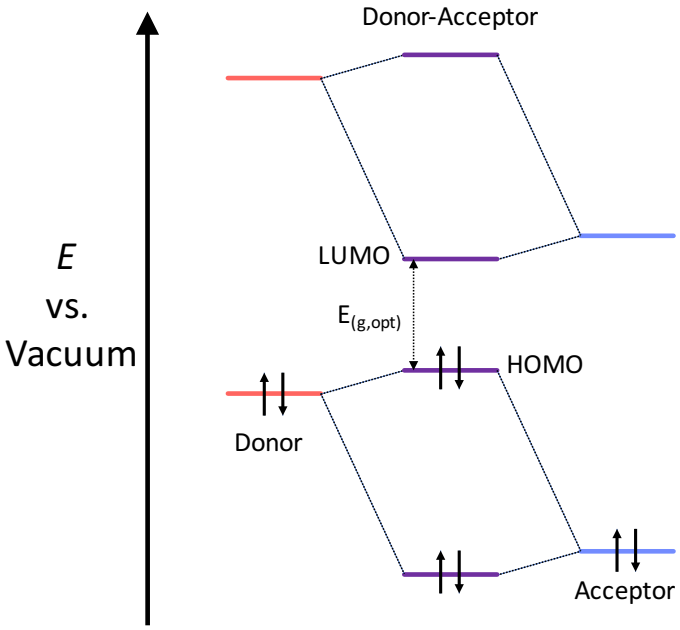

Figure 1.12 Formation of the frontier MOs of a donor-acceptor semiconductor.

The limited orbital mixing leads to a HOMO that primarily resides on the donor, and a LUMO mostly isolated on the acceptor. Orbital isolation has several effects on the electronic structure, and properties, of the donor-acceptor material. Since the donor unit has a higher HOMO level than the acceptor, and the LUMO of the acceptor is lower than that of the donor, donor-acceptor materials typically have a much lower HOMO-LUMO gap than the parent donor and acceptor units (Figure 1.12); often, these optical band gaps are in the near-infrared. The other consequence

of frontier orbital isolation in a donor-acceptor material is that the HOMO→LUMO transition takes on a degree of charge transfer character. This partial charge transfer character gives this transition a very large dipole moment, leading to a high optical extinction coefficient; however, orbital isolation should not be too great, as a lack of wavefunction overlap between the HOMO and LUMO can greatly decrease the transition's extinction coefficient. Additionally, because of the orbital isolation the excited electron resides primarily on the acceptor unit; this implies that electronic coupling between the acceptor unit and the n-type semiconductor is crucial for efficient exciton dissociation in an OPV.[49]

Both molecular and polymeric semiconductors can be synthesized with a donor-acceptor structure. One strategy, common to both small molecules and polymers, is to synthesize the donor and acceptor units separately and couple them at the end of the synthesis. Donor-acceptor polymers are often synthesized by Pd catalyzed cross-coupling reactions, such as Stille and Suzuki polymerizations.[30] These reactions require one monomer to be dihalogenated, and the other to have either two organotin reagents for Stille couplings or two organoboron species for Suzuki reactions; typically, the acceptor unit is the dihalogenated monomer, and the donor unit is the organotin, or boron, containing monomer. Donor-acceptor molecular semiconductors can also be synthesized by Pd catalyzed cross couplings; however, they can also be synthesized by other organic synthesis techniques, such as aldol condensation reactions.[43]

An early example of donor-acceptor polymers for OPVs is the series of carbazole-based polymers first produced by Blouin *et al* in 2007.[50,51] In the first cast case, an electron rich carbazole unit was juxtaposed with electron deficient benzothiadiazole, yielding poly[*N*-9′-heptadecanyl-2,7-carbazole-alt-5,5-(4′,7′-di-2-thienyl-2′,1′,3′-benzothiadiazole)] (PCDTBT) (Chart 1.3). Once optimized, PCDTBT:phenyl-C_{71}-butyric acid methyl ester ($PC_{71}BM$) solar cells achieved a PCE

of 7.5%.[52] The high performance of PCDTBT-based polymers is mostly due to the high V_{OC} (0.88 V) that results from PCDTBT's low E_{HOMO} (-5.45 eV). In order to fully understand the relationship between the polymer's structure and its optoelectronic properties, a series of these polymers were synthesized that varied the acceptor unit composition including such groups as benzoxadiazole, and pyridalthiadiazole.[51] While none of these outperformed the parent PCDTBT polymer, the frontier orbital energies and $E_{g,opt}$ could be tuned by changing the nature of the acceptor unit.

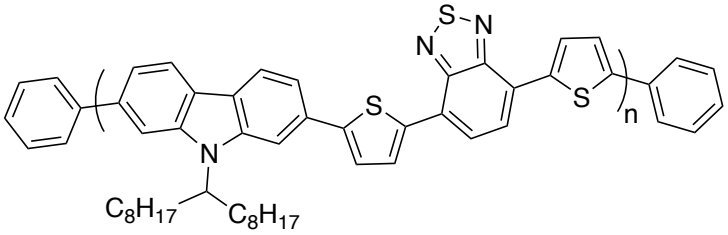

PCDTBT

Chart 1.3 PCDTBT, an early donor-acceptor polymer for high performance OPVs.

Alongside polymers, donor-acceptor molecular semiconductors also became popular in the last decade. In 2011, Sun *et al.* used a donor-acceptor small molecule with a central dithienylsilole unit (DTS($PTTh_2$)$_2$) (Chart 1.4) as the p-type semiconductor in the active layer of an OPV, and achieved a PCE of 6.7%.[53] The high V_{OC} (0.78 V) and J_{SC} (14.4 mA cm^{-2}) are the primary driving force behind this high PCE. This is also a particularly illustrative example of the effects of using a solvent additive in the active layer solution. A 70:30 blend of DTS($PTTh_2$)$_2$ and $PC_{70}BM$ in the active layer, in the absence of DIO, yielded an OPV with a PCE of 4.52%. Upon the addition of 0.25% (v/v) DIO to the active layer solution, the PCE increased to 6.7%; however, increasing the DIO loading to 0.60% (v/v) caused the PCE to fall to just 3.20%. The changes in the PCE values

obtained with DIO loading are driven primarily by increases in *FF*, with a small increase in J_{SC} offsetting a slight decrease in V_{OC}.

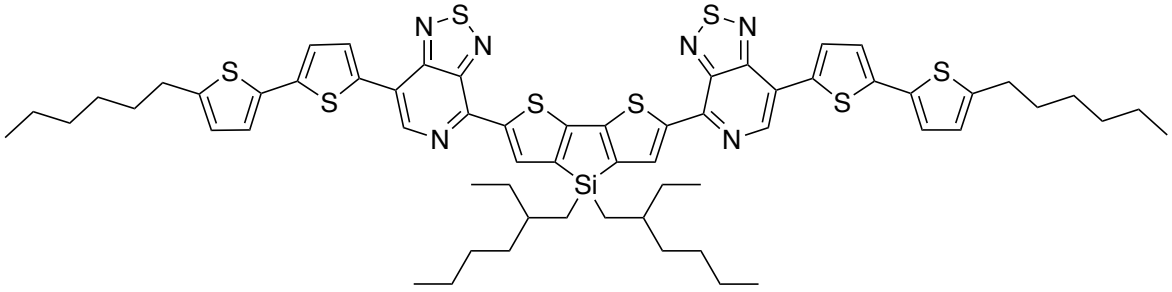

DTS(PTTh$_2$)$_2$

Chart 1.4 A molecular semiconductor with a donor-acceptor design DTS(PTTh$_2$)$_2$.[53]

In addition to these early examples, many donor and acceptor units have been combined to make donor-acceptor semiconductors over the last decade. While an exhaustive review is beyond the scope of this thesis, Chart 1.5 features common examples of donor and acceptor units.[30,54] As discussed already, silicon containing molecules such as dithienylsilole, and nitrogen containing structures such as carbazole have often been used.[51,55] However, the most common donor units are thiophene-based; these include oligomers of thiophene, as well as ring-fused thiophene derivatives, such as thienothiophenes, benzodithiophene, and dithienocylopentadiene. The increased planarity and conjugation of ring-fused thiophene derivatives *vs.* oligothiophenes have made them very prominent in donor-acceptor semiconductors.[16,56-58]

While most electron donors center around the use of thiophene, common electron acceptor units are more diverse. There are still some common themes, including the use of electron withdrawing functional groups such as amides and imides, or electronegative heteroatoms, such as N and F. Common acceptor units include: naphthalene diimide, perylene diimide,

benzothiadiazole, diketopyrrolopyrrole (DPP), and isoindigo.[30] Naphthalene and perylene diimide-based donor-acceptor semiconductors typically exhibit n-type behavior, while benzothiadiazole, DPP, and isoindigo have been combined with a wide variety of donor units to create both p-type and n-type semiconductors. Organic semiconductors based on the acceptor unit isoindigo are the focus of this thesis.

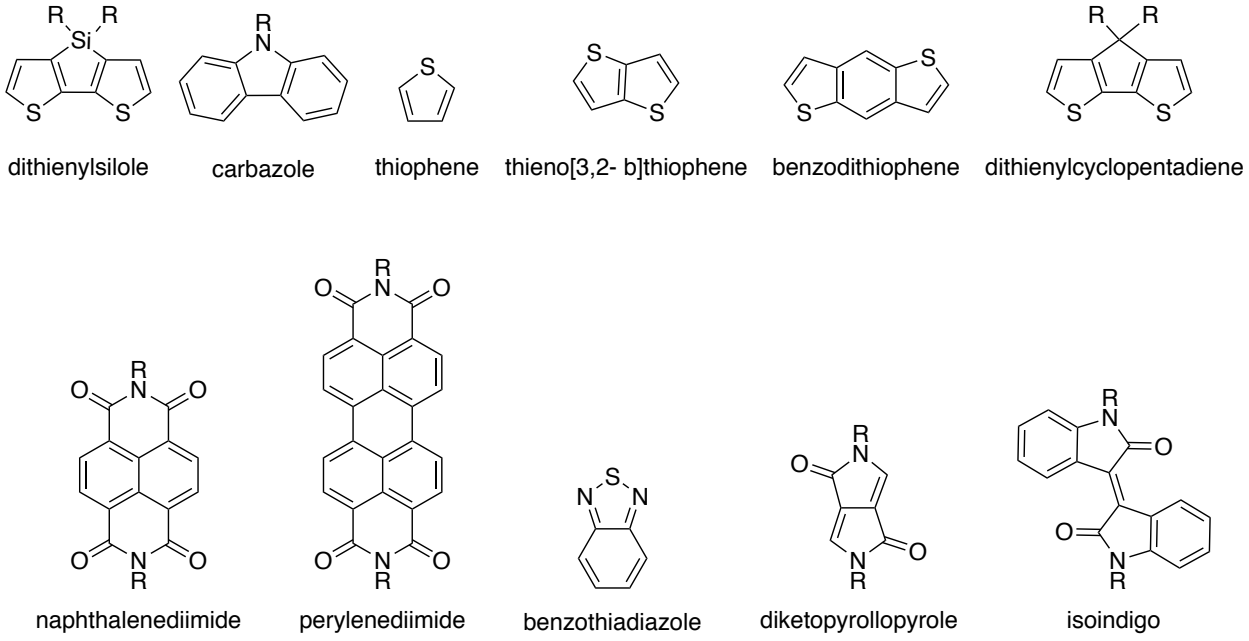

Chart 1.5 Common donor and acceptor units for organic semiconductors.

1.5 Isoindigo-based and isoindigo-inspired organic semiconductors

Isoindigo (Chart 1.6) is a π-conjugated compound containing two 5-membered lactam rings joined by an exocyclic double bond; each lactam is fused to a benzene ring.[59,60] The electron deficient, planar, and conjugated properties of isoindigo make it quite useful as an acceptor unit in donor-acceptor organic semiconductors.

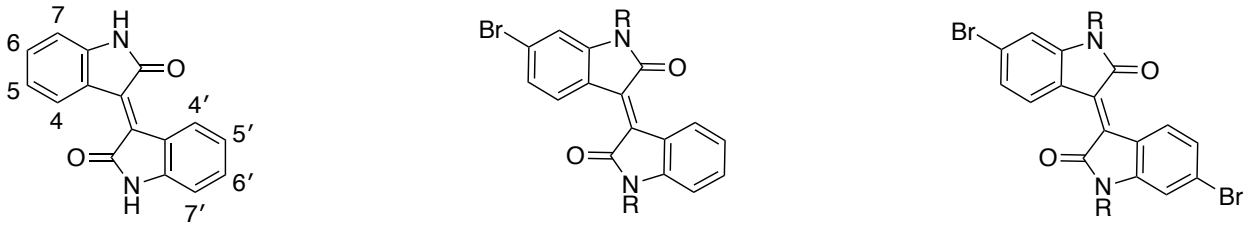

Chart 1.6 Isoindigo and its common derivatives for organic semiconductor synthesis.

For use in organic semiconductors, isoindigo is typically brominated at the 6 and/or 6′ positions to provide reactivity in Pd catalyzed coupling reactions. Both 6-bromoisoindigo and 6,6′-dibromoisoindigo are used in molecular semiconductors, and 6,6′-dibromoisoindigo has become a very common monomer in donor-acceptor polymers. While the 6 and 6′ positions of isoindigo are the most common sites for functionalization, donor-acceptor systems derived from 5,5′-dibromoisoindigo exist, and are good examples of the effect of cross-conjugation on organic semiconductors.[61,62] To impart solubility in common organic solvents, isoindigo is alkylated at the lactam nitrogens. This is typically accomplished by alkylation of the isoindigo unit with an alkyl halide and K_2CO_3 in *N,N*-dimethylformamide (DMF); however, under these conditions non-symmetrical isoindigo derivatives undergo a hydration of the exocyclic double bond followed by an aldol/retro-aldol decomposition and reformation, producing mixtures of the three possible products.[63,64] Since 2010, isoindigo has become one of the most common acceptor units for both donor-acceptor molecular and polymer organic semiconductors.

1.5.1 Isoindigo-based small molecule organic semiconductors

The first isoindigo-based organic semiconductors were reported by Mei *et al.* in 2010.[63] The two compounds reported in this work were donor-acceptor molecular semiconductors

composed of isoindigo and bithiophene in an acceptor-donor-acceptor (**M1**), or donor-acceptor-donor (**M2**) arrangement (Chart 1.7). Both molecules had low $E_{g,opt}$ (Table 1.1), and absorbed light into the near-infrared. The low HOMO level of these semiconductors (-5.6 eV) was promising for creating high V_{OC} OPVs. **M1** and **M2** were used in OPVs as the p-type material in the active layer blend with $PC_{61}BM$ and achieved PCEs of 0.55%, and 1.76% for **M1** and **M2** respectively (Table 1.1, at the end of Section 1.5.1). While both semiconductors absorb light well, poor *FF* and relatively low J_{SC} (Table 1.1) led to the low device efficiencies.

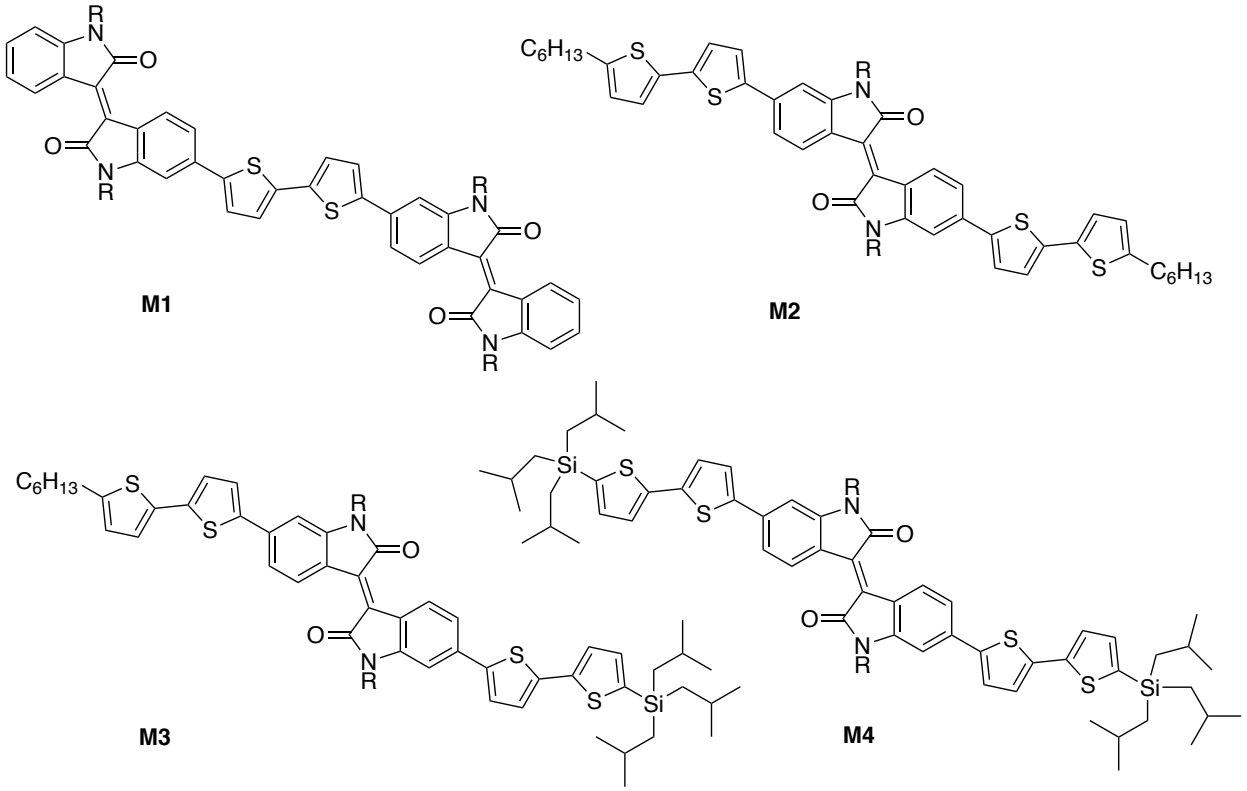

Chart 1.7 Isoindigo-based molecular semiconductors **M1**-**M4**, R = 2-ethylhexyl.

After the initial results were published, it was discovered that the **M2**-based OPVs had benefitted from the unintentional incorporation of poly(dimethylsiloxane) (PDMS) from the

syringes used to process the active layer solution.[65] Graham *et al.* determined that by intentionally incorporating PDMS as a blend additive in the active layer, the PCE of the resulting OPVs could be increased from 1.25 ± 0.37% with no PDMS to 2.16 ± 0.09% with 0.1 mg/ml PDMS in the active layer solution.[65] Improving the active layer morphology increased all of the device characteristics, but had the most pronounced effect on J_{SC}, which increased from 4.28 mA cm^{-2} without PDMS to 6.70 mA cm^{-2} with 0.75 mg/ml PDMS in the active layer solution. In addition to PDMS, other additives were studied in a follow up paper, leading to a maximum PCE of 3.67 ± 0.12% for OPVs of **M2**:$PC_{61}BM$ active layers incorporating both PDMS and tetraethyleneglycol.[66] Following this work on blend additives, Graham *et al.* studied tailor-made additives, derivatives of **M2** with either one (**M3**) or two (**M4**) tri(isobutyl)silyl groups in place of the hexyl chains on the bithiophene (Chart 1.7).[67] They showed that the use of **M3** as an additive (20% w/w) in an **M2**-based active layer helped control crystallinity and domain size, yielding OPVs with a PCE of 2.2%, compared to 1.3% for devices with no **M3** in the active layer.

In addition to Reynolds and coworkers, by 2013 other research groups began to produce isoindigo-based molecular organic semiconductors; a summary of the optoelectronic properties and OPV performance of some of these materials is found in Table 1.1. Yassin *et al.* published the synthesis and use of two different isoindigo-based small molecules in OPVs.[68] In **M5**, the isoindigo unit is flanked by two electron-rich benzofurans; in **M6**, the isoindigo is combined with two dithienopyrrole units (Chart 1.8). BHJ OPVs with **M5**:$PC_{61}BM$ active layers exhibited a maximum PCE of 0.26%, while those incorporating **M6** had a maximum PCE of 0.01% (Table 1.1). Additionally, a donor-acceptor-donor semiconductor with two triphenylamine groups on either side of isoindigo (**M7**) (Chart 1.8), reported by Yang *et al.,* was incorporated into OPV active layers as a p-type semiconductor achieving a maximum PCE of 0.84%.[69] The performance of **M5-**

M7 in OPVs was limited by low J_{SC} and very poor fill factors, usually caused by poor BHJ morphology (Table 1.1). These materials often exhibited a tendency to self-aggregate and exhibit large domains in active layers. It is also possible that these molecular semiconductors had poor charge carrier mobilities; however, this was not often measured in these early materials.

Also in 2013, Elsawy *et al.* studied the effects of the number of thiophene rings, and donor strength, in a series of donor-acceptor-donor isoindigo-based semiconductors.[70] The group studied thiophene (**M8**), bithiophene (**M9**), and terthiophene (**M10**), as well as two substituted thiophenes, 3-hexylthiophene (**M11**), and 3,4-ethylenedioxythiophene (**M12**) (Chart 1.8). As the number of thiophene units in the donor increased, the $E_{g,opt}$ decreased due to the increasing π-conjugation length, and donor strength, of the thiophene oligomer (Table 1.1). OPVs with **M8-M12**:$PC_{71}BM$ active layers were fabricated and the number of thiophene units directly correlated with OPV performance; the thiophene, bithiophene, and terthiophene containing semiconductors yielded max PCEs of 0.003%, 2.60%, and 3.20% respectively (Table 1.1). Despite a lower $E_{g,opt}$ due to the more electron rich nature of the ethylenedioxythiophene unit, **M12** did not perform significantly better than **M8** (Table 1.1). The poor performance of the semiconductors containing a single thiophene unit was ascribed to their poor charge carrier mobilities, which contributed to the low J_{SC}.

Another early isoindigo-based molecular semiconductor was reported by Wang *et al.*[71] In this case, the isoindigo unit was paired with an extended thiophene-thienothiophene donor unit in a donor-acceptor-donor fashion (**M13**) (Chart 1.8). The resulting semiconductor had a very low optical band gap of ~800 nm (~1.5 eV), and when combined with $PC_{61}BM$ in the active layer of an OPV produced a PCE of 1.41% (Table 1.1). The J_{SC} was relatively high owing to the material's

low bad gap; however, the PCE was adversely affected by a poor fill factor, due to poor blend morphology.

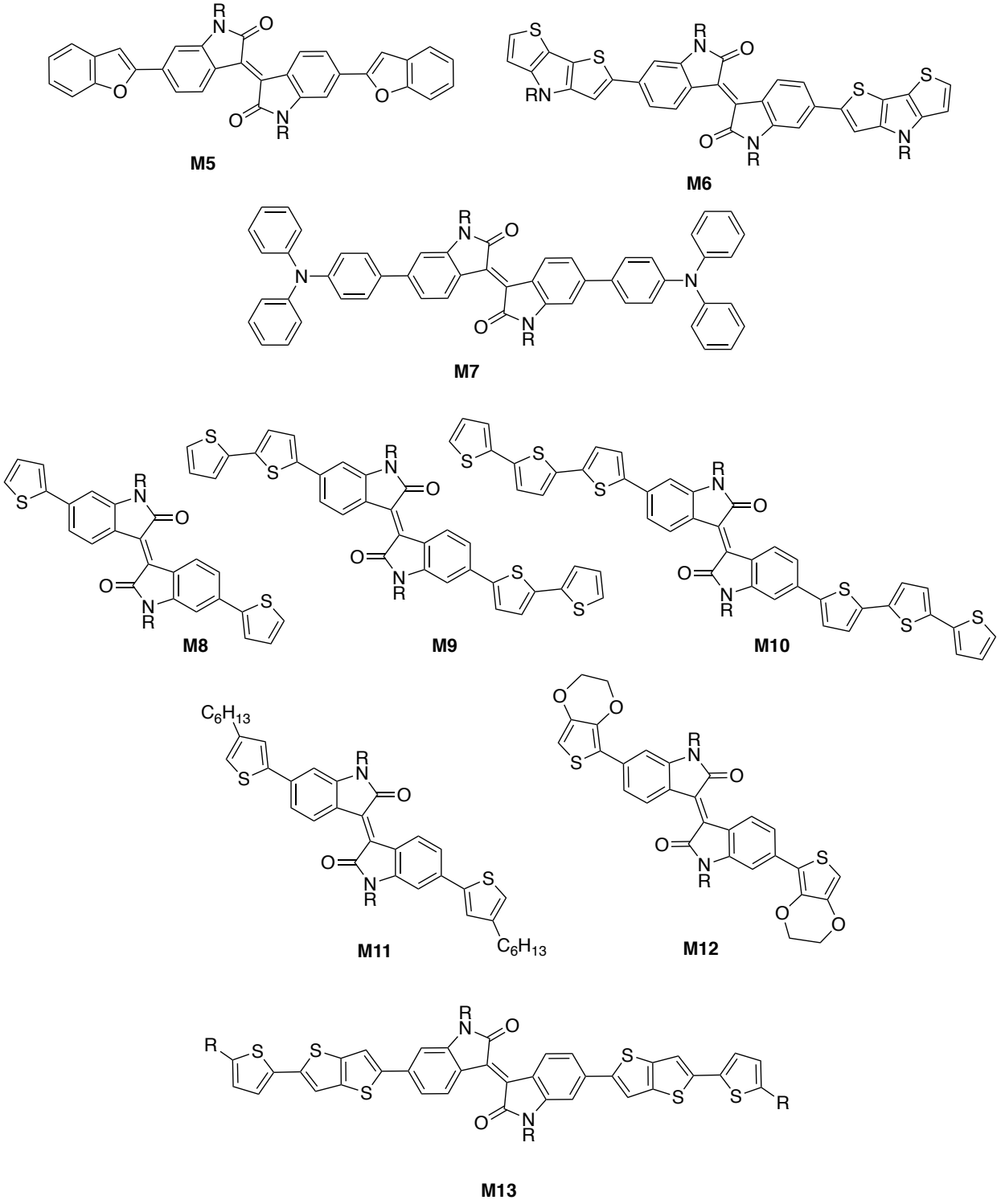

Chart 1.8 Isoindigo-based molecular semiconductors **M5**-**M13**, R = 2-ethylhexyl.

The isoindigo based semiconductors discussed so far have had a donor-acceptor-donor or acceptor-donor-acceptor structure. The donor-acceptor-donor design has proven more popular due to the ease of synthesis of the 6,6′-dibromoisoindigo unit compared to the reduced yields of 6-bromoisoindigo. After the initial wave of isoindigo-based molecular semiconductors, researchers began exploring a wider variety of molecular architectures and π-conjugated units to combine with isoindigo. Additionally, they began to explore using isoindigo-based small molecules as n-type semiconductors, replacing fullerene in OPV active layers.

Areephong *et al.* created an extended donor-acceptor molecule in which a central dithienylsilole unit was flanked by two isoindigos, each of which was bonded to a bithiophene unit (**M14**) (Chart 1.9).[72] This molecule's structure is similar to the benzothiadiazole-based donor-acceptor molecule, synthesized by Sun *et al.*, discussed in Section 1.3.2.[53] Thin films of **M14** cast from chloroform absorbed light down to 828 nm; this low band gap of 1.5 eV allows the compound to usefully harvest light into the near-infrared. When used in OPVs as the p-type semiconductor alongside $PC_{61}BM$, using 5% (v/v) DIO, an average PCE of 3.2 ± 0.2% was achieved. This was largely due to a very high J_{SC} (11.32 mA cm^{-2}) (Table 1.1), that resulted from the molecule's low band gap.[72]

A similar extended donor-acceptor motif was used by Tomassetti *et al.* to study the differences between linear (**M15)** and branched semiconductor structures (**M16/M17**) (Chart 1.9); the branched structure of **M16** and **M17** leads to a two-dimensional semiconductor.[73] The central acceptor in both cases is isoindigo, and each molecule contains a thiophene oligomer of either 3 or 4 thiophene units; the terminal thiophene is bonded to a cyanoacrylate ester. In the case of their branched semiconductors, the penultimate thiophene is bonded to an additional thiophene-cyanoacrylate group. The $E_{g,opt}$ of the linear and branched semiconductors were quite similar

(Table 1.1); however, owing to its extra thiophene, **M17** did have a slightly smaller electronic band gap ($E_{g,elec}$) of 1.71 eV. OPVs were fabricated using active layers of the isoindigo-based semiconductors and $PC_{61}BM$. To obtain maximum PCEs, solvent annealing treatments were used, and the linear molecule containing isoindigo and terthiophene (**M15)** produced the highest average efficiency of 1.6 ± 0.2% (Table 1.1). Atomic force microscopy (AFM) images of all three active layer blends revealed that, after solvent annealing treatment, the active layers of the **M15**-based OPVs had much smaller domain sizes than their branched counterparts **M16/M17**, which led to the increased PCE.[73]

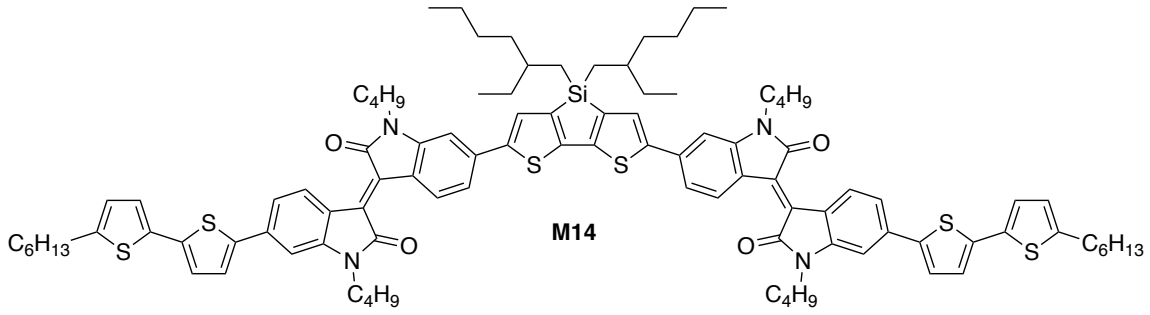

M14

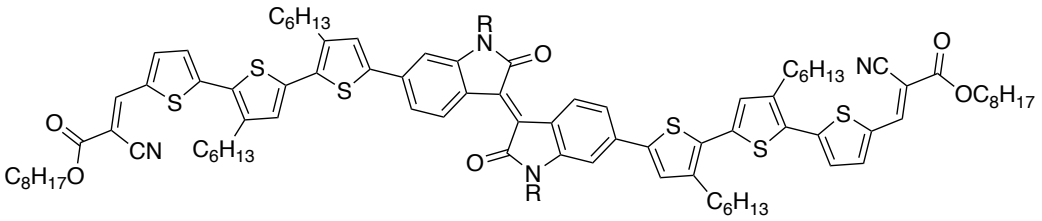

M15

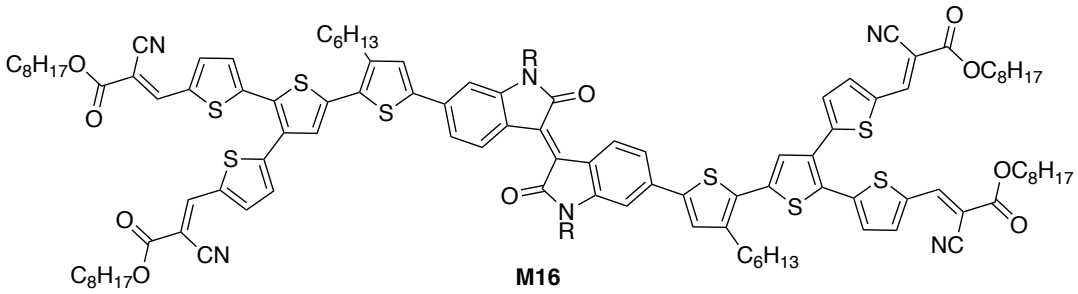

M16

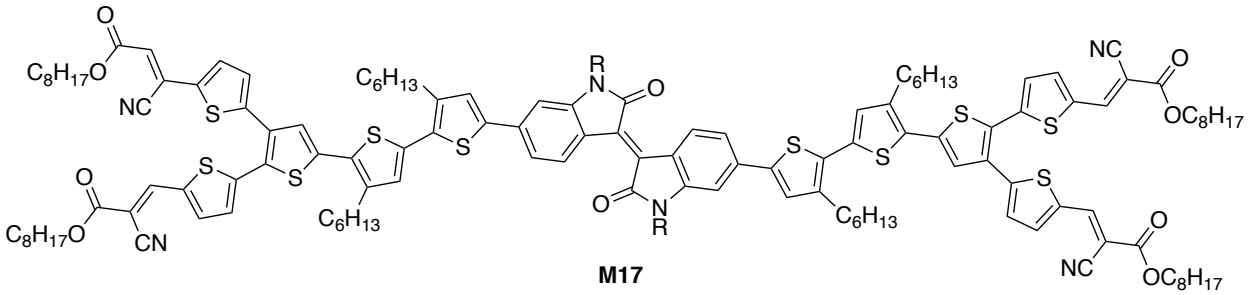

M17

Chart 1.9 Isoindigo-based molecular semiconductors **M14**-**M17**, R = 2-ethylhexyl.

Another example of multi-dimensional organic semiconductors can be found in the work of Liu *et al*, in which they synthesized triangular, isoindigo-based, n-type semiconductors.[74] These molecules were built around a central phenyl (**M18**) or triphenylamine (**M19**) core (Chart 1.10). The triphenylamine core of **M19** is a more electron-rich donor that the phenyl core of **M18**; this stronger donor-acceptor character makes the $E_{g,opt}$ of **M19** much smaller than **M18** (Table 1.1). Both **M18** and **M19** were used as the n-type semiconductor, with P3HT, in OPV active layers. The increased light absorption of **M19,** and better film morphology with P3HT led to higher J_{SC} and *FF* values, producing a maximum PCE 0.81% for **M19** as compared to 0.19% for **M18**.

Other n-type isoindigo-based molecular semiconductors have been synthesized to replace fullerenes in OPV active layers. An in-depth computational study by Rutledge *et al.* predicted donor-acceptor molecules with an isoindigo core to have appropriate energy levels to act as non-fullerene n-type semiconductors.[75] Based on this theoretical study, McAfee *et al.* synthesized a series of n-type molecular semiconductors including **M20** and **M21** (Chart 1.10).[76] Experimentally, it was found that increasing the steric bulk of the end group, from phthalimide to naphthalimide, and adding a chlorine to the isoindigo unit, significantly improved device efficiency by improving solid-state packing and enhancing the electron-deficient nature of the isoindigo unit. OPVs using **M20** and a molecular p-type semiconductor in the active layer achieved and average PCE of 1.07% (Table 1.1) compared to 0.93% for **M21**.[76]

Finally, in a break with convention, Jung *et al.* recently used isoindigo as the donor unit of a donor-acceptor molecular semiconductor (**M22**) paired with the even more electron deficient dithienyldiketopyrrolopyrrole (Chart 1.10).[77] In this case, the molecule's HOMO was localized to the isoindigo, while the LUMO resided on the diketopyrrolopyrrole units. This yielded a semiconductor with a low $E_{g,opt}$ (850 nm), and low frontier orbital energies; the LUMO energy was

-3.82 eV, and the HOMO -5.56 eV as measured by cyclic voltammetry (Table 1.1). These low-lying orbitals gave devices fabricated with **M22**:$PC_{71}BM$ active layers a high V_{OC} of 0.86 V (Table 1.1). After optimizing the devices by solvent annealing, an average PCE of 5.62% was achieved.

Since its first use in OPVs in 2010, a wide variety of isoindigo-based molecular semiconductors have been synthesized and incorporated into OPVs. Molecular semiconductors have several advantages over polymer semiconductors. They can be purified using simple recrystallization or chromatographic techniques, rather than the time and energy intensive Soxhlet extractions used in polymer synthesis. Additionally, polymers suffer from batch to batch variation in molecular weight, which can lead to large variations in OPV performance; the synthesis and purification of molecular semiconductors is much more repeatable, making their OPV performance more consistent.

However, there are drawbacks in the use of molecular semiconductors in OPVs. First, since these semiconductors are based on flat π-conjugated systems they tend to self-aggregate and π-stack, leading to over-crystallization of the active layer blends. This over-crystallization results in large domain sizes, causing inefficient exciton dissociation and low device performance. Secondly, polymer semiconductors often have higher charge carrier mobilites than molecular semiconductors because holes and electrons can pass down the length of a polymer chain via intramolecular charge transport, rather than hopping from molecule to molecule via intermolecular charge transport; this often leads to higher J_{SC} in polymer-based OPVs than in those using molecular organic semiconductors. These drawbacks have led to an intensifying focus on the development of polymer semiconductors in the last several years, including many donor-acceptor polymers incorporating isoindigo.

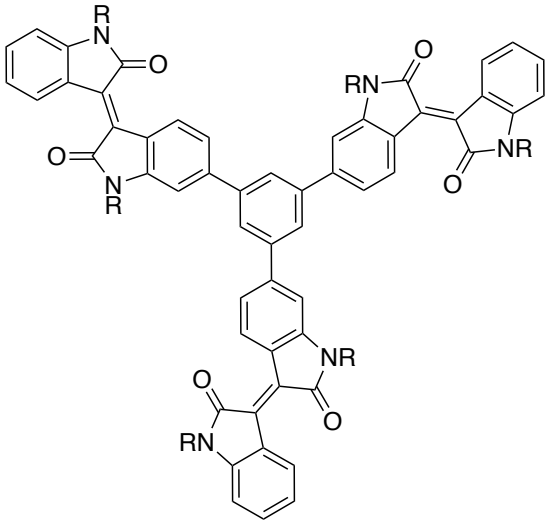

M18

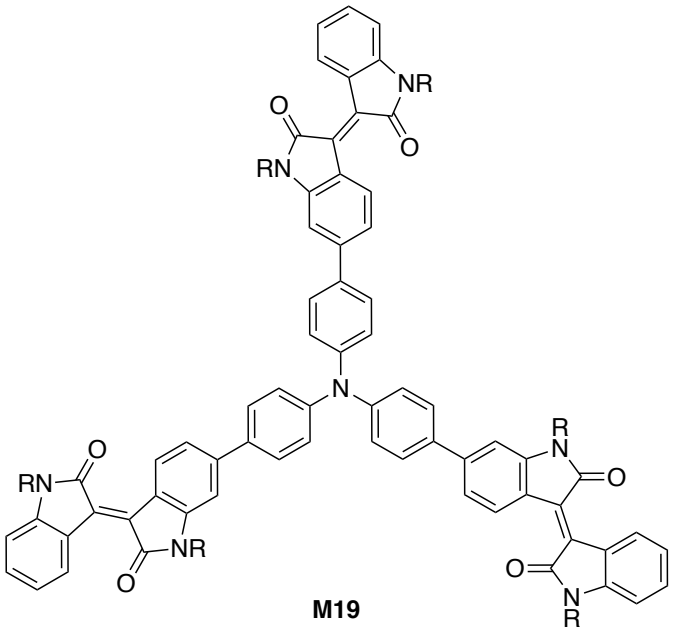

M19

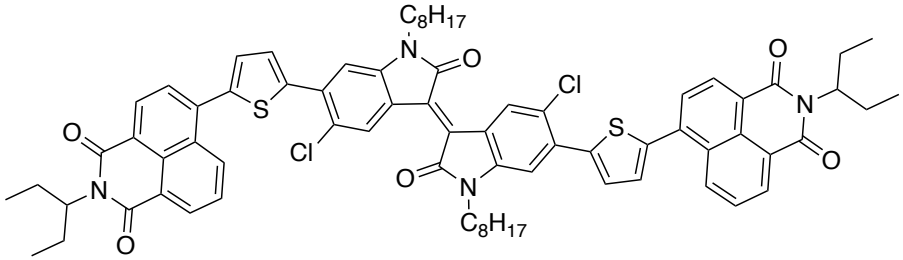

M20

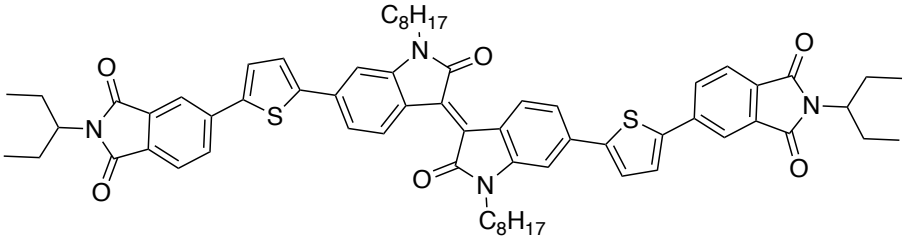

M21

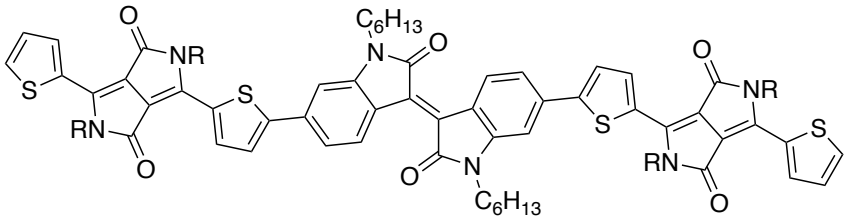

M22

Chart 1.10 Isoindigo-based molecular semiconductors **M18**-**M22**, R = 2-ethylhexyl.

Table 1.1 Optoelectronic properties and OPV performance of isoindigo-based molecular semiconductors **M1**-**M22**.

Molecule	HOMO[a] (eV)	LUMO[a] (eV)	$E_{g,Elec}$ (eV)	$E_{g,opt}$ (nm)	μ_h ($cm^2 V^{-1}s^{-1}$)	V_{OC} (V)	J_{SC} (mA cm^{-2})	*FF* (%)	PCE (%)	Ref
M1	-5.6	-3.8	1.7	655	-	0.74[b]	6.3[b]	38[b]	1.76[b]	63
M2	-5.6	-3.9	1.6	688	-	0.66[b]	2.4[b]	36[b]	0.55[b]	63
M5	-	-	-	551	-	0.6[b]	1[b]	38[b]	0.26[b]	68
M6	-	-	-	610	-	0.35[b]	0.15[b]	16[b]	0.01[b]	68
M7	-5.30[c]	-3.61[c]	1.69	734	2.49×10^{-4}	0.78[b]	2.94[b]	36.5[b]	0.84[b]	69
M8	-5.47	-3.60	1.87	685	1.4×10^{-2}	0.35[b]	0.003[b]	25.8[b]	0.003[b]	70
M9	-5.11	-3.57	1.54	729	3.6×10^{-2}	0.93[b]	6.58[b]	42.8[b]	2.60[b]	70
M10	-5.10	-3.63	1.47	775	9.7×10^{-4}	0.87[b]	8.21[b]	43.3[b]	3.20[b]	70
M11	-5.47	-3.61	1.86	689	1.1×10^{-3}	0.55[b]	0.21[b]	20.4[b]	0.04[b]	70
M12	-5.26	-3.62	1.64	700	3.2×10^{-5}	0.12[b]	0.002[b]	28.0[b]	0.002[b]	70
M13	-5.39[c]	-3.92[c]	1.47	805	-	0.72[b]	6.03[b]	32.5[b]	1.41[b]	71
M14	-5.17[c]	-3.66[c]	1.51	828	-	0.686	11.3	0.41	3.2	72
M15	-5.56[d]	-3.59[d]	1.97	800	3.66×10^{-3}	0.95[b]	4.46[b]	45[b]	1.92[b]	73
M16	-5.52[d]	-3.61[d]	1.91	765	1.86×10^{-5}	0.98[b]	1.60[b]	50[b]	0.78[b]	73
M17	-5.33[d]	-3.62[d]	1.71	785	3.44×10^{-5}	0.83[b]	3.29[b]	51[b]	1.39[b]	73
M18	-5.64[e]	-3.79[f]	-	670	-	1.15[b]	0.45[b]	36.7[b]	0.19[b]	74
M19	-5.54[e]	-3.77[f]	-	701	-	0.96[b]	1.91[b]	43.7[b]	0.81[b]	74
M20	-5.61[c]	-3.73[c]	1.88	711	-	0.82	2.94	44	1.07	76
M21	-5.58[c]	-3.67[c]	1.81	708	-	0.91	2.52	41	0.93	76
M22	-5.56[c]	-3.82[c]	1.74	850	-	0.86[b]	11.75[b]	58[b]	5.62	77

[a] HOMO/LUMO energies estimated from the onset of oxidation/reduction in voltammetry experiments, Fc/Fc^+ used as an internal reference. The Fc/Fc^+ redox couple is estimated as -5.1 eV with respect to vacuum. [b] OPV results from best device, all others are average performance. [c] Fc/Fc^+ redox couple estimated as -4.8 eV with respect to vacuum. [d] Fc/Fc^+ redox couple estimated as -4.98 eV with respect to vacuum. [e] $E_{HOMO} = -(E_{ox} + 4.54)$ eV.[74] [f] E_{LUMO} estimated from $E_{HOMO} + E_{g(opt)}$.

1.5.2 p-Type isoindigo-based polymer semiconductors

While the first publication of an isoindigo-based semiconductor was a small molecule, the field of isoindigo-based polymer semiconductors grew rapidly following this initial report. This is likely because 6,6′-dibromoisoindigo is an easily accessible, electron-deficient, co-monomer for the Pd catalyzed cross-coupling reactions commonly used to make donor-acceptor polymers. The first isoindigo-based polymers were reported by Stalder *et al.* in 2010.[78] The group synthesized a series of donor-acceptor polymers combining isoindigo with six donor units: thiophene (**P1a)**, 3,4-dioctylthiophene (**P2**), 3,4-propylenedioxythiophene (**P3**), ethene (**P4**), 9,9-dihexylfluorene (**P5a**), and 1,4-bis(hexyloxy)benzene (**P6**) (Chart 1.11). The semiconductors' physical and optoelectronic properties were characterized, and are summarized in Table 1.2 (entries 1-6). The polymers with thiophene (**P1a**), 3,4-propylenedioxythiophene (**P3**), and ethene (**P4**), featured the lowest $E_{g,opt}$ (>700 nm), and $E_{g,elec}$ <1.9 eV. The HOMO and LUMO energies of the polymers, as estimated by voltammetry, made them suitable as p-type semiconductors for OPV active layers.

Following this first report, researchers began using p-type isoindigo-based polymers in OPVs. In early 2011, three groups independently published the first OPVs incorporating isoindigo-based polymers in the active layer. Zhang *et al.* reported copolymers of isoindigo with thiophene (**P1b**), bis(2-ethylhexyloxy)-benzodithiophene (**P7**), and thienothiophene (**P8a/b**) donors (Chart 1.11).[79] The frontier orbital energies were similar to those of other isoindigo donor-acceptor polymers (Table 1.2, entries 7-9). All three polymers were incorporated into OPV active layers as the p-type semiconductor. The devices exhibited modest efficiencies (Table 1.2, entries 7-9), and the best performance was seen in devices incorporating **P7**, with a maximum PCE of 1.91%. At the time, the group blamed the modest efficiencies of their photovoltaics to a potential imbalance in charge carrier mobilities between the p-type and n-type semiconductors.

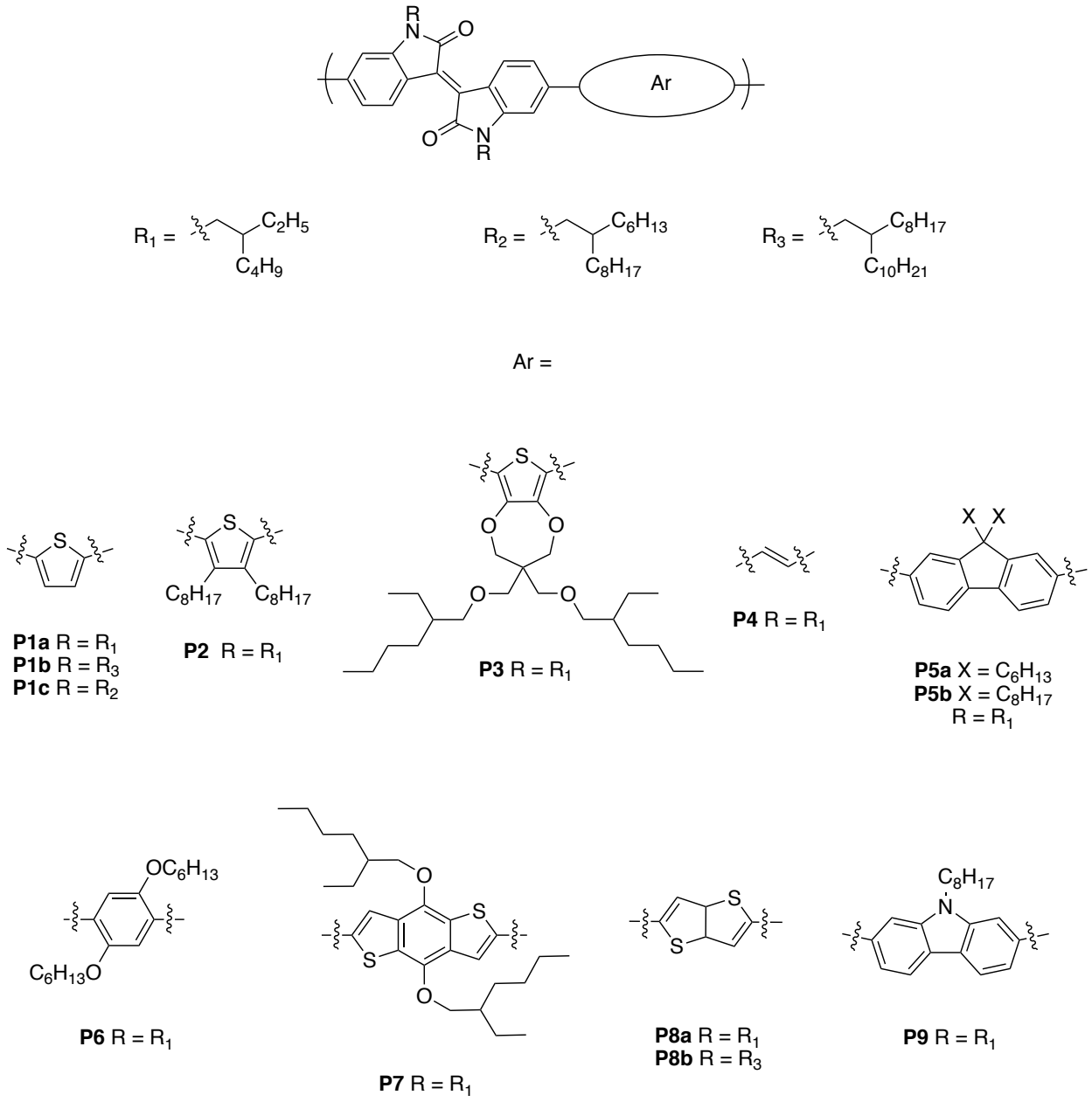

Chart 1.11 Isoindigo based p-type semiconductors **P1**-**P9**.

At nearly the same time, Liu *et al.* reported copolymers of isoindigo with 9,9-dioctylfluorene (**P5b**), bis(2-ethylhexyloxy)-benzodithiophene (**P7)**, and carbazole (**P9**), and incorporated them in OPV active layers with $PC_{61}BM$ (Table 1.2, entries 10-12). Again, the efficiency of the solar cells was modest, with a maximum PCE of 0.90% being obtained for

P7:$PC_{61}BM$ based devices; the low fill factor (0.41) of the OPVs pointed to poor active layer blend morphology as the cause of the low PCEs. In a third, nearly simultaneous, report, Wang *et al.* demonstrated the use of **P1c** as a p-type material in OPV active layers (Table 1.2, entry 13).[80] However, in this case, the researchers experimented with the use of DIO as an additive in their active layer solutions; the addition of DIO was key to successful use of isoindigo-based polymers in OPV applications. Wang *et al.* showed that the PCE of OPVs with a **P1c**:$PC_{71}BM$ active layer nearly doubled, from 1.7% to 3.0% when DIO was added to the active layer solution. The use of DIO (2.5 w/v% in o-dichlorobenzene) caused large changes in the active layer blend morphology; this improved blend morphology caused an increase in both J_{SC}, from 3.1 to 5.4 mA cm^{-2}, and *FF*, from 0.59 to 0.63.

Following this, Wang *et al.* reported the first use of the copolymer of isoindigo and terthiophene **P10a** (Chart 1.12). The optoelectronic properties of **P10a** were similar to those of **P1c**, though the increased donor strength of terthiophene *vs.* thiophene results in a slightly smaller optical band gap (Table 1.2, entry 14). While the optoelectronic properties of **P1c** and **P10a** were quite similar, the OPV performance was very different; optimized OPVs reached a PCE of 6.3%, twice as high as the PCE of optimized **P1c**:$PC_{71}BM$ based devices. This high PCE is due to a large increase in J_{SC}, from 5.4 mA cm^{-2} in OPVs using **P1c,** to 13.1 mA cm^{-2} for **P10a**. The fill factor also increases slightly, from 0.63 to 0.69, helping to offset the decrease in V_{OC} from 0.89 V to 0.70 V. As in **P1c** based devices, the PCE of OPVs with an **P10a**:$PC_{71}BM$ active layers increased dramatically when DIO was used. A PCE of 6.3% represented a major step for isoindigo-based polymer semiconductors, and led to a large amount isoindigo-oligothiophene copolymer research.

Table 1.2 Optoelectronic properties and OPV performance of isoindigo-based polymers **P1-P10A**.

Entry	Polymer	HOMO[a] (eV)	LUMO[a] (eV)	$E_{g,Elec}$ (eV)	$E_{g,opt}$ (nm)	V_{OC} (V)	J_{SC} (mA cm^{-2})	*FF* (%)	PCE (%)	Ref
1	**P1a**	-5.81	-3.95	1.86	775	-	-	-	-	[78]
2	**P2**	-5.74	-3.85	1.89	693	-	-	-	-	[78]
3	**P3**	-5.68	-3.91	1.77	800	-	-	-	-	[78]
4	**P4**	-5.76	-3.93	1.83	747	-	-	-	-	[78]
5	**P5a**	-5.83	-3.84	1.99	663	-	-	-	-	[78]
6	**P6**	-5.80	-3.87	1.93	708	-	-	-	-	[78]
7	**P7**	-5.20[c]	-3.66[d]	-	805	0.71[e]	7.93[e]	34[e]	1.91[e]	[79]
8	**P1b**	-5.49[c]	-3.91[d]	-	785	0.87[e]	1.76[e]	60[e]	0.92[e]	[79]
9	**P8a/b**	-5.43[c]	-3.88[d]	-	800	0.84[e]	3.90[e]	53[e]	1.74[e]	[79]
10	**P9**	-5.23[c]	-3.6[c]	1.63	743	0.49[e]	2.98[e]	25[e]	0.4[e]	[81]
11	**P5b**	-5.14	-3.51	1.63	693	0.53[e]	0.13[e]	26[e]	0.02[e]	[81]
12	**P7**	-5.11	-3.66	1.45	806	0.56[e]	3.81[e]	41[e]	0.9[e]	[81]
13	**P1c**	-5.85	-3.88	1.97	775	0.89[e]	5.4[e]	63[e]	3.0[e]	[80]
14	**P10a**	-5.82	-3.83	1.99	826	0.70[e]	13.1[e]	69[e]	6.3[e]	[82]

[a] HOMO/LUMO energies estimated from the onset of oxidation/reduction in voltammetry experiments, Fc/Fc^+ used as an internal reference. The Fc/Fc^+ redox couple is estimated as -5.1 eV with respect to vacuum. [b] Optoelectronic characterization performed with **P8b**, OPVs fabricated with **P8a**. [c] The Fc/Fc^+ redox couple is estimated as -4.8 eV with respect to vacuum. [d] $E_{LUMO} = E_{HOMO} + E_{gap}$ (opt). [e] OPV results from best device, all others are average performance

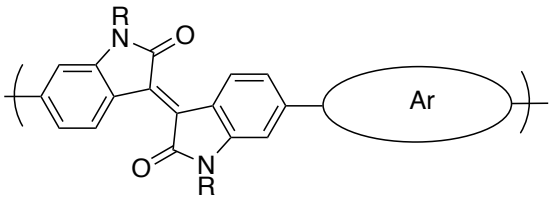

R_1 = 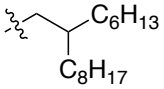 $R_2 = C_8H_{17}$

Ar =

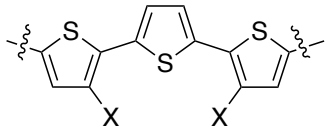

P10a X = C_8H_{17}
P10b X = C_6H_{13}
R = R_1

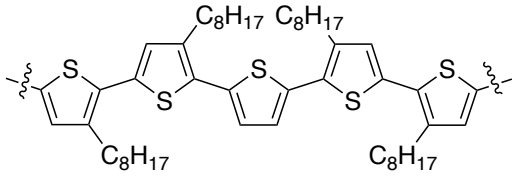

P11 R = R_1

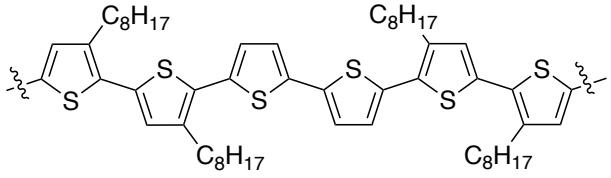

P12 R = R_1

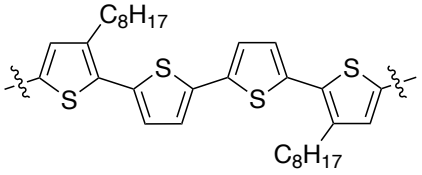

P13 R = R_1

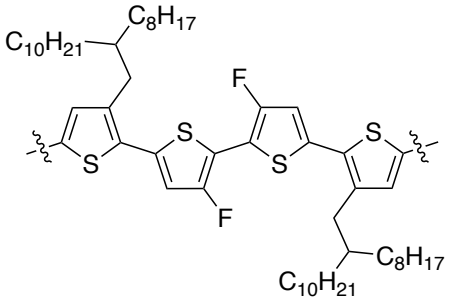

P14 R = R_2

Chart 1.12 Isoindigo-oligothiophene p-type donor-acceptor polymers **P10a**-**P14**.

Table 1.3 Optoelectronic properties and OPV performance of isoindigo-oligothiophene copolymers **P1c** and **P10A-P14**.

Entry	Polymer	HOMO[a] (eV)	LUMO[a] (eV)	$E_{g,opt}$ (nm)	μ_h ($cm^2 V^{-1}s^{-1}$)	μ_e ($cm^2 V^{-1}s^{-1}$)	V_{OC} (V)	J_{SC} (mA cm^{-2})	*FF* (%)	PCE (%)	Ref
1	**P1c**	-5.78	-3.95	800	1.0×10^{-3}	8.1×10^{-3}	0.91[b]	7.16[b]	66[b]	4.30[b]	83
2	**P10a**	-5.69	-3.97	827	3.0×10^{-2}	5.0×10^{-3}	0.72[b]	14.63[b]	66[b]	6.90[b]	83
3	**P11**	-5.64	-3.94	810	3.6×10^{-3}	5.3×10^{-4}	0.69[b]	11.28[b]	67[b]	5.36[b]	83
4	**P12**	-5.47	-3.94	816	7.4×10^{-3}	2.3×10^{-4}	0.65[b]	10.51[b]	66[b]	4.65[b]	83
5	**P10a**	-5.49	-3.90	780	$3.68^c \times 10^{-5}$	-	0.73	13.8	63.6	6.4	84
6	**P13**	-5.48	-3.90	785	$3.17^c \times 10^{-4}$	-	0.76	13.5	57.9	5.96	84
7	**P11**	-5.44	-3.86	785	$2.80^c \times 10^{-5}$	-	0.72	8.3	61.8	3.7	84
8	**P12**	-5.37	-3.80	790	$8.93^c \times 10^{-5}$	-	0.71	15.7	63.9	7.10	84
9	**P1**	-5.59	-3.90	765	4×10^{-2}	1×10^{-1}	0.90	5.8	55	2.9	85
10	**P10b**	-5.57	-3.93	785	5×10^{-2}	-	0.70	15.2	62	6.6	85
11	**P14**	-5.30[d]	-3.78[e]	816	$3.4^c \times 10^{-3}$	-	0.8	13.3	60.9	6.7	86

[a] HOMO/LUMO energies estimated from the onset of oxidation/reduction in voltammetry experiments, Fc/Fc^+ used as an internal reference. The Fc/Fc^+ redox couple is estimated as -5.1 eV with respect to vacuum. [b] OPV results from best device, all others are average performance. [c] Hole mobilities measured on polymer:acceptor active layers in hole-only devices with a space charge limited current model. [d] Reference value of Fc/Fc^+ redox couple unstated. [e] LUMO energy determined from $E_{LUMO} = E_{HOMO} + E_{g,opt}$.

Isoindigo-oligothiophene polymers with 1-6 thiophenes in the repeat unit (Chart 1.12) have since been studied and incorporated into OPVs; their optoelectronic properties, and photovoltaic performance are summarized in Table 1.3. In late 2013, and early 2014, a pair of parallel studies were performed by Ma *et al.* and Ho *et al.* which explored the effects of the number of thiophene rings in the donor unit of isoindigo-oligothiophene copolymers.[83,84] Ma *et al.* reported isoindigo-thiophene polymers with one (**P1c)**, three (**P10a**), five (**P11**), and six (**P12**) thiophenes in the donor unit (Table 1.3, entries 1-4). The LUMO levels of all four polymers were nearly identical, owing to the common isoindigo acceptor unit; however, the group discovered that the driving force for exciton dissociation increased with increasing number of thiophene units, in spite of the nearly constant LUMO energy. The hole mobilites of the polymers were also found to improve slightly with increasing numbers of thiophene units. Despite this, they found that the OPV efficiency peaked for devices fabricated with **P10a**:$PC_{71}BM$ active layers at 6.90%, and decreased in the longer pentathiophene (**P11**) and sexithiophene (**P12**) polymers. To assess the morphology of the active layer blends, the group performed transmission electron microscopy (TEM) and grazing incidence wide angle x-ray scattering (GIWAXS). They showed that **P11** and **P12** containing polymers formed active layer blends with domain sizes too large for efficient exciton migration to the p/n interface. These large domain sizes lowered the J_{SC} and *FF* of the **P11** and **P12**-based devices.

In a similar report, Ho *et al.* studied the photovoltaic performance of isoindigo-oligothiophene polymers with three (**P10a**), four (**P13**) (Chart 1.12), five (**P11**), and six (**P12**) thiophenes in the donor unit (Table 1.3, entries 5-8).[84] This group also found that OPVs incorporating **P10a** in the active layer performed better than the quarterthiophene (**P13**) and pentathiophene (**P11**)-based OPVs, owing chiefly to a larger J_{SC}. However, unlike the previous

report of **P12**:$PC_{71}BM$ cells, the group found that they could achieve an optimal active layer morphology using chlorobenzene as the solvent with the blend additive chloronaphthalene, rather than the dichlorobenzene and DIO used by Ma *et al.* By switching solvents and blend additives, Ho *et al.* achieved a maximum PCE of 7.25% in their **P12**:$PC_{71}BM$ OPVs due to a much higher J_{SC} than was reported by Ma *et al*.

While these studies described trends in photovoltaic performance amongst isoindigo-oligothiophene copolymers, uncertainty still existed surrounding why isoindigo-terthiophene copolymers (**P10**) performed much better than isoindigo-thiophene copolymers (**P1c**) in OPVs. Both materials are energetically and structurally very similar, yet **P10a**-based solar cells exhibited PCEs three times higher than those of **P1c**; three publications in 2016 by Reynolds and coworkers explored these differences in OPV performance.

First, Stalder *et al.* explored charge carrier mobilites and solid state packing in a series of isoindigo-thiophene copolymers.[87] The report's key findings centered around using 2D nuclear magnetic resonance (NMR) spectroscopy experiments investigating packing motifs in **P1c** and **P10b** (Chart 1.10) to explain the differences in charger carrier mobility between the two polymers. The higher electron mobility of **P1c** was determined to be due to co-facial stacking of isoindigo units between polymer chains, while in **P10b** isoindigo was arranged slip-stack with the terthiophene units of adjacent polymers chains. This result helped to determine the reason for the difference in n-type mobility between the two polymers, but left the reason for their dramatically different OPV performance unclear.

Following this work, Lai *et al.* studied blends of **P1c** or **P10b** with $PC_{71}BM$ using transient photoluminescence, as well as sub-band gap external quantum efficiency (EQE), and geometric capacitance measurements. By transient photoluminescence experiments, they showed that

P10b:$PC_{71}BM$ blends exhibited much faster excited state decay than **P1c**:$PC_{71}BM$ blends, 143 ± 1 ps for **P10b** *vs.* 987 ± 2 ps for **P1c**. The faster excited state decay is evidence of faster electron transfer from the **P10b** excited state to $PC_{71}BM$. The photoluminescence results were supported by geometric capacitance measurements showing that the dielectric constant of the **P10b**:$PC_{71}BM$ blends (4.76 ± 0.18) was higher than that of the **P1c**:$PC_{71}BM$ blend (4.22 ± 0.11). The larger dielectric constant of the **P10b**:$PC_{71}BM$ blends is indicative of a stronger electronic coupling between $PC_{71}BM$ and **P10b** than with **P1**. The strong electronic coupling between **P10b** and $PC_{71}BM$ enhances exciton dissociation and helps explain the difference in J_{SC} values between **P1c** and **P10b**-based OPVs.

In the final paper of the series, Grand *et al.* brought these conclusions together into a comprehensive study of structure-property relationships in poly(isoindigo-oligothiophene):$PC_{71}BM$ bulk heterojunction OPVs (Table 1.3, entries 9 and 10).[85] This work reviewed previously published isoindigo-oligothiophene copolymers and proceeded to study the effects of DIO on active layer morphology in **P1c** and **P10b**:$PC_{71}BM$ OPVs, as well as exploring the fate of DIO after deposition of the active layer film. Using x-ray photoelectron spectroscopy, the group determined that the DIO evaporates when the devices are placed under high vacuum for deposition of the top electrode. In addition to the comprehensive study of blend additives, both normal and inverted architecture OPVs were optimized and no significant difference in performance was found; normal architecture devices achieved average PCEs of 2.9% and 6.6% for **P1c** and **P10b**-based active layers respectively, while the average PCE in inverted devices was 2.4% and 6.5% (**P1c** and **P10b** respectively).

Finally, in an attempt to optimize p-type and n-type semiconductor interactions, Hu *et al.* explored the idea of reducing the steric crowding around isoindigo by moving most of the

solubilizing steric bulk to the donor unit of their isoindigo-quarterthiophene polymers.[86] The polymers featured short, linear, octyl chains on the isoindigo unit, and large bulk 2-octyldodecyl groups on the quatrithiophene unit. In addition to this, **P14** incorporates two fluorines in the central bithiophene to promote planarity in the thiophene backbone (Chart 1.12). By increasing backbone planarity and improving isoindigo-fullerene interaction the group could increase the PCE of OPVs incorporating **P14**:$PC_{71}BM$ active layers to 6.7% (Table 1.3, entry 11), a significant improvement over other isoindigo-quarterthiophene polymers.

1.5.3 n-Type isoindigo-based polymer organic semiconductors

While most of the isoindigo-based polymers reported to date have been p-type semiconductors, a significant number of n-type isoindigo based polymer semiconductors have been reported. Soon after the first reports of isoindigo semiconductors, Stalder *et al.* published poly(isoindigo) (**P15**), as well as a copolymer of isoindigo and benzothiadiazole (**P16**) (Chart 1.13).[88] The $E_{g,opt}$ of the polymers were both above 700 nm, and the low LUMO levels (-3.84 eV for **P15** and -3.90 eV for **P16**) made them suitable for use as n-type semiconductors in OPV active layers with P3HT. However, their performance in OPVs was modest; a maximum PCE of 0.47% was achieved with P3HT:**P15**-based OPVs. Low *FF* and J_{SC}, likely resulting from poor blend morphology, were responsible for the poor performance.

After this, Grenier *et al.* produced a series of n-type isoindigo copolymers (Chart 1.13, **P17-P19**); while they were not used in OPVs, their optoelectronic properties and charge carrier mobilities in organic field effect transistors (OFETs) are summarized in Table 1.4.[89] The copolymer of isoindigo and dithienyl diketopyrrolopyrrole (**P17**) had a low band gap of just 1.35 eV. The best electron mobility was observed in OFETs fabricated with a copolymer of isoindigo

and 5,5′-dioctyl-1,1′-4H-bithieno[3,4-c]pyrrole-4,4′,6,6′(5H,5′H)-tetrone (BTD) (**P19**). The higher electron mobility in **P19** was credited to its centrosymmetric nature improving the molecular packing to aid in charge transport.[89]

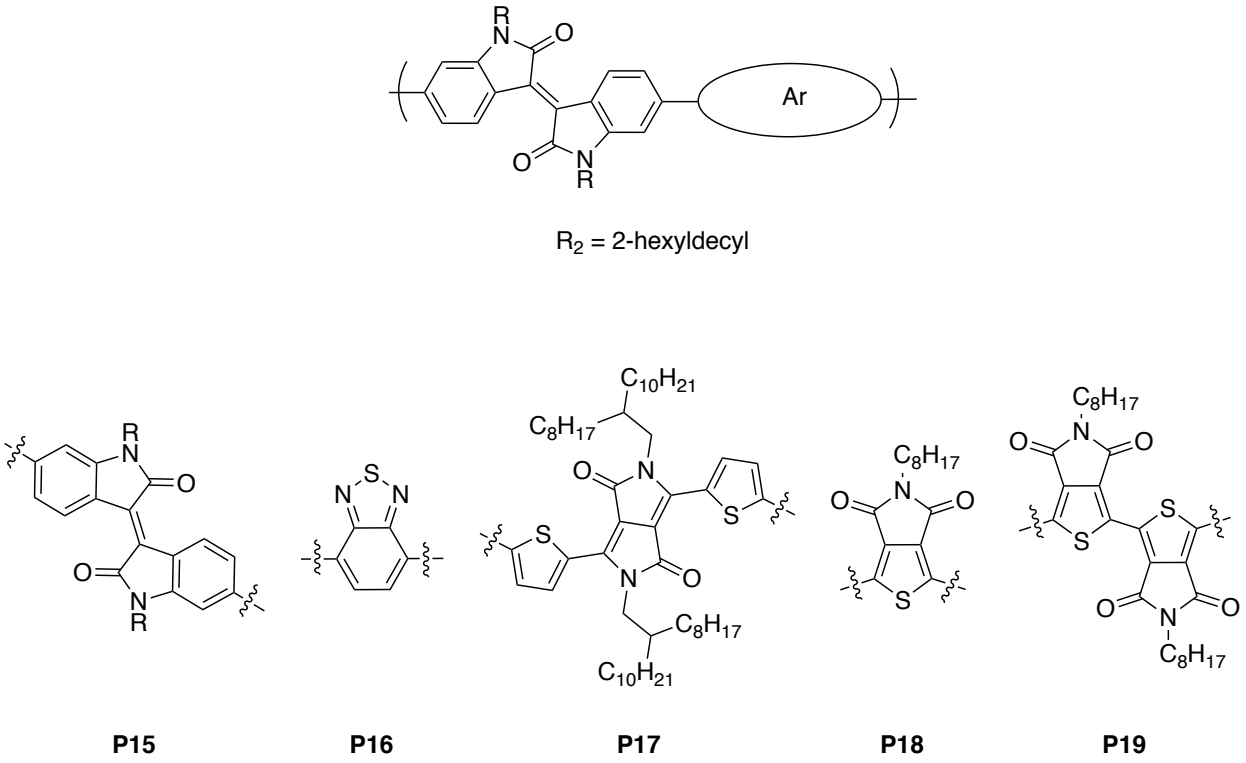

Chart 1.13 n-Type isoindigo-based donor-acceptor copolymers **P15**-**P19**.

Table 1.4 Optoelectronic properties and OPV performance of n-type isoindigo-based polymers **P15-P19**.

Polymer	HOMO[a] (eV)	LUMO[a] (eV)	$E_{g,opt}$ (nm)	μ_e ($cm^2 V^{-1}s^{-1}$)	V_{OC} (V)	J_{SC} ($mA\ cm^{-2}$)	*FF* (%)	PCE (%)	Ref
P15	-5.54[b]	-3.84	729	3.7×10^{-7}	0.62[c]	1.91[c]	41[c]	0.47[c]	[88]
P16	-5.67[b]	-3.90	700	-	-	-	-	-	[88]
P17	-5.3	-4.0	918	2.7×10^{-4}	-	-	-	-	[89]
P18	-6.0	-4.2	721	3.0×10^{-4}	-	-	-	-	[89]
P19	-6.1	-4.2	708	3.5×10^{-3}	-	-	-	-	[89]

[a] HOMO/LUMO energies estimated from the onset of oxidation/reduction in voltammetry experiments, Fc/Fc^+ used as an internal reference. The Fc/Fc^+ redox couple is estimated as -5.1 eV with respect to vacuum. [b] E_{HOMO} energy determined from $E_{HOMO} = E_{LUMO} + E_{gap}$ (opt). [d] OPV results from best device.

1.5.4 Modified isoindigo structures in organic semiconductors

The works summarized so far use 6-bromoisoindigo or 6,6′-dibromoisoindigo to build donor-acceptor semiconductors, and the majority of isoindigo-based organic semiconductors use one of these two building blocks, chiefly due to their ease of synthesis. However, as the popularity of isoindigo has grown, reports of modified isoindigo structures have increased in number, and modified isoindigos as acceptor units in donor-acceptor organic semiconductors have become common. These modified isoindigos fall into three main categories: heteroatom substituted isoindigos, thienoisoindigos, and extended isoindigos. The optoelectronic properties and OPV performance of a number semiconductors based on modified isoindigo structures are summarized in Table 1.5.

Heteroatom substituted isoindigos have one or more electronegative heteroatoms incorporated into the isoindigo structure; common examples are haloisoindigos and azaisoindigo. In haloisoindigos one or more hydrogens are replaced by a halogen (typically Cl or F); in azaisoindigo, one or more of the carbon atoms are replaced with nitrogen. Lei *et al.* first reported the synthesis, and use, of 7,7′-difluoroisoindigo in 2012.[90] Difluoroisoindigo was incorporated into a donor-acceptor copolymer with bithiophene (**P20**, Chart 1.14), and its performance in OFETs was compared with the analogous non-fluorinated polymer **P21** (Table 1.5). It was found that the fluorinated polymer exhibited improved charge carrier mobilities over the non-fluorinated polymer. In particular, **P20** had an electron mobility an order of magnitude higher than the non-fluorinated analogue. AFM and GIWAXS studies showed that **P20** packed in a more crystalline manner in the solid state, with different intermolecular interactions than **P21**, facilitating the higher charge carrier mobilities.

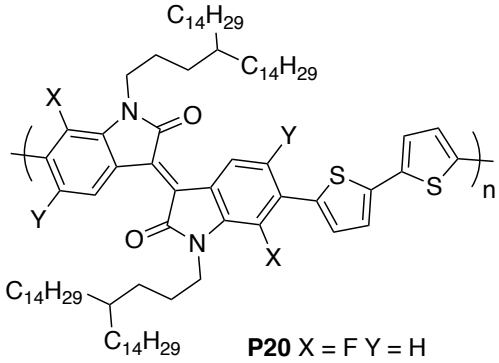

P20 X = F Y = H
P21 X = H Y = H
P22 X = H Y = Cl

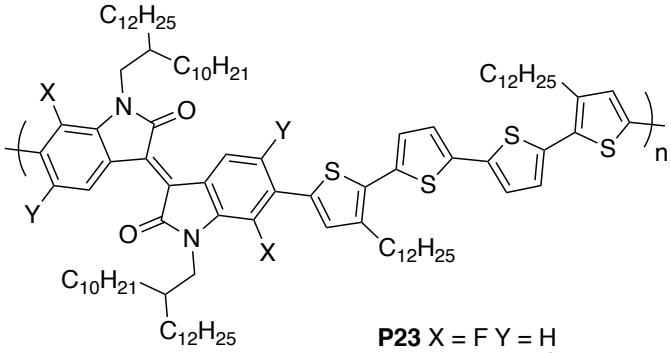

P23 X = F Y = H
P24 X = H Y = Cl
P25 X = H Y = H

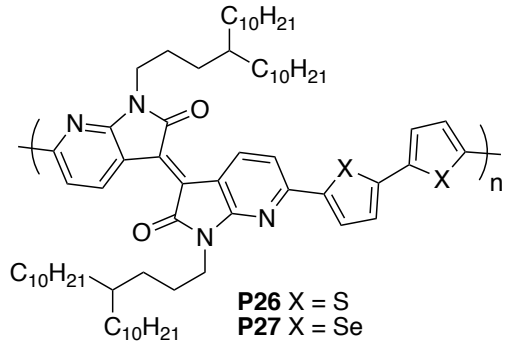

P26 X = S
P27 X = Se

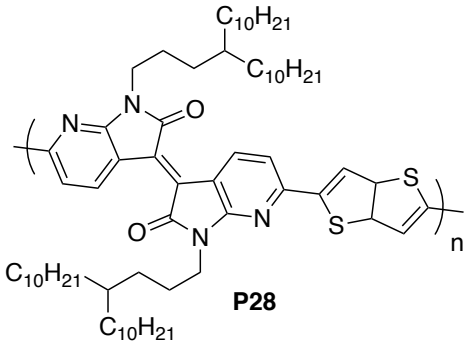

P28

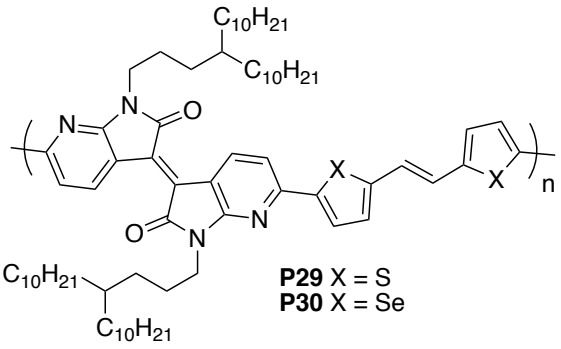

P29 X = S
P30 X = Se

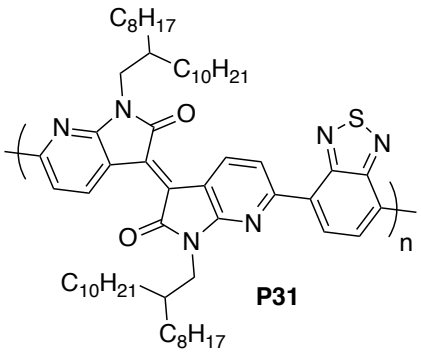

P31

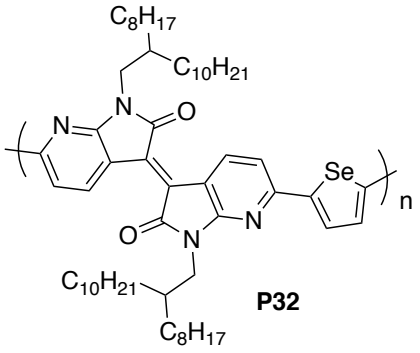

P32

Chart 1.14 Modified isoindigo-based semiconductors featuring heteroatom substitution **P20**-**P32**.

Following their work on 7,7′-difluoroisoindigo, Lei *et al.* synthesized a 5,5′-dichloroisoindigo-bithiophene polymer **P22** (Chart 1.14) by direct chlorination of the 6,6′-dibromoisoindigo monomer, and subsequent copolymerization with bithiophene.[91] Chlorination of isoindigo was found to have effects similar to fluorination on the optoelectronic properties of isoindigo-based polymers (Table 1.5). However, while the resulting polymer exhibited ambipolar charge carrier mobility higher than the non-halogenated derivative, the hole mobility was diminished compared to the fluorinated **P21**.

After their initial reports of both haloisoindigo derivatives, Zheng *et al.* performed an in-depth study of the effects of halogenation on the solid state packing of isoindigo-quarterthiophene polymers **P23-P25**.[92] They found that fluorine substitution increased backbone planarity, leading to higher charge carrier mobility in OFETs; the same planarization reduced efficiency in OPVs because it increased domain sizes in the active layer. Conversely, the large chlorine atoms disrupted backbone planarity, reducing charge carrier mobility, but improving OPV performance by decreasing domain size in the active layer blend.

In addition to halogen substitution, electronegative nitrogen atoms have been incorporated into several isoindigo-based semiconductors by the Kelly research group and several others. In late 2013, the Kelly group reported the use of 7-azaisoindigo in molecular donor-acceptor semiconductors; this research will be discussed in-depth in Chapters 2 and 3.[64,93] Following this, de Miguel *et al.* reported the synthesis and characterization of 7,7′-diazaisoindigo, and two separate research groups incorporated 7,7′-diazaisoindigo into donor-acceptor polymers for ambipolar OFETs.[94-97] Huang *et al.* reported a copolymer of diazaisoindigo and bithiophene, **P26**, (Chart 1.14) which exhibited high and balanced hole and electron mobilities (Table 1.5).[95] Following this, the group went on to synthesize a series of diazaisoindigo copolymers with

biselenophene (**P27**), thienothiophene (**P28**), dithienylethene (**P29**), and diselenophenylethene (**P30**) donor units (Chart 1.13).[96] The optoelectronic properties and OFET performance of these polymers are summarized in Table 1.5 (entries 5-8). Yue *et al.* also synthesized diazaisoindigo copolymers with benzothiadiazole (**P31)** and selenophene (**P32)** (Chart 1.14).[97] These polymers were also incorporated into ambipolar and n-type field effect transistors (Table 1.5) with high charge carrier mobilities. The promising OFET performance of these azaisoindigo-based polymers was caused by the increase in planarity induced by substituting the single N atom for the relatively bulkier CH group. However, the increased planarity also likely induces aggregation in active layer blends, possibly explaining why these materials have not been successful in OPV applications despite promising OFET performance.

The second class of modified isoindigo is thienoisoindigo; in this structure, the two benzene rings of isoindigo have been replaced with thiophenes fused across the 2 and 3 positions to the isoindigo lactams. Thienoisoindigo was first reported as an acceptor unit in 2012 by Ashraf *et al.* with the synthesis and characterization of a thienoisoindigo-benzothiadiazole copolymer **P33** (Chart 1.15).[98] The resulting polymer had a very small optical band gap of 0.92 eV (Table 1.5, entry 11), absorbing light well into the near-infrared. **P33** was incorporated into OFETs and exhibited balanced ambipolar charge carrier mobilities, with both μ_h and μ_e values of approximately 0.1 $cm^2V^{-1}s^{-1}$. The high charge carrier mobility is due to the increased planarity of thienoisoindigo. In isoindigo there is steric repulsion between the hydrogen at position 4 and the lactam oxygen; in thienoisoindigo this steric repulsion is replaced with a favorable intramolecular interaction between the sulfur of the thiophene and the carbonyl oxygen of the lactam. Since this first report of thienoisoindigo, many donor-acceptor semiconductors have been synthesized incorporating it as the acceptor unit.[99-102] Unlike isoindigo containing semiconductors,

thienoisoindigo-based polymers have found their primary use as high performance materials for OFETs. Of note is the copolymer of thienoisoindigo and naphthalene (**P34)** reported by Kim *et al.* (Chart 1.15); when this polymer was used as the p-channel material in a top-gate bottom-contact OFET a very high μ_h of 14.4 $cm^2 V^{-1}s^{-1}$ was achieved (Table 1.5).[103] This exceptional hole mobility was largely due to the highly planar nature of the polymer repeat unit.

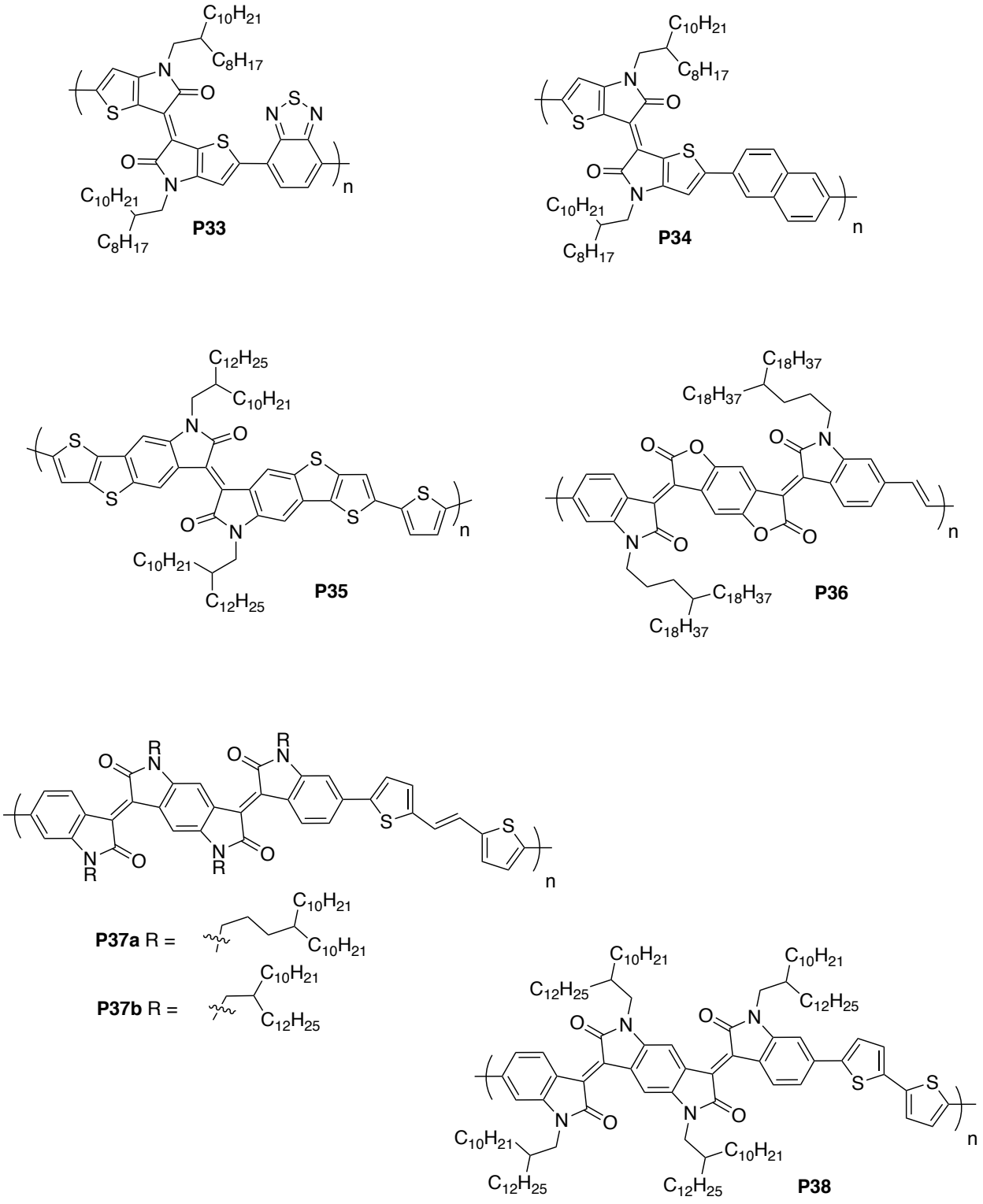

Chart 1.15 Thienoisoindigo-containing and expanded isoindigo-based semiconductors **P33**-**P38**.

The final category of modified isoindigo structures are expanded isoindigo units. These structures take one of two forms; either they have additional aromatic rings fused to the phenyl ring of isoindigo, or have additional conjugated units inserted into the exocyclic double bond of isoindigo using crossed aldol reactions. In an example of fusing additional aromatic rings to the phenyl rings of isoindigo, Yue *et al.* produced a thieno[2,3-b]benzothiophene-fused isoindigo monomer which was copolymerized with thiophene to produce polymer **P35** (Chart 1.15).[104] The low $E_{g,opt}$ (771 nm, or 1.6 eV) of this polymer, combined with its high μ_h (0.31 $cm^2\ V^{-1}\ s^{-1}$), and high LUMO level (-3.5 eV) made it an ideal p-type semiconductor for OPV applications. OPVs fabricated with **P35**:$PC_{71}BM$ active layers exhibited a maximum PCE of 9.1% (Table 1.5); this high PCE was primarily due to very large J_{SC} of 17.7 mA cm^{-2}. This device represents the most efficient OPV fabricated with isoindigo-based materials to date, and is remarkable because it performs very well without thermal annealing or solvent additives.

The other type of expanded isoindigo structure features conjugated units added between the lactam rings of isoindigo, typically synthesized by using double crossed aldol reactions. The most popular structure with this motif is benzodifuran-based oligo-*p*-phenylenevinylene (BDOPV), in which a benzodifurandione group is added between the two lactam rings of isoindigo. It was first reported by Lei *et al.* in 2013, in which they synthesized the BDOPV unit and polymerized it with bis(tributylstannyl)ethylene to yield the polymer **P36** (Chart 1.15).[105] They compared the structure to PPV, in which two of the three vinyl groups in the polymer repeat unit are forced into a planar geometry by the furan and pyrrole rings of the benzofuran and isatin groups. The electron-withdrawing nature of the lactam and lactone moieties also helped increase the electron mobility of the resulting polymer to 1.1 $cm^2\ V^{-1}\ s^{-1}$ (Table 1.5, entry 14). Several other

copolymers based on BDOPV have been developed, and exhibit similar optoelectronic properties and OFET performance.[106-109]

Recently, two research groups reported the tetra-lactam derivative of BDOPV; this resembles two isoindigos which share one of their benzene rings.[110,111] The central benzene ring of this unit is fused to two lactam rings *para*- to one another. Both groups synthesized copolymers of their expanded isoindigo with dithienylethene to yield **P37** (Chart 1.15), with He *et al.* also producing a bithiophene-containing polymer, **P38** (Chart 1.15). The optoelectronic properties, and charge carrier mobilities of both polymers are summarized in Table 1.5. The absorption spectra of these polymers extend to almost 1000 nm, making them very effective light absorbers. Both groups incorporated their expanded isoindigo-based polymers into the active layers of OFETs; He *et al.* found **P38** to have ambipolar charge carrier characteristics, while Cao *et al.* determined that **P37a** had a very high hole mobility of 1.92 $cm^2\ V^{-1}\ s^{-1}$. The difference in hole mobilites found by both groups for **P37** can be attributed to the different alkyl groups used in their expanded isoindigo units. By using an alkyl unit branched at the 4-position (**P37a**), Cao *et al.* observed an order of magnitude higher μ_h than He *et al.*, who chose a 2-position branched 2-decyltetradecyl alkyl unit (**P37b**).

Finally, in 2016 two groups independently reported the synthesis and use of a ring-fused isoindigo dimer synthesized using a double crossed aldol reaction. Work on this expanded isoindigo derivative is described in Chapters 4 and 5 of this thesis.[112,113] Immediately following this work, Jiang *et al.* used a different synthetic route to make their expanded isoindigo unit, and incorporated it into donor-acceptor polymers with thiophene (**P39**), bithiophene (**P40**), and dithienylethene (**P41**) (Chart 1.16). The polymers had low frontier orbital energy levels and small optical band gaps; **P41** exhibited the highest ambipolar charge carrier mobilities of the three

polymers (Table 1.5) due to its highly planar dithienylethene donor unit. Modified isoindigos of all three varieties offer a fantastic opportunity to study structure-property relationships in organic semiconductors, and help develop guidelines to synthesize materials in the future.

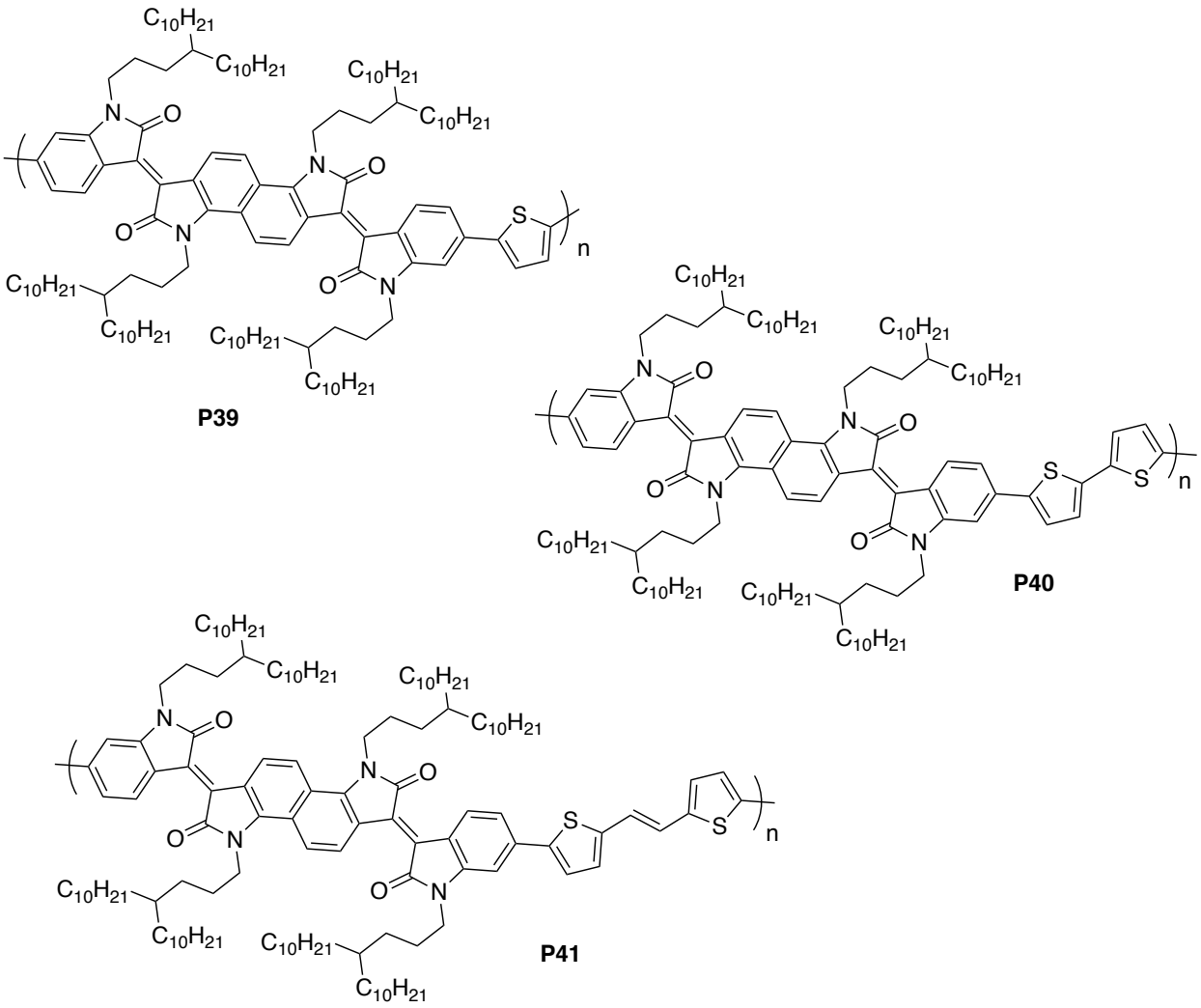

Chart 1.16 Expanded isoindigo-based semiconductors featuring fused isoindigo units **P39-P41**.

Table 1.5 Optoelectronic properties and OPV performance of modified isoindigo-based semiconductors **P20-P41**.

Polymer	HOMO[a] (eV)	LUMO[a] (eV)	$E_{g,opt}$ (nm)	μ_h ($cm^2 V^{-1}s^{-1}$)	μ_e ($cm^2 V^{-1}s^{-1}$)	V_{OC}[b] (V)	J_{SC}[b] ($mA\ cm^{-2}$)	FF[b] (%)	PCE[b] (%)	Ref
P20	-5.60	-3.88	827	1.41	0.38					90
P21	-5.42	-3.70	790	1.44	0.004					90
P22	-5.63	-3.86	810	0.51	0.42					90
P23	-5.51	-3.92	855	0.69	-	0.63	4.26	44	1.19	92
P24	-5.53	-3.85	827	0.08	-	0.75	10.00	61	4.60	92
P25	-5.63	-3.63	751	-	-	0.76	7.95	57	3.42	92
P26	-5.67[c]	-3.64[c]	827	1.89	0.48	-	-	-	-	95
P27	-5.58[c]	-3.66[c]	838	2.38	0.32	-	-	-	-	96
P28	-5.68[c]	-3.70[c]	810	0.78	1.12	-	-	-	-	96
P29	-5.56[c]	-3.60[c]	800	1.59	0.02	-	-	-	-	96
P30	-5.54[c]	-3.65[c]	810	0.73	0.14	-	-	-	-	96
P31	-5.8[d]	-4.1[e]	729	-	1.0[g]	-	-	-	-	97
P32	-5.6[d]	-4.0[e]	775	0.2[g]	0.5[g]	-	-	-	-	97
P33	-4.86[f]	-3.73[f]	1348	0.1	0.14	-	-	-	-	98
P34	-5.12	-3.49	912	12.0	0.092	-	-	-	-	103
P35	-5.1[d]	-3.5[e]	775	0.31[g]	-	0.72	17.7	71	9.1	104
P36	-6.21	-4.24	873	-	0.84	-	-	-	-	105
P37a	-5.32[d]	-4.05[e]	976	1.92[g]	-	-	-	-	-	114
P37b	-5.71	-3.70	1016	0.10[g]	0.075[g]	-	-	-	-	111
P38	-5.60	-3.71	1008	0.19[g]	0.088[g]	-	-	-	-	111
P39	-5.16	-3.66	961	3.0×10^{-3}	3.7×10^{-3}	-	-	-	-	115
P40	-5.16	-3.58	946	1.29	0.14	-	-	-	-	115
P41	-5.24	-3.58	961	1.47	0.11	-	-	-	-	115

[a] HOMO/LUMO energies estimated from the onset of oxidation/reduction in voltammetry experiments, Fc/Fc^+ used as an internal reference. The Fc/Fc^+ redox couple is estimated as -4.8 eV with respect to vacuum. [b] OPV results from best device. [c] HOMO/LUMO energies calculated using $E_{MO} = (E_{onset} - 4.40\ eV)$.[95,96] [d] E_{HOMO} = IP measured using photoelectron spectroscopy. [e] E_{LUMO} values are electron affinities calculated using EA = IP + $E_{g,opt}$. [f] Maximum charge carrier mobility achieved, all others are average. [g] energy of Fc/Fc^+ redox couple vs vacuum unstated.

1.6 Research objectives

The goal of this thesis is to explore how differences in the structure of isoindigo-based organic semiconductors affect the optoelectronic properties of the resulting materials, typically by incorporating them into organic electronic devices such as OPVs and OFETs. As seen in Section 1.5.4, semiconductors based on modified isoindigos can exhibit very different optoelectronic properties than those based on isoindigo. Over the course of four major projects this thesis describes the synthesis of three modified isoindigo structures, their incorporation into organic semiconductors, and the characterization of their optoelectronic properties and device performance.

In Chapters 2 and 3, a nitrogen-containing derivative of isoindigo, 7-azaisoindigo, will be discussed. In this work, four isoindigo-based molecular semiconductors were synthesized; two of these contained 7-azaisoindigo, while the two controls contained isoindigo. The goal of this project was to study the effects of the electronegative nitrogen on the frontier molecular orbital energies of the resulting semiconductors; it was theorized that by adding electronegative heteroatoms to the acceptor unit of the donor-acceptor semiconductors would lower their LUMO energy leading to a lower optical band gap. The incorporation of 7-azaisoindigo was found to have a small effect on the frontier orbital energies of the semiconductors. However, the presence of the nitrogen heteroatom caused a large decrease in OPV efficiency.

While the incorporation of nitrogen did not have a large effect on the semiconductors' optoelectronic properties, it does offer a lone pair which can act as a Lewis base. In Chapter 3, the coordination of this lone pair to the Lewis acids, H^+ and BF_3, is studied; it was hypothesized that the coordination of a Lewis acid would increase the electron withdrawing strength of the azaisoindigo unit, leading to materials with a very low optical band gap. It was discovered that the

coordination of a Lewis acid caused a large red-shift in the HOMO→LUMO transition of the azaisoindigo-based semiconductors. The identity of the Lewis adduct formed was studied using UV/vis spectroscopy, time dependent density functional theory (TDDFT) calculations, and ^{1}H NMR spectroscopy. After the Lewis adduct had been identified, it was determined that the coordination could take place at the solid-vapor interface, allowing for doping of thin-films of the azaisoindigo semiconductors using BF_3 vapor.

Chapter 4 introduces a second modified isoindigo structure, bisisoindigo, a dimer fused at the 6 and 7 positions of isoindigo. By extending the π-conjugation of the acceptor unit across two coplanar isoindigo groups, it was theorized that the LUMO energy of the resulting semiconductors would be lower and that their light absorption would extend into the near-infrared. This highly planar expanded isoindigo structure was synthesized via a crossed aldol condensation between a fused isatin dimer and two equivalents of 6-bromo-2-oxindole. Bisisoindigo, as well as a donor-acceptor molecular semiconductor incorporating bisisoindigo and two bithiophene units, were synthesized, characterized, and incorporated into OPVs. Bisisoindigo had a much lower band gap than isoindigo due to its extended conjugation. The donor-acceptor-donor molecule exhibited an even lower band gap, and much higher extinction coefficient, consistent with the partial charge-transfer character of the HOMO→ LUMO transition in donor-acceptor materials. While the optical band gaps and extinction coefficients of the semiconductors were very good, their performance when incorporated into an OPV active layer blend with $PC_{71}BM$ was poor. This low OPV efficiency was attributed to poor blend morphology, as it was discovered by AFM that both semiconductors tended to over-crystallize in the solid state and form domains much larger than desired.

In Chapter 5 another isoindigo dimer is introduced, diisoindigo; this structure consists of two isoindigo units joined by a single bond at their 6 positions. Using diisoindigo and bisisoindigo, the effect of acceptor unit number and size on the optoelectronic properties of donor-acceptor-acceptor polymers was studied. A series of six polymers was synthesized and characterized, combining the acceptor units isoindigo, bisisoindigo, and diisoindigo with the donor units thiophene and terthiophene. It was found that diisoindigo containing polymers had lower frontier orbital energies than their isoindigo analogues, as well as lower hole mobilities, and higher electron mobilities. Polymers incorporating bisisoindigo had the lowest frontier orbital energies, as well as much smaller optical band gaps than the isoindigo and diisoindigo-based polymers, consistent with their increased conjugation length. When incorporated into OPVs, the isoindigo-based polymers performed better than the diisoindigo analogues, while the bisisoindigo-based polymers performed the worst. The lower LUMO energy of the diisoindigo and bisisoindigo polymers reduced the energetic driving force for exciton dissociation at the polymer:$PC_{71}BM$ interface, leading to poor J_{SC} and PCE values.

Finally, in Chapter 6, the results of all four projects will be compared and discussed. By comparing all three modified isoindigo structures, broader conclusions can be made about the effects different structural variations have on the performance of organic semiconductors. While these studies were performed on derivatives of isoindigo, some general conclusions can be drawn about the effects of the synthetic designs employed, such as extended conjugation or added electronegative heteroatoms, on the optoelectronic properties of organic semiconductors as a whole. In addition, future directions for these projects, such as new synthetic designs and further use of the expanded isoindigos reported in this thesis, will be discussed.

1.7 References

(1) *IPCC, 2013: Climate Change 2013: The Physical Science Basis. Contribution of Working Group I to the Fifth Assessment Report of the Intergovern- mental Panel on Climate Change.* Stocker, T.F., D. Qin, G.-K. Plattner, M. Tignor, S.K. Allen, J. Boschung, A. Nauels, Y. Xia, V. Bex and P.M. Midgley Eds.; Cambridge University Press: Cambridge, United Kingdom and New York, NY, USA, **2013**, pp. 1535.

(2) Chu, S.; Cui, Y.; Liu, N. The Path Towards Sustainable Energy. *Nat. Mater.* **2017**, *16*, 16–22.

(3) Nelson, J. *The Physics of Solar Cells*; Imperial College Press: London, **2003**.

(4) Kurtz, S.; Haegel, N.; Sinton, R.; Margolis, R. The Future of Photonics. *Nat. Photonics* **2017**, *11*, 3–5.

(5) Li, G.; Zhu, R.; Yang, Y. Polymer Solar Cells. *Nat. Photonics* **2012**, *6*, 153–161.

(6) New BMBF Research Project Started: Transparent Organic Photovoltaic Glass Façade. http://www.heliatek.com/en/press/press-releases/details/new-bmbf-research-project-started-transparent-organic-photovoltaic-glass-façade (accessed 11/09/2017).

(7) Mishra, A.; Bäuerle, P. Small Molecule Organic Semiconductors on the Move: Promises for Future Solar Energy Technology. *Angew. Chem. Int. Ed.* **2012**, *51*, 2020–2067.

(8) Herwig, P. T.; Müllen, K. A Soluble Pentacene Precursor: Synthesis, Solid-State Conversion Into Pentacene and Application in a Field-Effect Transistor. *Adv. Mater.* **1999**, *11*, 480–483.

(9) Nelson, S. F.; Lin, Y. Y.; Gundlach, D. J.; Jackson, T. N. Temperature-Independent Transport in High-Mobility Pentacene Transistors. *Appl. Phys. Lett.* **1998**, *72*, 1854–1856.

(10) *Functional Organic Materials*; Müller, T. J. J., Bunz, U. H. F., Eds.; Wiley-VCH; Weinheim, **2007**.

(11) Grand, C. Controlling Electronic Properties and Morphology of Isoindigo-Based Polymers for Photovoltaic Applications. PhD Thesis; Georgia Institute of Technology, **2015,** 1-72.

(12) Savoie, B. M.; Jackson, N. E.; Marks, T. J.; Ratner, M. A. Reassessing the Use of One-Electron Energetics in the Design and Characterization of Organic Photovoltaics. *Phys. Chem. Chem. Phys.* **2013**, *15*, 4538-4547.

(13) Shirakawa, H.; Louis, E. J.; MacDiarmid, A. G.; Chiang, C. K.; Heeger, A. J. Synthesis of Electrically Conducting Organic Polymers: Halogen Derivatives of Polyacetylene, $(CH)_x$. *J. Chem. Soc., Chem. Commun.* **1977**, *16*, 578-580.

(14) Swager, T. M. 50th Anniversary Perspective: Conducting/Semiconducting Conjugated Polymers. a Personal Perspective on the Past and the Future. *Macromolecules* **2017**, *50*, 4867-4886.

(15) Heeger, A. J. Semiconducting Polymers: the Third Generation. *Chem. Soc. Rev.* **2010**, *39*, 2354–2371.

(16) Chen, J.; Cao, Y. Development of Novel Conjugated Donor Polymers for High-Efficiency Bulk-Heterojunction Photovoltaic Devices. *Acc. Chem. Res.* **2009**, *42*, 1709–1718.

(17) *Design and Synthesis of Conjugated Polymers*; Leclerc, M., Morin, J. F., Eds.; Wiley-VCH: Weinheim, **2010**.

(18) Burroughes, J. H.; Bradley, D.; Brown, A. R.; Marks, R. N. Light-Emitting Diodes Based on Conjugated Polymers. *Nature* **1990,** *347,* 539-541.

(19) Greenham, N. C.; Moratti, S. C.; Bradley, D.; Friend, R. H. Efficient Light-Emitting Diodes Based on Polymers with High Electron Affinities. *Nature* **1993**, *365,* 628-630.

(20) Sariciftci, N. S.; Smilowitz, L.; Heeger, A. J.; Wudl, F. Photoinduced Electron Transfer From a Conducting Polymer to Buckminsterfullerene. *Science* **1992**, *258*, 1474–1476.

(21) Sariciftci, N. S.; Braun, D.; Zhang, C.; Srdanov, V. I.; Heeger, A. J.; Stucky, G.; Wudl, F. Semiconducting Polymer-Buckminsterfullerene Heterojunctions: Diodes, Photodiodes, and Photovoltaic Cells. *Appl. Phys. Lett.* **1993**, *62*, 585–587.

(22) Brabec, C. J.; Gowrisanker, S.; Halls, J. J. M.; Laird, D.; Jia, S.; Williams, S. P. Polymer-Fullerene Bulk-Heterojunction Solar Cells. *Adv. Mater.* **2010**, *22*, 3839–3856.

(23) Melzer, C.; Koop, E. J.; Mihailetchi, V. D.; Blom, P. W. M. Hole Transport in Poly(Phenylene Vinylene)/Methanofullerene Bulk-Heterojunction Solar Cells. *Adv. Funct. Mater.* **2004**, *14*, 865–870.

(24) Roncali, J. Conjugated Poly(Thiophenes): Synthesis, Functionalization, and Applications. *Chem. Rev.* **1992**, *92*, 711–738.

(25) McCullough, R. D.; Lowe, R. D.; Jayaraman, M. Design, Synthesis, and Control of Conducting Polymer Architectures: Structurally Homogeneous Poly(3-Alkylthiophenes). *J. Org. Chem.* **1993**, *58*, 904–912.

(26) Padinger, F.; Rittberger, R. S. Effects of Postproduction Treatment on Plastic Solar Cells. *Adv. Funct. Mater.* **2003**, *13*, 85–88.

(27) Kasap, S. O. *Principles of Electronic Materials and Devices*, 3rd ed.; New York, 2006.

(28) Servaites, J. D.; Ratner, M. A.; Marks, T. J. Organic Solar Cells: a New Look at Traditional Models. *Energy Environ. Sci.* **2011**, *4*, 4410-4422.

(29) Kippelen, B.; Brédas, J.-L. Organic Photovoltaics. *Energy Environ. Sci.* **2009**, *2*, 251–261.

(30) *Organic Solar Cells: Fundamentals, Devices, and Upscaling*; Rand, B. P.; Richter, H. Eds.; Pan Stanford Publishing: Singapore, **2014**.

(31) Thompson, B. C.; Kim, Y.-G.; McCarley, T. D.; Reynolds, J. R. Soluble Narrow Band Gap and Blue Propylenedioxythiophene-Cyanovinylene Polymers as Multifunctional Materials for Photovoltaic and Electrochromic Applications. *J. Am. Chem. Soc.* **2006**, *128*, 12714–12725.

(32) Tang, C. W. Two-Layer Organic Photovoltaic Cell. *Appl. Phys. Lett.* **1986**, *48*, 183–185.

(33) Mikhnenko, O. V.; Blom, P. W. M.; Nguyen, T.-Q. Exciton Diffusion in Organic Semiconductors. *Energy Environ. Sci.* **2015**, *8*, 1867–1888.

(34) Yu, G.; Gao, J.; Hummelen, J. C.; Wudl, F.; Heeger, A. J. Polymer Photovoltaic Cells: Enhanced Efficiencies via a Network of Internal Donor-Acceptor Heterojunctions. *Science* **1995**, *270*, 1789-1791.

(35) Kirchartz, T.; Agostinelli, T.; Campoy-Quiles, M.; Gong, W.; Nelson, J. Understanding the Thickness-Dependent Performance of Organic Bulk Heterojunction Solar Cells: the Influence of Mobility, Lifetime, and Space Charge. *J. Phys. Chem. Lett.* **2012**, *3*, 3470–3475.

(36) Li, G.; Shrotriya, V.; Huang, J.; Yao, Y.; Moriarty, T.; Emery, K.; Yang, Y. High-Efficiency Solution Processable Polymer Photovoltaic Cells by Self-Organization of Polymer Blends. *Nat. Mater.* **2005**, *4*, 864–868.

(37) Amb, C. M.; Chen, S.; Graham, K. R.; Subbiah, J.; Small, C. E.; So, F.; Reynolds, J. R. Dithienogermole as a Fused Electron Donor in Bulk Heterojunction Solar Cells. *J. Am. Chem. Soc.* **2011**, *133*, 10062–10065.

(38) Henson, Z. B.; Müllen, K.; Bazan, G. C. Design Strategies for Organic Semiconductors Beyond the Molecular Formula. *Nat. Chem.* **2012**, *4*, 699–704.

(39) Lee, J. K.; Ma, W. L.; Brabec, C. J.; Yuen, J.; Moon, J. S.; Kim, J. Y.; Lee, K.; Bazan, G. C.; Heeger, A. J. Processing Additives for Improved Efficiency From Bulk Heterojunction Solar Cells. *J. Am. Chem. Soc.* **2008**, *130*, 3619–3623.

(40) Mazzio, K. A.; Luscombe, C. K. The Future of Organic Photovoltaics *Chem. Soc. Rev.* **2014**, *44*, 78–90.

(41) *Progress in High-Efficient Solution Process Organic Photovoltaic Devices*; Yang, Y.; Li, G. Eds.; Springer; Berlin and Heidelberg, **2015**.

(42) Yip, H.-L.; Jen, A. K. Y. Recent Advances in Solution-Processed Interfacial Materials for Efficient and Stable Polymer Solar Cells. *Energy Environ. Sci.* **2012**, *5*, 5994.

(43) Ashraf, R. S.; Wadsworth, A.; Baran, D.; Yousaf, S. A.; Nielsen, C. B.; Tan, C.-H.; Dimitrov, S. D.; Shang, Z.; Gasparini, N.; Alamoudi, M.; Laquai, F. E. D. E. R.; Brabec, C. J.; Salleo, A.; Durrant, J. R.; Holliday, S.; McCulloch, I. High-Efficiency and Air-Stable P3HT-Based Polymer Solar Cells with a New Non-Fullerene Acceptor. *Nat. Commun.* **2016**, *7*, 11585.

(44) Liu, D.; Kelly, T. L. Perovskite Solar Cells with a Planar Heterojunctionstructure Prepared Using Room-Temperaturesolution Processing Techniques. *Nat. Photonics* **2013**, *8*, 133–138.

(45) Jørgensen, M.; Krebs, F. C. *Degradation of Polymer-Based OPV*; Krebs, F. C., Ed.; John Wiley & Sons, 2012; pp 1–20.

(46) Scharber, M. C.; Mühlbacher, D.; Koppe, M.; Denk, P.; Waldauf, C.; Heeger, A. J.; Brabec, C. J. Design Rules for Donors in Bulk-Heterojunction Solar Cells—Towards 10 % Energy-Conversion Efficiency. *Adv. Mater.* **2006**, *18*, 789–794.

(47) Zhang, Q.; Kan, B.; Liu, F.; Long, G.; Wan, X.; Chen, X.; Zuo, Y.; Ni, W.; Zhang, H.; Li, M.; Hu, Z; Huang, F.; Cao, Y.; Liang, Z.; Zhang, M.; Russell, T.P; Chen, Y. Small-Molecule Solar Cells with Efficiency Over 9%. *Nat. Photonics* **2014**, *9*, 35–41.

(48) Walker, B.; Kim, C.; Nguyen, T.-Q. Small Molecule Solution-Processed Bulk Heterojunction Solar Cells. *Chem. Mater.* **2011**, *23*, 470–482.

(49) Graham, K. R.; Cabanetos, C.; Jahnke, J. P.; Idso, M. N.; Labban, El, A.; Ngongang Ndjawa, G. O.; Heumueller, T.; Vandewal, K.; Salleo, A.; Chmelka, B. F.; Amassian, A.; Beaujuge, P. M.; McGehee, M. D. Importance of the Donor:Fullerene Intermolecular Arrangement for High-Efficiency Organic Photovoltaics. *J. Am. Chem. Soc.* **2014**, *136*, 9608–9618.

(50) Blouin, N.; Michaud, A.; Leclerc, M. A Low-Bandgap Poly(2,7-Carbazole) Derivative for Use in High-Performance Solar Cells. *Adv. Mater.* **2007**, *19*, 2295–2300.

(51) Blouin, N.; Michaud, A.; Gendron, D.; Wakim, S.; Blair, E.; Neagu-Plesu, R.; Belletête, M.; Durocher, G.; Tao, Y.; Leclerc, M. Toward a Rational Design of Poly(2,7-Carbazole) Derivatives for Solar Cells. *J. Am. Chem. Soc.* **2008**, *130*, 732–742.

(52) Wang, D. H.; Kim, J. K.; Seo, J. H.; Park, I.; Hong, B. H.; Park, J. H.; Heeger, A. J. Transferable Graphene Oxide by Stamping Nanotechnology: Electron-Transport Layer for Efficient Bulk-Heterojunction Solar Cells. *Angew. Chem. Int. Ed.* **2013**, *52*, 2874–2880.

(53) Sun, Y. Solution-Processed Small-Molecule Solar Cells with 6.7% Efficiency. *Nat. Mater.* **2011**, *11*, 44–48.

(54) Collins, S. D.; Ran, N. A.; Heiber, M. C.; Nguyen, T.-Q. Small Is Powerful: Recent Progress in Solution-Processed Small Molecule Solar Cells. *Adv. Energy Mater.* **2017**, *6*, No. 1602242.

(55) Sun, W.; Ma, Z.; Dang, D.; Zhu, W.; Andersson, M. R.; Zhang, F.; Wang, E. An Alternating D–A1–D–A2 Copolymer Containing Two Electron-Deficient Moieties for Efficient Polymer Solar Cells. *J. Mater. Chem. A* **2013**, *1*, 11141–11144.

(56) McCulloch, I.; Heeney, M.; Chabinyc, M. L.; DeLongchamp, D.; Kline, R. J.; Cölle, M.; Duffy, W.; Fischer, D.; Gundlach, D.; Hamadani, B.; Hamilton, R.; Richter, L.; Salleo, A.; Shkunov, M.; Sparrowe, D.; Tierney, S.; Zhang, W. Semiconducting Thienothiophene Copolymers: Design, Synthesis, Morphology, and Performance in Thin-Film Organic Transistors. *Adv. Mater.* **2009**, *21*, 1091–1109.

(57) Peet, J.; Kim, J. Y.; Coates, N. E.; Ma, W. L.; Moses, D.; Heeger, A. J.; Bazan, G. C. Efficiency Enhancement in Low-Bandgap Polymer Solar Cells by Processing with Alkane Dithiols. *Nat. Mater.* **2007**, *6*, 497–500.

(58) Liang, Y.; Yu, L. A New Class of Semiconducting Polymers for Bulk Heterojunction Solar Cells with Exceptionally High Performance. *Acc. Chem. Res.* **2010**, *43*, 1227–1236.

(59) Stalder, R.; Mei, J.; Graham, K. R.; Estrada, L. A.; Reynolds, J. R. Isoindigo, a Versatile Electron-Deficient Unit for High-Performance Organic Electronics. *Chem. Mater.* **2014**, *26*, 664–678.

(60) Wang, E.; Mammo, W.; Andersson, M. R. 25th Anniversary Article: Isoindigo-Based Polymers and Small Molecules for Bulk Heterojunction Solar Cells and Field Effect Transistors. *Adv. Mater.* **2014**, *26*, 1801–1826.

(61) Ganguly, A.; Zhu, J.; Kelly, T. L. Effect of Cross-Conjugation on Derivatives of Benzoisoindigo, an Isoindigo Analogue with an Extended π-System. *J. Phys. Chem. C* **2017**, *121*, 9110-9119.

(62) Estrada, L. A.; Stalder, R.; Abboud, K. A.; Risko, C.; Brédas, J.-L.; Reynolds, J. R. Understanding the Electronic Structure of Isoindigo in Conjugated Systems: a Combined Theoretical and Experimental Approach. *Macromolecules* **2013**, *46*, 8832–8844.

(63) Mei, J.; Graham, K. R.; Stalder, R.; Reynolds, J. R. Synthesis of Isoindigo-Based Oligothiophenes for Molecular Bulk Heterojunction Solar Cells. *Org. Lett.* **2010**, *12*, 660–663.

(64) Randell, N. M.; Douglas, A. F.; Kelly, T. L. 7-Azaisoindigo as a New Electron Deficient Component of Small Molecule Chromophores for Organic Solar Cells. *J. Mater. Chem. A* **2014**, *2*, 1085–1092.

(65) Graham, K. R.; Mei, J.; Stalder, R.; Shim, J. W.; Cheun, H.; Steffy, F.; So, F.; Kippelen, B.; Reynolds, J. R. Polydimethylsiloxane as a Macromolecular Additive for Enhanced Performance of Molecular Bulk Heterojunction Organic Solar Cells. *ACS Appl. Mater. Interfaces* **2011**, *3*, 1210–1215.

(66) Graham, K. R.; Wieruszewski, P. M.; Stalder, R.; Hartel, M. J.; Mei, J.; So, F.; Reynolds, J. R. Improved Performance of Molecular Bulk-Heterojunction Photovoltaic Cells Through Predictable Selection of Solvent Additives. *Adv. Funct. Mater.* **2012**, *22*, 4801–4813.

(67) Graham, K. R.; Stalder, R.; Wieruszewski, P. M.; Patel, D. G.; Salazar, D. H.; Reynolds, J. R. Tailor-Made Additives for Morphology Control in Molecular Bulk-Heterojunction Photovoltaics. *ACS Appl. Mater. Interfaces* **2013**, *5*, 63–71.

(68) Yassin, A.; Leriche, P.; Allain, M.; Roncali, J. Donor–Acceptor–Donor (D–a–D) Molecules Based on Isoindigo as Active Material for Organic Solar Cells. *New J. Chem.* **2013**, *37*, 502–507.

(69) Yang, M.; Chen, X.; Zou, Y.; Pan, C.; Liu, B.; Zhong, H. A Solution-Processable D–A–D Small Molecule Based on Isoindigo for Organic Solar Cells. *J Mater Sci* **2013**, *48*, 1014–1020.

(70) Elsawy, W.; Lee, C.-L.; Cho, S.; Oh, S.-H.; Moon, S.-H.; Elbarbary, A.; Lee, J.-S. Isoindigo-Based Small Molecules for High-Performance Solution-Processed Organic Photovoltaic Devices: the Electron Donating Effect of the Donor Group on Photo-Physical Properties and Device Performance. *Phys. Chem. Chem. Phys.* **2013**, *15*, 15193–15203.

(71) Wang, T.; Chen, Y.; Bao, X.; Du, Z.; Guo, J.; Wang, N.; Sun, M.; Yang, R. A New Isoindigo-Based Molecule with Ideal Energy Levels for Solution-Processable Organic Solar Cells. *Dyes Pigm.* **2013**, *98*, 11–16.

(72) Areephong, J.; Juan, R. R. S.; Payne, A.-J.; Welch, G. C. A Narrow Band Gap Isoindigo Based Molecular Donor for Solution Processed Organic Solar Cells. *New J. Chem.* **2015**, *39*, 5075–5079.

(73) Tomassetti, M.; Ouhib, F.; Cardinaletti, I.; Verstappen, P.; Salleo, A.; Jérôme, C.; Manca, J.; Maes, W.; Detrembleur, C. Branched and Linear A_2–D–A_1–D–A_2 Isoindigo- Based Solution-Processable Small Molecules for Organic Field-Effect Transistors and Solar Cells. *RSC Adv.* **2015**, *5*, 85460–85469.

(74) Liu, X.; Xie, Y.; Zhao, H.; Cai, X.; Wu, H.; Su, S.-J.; Cao, Y. Star-Shaped Isoindigo-Based Small Molecules as Potential Non-Fullerene Acceptors in Bulk Heterojunction Solar Cells. *New J. Chem.* **2015**, *39*, 8771–8779.

(75) Rutledge, L. R.; McAfee, S. M.; Welch, G. C. Design and Computational Characterization of Non-Fullerene Acceptors for Use in Solution-Processable Solar Cells. *J. Phys. Chem. A* **2014**, *118*, 7939–7951.

(76) McAfee, S. M.; Topple, J. M.; Sun, J.-P.; Hill, I. G.; Welch, G. C. The Structural Evolution of an Isoindigo-Based Non-Fullerene Acceptor for use in Organic Photovoltaics. *RSC Adv.* **2015**, *5*, 80098–80109.

(77) Jung, J. W. A Low Band Gap Conjugated Small Molecule Based on Isoindigo Flanked with Diketopyrrolopyrrole for Efficient Organic Solar Cells. *Dyes Pigm.* **2017**, *137*, 512–517.

(78) Stalder, R.; Mei, J.; Reynolds, J. R. Isoindigo-Based Donor−Acceptor Conjugated Polymers. *Macromolecules* **2010**, *43*, 8348–8352.

(79) Zhang, G.; Fu, Y.; Xie, Z.; Zhang, Q. Synthesis and Photovoltaic Properties of New Low Bandgap Isoindigo-Based Conjugated Polymers. *Macromolecules* **2011**, *44*, 1414–1420.

(80) Wang, E.; Ma, Z.; Zhang, Z.; Henriksson, P.; Inganäs, O.; Zhang, F.; Andersson, M. R. An Isoindigo-Based Low Band Gap Polymer for Efficient Polymer Solar Cells with High Photo-Voltage. *Chem. Commun.* **2011**, *47*, 4908–4910.

(81) Liu, B.; Zou, Y.; Peng, B.; Zhao, B.; Huang, K.; He, Y.; Pan, C. Low Bandgap Isoindigo-Based Copolymers: Design, Synthesis and Photovoltaic Applications. *Polym. Chem.* **2011**, *2*, 1156–1162.

(82) Wang, E.; Ma, Z.; Zhang, Z.; Vandewal, K.; Henriksson, P.; Inganäs, O.; Zhang, F.; Andersson, M. R. An Easily Accessible Isoindigo-Based Polymer for High-Performance Polymer Solar Cells. *J. Am. Chem. Soc.* **2011**, *133*, 14244–14247.

(83) Ma, Z.; Sun, W.; Himmelberger, S.; Vandewal, K.; Tang, Z.; Bergqvist, J.; Salleo, A.; Andreasen, J. W.; Inganäs, O.; Andersson, M. R.; Muller, C.; Zhang, F.; Wang, E. Structure–Property Relationships of Oligothiophene–Isoindigo Polymers for Efficient Bulk-Heterojunction Solar Cells. *Energy Environ. Sci.* **2014**, *7*, 361–369.

(84) Ho, C.-C.; Chen, C.-A.; Chang, C.-Y.; Darling, S. B.; Su, W.-F. Isoindigo-Based Copolymers for Polymer Solar Cells with Efficiency Over 7%. *J. Mater. Chem. A* **2014**, *2*, 8026–8032.

(85) Grand, C.; Baek, S.; Lai, T.-H.; Deb, N.; Zajaczkowski, W.; Stalder, R.; Müllen, K.; Pisula, W.; Bucknall, D. G.; So, F.; Reynolds, J. R. Structure–Property Relationships Directing Transport and Charge Separation in Isoindigo Polymers. *Macromolecules* **2016**, *49*, 4008–4022.

(86) Hu, H.; Jiang, K.; Kim, J.-H.; Yang, G.; Li, Z.; Ma, T.; Lu, G.; Qu, Y.; Ade, H.; Yan, H. Materials Chemistry A. *J. Mater. Chem. A* **2016**, *4*, 5039–5043.

(87) Stalder, R.; Puniredd, S. R.; Hansen, M. R.; Koldemir, U.; Grand, C.; Zajaczkowski, W.; Müllen, K.; Pisula, W.; Reynolds, J. R. Ambipolar Charge Transport in Isoindigo-Based Donor–Acceptor Polymers. *Chem. Mater.* **2016**, *28*, 1286–1297.

(88) Stalder, R.; Mei, J.; Subbiah, J.; Grand, C.; Estrada, L. A.; So, F.; Reynolds, J. R. N-Type Conjugated Polyisoindigos. *Macromolecules* **2011**, *44*, 6303–6310.

(89) Grenier, F.; Berrouard, P.; Pouliot, J.-R.; Tseng, H.-R.; Heeger, A. J.; Leclerc, M. Synthesis of New N-Type Isoindigo Copolymers. *Polym. Chem.* **2013**, *4*, 1836.

(90) Lei, T.; Dou, J.-H.; Ma, Z.-J.; Yao, C.-H.; Liu, C.-J.; Wang, J.-Y.; Pei, J. Ambipolar Polymer Field-Effect Transistors Based on Fluorinated Isoindigo: High Performance and Improved Ambient Stability. *J. Am. Chem. Soc.* **2012**, *134*, 20025–20028.

(91) Lei, T.; Dou, J.-H.; Ma, Z.-J.; Liu, C.-J.; Wang, J.-Y.; Pei, J. Chlorination as a Useful Method to Modulate Conjugated Polymers: Balanced and Ambient-Stable Ambipolar High-Performance Field-Effect Transistors and Inverters Based on Chlorinated Isoindigo Polymers. *Chem. Sci.* **2013**, *4*, 2447–2452.

(92) Zheng, Y.-Q.; Wang, Z.; Dou, J.-H.; Zhang, S.-D.; Luo, X.-Y.; Yao, Z.-F.; Wang, J.-Y.; Pei, J. Effect of Halogenation in Isoindigo-Based Polymers on the Phase Separation and Molecular Orientation of Bulk Heterojunction Solar Cells. *Macromolecules* **2015**, *48*, 5570–5577.

(93) Randell, N. M.; Fransishyn, K. M.; Kelly, T. L. Lewis Acid–Base Chemistry of 7-Azaisoindigo-Based Organic Semiconductors. *ACS Appl. Mater. Interfaces*, **2017**, *9*, 24788–24796.

(94) de Miguel, G.; Camacho, L.; a-Frutos, E. M. G. X. 7,7′-Diazaisoindigo: A Novel Building Block for Organic Electronics. *J. Mater. Chem. C* **2016**, *4*, 1208–1214.

(95) Huang, J.; Mao, Z.; Chen, Z.; Gao, D.; Wei, C.; Zhang, W.; Yu, G. Diazaisoindigo-Based Polymers with High-Performance Charge-Transport Properties: From Computational Screening to Experimental Characterization. *Chem. Mater.* **2016**, *28*, 2209–2218.

(96) Huang, J.; Chen, Z.; Mao, Z.; Gao, D.; Wei, C.; Lin, Z.; Li, H.; Wang, L.; Zhang, W.; Yu, G. Tuning Frontier Orbital Energetics of Azaisoindigo-Based Polymeric Semiconductors to Enhance the Charge-Transport Properties. *Adv. Electron. Mater.* **2017**, No. 1700078.

(97) Yue, W.; Nikolka, M.; Xiao, M.; Sadhanala, A.; Nielsen, C. B.; White, A. J. P.; Chen, H.-Y.; Onwubiko, A.; Sirringhaus, H.; McCulloch, I. Azaisoindigo Conjugated Polymers for High Performance n-Type and Ambipolar Thin Film Transistor Applications. *J. Mater. Chem. C* **2016**, *4*, 9704–9710.

(98) Ashraf, R. S.; Kronemeijer, A. J.; James, D. I.; Sirringhaus, H.; McCulloch, I. A New Thiophene Substituted Isoindigo Based Copolymer for High Performance Ambipolar Transistors. *Chem. Commun.* **2012**, *48*, 3939-3941.

(99) Koizumi, Y.; Ide, M.; Saeki, A.; Vijayakumar, C.; Balan, B.; Kawamoto, M.; Seki, S. Thienoisoindigo-Based Low-Band Gap Polymers for Organic Electronic Devices. *Polym. Chem.* **2013**, *4*, 484–494.

(100) Hasegawa, T.; Ashizawa, M.; Hiyoshi, J.; Kawauchi, S.; Mei, J.; Bao, Z.; Matsumoto, H. An Ultra-Narrow Bandgap Derived From Thienoisoindigo Polymers: Structural Influence on Reducing the Bandgap and Self-Organization. *Polym. Chem.* **2016**, *7*, 1181–1190.

(101) Dutta, G. K.; Han, A.-R.; Lee, J.; Kim, Y.; Oh, J. H.; Yang, C. Visible-Near Infrared Absorbing Polymers Containing Thienoisoindigo and Electron-Rich Units for Organic Transistors with Tunable Polarity. *Adv. Funct. Mater.* **2013**, *23*, 5317–5325.

(102) Vybornyi, O.; Jiang, Y.; Baert, F.; Demeter, D.; Roncali, J.; Blanchard, P.; Cabanetos, C. Solution-Processable Thienoisoindigo-Based Molecular Donors for Organic Solar Cells with High Open-Circuit Voltage. *Dyes Pigm.* **2015**, *115*, 17–22.

(103) Kim, G.; Kang, S.-J.; Dutta, G. K.; Han, Y.-K.; Shin, T. J.; Noh, Y.-Y.; Yang, C. A Thienoisoindigo-Naphthalene Polymer with Ultrahigh Mobility of 14.4 $cm^2 v^{-1} s^{-1}$ That Substantially Exceeds Benchmark Values for Amorphous Silicon Semiconductors. *J. Am. Chem. Soc.* **2014**, *136*, 9477–9483.

(104) Yue, W.; Ashraf, R. S.; Nielsen, C. B.; Collado-Fregoso, E.; Niazi, M. R.; Yousaf, S. A.; Kirkus, M.; Chen, H.-Y.; Amassian, A.; Durrant, J. R.; McCulloch, I. A Thieno[3,2-b][1]Benzothiophene Isoindigo Building Block for Additive- and Annealing-Free High-Performance Polymer Solar Cells. *Adv. Mater.* **2015**, *27*, 4702–4707.

(105) Lei, T.; Dou, J.-H.; Cao, X.-Y.; Wang, J.-Y.; Pei, J. Electron-Deficient Poly(P-Phenylene Vinylene) Provides Electron Mobility Over 1 $cm^2 v^{-1} s^{-1}$ Under Ambient Conditions. *J. Am. Chem. Soc.* **2013**, *135*, 12168–12171.

(106) Lei, T.; Dou, J.-H.; Cao, X.-Y.; Wang, J.-Y.; Pei, J. A BDOPV-Based Donor-Acceptor Polymer for High-Performance n-Type and Oxygen-Doped Ambipolar Field-Effect Transistors. *Adv. Mater.* **2013**, *25*, 6589–6593.

(107) Zhou, X.; Ai, N.; Guo, Z.-H.; Zhuang, F.-D.; Jiang, Y.-S.; Wang, J.-Y.; Pei, J. Balanced Ambipolar Organic Thin-Film Transistors Operated Under Ambient Conditions: Role of the Donor Moiety in BDOPV-Based Conjugated Copolymers. *Chem. Mater.* **2015**, *27*, 1815–1820.

(108) Lei, T.; Wang, J.-Y.; Pei, J. Design, Synthesis, and Structure–Property Relationships of Isoindigo-Based Conjugated Polymers. *Acc. Chem. Res.* **2014**, *47*, 1117–1126.

(109) Dou, J.-H.; Zheng, Y.-Q.; Yao, Z.-F.; Yu, Z.-A.; Lei, T.; Shen, X.; Luo, X.-Y.; Sun, J.; Zhang, S.-D.; Ding, Y.-F.; Han, G.; Yi, Y.; Wang, J.-Y.; Pei, J. Fine-Tuning of Crystal Packing and Charge Transport Properties of BDOPV Derivatives Through Fluorine Substitution. *J. Am. Chem. Soc.* **2015**, *137*, 15947–15956.

(110) Cao, Y.; Yuan, J.-S.; Zhou, X.; Wang, X.-Y.; Zhuang, F.-D.; Wang, J.-Y.; Pei, J. N-Fused BDOPV: a Tetralactam Derivative as a Building Block for Polymer Field-Effect Transistors. *Chem. Commun.* **2015**, *51*, 10514–10516.

(111) He, Y.; Guo, C.; Bin Sun; Quinn, J.; Li, Y. (*3E,7E*)-3,7-Bis(2-oxoindolin-3-ylidene)-5,7- dihydropyrrolo[2,3-*f*]indole-2,6(*1H,3H*)-dione based polymers for ambipolar organic thin film transistors. *Chem. Commun.* **2015**, *51*, 8093–8096.

(112) Randell, N. M.; Boutin, P. C.; Kelly, T. L. Bisisoindigo: Using a Ring-Fusion Approach to Extend the Conjugation Length of Isoindigo. *J. Mater. Chem. A* **2016**, *4*, 6940–6945.

(113) Randell, N. M.; Radford, C.L.; Yang, J.; Quinn, J.; Hou, D.; Li, Y.; Kelly, T. L. Acceptor Unit Length and Strength in Isoindigo-Inspired Donor-Acceptor-Acceptor Polymer Semiconductors. **2017**, *In Preparation*

(114) Cao, Y.; Yuan, J.-S.; Zhou, X.; Wang, X.-Y.; Zhuang, F.-D.; Wang, J.-Y.; Pei, J. N-Fused BDOPV: a Tetralactam Derivative as a Building Block for Polymer Field-Effect Transistors. *Chem. Commun.* **2015**, *51*, 10514–10516.

(115) Jiang, Y.; Gao, Y.; Tian, H.; Ding, J.; Yan, D.; Geng, Y.; Wang, F. Synthesis and Characterization of Isoindigo[7,6-g]Isoindigo-Based Donor–Acceptor Conjugated Polymers. *Macromolecules* **2016**, *49*, 2135–2144.

Chapter 2

7-Azaisoindigo as a New Electron Deficient Component of Small Molecule Chromophores for Organic Solar Cells

Reproduced from

Randell, N. M.; Douglas, A. F.; Kelly, T. L.

Journal of Materials Chemistry A, **2014**, *2*, 1085–1092. DOI: 10.1039/C3TA14263A

with permission from the Royal Society of Chemistry.

Consent was obtained from all co-authors to include this manuscript in the thesis. Unless otherwise noted, I performed all experimental work and wrote the first draft of the manuscript. A.F. Douglas synthesized of 5,5′-bis(trimethylstannyl)-3,3′-bisdodecyloxy-2,2′-bithiophene. T.L Kelly directed the study and revised manuscript.

Transition

This chapter focuses on my initial work using 7-azaisoindigo as an electron acceptor unit in donor-acceptor organic semiconductors. The purpose of this work was to investigate the effects of electronegative heteroatoms on the optoelectronic properties of organic semiconductor; in particular, the effects this had on the HOMO and LUMO levels of the resulting materials.

The introduction section of this chapter contains some material that is repetitive from Chapter 1 of the thesis including a brief introduction to OPVs and donor-acceptor semiconductors, as well as a summary of isoindigo-based semiconductors. However, I feel this

repetition is important in that it gives context to the work; this section was current as of 2013 when this paper was first submitted and gives important information about the state of the field of OPV research at that time. For example, the record OPV efficiency discussed in this chapter is no longer current, and far more research on isoindigo-based semiconductors, including further azaisoindigo-based semiconductors, has since been published, but these details reflect the state of the field at the time of writing.

2.1 Introduction

Research in the area of OPVs has recently produced substantial gains in device efficiency.[1-7] The current record for PCE in an OPV is a tandem, small molecule based cell with 12% PCE produced by the German company Heliatek.[8] The use of oligomeric materials in this record breaking cell is an excellent example of how small molecule dyes can hold several advantages over their polymeric counterparts. These include their inherent monodispersity, greater reproducibility in their syntheses, and increased crystallinity. Polymeric OPV components often suffer from a broad distribution in molecular weights that can negatively affect cell performance, whereas small molecules can be readily obtained in extremely high purity using conventional synthetic organic techniques. Additionally, the increased crystallinity of small molecule chromophores can drive increases in charge carrier mobility, which in turn can lead to improvements in device efficiency.[9,10]

Further increases in OPV efficiency will require the design of new dye molecules tailored to better overlap with the AM1.5G solar spectrum (which extends well into the near-infrared).[11] In both polymer and small molecule materials the juxtaposition of an electron donor with an electron acceptor is a common design strategy used to produce low bandgap materials.[3,12-16] The HOMOs of these molecules reside largely on the donor component, while in turn the LUMO is predominantly localized on the electron acceptor. This increases the charge transfer character of the HOMO to LUMO transition, leading to both a substantial red-shift of the absorption band and an increase in molar extinction coefficient.

Electron deficient sub-units bearing amide or imide functionalities, such as DPP[3,17-19] and perylene bisimide,[20-23] have been thoroughly explored as the acceptor portion of these donor-acceptor (DA) dyes. The electron deficient nature of these molecules lowers their

frontier orbital energy levels, producing efficient low bandgap chromophores when coupled to appropriate electron donors. In 2010, Mei *et al.* first reported the use of isoindigo as a new electron deficient sub-unit in oligomeric DA chromophores.[14] Since then, numerous research groups have made use of the isoindigo motif in new conjugated materials.[24] These include the poly(isoindigo) homopolymer,[25] DA oligomers[26,27] and copolymers,[13,25,28-32] various n-type copolymers,[25,33] and dyes for metal-free dye sensitized solar cells.[34] However, despite the extensive amount of research on isoindigo-containing compounds, relatively little work has been carried out on variants of the isoindigo core structure. While copolymers containing chloro- and fluoro- substituted isoindigo have been studied for their ambipolar charge transport characteristics in organic field effect transistors,[35,36] and as a component in polymer solar cells,[37] little other work has been done in this area.

Here the use of 7-azaisoindigo as an electron deficient moiety in DA small molecule chromophores containing 2,2′-bithiophene donors is reported. The presence of the heteroatom in the 7-azaisoindigo structure serves to fine-tune the energy of the LUMO, which is localized on the azaisoindigo sub-unit. In order to independently probe the effects of the electron withdrawing and donating components, a series of four chromophores were synthesized using a modular synthetic approach. Each contained either isoindigo or 7-azaisoindigo as the electron deficient sub-unit, and either 2,2′-bithiophene or 3,3′-bis(dodecyloxy)-2,2′-bithiophene as the electron donating component. The electronic structure of all four dyes was characterized by DFT calculations, cyclic voltammetry, and electronic spectroscopy. Finally, the chromophores were combined with $PC_{61}BM$ and tested in prototype BHJ solar cells.

2.2 Experimental

2.2.1 Materials and methods

Prior to use, dimethylsulfoxide (DMSO), DMF, toluene and tetrahydrofuran (THF) were dried over activated 3 Å molecular sieves and stored under N_2. $Pd(PPh_3)_4$ was stored in an inert atmosphere N_2 glove box when not in use. All other solvents and reagents were used as received. NMR spectra were obtained using a Bruker Avance 500 MHz spectrometer. UV/vis spectroscopy measurements were performed in $CHCl_3$ or as thin films on glass substrates using a Cary 6000 UV/Visible spectrophotometer. AFM measurements were carried out using a Dimensions Hybrid Nanoscope system (Veeco Metrology Group). Mass spectra were recorded using a matrix assisted laser desorption ionization time-of-flight (MALDI-TOF) mass spectrometer, in positive ion reflectron mode, using a matrix of either α-Cyano-4-hydroxycinnamic acid/trifluoroacetic acid (compounds **15-17**) or 2,5-dihydroxybenzoic acid (compound **18**). Cyclic voltammetry was carried out in 0.05 mol L^{-1} tetrabutylammonium hexafluorophosphate dissolved in dry, degassed CH_2Cl_2. The working electrode was glassy carbon, the counter electrode was a Pt wire, and the reference electrode was a Ag wire. Voltammagrams were referenced to an internal Fc/Fc^+ standard. All scans were acquired at a scan rate of 20 mV s^{-1}.

2.2.3 Device fabrication and characterization

Pre-cleaned ITO coated glass substrates (Delta Technologies) ($R_s \approx 6\ \Omega/\square$) were UV-ozone cleaned for 15 min immediately prior to use. A layer of poly(3,4-ethylenedioxythiophene:polystyrene sulfonate (Clevios P VP AI 4083) was spin coated onto the ITO substrates and annealed at 150 °C before being placed in an N_2-atmosphere glove box.

The active layer solution (60:40 **15-18**:$PC_{61}BM$ by mass, total solid concentration of 18 mg/mL in chlorobenzene) was then deposited by spin coating. The samples were allowed to dry at ambient temperature for 2 hours, and then annealed at 100 °C for 20 min. Donor to acceptor ratios, concentrations, and annealing conditions were previously optimized for **15** by Mei *et al.*,[14] and were left unchanged for **15**–**18**. LiF (0.8 nm) and Al (100 nm) were then thermally evaporated onto the substrates at a base pressure of 10^{-6} mbar.

Current-voltage measurements were made inside a N_2-atmosphere glove box using a Keithley 2400 source-measure unit. The cells were illuminated by a 450 W Class AAA solar simulator equipped with an AM1.5G filter (Sol3A, Oriel instruments) at a calibrated intensity of 100 mW/cm^2, as determined by a standard silicon reference cell (91150V, Oriel Instruments). The cell area was defined by a non-reflective anodized aluminium mask to be 0.07065 cm^2. Incident photon to current efficiency (IPCE) measurements were performed on the highest efficiency devices under ambient conditions using a QE-PV-SI system (Oriel Instruments) consisting of a 300 W Xe arc lamp, monochromator, chopper, lock-in amplifier and certified silicon reference cell. Measurements were made using a 30 Hz chop frequency.

2.2.3. Detailed synthetic procedures

1-(2-Ethylhexyl)-7-azaindole (**1**)[38]

7-Azaindole (355 mg, 3.00 mmol) was dissolved in 10 mL of dimethylacetamide (DMA). NaH (98.2 mg, 4.09 mmol) was added and the reaction was stirred for 30 min under N_2. 2-Ethyl-1-hexylbromide (679 mg, 3.51 mmol) was dissolved in 2 mL of DMA and added slowly to the reaction mixture via syringe and the reaction mixture was stirred for 18 hours at room temperature. The reaction mixture was quenched with H_2O and extracted with CH_2Cl_2; the

combined organic phases were washed with deionized water, dried over $MgSO_4$ and concentrated under reduced pressure. The crude 1-(2-ethylhexyl)-7-azaindole was purified by column chromatography on silica gel (eluent: CH_2Cl_2) and dried under high vacuum to yield a clear colourless viscous liquid (579 mg, 83.7%). ^{1}H NMR (500 MHz, $CDCl_3$ δ, ppm): 8.32 (dd, J_1 = 1.2 Hz, J_2 = 4.6 Hz, 1H), 7.89 (dd, J_1 = 1.4 Hz, J_2 = 7.8 Hz, 1H), 7.19 (d, J = 3.4 Hz, 1H), 7.01-7.05 (m, 1H), 6.45 (d, J = 3.4 Hz, 1H), 4.19 (d, J = 7.4 Hz, 2H), 1.92-2.02 (m, 1H), 1.20-1.35 (m, 9H), 0.82-0.91 (m, 6H).

1-(2-Ethylhexyl)-7-azaisatin (**2**)[38]

1-(2-Ethylhexyl)-7-azaindole (**1**) (1.02 g, 4.45 mmol) was dissolved in 20 mL of dry DMSO under N_2. *N*-bromosuccinimide (1.60g mg, 8.98 mmol) was added to the flask and the reaction mixture was stirred at 60 °C while sparging with N_2. After 5 hours the temperature was increased to 100 °C and the reaction mixture was heated while sparging with N_2 for 21 hours. The reaction mixture was quenched with 100 mL of H_2O and extracted with CH_2Cl_2. The combined organic phases were washed with deionized water, dried over $MgSO_4$ and concentrated under reduced pressure. The crude 1-(2-ethylhexyl)-7-azaisatin was purified by column chromatography on silica gel (eluent: 1:3 ethyl acetate:hexanes) and dried under high vacuum to yield a yellow-orange solid (395 mg, 34%). ^{1}H NMR (500 MHz, $CDCl_3$, δ, ppm): 8.35 (dd, J_1 = 5.2 Hz, J_2 =1.6 Hz, 1H), 7.72, (dd, J_1 = 7.3 Hz, J_2 =1.6 Hz, 1H), 6.96-6.99 (m, 1H), 3.65 (dd J_1 = 7.1 Hz, J_2 = 1.3 Hz, 2H), 1.90 (m, 1H), 1.10-1.40 (m, 10H), 0.70-0.90 (m, 7H).

1-(2-Ethylhexyl)-7-aza-6′-bromoisoindigo (**3**)[14]

1-(2-Ethylhexyl)-7-azaisatin (**2**) (308 mg, 1.45 mmol) and 6-bromo-2-oxindole (369 mg, 1.42 mmol) were dissolved in 12 mL of glacial acetic acid. Concentrated hydrochloric acid (0.1 mL) was added to the flask and the reaction mixture was heated at reflux for 24 hours under N_2. The reaction mixture was cooled to room temperature and diluted with 5% aqueous $NaHCO_3$ (w/v). The product was isolated by suction filtration, washed with $NaHCO_3$(aq) three times, H_2O three times and 1:1 EtOH:H_2O three times and dried under high vacuum to yield 1-(2-ethylhexyl)-7-aza-6′-bromoisoindigo as a red-black solid (592 mg, 92.3%). ^{1}H NMR (500 MHz, D_6-DMF, δ, ppm): 11.21 (s, 1H), 9.43 (dd, J = 7.8 Hz, J_2 1.4 Hz, 1H), 9.19 (d, J = 8.6 Hz, 1H), 8.32 (dd, J_1 = 5.0 Hz, J_2 = 1.4 Hz, 1H), 7.30 (dd, J_1 = 8.7 Hz, J_2 = 1.9 Hz, 1H), 7.19 (d, J = 1.9 Hz, 1H), 7.12-7.15 (m, 1H), 3.82 (d, J = 7.6 Hz, 2H), 2.04 (m, 1H), 1.25-1.45 (m, 9H), 0.84-0.96 (m, 6H).

1,1′-Bis(2-ethylhexyl)-7-aza-6′-bromoisoindigo (**4-6**)[14]

1-(2-Ethylhexyl)-7-aza-6′-bromoisoindigo (**3**) (57.4 mg, 0.126 mmol) was dissolved in 2 mL of dry DMF under N_2. K_2CO_3 (119 mg, 0.859 mmol) was added and the reaction mixture was stirred for 30 min. 2-Ethyl-1-hexylbromide (0.10 mL, 0.56 mmol) was added and the reaction was stirred at 100 °C for 20 hours. The reaction mixture was poured over 50 mL of brine and extracted with CH_2Cl_2. The combined organic phases were washed three times with brine, dried over $MgSO_4$ and concentrated under reduced pressure. The resulting three products were separated by column chromatography on silica gel (eluent: CH_2Cl_2) and dried under high vacuum to yield red-black solids.

1,1′-Bis(2-ethylhexyl)-7-aza-6′-bromoisoindigo (**4**)**:** (13 mg, 17%), ^{1}H NMR (500 MHz, $CDCl_3$, δ, ppm): 9.37 (dd, *J*= 7.9 Hz, J_2 = 1.3 Hz, 1H), 9.145 (d, *J* = 8.6 Hz 1H), 8.21 (dd, *J* = 5.1 Hz, J_2 = 1.4 Hz, 1H), 7.20 (dd, *J* = 8.6 Hz, J_2 = 1.7 Hz, 1H), 6.96-6.99 (m, 1H), 6.92 (d. *J* = 1.6 Hz, 1H), 3.79-3.82 (m, 2H), 3.60-3.68 (m, 2H), 2.02-2.04 (m, 1H), 1.82-1.85 (m, 1H), 1.25-1.38 (m, 19H), 0.79-0.95 (m, 15H).

1,1′-Bis(2-ethylhexyl)-6,6′-dibromoisoindigo (**5**): (24 mg, 34%), ^{1}H NMR (500 MHz, $CDCl_3$, δ, ppm): 9.04 (d, *J* = 8.6 Hz, 2H), 7.17 (dd, *J* = 8.6 Hz, J_2 = 1.6 Hz, 2H), 6.89 (s, 2H), 3.60-3.65 (m, 4H), 1.81-1.84 (m, 2H), 1.25-1.40 (m, 27H), 0.82-0.95 (m, 19H)

1,1′-Bis(2-ethylhexyl)-7,7′-diazaisoindigo (**6**): (7 mg, 10%), ^{1}H NMR (500MHz, $CDCl_3$, δ, ppm): 9.45 (dd, J_1 = 4.8 Hz, J_2 = 1.3 Hz, 2H), 8.23 (dd, *J* = 5.06 Hz, J_2 = 1.3 Hz, 2H), 6.99-7.02 (m, 2H), 3.80-3.81 (m, 4H), 2.02-2.05 (m, 2H), 1.25-1.41 (m, 23H), 0.86-0.94 (m, 18H).

6-Bromoisoindigo (**7**)[14]

To a slurry of 6-bromoisatin (131 mg, 0.892 mmol) and 6-bromo-2-oxindole (187 mg, 0.880 mmol) in 5.6 mL of glacial acetic acid, was added 0.05 mL of concentrated hydrochloric acid. The reaction mixture was heated to reflux for 24 hours. The reaction mixture was cooled and the product was isolated by suction filtration. The resulting red-black solid was washed with H_2O three times, ethanol (EtOH) three times, and dried under high vacuum to yield 6-bromoisoindigo (246 mg, 82.0%).

1,1′-Bis(2-ethylhexyl)-6-bromoisoindigo (**8**)

6-Bromoisoindigo (**7**) (246 mg, 0.721 mmol), and K_2CO_3 (637 mg, 4.61 mmol) were dissolved in 15 mL of dry DMF under N_2. 2-Ethyl-1-hexylbromide (0.40 mL, 2.25 mmol) was added via

syringe and the reaction mixture was stirred at 100 °C for 18 hours. The reaction mixture was poured over 100 mL H_2O and extracted with CH_2Cl_2. The combined organic phases were washed with brine, dried over $MgSO_4$, and concentrated under reduced pressure. The crude 1,1′-bis(2-ethylhexyl)-6-bromoisoindigo was purified by column chromatography on silica gel (eluent: 3:2 hexane: CH_2Cl_2), and dried under high vacuum to yield a red solid (112 mg, 27.5%). ^{1}H NMR (500MHz, $CDCl_3$, δ ppm): 9.13 (d, J = 7.9 Hz, 1H), 9.05 (d, J = 8.5 Hz, 1H), 7.35 (t, J = 7.5 Hz, 1H), 7.15 (d, J = 8.4 Hz, 1H), 7.04 (t, J = 7.6 Hz, 1H), 6.88 (s, 1H), 6.76 (d, J = 7.7 Hz, 1H), 3.56-3.70 (m, 4H), 1.77-1.88 (m, 2H), 1.22-1.45 (m, 18H), 0.82-0.97, (m, 14H).

2,2′-Bithiophene (**9**)[39]

To Mg turnings (0.9460 g, 0.0201 mol) and trace I_2 in 15 mL of dry THF under N_2, was added 0.5 mL of 2-bromothiophene (2.4 mL, 0.025 mol) to initiate an exothermic reaction. Once the reaction began, the remaining 2-bromothiophene was added dropwise and the reaction mixture was stirred at reflux for 45 min. The solution was cooled to room temperature and added via syringe to a solution of Ni(dppp)Cl_2 (17 mg, 0.031 mmol) and 2-bromothiophene (1.95 mL, 0.0120 mol) in 10 mL of dry THF at 0 °C. The mixture was then heated to reflux for 4 hours. The resulting mixture was poured over 50 mL H_2O and extracted with CH_2Cl_2. Dilute aqueous hydrochloric acid was required to break the resulting emulsion. The organic layers were washed with 5% aqueous $NaHCO_3$ (w/v) and brine, dried over $MgSO_4$ and concentrated under reduced pressure. The crude 2,2′-bithiophene was purified by column chromatography on silica gel (eluent: hexanes) and dried under high vacuum to yield a white solid (2.642 g, 78.9%). ^{1}H

NMR (500 MHz, $CDCl_3$, δ ppm): 7.21 (d, J = 5.1 Hz, 1H), 7.18 (d, J = 3.5 Hz, 1H), 7.02 (t, J = 3.7 Hz, 1H).

5,5′-Di(tributylstannyl)-2,2′-bithiophene (**10**)[40]

2,2′-Bithiophene (**9**) (53.1 mg, 0.319 mmol), was dissolved in 3 mL of dry THF under N_2. The solution was cooled to –78 °C and *n*-butyllithium (2.5 mol/L in hexanes, 0.29 mL, 0.725 mmol) was added to the solution dropwise. A white precipitate formed and the suspension was warmed to room temperature and stirred for 1 hour. Tributyltin chloride (0.19 mL, 0.70 mmol) was added and the reaction mixture was heated at reflux for 1 hour. The mixture was then cooled to room temperature and 7 mL of hexane was added. The organic layer was washed with 5% aqueous $NaHCO_3$ (w/v) and water, dried over $MgSO_4$ and concentrated under high vacuum to yield 5,5′-di(tributylstannyl)-2,2′-bithiophene as a viscous green liquid (172 mg, 72.6%). ^{1}H NMR (500 MHz, $CDCl_3$, δ ppm): 7.29 (d, J = 3.33 Hz 1H), 7.05 (d, J = 3.45 Hz 1H), 1.57 (m 7H), 1.34 (m 7H), 1.11 (m, 7H), 0.91 (m 11H).

3-Dodecyloxythiophene (**11**)[15]

3-Methoxythiophene (1.4 mL, 18 mmol) was dissolved in 15 mL of dry toluene. 1-Dodecanol (7.8 mL, 35 mmol) was added, followed by *p*-toluenesulfonic acid (0.33 g, 1.8 mmol). The reaction mixture was heated at reflux under N_2 overnight. The reaction mixture was diluted with 50 mL of CH_2Cl_2 and washed with water and brine. The organic layer was dried over $MgSO_4$ and concentrated to dryness under reduced pressure. The crude 3-dodecyloxythiophene was purified by column chromatography on silica gel (eluent: hexanes, gradient to 25% CH_2Cl_2 in hexanes) and concentrated under reduced pressure to yield 2.26 g of a colorless oil. This

product was dried under high vacuum to a final yield of 1.82 g (38.8%). ^{1}H NMR (500 MHz, $CDCl_3$, δ ppm): 7.17 (m, 1H), 6.75 (d, J = 5.18 Hz, 1H), 6.23 (t, J = 1.51 Hz, 1H), 3.94 (t, J = 6.53 Hz, 2H), 1.74-1.79(m, 2H), 1.41-1.47 (m, 2H), 1.23-1.36 (m, 18H).

2-Bromo-3-dodecyloxythiophene (**12**)[15]

3-Dodecyloxythiophene (**11**) (1.82 g, 6.78 mmol) was dissolved in 15 mL of dry THF. The solution was cooled to 0 °C in an ice bath under N_2. *N*-bromosuccinimide (1.21 g, 6.78 mmol) was added. The reaction mixture was warmed slowly to room temperature, and stirred for 20 hours. The reaction mixture was diluted with 50 mL diethyl ether, washed with water, dried over $MgSO_4$, filtered, and concentrated under reduced pressure. The crude 2-bromo-3-dodecyloxythiophene was purified by column chromatography on silica gel (eluent: hexanes), concentrated under reduced pressure and dried under high vacuum to yield an off-white solid (1.29 g, 55%). ^{1}H NMR (500 MHz, $CDCl_3$, δ ppm): 7.18 (d, J = 5.95 Hz, 1H), 6.74 (d, J = 5.95 Hz, 1H), 4.03 (t, J = 6.57 Hz, 2H), 1.72-1.78 (m, 2H), 1.42-1.47 (m, 2H), 1.23-1.37 (m, 17H).

3,3′-Bis(dodecyloxy)-2,2′-bithiophene (**13**)[15]

Bis(cyclooctadienyl)nickel(0) (1.535 g, 5.57 mmol) was dissolved in 15 mL of anhydrous DMF. 2,2′-Bipyridine (0.87 g, 5.6 mmol) and cyclooctadiene (0.45 mL, 3.7 mmol) were added and the reaction mixture was heated at 80 °C for 1 hour. 2-Bromo-3-dodecyloxythiophene (**12**) (1.29 g, 3.71 mmol) was dissolved in 25 mL of dry toluene and added to the reaction mixture dropwise. The reaction mixture was subsequently stirred overnight at 80 °C. The reaction mixture was diluted with 100 mL of CH_2Cl_2 and washed with 10% aqueous hydrochloric acid and water, dried over $MgSO_4$ and concentrated to dryness under reduced pressure. The crude

3,3′-Bis(dodecyloxy)-2,2′-bithiophene was purified by column chromatography on silica gel (eluent: hexanes, gradient to 20% CH_2Cl_2 in hexanes) and dried under high vacuum to yield a pale yellow solid (0.300 g, 30.2%). ^{1}H NMR (500 MHz, $CDCl_3$, δ ppm): 7.07 (d, J = 5.55 Hz, 2H), 6.83 (d, J = 5.56 Hz, 2H), 4.09 (t, J = 6.52 Hz, 4H), 1.81-1.87 (m 5H), 1.48-1.56 (m, 10H), 1.22-1.39 (m, 42H).

5,5′-Di(tributylstannyl)-3,3′-bisdodecyloxy-2,2′-bithiophene (**14**)[15]

3,3′-Bis(dodecyloxy)-2,2′-bithiophene (**13**) (230 mg, 0.43 mmol) was dissolved in 5 mL of dry THF and cooled to –78 °C, *n*-butyllithium (0.38 mL, 0.95 mmol) was added dropwise and the reaction mixture was stirred at –78 °C for 1 hour. It was then warmed to room temperature and stirred for an additional 1 hour. The reaction mixture was, again, cooled to –78 °C and tributyltin chloride (0.20 mL, 0.95 mmol) was added. The mixture was stirred at –78 °C for 10 min before being warmed to room temperature and stirred for 2.5 hours. The reaction mixture was diluted with 20 mL of ethyl acetate, washed with water and brine, dried over $MgSO_4$, filtered, and concentrated under reduced pressure to yield 5,5′-di(tributylstannyl)-3,3′-bisdodecyloxy-2,2′-bithiophene as a yellow oil (657 mg, 137%). ^{1}H NMR (500 MHz, $CDCl_3$, δ ppm): 6.83 (s, 1H), 4.10 (t, J = 6.41 Hz, 1H), 1.82-1.88 (m, 3H), 1.51-1.67 (m 20H), 1.43-1.50 (m, 2H), 1.22-1.39 (m, 47H), 1.02-1.17 (m, 12H), 0.86-0.94 (m, 32H), 0.78-0.82 (m, 2H).

Compound **15**[14]

5,5′-di(tributylstannyl)-2,2′-bithiophene (**10**) (29.2 mg, 0.0392 mmol) was dissolved in 5 mL of dry toluene and degassed using three freeze pump thaw cycles. 1,1′-Bis(2-ethylhexyl)-6-bromoisoindigo (**8**) (51.4 mg, 0.0909 mmol) and $Pd(PPh_3)_4$ (3.6 mg, 0.0031 mmol) were added

to the solution and the reaction mixture was stirred at reflux for 45 hours. The solvent was removed under reduced pressure; the crude **15** was purified by chromatography on silica gel (eluent: 1:1 CH_2Cl_2:hexanes, gradient to 5:3 CH_2Cl_2:hexanes) and dried under high vacuum to yield a dark purple solid (32 mg, 72%). ^{1}H NMR (500 MHz, $CDCl_3$, δ ppm): 9.20 (d, J = 8.4 Hz, 2H), 9.15 (d, J = 8.0 Hz, 2H), 7.28-7.38 (m, 6H), 7.05 (t, J = 8.5 Hz, 2H), 6.99 (d, J = 1.5 Hz, 2H), 6.78 Hz (d, J = 7.8 Hz, 2H), 3.63-3.80 (m, 9H), 1.84-1.94 (m, 5H), 1.28-1.47 (m, 44H), 0.86-1.00 (m, 31H). MALDI-TOF MS (m/z): $(M+H)^+$ (calc'd): 1135.6, (found): 1135.7.

Compound **16**

5,5′-Di(tributylstannyl)-2,2′-bithiophene (**10**) (31.7 mg, 0.0426 mmol) was dissolved in 5 mL of freshly degassed (using three freeze pump thaw cycles) dry toluene. 1,1′-Bis(2-ethylhexyl)-7-aza-6′-bromoisoindigo (**4**) (53.2 mg 0.0939 mmol) and $Pd(PPh_3)_4$ (3.2 mg, 0.0028 mmol) were added and the reaction mixture was stirred at reflux for 48 hours. The solvent was removed under reduced pressure and the crude **16** was purified by column chromatography on silica gel (eluent: CH_2Cl_2) and dried under high vacuum to yield a dark purple solid (34.2 mg, 70.6%). ^{1}H NMR (500 MHz, $CDCl_3$, δ ppm): 9.36 (dd, J_1 = 7.8; J_2 = 1.3 Hz, 1H), 9.27 (d, J = 8.4 Hz, 1H), 8.19 (dd, J_1 = 4.9; J_2 = 1.2 Hz, 1H), 7.36-7.41 (m, 2H), 7.31 (dd, J_1 = 8.4; J_2 = 1.5 Hz, 1H), 6.94-6.99 (m, 2H), 3.50-3.88 (m 7H), 2.01-2.05 (m, 1H), 1.85-1.93 (m, 1H), 1.19-1.50 (m, 32H), 0.79-1.01 (m, 23H). ^{13}C NMR (500 MHz, $CDCl_3$, δ ppm) 168.6, 168.0, 162.7, 158.1, 157.9, 157.7, 149.6, 146.2, 143.0, 137.93, 137.88, 136.7, 133.7, 130.9, 130.8, 130.2, 130.0, 125.5, 125.3, 122.6, 120.8, 119.2, 118.8, 116.9, 116.4, 113.1, 104.8, 104.7, 100.0, 57.8, 55.4, 44.2, 43.5, 37.8, 37.4, 30.8, 30.5, 28.9, 28.5, 27.89, 27.88, 26.9, 24.3, 24.27, 23.9, 23.1,

22.7, 17.5, 14.2, 14.18, 12.1, 13.6, 10.8, 10.6, 1.0. MALDI-TOF MS (m/z): $(M+H)^+$ (calc'd): 1137.6, (found): 1137.7 .

Compound **17**

5,5′-Di(tributylstannyl)-3,3′-bisdodecyloxy-2,2′-bithiophene (**14**) (210.7 mg, 0.1893 mmol) was dissolved in 13 mL of dry toluene and degassed using three freeze pump thaw cycles. 1,1′-Bis(2-ethylhexyl)-6-bromoisoindigo (**8**) (215.0 mg, 0.3801 mmol) and $Pd(PPh_3)_4$ (12.9 mg, 0.0112 mmol) were added and the reaction mixture was stirred at reflux for 20 hours. The solvent was removed under reduced pressure; the crude **17** was purified by column chromatography on silica gel (eluent: 1:1 CH_2Cl_2:hexanes, gradient to 3:2 CH_2Cl_2:hexanes) and dried under high vacuum to yield a dark blue solid (147.2 mg, 51.7%). ^{1}H NMR (500 MHz, CD_2Cl_2, δ ppm): 9.20 (d, J = 8.4 Hz, 1H), 9.14 (d, J = 7.9, Hz), 7.35 (t, J = 7.7 Hz, 1H), 7.30 (d, J = 8.4 Hz, 1H), 7.26 (s, 1H), 7.01-7.04 (m, 2H), 6.82 (d, J = 7.89 Hz, 1H), 4.26 (t, J = 7.44 Hz, 2H), 3.63-3.78 (m, 4H), 1.84-2.01 (m, 4H), 1.56-1.66 (m, 2H), 1.17-1.50 (m, 35H), 0.80-1.04 (m, 16H). ^{13}C NMR (500 MHz, CD_2Cl_2, δ ppm) 168.5, 168.2, 153.4, 146.0, 145.1, 139.0, 137.9, 132.6, 121.9, 120.9, 115.8, 103.8, 72.3, 44.3, 44.02, 44.01, 44.0, 43.0, 37.8, 37.6, 31.9, 30.8, 30.7, 29.73, 29.67, 29.5, 29.4, 28.8, 28.7, 27.8, 26.1, 24.2, 24.1, 23.1, 22.7, 19.6, 13.90, 13.86, 13.8, 10.6, 10.5, 0.8. MALDI-TOF MS (m/z): (M^+): (calc'd): 1503.98, (found): 1504.0.

Compound **18**

5,5′-Di(tributylstannyl)-3,3′-bisdodecyloxy-2,2′-bithiophene (**14**) (106.3 mg, 0.0955 mmol) was dissolved in 13 mL of dry toluene and degassed using three freeze pump thaw cycles. 1,1′-Bis(2-ethylhexyl)-7-aza-6′-bromoisoindigo (**4**) (115.5 mg 0.2039 mmol) and $Pd(PPh_3)_4$ (6.4

mg, 0.00554 mmol) were added and the reaction was stirred at reflux for 20 hours. The solvent was removed under reduced pressure; the crude **18** was purified by column chromatography on silica gel (eluent: CH_2Cl_2, gradient to 1% methanol in CH_2Cl_2) and concentrated under high vacuum to yield a dark blue solid (125.3 mg, 87%). ^{1}H NMR (500 MHz, $CDCl_3$, δ ppm): 9.36 (d, J = 7.70 Hz, 1H), 9.25 (d, J = 8.43 Hz, 1H), 8.19 (d, J = 4.93 Hz, 1H), 7.31 (d, J = 8.03 Hz, 1H), 7.20 (s, 1H), 6.97 (m, 2H), 4.24 (t, J = 6.44 Hz, 2H), 3.83 (d, J = 7.11 Hz, 2H), 3.71-3.76 (m, 2H), 2.02-2.10 (m, 1H), 1.87-2.00 (m, 3H), 1.54-1.66 (m, 10H), 1.20-1.48 (m, 43H), 0.80-1.02 (m, 22H). ^{13}C NMR (500 MHz, $CDCl_3$, δ ppm), 168.8, 168.2, 157.6, 153.4, 149.4, 146.2, 139.1, 138.7, 136.6, 133.8, 130.8, 129.6, 120.5, 118.5, 118.1, 116.6, 116.3, 113.1, 104.0, 72.2, 44.2, 43.4, 37.8, 37.5, 31.9, 30.9, 30.5, 29.72, 29.69, 29.61, 28.8, 28.5, 26.1, 24.2, 23.9, 23.13, 23.10, 22.7, 14.1, 10.9, 10.6, 1.04. MALDI-TOF MS: (M^+): (calc'd): 1505.97, (found): 1506.0.

2.3 Results and discussion

2.3.1 Synthesis of donor-acceptor chromophores

The synthesis of DA chromophores is often carried out in a modular fashion, synthesizing the donor and acceptor sub-units separately and combining them late in the synthesis using metal-catalyzed cross-coupling reactions. This modular approach was adopted here, enabling the efficient synthesis of four dyes with an acceptor-donor-acceptor structure.

7-Azaisoindigo was synthesized in order to provide a more electron deficient analogue to isoindigo (Scheme 2.1). While 7-azaisoindigo derivatives have been explored for their use in medicinal chemistry,[38,41] no work has been done to evaluate their utility in optoelectronic applications. The synthesis started from the commercially available 7-azaindole, which was *N*-alkylated and then oxidized to the corresponding 1-alkyl-7-azaisatin (**2**). An aldol condensation

with 6-bromo-2-oxindole was then used to form the 7-aza-6′-bromoisoindigo sub-unit (**3**).[14] As shown by Mei *et al*.,[14] due to the hydrolysable nature of the exocyclic double bond in the isoindigo backbone, upon exposure to base, these molecules undergo a retro-aldol/aldol decomposition and reformation process. This same process was found to occur during alkylation of 7-aza-6′-bromoisoindigo (**4**), and produced a mixture of all three possible compounds (**4-6**), which were separated by chromatography.

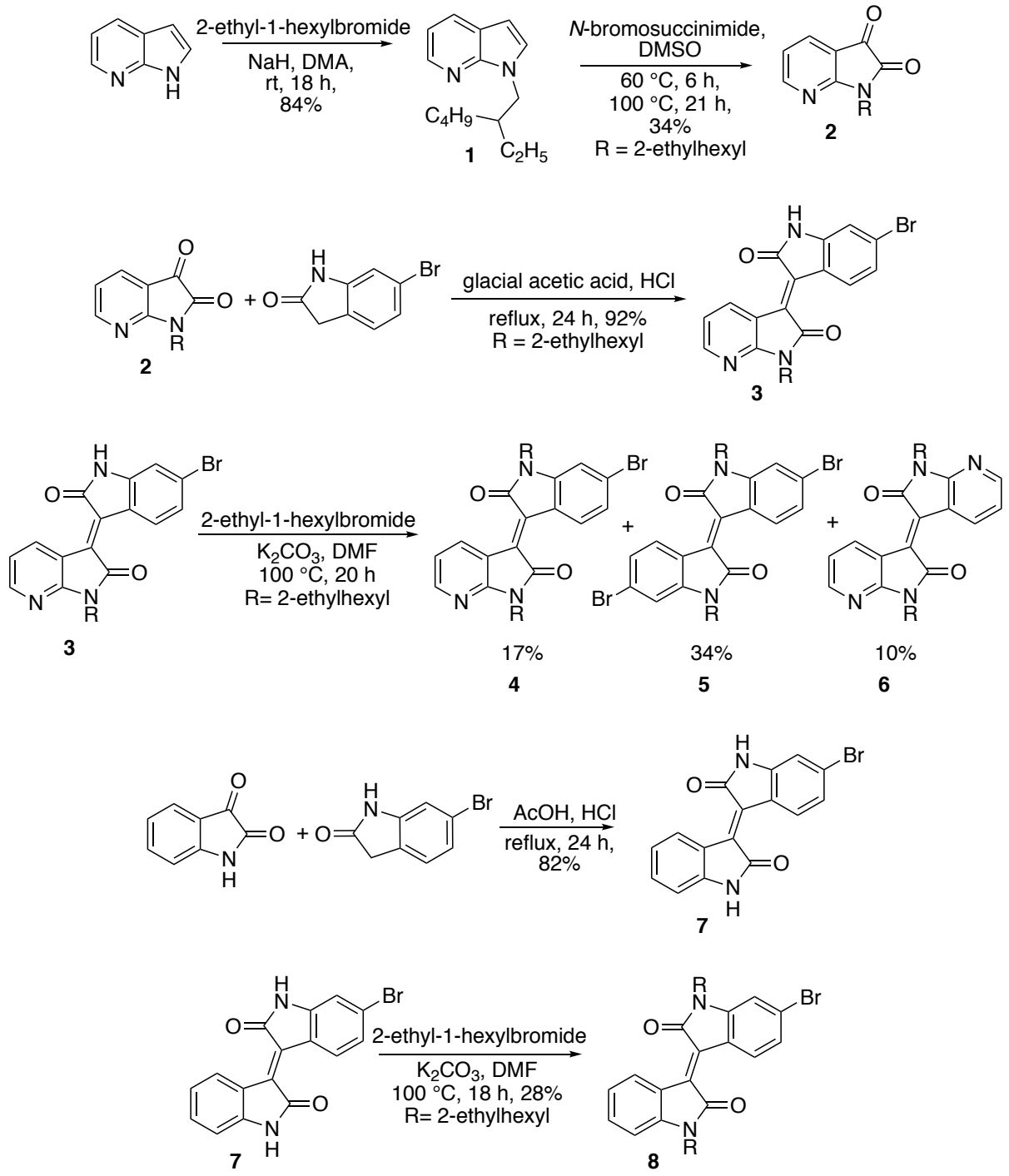

Scheme 2.1 Synthesis of acceptor units 7-aza-6′-bromoisoindigo (**4**) and 6-bromoisoindigo (**8**).

The electron donor groups chosen for this work were 2,2′-bithiophene and 3,3′-bis(dodecyloxy)-2,2′-bithiophene. 2,2′-Bithiophene was chosen in order to provide a direct comparison to previous work.[14] It was decided that in addition to using the more electron deficient azaisoindigo, an electron rich 3,3′-bis(dodecyloxy)-2,2′-bithiophene would also be synthesized. In this manner the relative effects of electron withdrawing and donating groups could be tested separately. Both 5,5′-bis(tributylstannyl)-2,2′-bithiophene (**10**)[39,40] and 5,5′-bis(tributylstannyl)-3,3′-bis(dodecyloxy)-2,2′-bithiophene (**14**)[15] were synthesized using previously reported methods (Scheme 2.2).

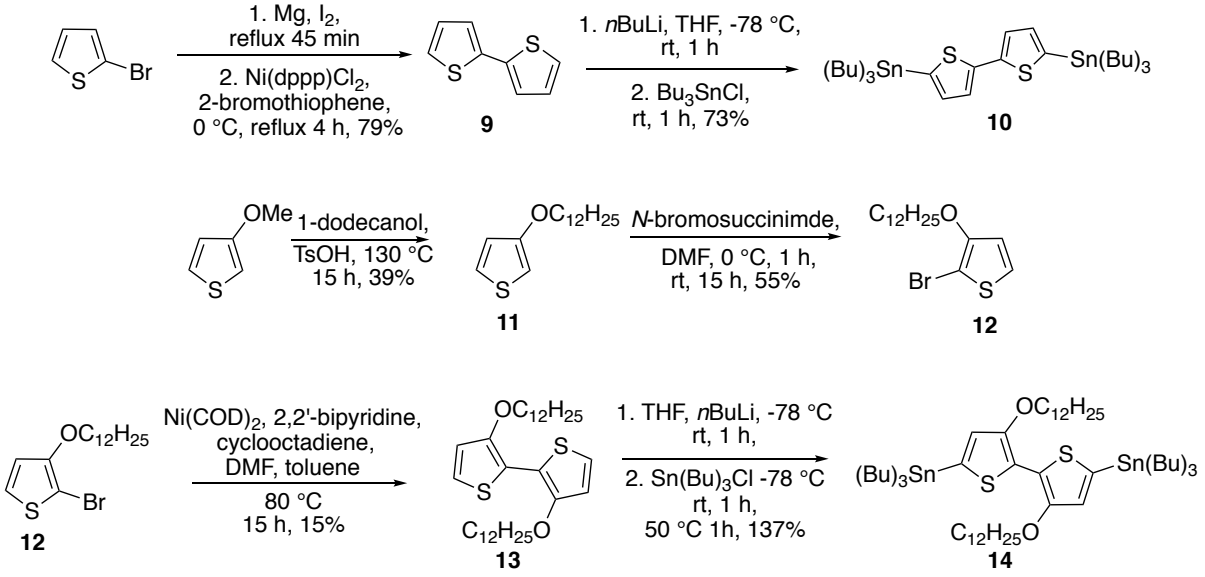

Scheme 2.2 Synthesis of donor units 2,2′-bithiophene (**10**) and 3,3′-bis(dodecyloxy)-2,2′-bithiophene (**14**).

Finally, the donor and acceptor portions of the dyes were combined via a metal-catalyzed cross-coupling. Because of the sensitivity of the isoindigo framework to basic conditions, a Stille coupling (rather than a Suzuki coupling) was chosen to couple the donor

and acceptor sub-units (Scheme 2.3). The effect of coupling the donor and acceptor was immediately visible, with the red (aza)isoindigo solutions turning a deep purple when combined with 2,2′-bithiophene and dark blue when coupled to 3,3′-bis(dodecyloxy)-2,2′-bithiophene.

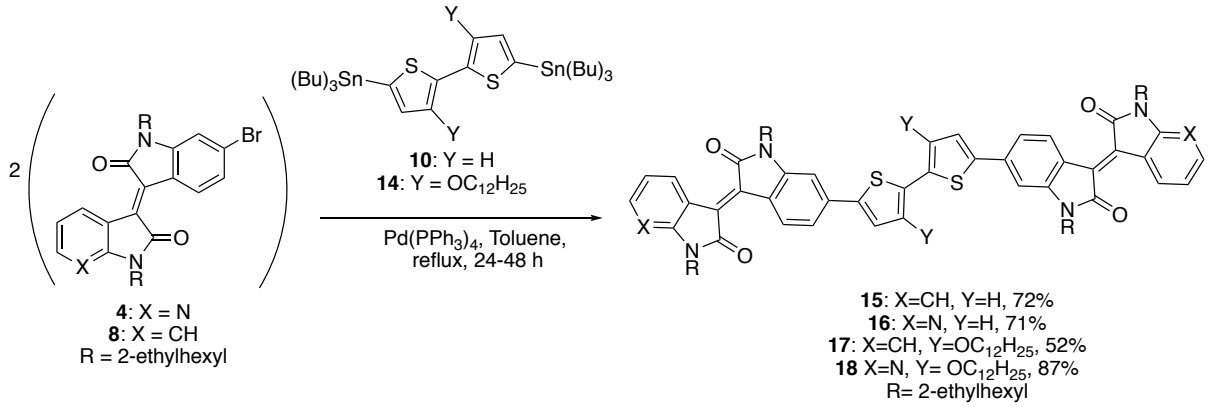

Scheme 2.3 Synthesis of compounds **15-18** via the Stille coupling of bithiophene donor units (**10** and **14**) with (aza)isoindigo acceptor units (**4** and **8**).

2.3.2 Orbital energy calculations

DFT calculations carried out using the B3LYP exchange-correlation functional with a 6-31G(d,p) basis set, were used to determine the optimized geometries and frontier orbital energy levels for each of the synthesized oligomers; the results are summarized in Table 2.1. It was anticipated that the nitrogen-containing azaisoindigo would lower the LUMO energy of the dye, while adding alkoxy groups to the bithiophene core was expected to raise the energy of the HOMO with respect to vacuum. Both of these alterations were expected to lower the HOMO/LUMO gap of the oligomers.

The effect of aza-substitution can be seen in the lower lying energy levels of **16** and **18** relative to their isoindigo counterparts; however, it appears that the inductive effect of the

nitrogen atom affects both the HOMO and LUMO equally. There is no difference in the HOMO-LUMO gap between compounds **15** and **16** and only a minor change between compounds **17** and **18**. The absolute energy of these orbitals, however, is dependent on the presence of the nitrogen heteroatom. Comparing **15** to **16** there is a 150 meV shift towards lower energies for both the HOMO and the LUMO. The effect on the 3,3′-bisalkoxybithiophene-based dyes is similar. In comparing **17** and **18**, the LUMO level decreases by 150 meV while the HOMO energy drops by 120 meV, leading to a 30 meV reduction in HOMO-LUMO gap.

The effect of alkoxy-substitution on the frontier orbital energy levels and bandgap is more pronounced. In the isoindigo-based dyes (**15** and **17**) the addition of alkoxy groups to the bithiophene core increases the HOMO energy by 420 meV, while the LUMO energy is only raised by 70 meV, leading to a red-shift in the HOMO/LUMO gap of 350 meV. A similar shift is seen in the azaisoindigo-based dyes (**16** and **18**). The HOMO level increases by 450 meV while the LUMO increases by 70 meV, lowering the HOMO-LUMO gap energy by 370 meV.

Figure 2.1 depicts the frontier molecular orbitals for **15-18**. As expected, the HOMO is predominantly localized on the electron-rich bithiophene core, while the LUMO is more localized on the (aza)isoindigo sub-units. One notable difference in the structure of the frontier orbitals is that they are much more localized in **17** and **18** than in **15** and **16**. This is attributed to the presence of the dodecyloxy groups in **17** and **18**. In these compounds the relative energies of the bithiophene π-orbitals are substantially higher than those of the (aza)isoindigo sub-unit, limiting the amount of orbital mixing that can occur. This increase in localization agrees well with the fact that there was no change in the HOMO-LUMO gap for **15** and **16** but that there is a 30 meV difference in the gap energy for **17** and **18**.

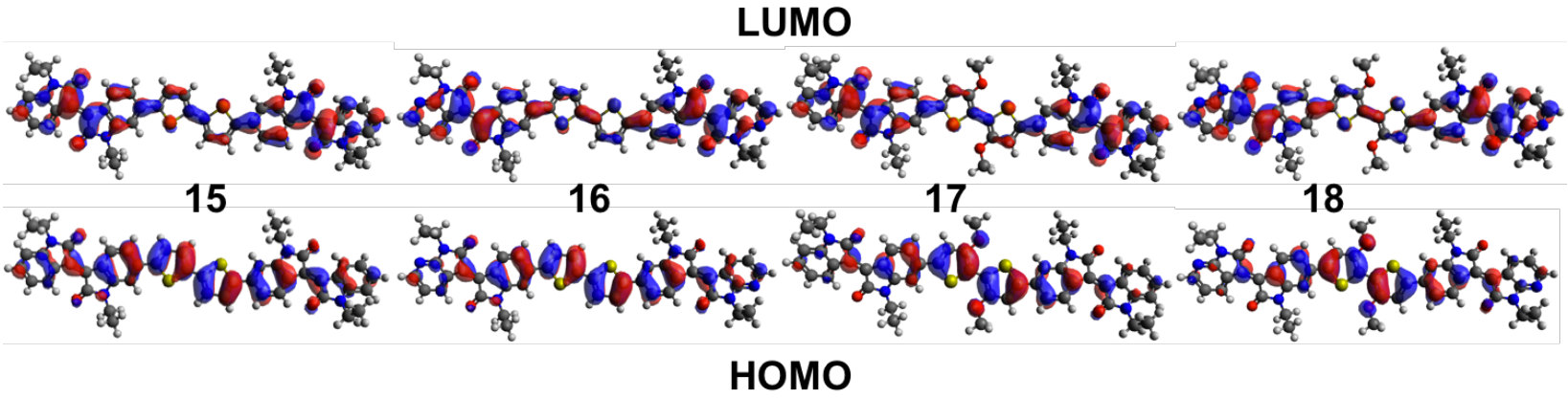

Figure 2.1 Frontier molecular orbitals of **15-18** calculated using the B3LYP exchange-correlation functional with a 6-31G(d,p) basis set.

Table 2.1 Calculated and experimental frontier orbital energy levels and electronic spectroscopy data of compounds **15-18**.

Compound	E_{HOMO} (Calc[a])(eV)	E_{LUMO} (Calc[a])(eV)	ΔE (Calc)(eV)	λ_{max} (soln)(nm)	$\varepsilon/10^4$ (soln)($M^{-1}cm^{-1}$)	$E_{g,opt}$[b] (eV)	E_{HOMO}[c] (Elec)(eV)	E_{LUMO}[c] (Elec)(eV)	ΔE (Elec)(eV)
15	-5.10	-2.85	2.25	571	2.5	1.77	-5.64	-3.86	1.78
16	-5.25	-3.00	2.25	569	1.6	1.74	-5.68	-3.92	1.76
17	-4.68	-2.78	1.90	653	5.4	1.50	-5.23	-3.95	1.28
18	-4.80	-2.93	1.87	663	4.1	1.46	-5.25	-3.92	1.33

[a]Carried out using the B3LYP exchange-correlation functional with a 6-31G(d,p) basis set. To reduce the complexity of the calculations 2-ethylhexyl groups were replaced with ethyl groups, dodecyloxy groups were replaced with methoxy groups and the calculations were performed in vacuum. [b]Optical bandgaps were taken from the absorption edge of thin film spectra. [c]Voltammagrams were referenced to the Fc/Fc^+ redox couple and subsequently referenced to vacuum (the Fc/Fc^+ redox couple was assumed to be 5.1 eV with respect to vacuum).[42] HOMO and LUMO values were taken from the onset of oxidation and reduction respectively

2.3.3 Cyclic voltammetry

The effects of both alkoxy and aza functionalities on the frontier orbital energy levels were experimentally studied by cyclic voltammetry (Figure 2.2). Both **15** and **17** show partially symmetrical peaks for both oxidation and reduction processes, with > 59 mV separation between the corresponding anodic and cathodic peaks. This is consistent with quasi-reversible behaviour. In contrast, the aza-substituted dyes have less pronounced features. Both the oxidation and reduction processes observed in **16** appear to be largely irreversible, and while **18** undergoes an oxidation process consistent with quasi-reversible behaviour, the reversibility of its first reduction peak is poor. Since this same reduction process appears to be poorly reversible in both **16** and **18**, it suggests that the reduced azaisoindigo moiety is chemically reactive. Compound **18** also shows an additional reduction process at more negative potential; however, the reversibility of the first reduction was not improved by changing sweep direction immediately after the first peak, before the second reduction occurred.

Analysis of the peak positions reveals a dramatic shift in the potential of the peak anodic current when the bithiophene is substituted with alkoxy groups. The oxidation potential is shifted to lower potentials by 0.40 V between **15** and **17**, and by 0.50 V between **16** and **18**. The replacement of isoindigo with azaisoindigo, however, has little effect on the position of the reduction peak. The differences in reduction potentials between **15** and **16** and between **17** and **18** are within experimental error.

The HOMO and LUMO energies measured using cyclic voltammetry exhibit qualitatively the same trends as those determined using DFT. Placement of alkoxy groups on the bithiophene raises the HOMO energy level by 0.4-0.5 eV, while replacing isoindigo with azaisoindigo has only a relatively minor effect on the LUMO energy. The differences in ΔE between the voltammetry

and DFT results are likely the result of the DFT calculations being carried out in the absence of a dielectric continuum or solvent model.

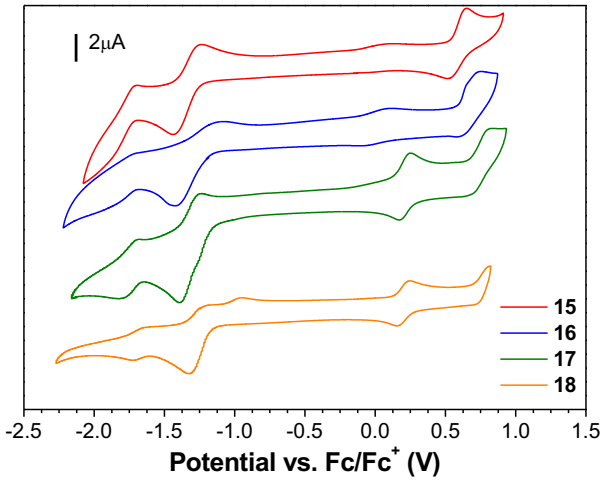

Figure 2.2 Cyclic voltammetry of **15-18** performed in 0.05 mol L^{-1} $TBAPF_6$ in CH_2Cl_2 and referenced to an internal Fc/Fc^+ standard.

2.3.4 UV/visible spectroscopy

Solution and solid state UV/visible spectroscopy were carried out on all four compounds to determine their suitability as OPV dyes (Figure 2.3). Extinction coefficients and λ_{max} values, as well as solid state optical bandgaps, are listed in Table 2.1. One of the most pronounced differences in the UV/visible spectra is that the addition of alkoxy groups to the bithiophene donor more than doubles the extinction coefficient of the broad, low energy absorption band. Since the oscillator strength of a transition is proportional to the transition dipole moment, this dramatic change in extinction coefficient is likely due to an increase in the degree of charge transfer character associated with the transition. This is in agreement with the increased localization observed in the frontier orbitals (Figure 2.1).

The inclusion of alkoxy substituents also red-shifts the λ_{max} by 82 nm in the isoindigo dyes (**15** and **17**) and by 94 nm in the azaisoindigo dyes (**16** and **18**). The presence of azaisoindigo has a much smaller effect, very slightly blue-shifting the λ_{max} from 571 nm to 569 nm between **15** and **16** and providing a slight red shift of 10 nm between **17** and **18**. The bathochromic shift between **17** and **18** is further evidence of increased orbital localization in these two dyes (Figure 2.1). Localization of the frontier orbitals would increase the inductive effect of the nitrogen on the LUMO, while decreasing its effect on the primarily bithiophene-centred HOMO.

When the chromophores are spin cast as thin films on glass slides, the features of the UV/visible spectra change dramatically (Figure 2.3b). All four dyes develop a shoulder on the low energy side of the most prominent absorption band, indicative of intermolecular interactions in the solid state. This feature is most prominent in **15**. The calculated optical bandgaps for the chromophores are summarized in Table 2.1. In all cases the band edge in the solid state occurs at lower energy than the solution phase HOMO-LUMO gap. In the case of **16**, the λ_{max} value shifts to slightly higher energy in the thin film than in solution; however, the growth of a prominent shoulder feature nonetheless red-shifts the absorption edge. In the solid state both **17** and **18** absorb well into the near- infrared, which is highly promising for their application in bulk heterojunction solar cells.

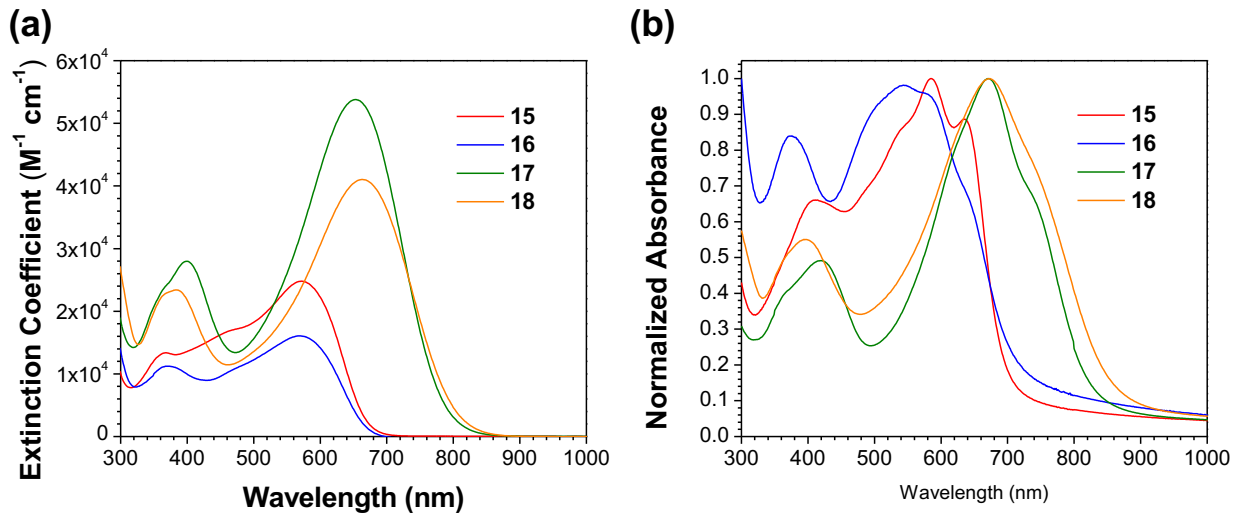

Figure 2.3 UV/visible spectra of **15-18**: (a) in chloroform solution, and (b) as thin films on glass substrates.

2.3.5 Photovoltaic cell performance

The frontier orbital energy levels of **15**–**18** may make them suitable for use as either the electron accepting or donating component of the active layer in a bulk heterojunction solar cell. The most electron deficient dyes (**15** and **16**) were first evaluated for their ability to act as electron acceptors by blending them with P3HT and fabricating OPV devices. These devices performed very poorly (Table 2.2, Figure 2.4 and 2.5), with maximum PCEs of 0.016% and 0.002% for **15** and **16**, respectively. Since the more electron-rich alkoxy-substituted compounds **17** and **18** are unlikely to perform better as electron acceptors, this suggests that these compounds are best utilized as electron donors in BHJ devices.

Table 2.2 Performance of ITO/PEDOT:PSS/8:10 P3HT:**15** or **16**/LiF/Al BHJ solar cells.

Compound	V_{OC}[a] (V)	J_{SC}[a] (mA cm^{-2})	Fill Factor[a] (%)	PCE[a] (%)	Best PCE (%)
15	0.2 ± 0.1	0.15 ± 0.03	27 ± 1	0.008 ± 0.005	0.016
16	0.25 ± 0.06	0.022 ± 0.005	28 ± 1	0.0015 ± 0.0005	0.002

[a]Averages and standard deviations for each data set were determined from measurements on a minimum of 6 separate devices

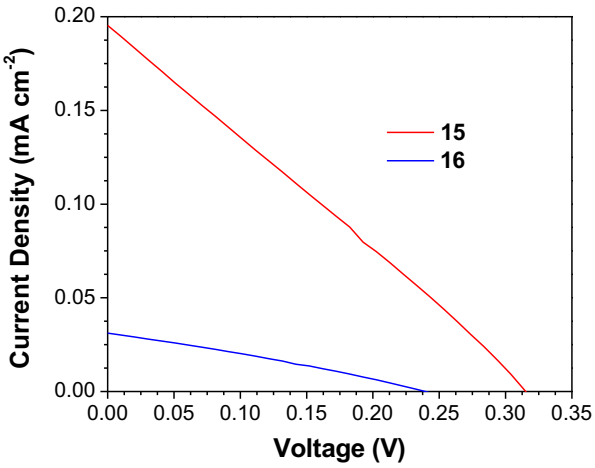

Figure 2.4 Current-voltage curves for the most efficient BHJ solar cells based on active layers of P3HT:**15-16** (10:8 by mass). All devices were based on the ITO/PEDOT:PSS/P3HT:**15** or **16**/LiF/Al architecture.

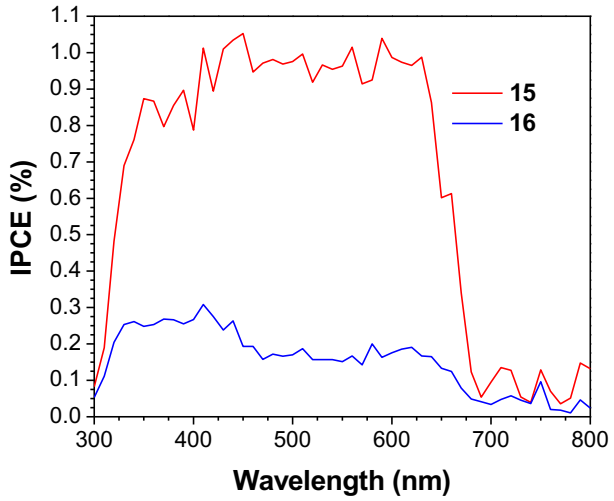

Figure 2.5 IPCE spectra of the most efficient BHJ solar cells based on active layers of P3HT:**15**-**16** (10:8 by mass). All devices were based on the ITO/PEDOT:PSS/P3HT:**15** or **16**/LiF/Al architecture.

In order to assess the performance of **15**–**18** as electron donors, OPV devices were fabricated by blending each of the four dyes with $PC_{61}BM$, and the *J*-*V* characteristics of the highest performing devices are shown in Figure 2.6. The performance of OPVs incorporating **15** and $PC_{61}BM$ is in good agreement with the previous report of Mei *et al.*[14] Table 2.3 summarizes the device performance parameters of the cells based on each of the four oligomers.

From the data in Table 2.3, two major trends can be observed. The first is that alkoxy substitution of the bithiophene core (compound **17** compared to **15**) results in a net improvement in PCE. The average data suggests that this increase in efficiency is primarily due to an increase in the fill factor; however, from the *J*–*V* curves of the most efficient cells, it can also be observed that an increase in J_{SC} also plays a role. Further evidence for this can be found by comparing the IPCE spectra of the most efficient devices (Figure 2.7). The IPCE of cells containing **17** is substantially higher across the entire spectrum than the IPCE of cells containing **15**, reflecting the larger extinction coefficient of **17**. Furthermore, the IPCE spectrum of the device containing **17**

extends substantially further into the near-infrared. Both spectra match well to the absorption spectra of thin films of **15** and **17**.

Table 2.3 Performance of ITO/PEDOT:PSS/60:40 **15-18**:PC61BM/LiF/Al BHJ solar cells.

Compound	V_{OC}[a] (V)	J_{SC}[a] (mA cm^{-2})	Fill Factor[a] (%)	PCE[a] (%)	Best PCE(%)
15	0.66 ± 0.05	2.7 ± 0.3	31 ± 3	0.6 ± 0.1	0.74
16	0.28 ± 0.09	0.22 ± 0.04	28 ± 2	0.018 ± 0.006	0.03
17	0.67 ± 0.01	2.5 ± 0.9	40 ± 3	0.7 ± 0.2	0.93
18	0.3 ± 0.1	0.6 ± 0.2	22 ± 2	0.04 ± 0.02	0.07

[a]Averages and standard deviations for each data set were determined from measurements on a minimum of 23 devices.

The second, and most notable, trend in device performance is that the devices incorporating the azaisoindigo-based dyes (**16** and **18**) performed very poorly when compared to **15** and **17**. The devices that used the azaisoindigo-based dye **16** were over an order of magnitude less efficient than those that used the isoindigo-based analogue **15**. Similar results are obtained when the performance of devices based on compounds **17** (0.67%) and **18** (0.04%) is compared. The IPCE spectra of devices based on **16** and **18** are shown in Figure 2.8, and reflect the poor J_{SC} values of both devices. Given the very similar frontier orbital energy levels and solid-state UV/visible spectra of compounds **15** and **16**, and compounds **17** and **18**, these results are somewhat surprising.

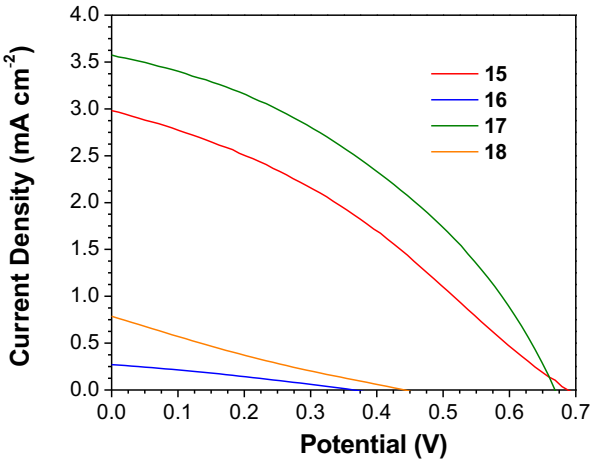

Figure 2.6 Current-voltage curves for the most efficient BHJ solar cells based on active layers of **15-18**:$PC_{61}BM$ (60:40 by mass). All devices were based on the ITO/PEDOT:PSS/**15-18**:$PC_{61}BM$/LiF/Al architecture.

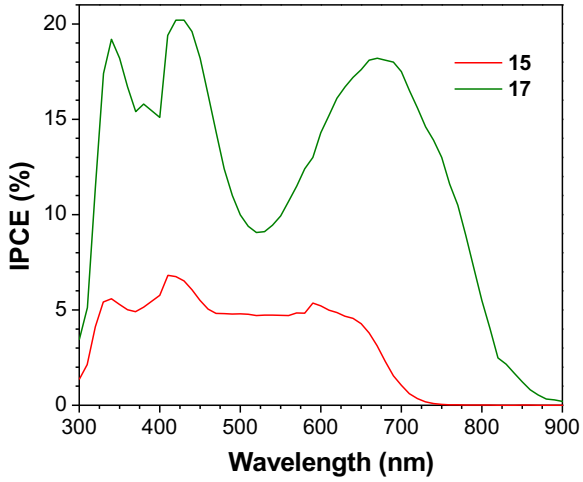

Figure 2.7 IPCE spectra of the most efficient BHJ solar cells based on active layers of **15** or **17**:$PC_{61}BM$ (60:40 by mass). All devices were based on the ITO/PEDOT:PSS/**15** or **17**:$PC_{61}BM$/LiF/Al architecture.

From Table 2.3, it can be seen that one of the main causes of the poor efficiency for the devices that use the azaisoindigo-based dyes is a poor fill factor. From the slope of the *J*–*V* curve as it approaches V_{OC} (Figure 2.6) it can be seen that this is caused by a low R_{Sh}. The low R_{Sh} also explains the very low values of V_{OC}, which are much lower than would be predicted from the

difference between the donor HOMO and the LUMO of $PC_{61}BM$. This suggests that recombination within the active layer may be a substantial obstacle to the use of **16** and **18** in OPV devices. **18** performed slightly better than **16** in test devices, owing to its more intense and red-shifted absorption bands (Figure 2.3b), which produced slightly higher values of both IPCE (Figure 2.8) and J_{SC}.

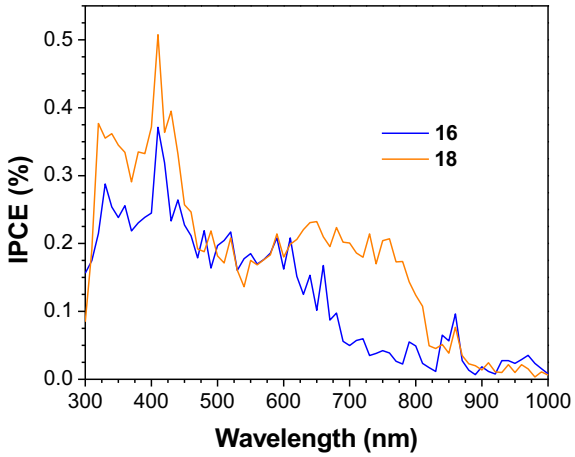

Figure 2.8 IPCE spectra of the most efficient BHJ solar cells based on active layers of **16** or **18**:$PC_{61}BM$ (60:40 by mass). All devices were based on the ITO/PEDOT:PSS/**16** or **18**:$PC_{61}BM$/LiF/Al architecture.

2.3.6 Atomic force microscopy

One possible explanation for the poor performance of **16** and **18** is that the presence of the nitrogen atom in the isoindigo structure negatively affected the morphology of the bulk heterojunction. In order to determine if this was the case, AFM images were recorded of films of dyes **15**–**18** blended with $PC_{61}BM$. Measurements were conducted on OPV substrates in areas lacking the metal cathode, and the height contrasted AFM images for each active layer blend are shown in Figure 2.9. The film morphology of **1** and $PC_{61}BM$ closely resembles that of previous

reports.[14] The morphologies of the blends containing **16** and **18** were not substantially different from those of **15** and **17**, and no definite correlations could be drawn between the blend morphologies of the azaisoindigo-based dyes and their poor photovoltaic performance. The root-mean-square roughness (R_q) of all films is similar, again suggesting that the morphology is not responsible for the observed decrease in performance. Additionally, since the energy levels of **16** and **18** are quite similar to those of **15** and **17** (Table 2.1), it is unlikely that a decrease in the amount of exciton dissociation is responsible for the lower efficiencies.

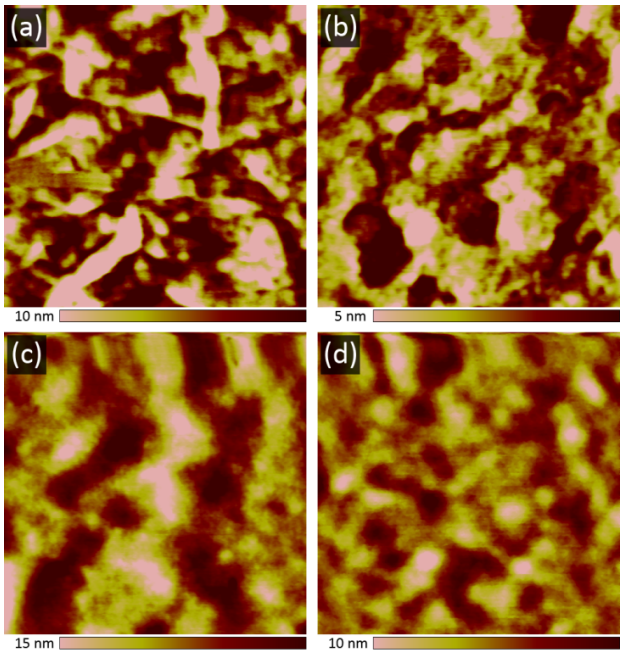

Figure 2.9 Tapping mode AFM height images of 60:40 blends of: (a) **15**:$PC_{61}BM$, (b) **16**:$PC_{61}BM$, (c) **17**:$PC_{61}BM$, and (d) **18**:$PC_{61}BM$. Blends were spin coated from chlorobenzene onto thin films of PEDOT:PSS and annealed at 100 °C for 20 min. R_q values: (a) 4.6 nm, (b) 1.8 nm, (c) 3.8 nm, (d) 2.0 nm. All images have dimensions of 1 μm × 1 μm.

After ruling out morphological effects, it is most likely that the poor performance of the OPVs incorporating **16** and **18** is due to a reduced hole mobility in the electron donor. In their work on benzothiadiazole-based polymers, Blouin *et al*. also synthesized a pyridalthiadiazole -

based system[43] and found that the pyridal analogue had a hole mobility two orders of magnitude lower than the benzothiadiazole-based parent polymer. Steinberger *et al*. have also developed similar DA oligomers based on pyridalthiadiazole,[44] and found that while the compounds worked well when incorporated into planar junction solar cells, when incorporated into a BHJ the performance dropped dramatically. This is consistent with the findings of Blouin *et al*., since there should be an increased dependence on charge carrier mobility in the BHJ device. These precedents lend credence to the hypothesis that a low hole mobility is the driving force behind the relatively poor efficiency of **16** and **18** in OPV devices.

2.4 Conclusions

In conclusion, the use of azaisoindigo in optoelectronic applications for the first time has been presented. Using a modular synthetic strategy, a series of acceptor-donor-acceptor dyes incorporating either azaisoindigo or isoindigo as the electron acceptor and either 2,2′-bithiophene or 3,3′-bis(dodecyloxy)-2,2′-bithiophene as the electron donor have been synthesized. The electronic structure of these dyes was investigated using DFT calculations, cyclic voltammetry and electronic spectroscopy. It was discovered that the dyes incorporating 3,3′-bis(dodecyloxy)-2,2′-bithiophene had large extinction coefficients and also absorbed well into the near-infrared, meeting two important criteria for their use in OPV applications. The replacement of isoindigo with 7-azaisoindigo induced a slight red-shift in the absorption spectrum of dyes bearing the bis(alkoxythiophene) donors; however, the effects of aza-substitution of isoindigo were small compared with the electron donating effects of the dodecyloxy groups.

All four dyes were subsequently used as the electron donor in the active layer of bulk heterojunction solar cells. Devices that used the isoindigo/bis(alkoxythiophene) dye (**17**)

performed the best, with PCEs reaching 0.93%. Both compounds based on 7-azaisoindigo performed poorly relative to their isoindigo counterparts, likely due to a reduction in hole mobility. These results clearly demonstrate a number of important structure-property relationships in the design of small molecule chromophores for organic photovoltaic devices.

2.5 Acknowledgements

The Natural Science and Engineering Research Council of Canada (NSERC) and the University of Saskatchewan are acknowledged for financial support. T.L.K. is a Canada Research Chair in Photovoltaics. This research was undertaken, in part, thanks to funding from the Canada Research Chairs Program. N.M.R. thanks NSERC and the Government of Saskatchewan (Saskatchewan Opportunity and Innovation scholarship) for scholarship funding.

2.6 References

(1) Henson, Z. B.; Welch, G. C.; van der Poll, T.; Bazan, G. C. Pyridalthiadiazole-Based Narrow Band Gap Chromophores. *J. Am. Chem. Soc.* **2012**, *134*, 3766–3779.

(2) Sun, Y. Solution-Processed Small-Molecule Solar Cells with 6.7% Efficiency. *Nat Mater.* **2011**, *11*, 44–48.

(3) Tamayo, A. B.; Walker, B.; Nguyen, T.-Q. A Low Band Gap, Solution Processable Oligothiophene with a Diketopyrrolopyrrole Core for Use in Organic Solar Cells. *J. Phys. Chem. C* **2008**, *112*, 11545–11551.

(4) Weidelener, M.; Wessendorf, C. D.; Hanisch, J.; Ahlswede, E.; Götz, G.; Lindén, M.; Schulz, G.; Mena-Osteritz, E.; Mishra, A.; Bäuerle, P. Dithienopyrrole-Based Oligothiophenes for Solution-Processed Organic Solar Cells. *Chem. Commun.* **2013**, *49*, 10865-10867.

(5) Haid, S.; Marszalek, M.; Mishra, A.; Wielopolski, M.; Teuscher, J.; Moser, J.-E.; Humphry-Baker, R.; Zakeeruddin, S. M.; Grätzel, M.; Bäuerle, P. Significant Improvement of Dye-Sensitized Solar Cell Performance by Small Structural Modification in π-Conjugated Donor–Acceptor Dyes. *Adv. Funct. Mater.* **2012**, *22*, 1291–1302.

(6) Steinberger, S.; Mishra, A.; Reinold, E.; Mena-Osteritz, E.; Müller, H.; Uhrich, C.; Pfeiffer, M.; Bäuerle, P. Synthesis and Characterizations of Red/Near-IR Absorbing A–D–A–D–A-Type Oligothiophenes Containing Thienothiadiazole and Thienopyrazine Central Units. *J. Mater. Chem.* **2012**, *22*, 2701–2712.

(7) Welch, G. C.; Perez, L. A.; Hoven, C. V.; Zhang, Y.; Dang, X.-D.; Sharenko, A.; Toney, M. F.; Kramer, E. J.; Nguyen, T.-Q.; Bazan, G. C. A Modular Molecular Framework for Utility in Small-Molecule Solution-Processed Organic Photovoltaic Devices. *J. Mater. Chem.* **2011**, *21*, 12700-12709.

(8) Heliatek Consolidates Its Technology Leadership by Establishing a New World Record for Organic Solar Technology with a Cell Efficiency of 12% http://www.heliatek.com/wp-content/uploads/2013/01/130116_PR_Heliatek_achieves_record_cell_effiency_for_OPV.pdf, retrieved October 8, 2013.

(9) Lin, Y.; Li, Y.; Zhan, X. Small Molecule Semiconductors for High-Efficiency Organic Photovoltaics. *Chem. Soc. Rev.* **2012**, *41*, 4245-4272.

(10) Mishra, A.; Bäuerle, P. Small Molecule Organic Semiconductors on the Move: Promises for Future Solar Energy Technology. *Angew. Chem. Int. Ed.* **2012**, *51*, 2020–2067.

(11) Dennler, G.; Scharber, M. C.; Brabec, C. J. Polymer-Fullerene Bulk-Heterojunction Solar Cells. *Adv. Mater.* **2009**, *21*, 1323–1338.

(12) Shang, H.; Fan, H.; Liu, Y.; Hu, W.; Li, Y.; Zhan, X. A Solution-Processable Star-Shaped Molecule for High-Performance Organic Solar Cells. *Adv. Mater.* **2011**, *23*, 1554–1557.

(13) Wan, M.; Zhu, H.; Deng, H.; Jin, L.; Guo, J.; Huang, Y. Low Band-Gap Modulation of Isoindigo-Based Copolymers Toward High Open-Circuit Voltage of Polymer Solar Cells. *J. Polym. Sci. A Polym. Chem.* **2013**, *51*, 3477–3485.

(14) Mei, J.; Graham, K. R.; Stalder, R.; Reynolds, J. R. Synthesis of Isoindigo-Based Oligothiophenes for Molecular Bulk Heterojunction Solar Cells. *Org. Lett.* **2010**, *12*, 660–663.

(15) Guo, X.; Watson, M. D. Conjugated Polymers From Naphthalene Bisimide. *Org. Lett.* **2008**, *10*, 5333–5336.

(16) Chen, J.; Cao, Y. Development of Novel Conjugated Donor Polymers for High-Efficiency Bulk-Heterojunction Photovoltaic Devices. *Acc. Chem. Res.* **2009**, *42*, 1709–1718.

(17) Karsten, B. P.; Bijleveld, J. C.; Janssen, R. A. J. Diketopyrrolopyrroles as Acceptor Materials in Organic Photovoltaics. *Macromol. Rapid Commun.* **2010**, *31*, 1554–1559.

(18) Wienk, M. M.; Turbiez, M.; Gilot, J.; Janssen, R. A. J. Narrow-Bandgap Diketo-Pyrrolo-Pyrrole Polymer Solar Cells: the Effect of Processing on the Performance. *Adv. Mater.* **2008**, *20*, 2556–2560.

(19) Bijleveld, J. C.; Zoombelt, A. P.; Mathijssen, S. G. J.; Wienk, M. M.; Turbiez, M.; de Leeuw, D. M.; Janssen, R. A. J. Poly(Diketopyrrolopyrrole−Terthiophene) for Ambipolar Logic and Photovoltaics. *J. Am. Chem. Soc.* **2009**, *131*, 16616–16617.

(20) Howard, I. A.; Laquai, F.; Keivanidis, P. E.; Friend, R. H.; Greenham, N. C. Perylene Tetracarboxydiimide as an Electron Acceptor in Organic Solar Cells: a Study of Charge Generation and Recombination. *J. Phys. Chem. C* **2009**, *113*, 21225–21232.

(21) Zhang, X.; Lu, Z.; Ye, L.; Zhan, C.; Hou, J.; Zhang, S.; Jiang, B.; Zhao, Y.; Huang, J.; Zhang, S.; Liu, Y.; Shi, Q.; Liu, Y.; Yao, J. A Potential Perylene Diimide Dimer-Based Acceptor Material for Highly Efficient Solution-Processed Non-Fullerene Organic Solar Cells with 4.03% Efficiency. *Adv. Mater.* **2013**, *25*, 5791–5797.

(22) Chen, Z.; Zheng, Y.; Yan, H.; Facchetti, A. Naphthalenedicarboximide- vs Perylenedicarboximide-Based Copolymers. Synthesis and Semiconducting Properties in Bottom-Gate N-Channel Organic Transistors. *J. Am. Chem. Soc.* **2009**, *131*, 8–9.

(23) Segura, J. L.; Herrera, H.; Bäuerle, P. Oligothiophene-Functionalized Naphthalimides and Perylene Imides: Design, Synthesis and Applications. *J. Mater. Chem.* **2012**, *22*, 8717-8733.

(24) Stalder, R.; Mei, J.; Graham, K. R.; Estrada, L. A.; Reynolds, J. R. Isoindigo, a Versatile Electron-Deficient Unit for High-Performance Organic Electronics. *Chem. Mater.* **2014**, *26*, 664–678.

(25) Stalder, R.; Mei, J.; Subbiah, J.; Grand, C.; Estrada, L. A.; So, F.; Reynolds, J. R. n-Type Conjugated Polyisoindigos. *Macromolecules* **2011**, *44*, 6303–6310.

(26) Wang, T.; Chen, Y.; Bao, X.; Du, Z.; Guo, J.; Wang, N.; Sun, M.; Yang, R. A New Isoindigo-Based Molecule with Ideal Energy Levels for Solution-Processable Organic Solar Cells. *Dyes Pigm.* **2013**, *98*, 11–16.

(27) Yang, M.; Chen, X.; Zou, Y.; Pan, C.; Liu, B.; Zhong, H. A Solution-Processable D–A–D Small Molecule Based on Isoindigo for Organic Solar Cells. *J. Mater. Sci.* **2013**, *48*, 1014–1020.

(28) Cao, K.; Wu, Z.; Li, S.; Sun, B.; Zhang, G.; Zhang, Q. A Low Bandgap Polymer Based on Isoindigo and Bis(Dialkylthienyl)Benzodithiophene for Organic Photovoltaic Applications. *J. Polym. Sci. A Polym. Chem.* **2012**, *51*, 94–100.

(29) Wang, E.; Ma, Z.; Zhang, Z.; Vandewal, K.; Henriksson, P.; Inganäs, O.; Zhang, F.; Andersson, M. R. An Easily Accessible Isoindigo-Based Polymer for High-Performance Polymer Solar Cells. *J. Am. Chem. Soc.* **2011**, *133*, 14244–14247.

(30) Wang, C.; Zhao, B.; Cao, Z.; Shen, P.; Tan, Z.; Li, X.; Tan, S. Enhanced Power Conversion Efficiencies in Bulk Heterojunction Solar Cells Based on Conjugated Polymer with Isoindigo Side Chain. *Chem. Commun.* **2013**, *49*, 3857-3859.

(31) Mahmood, K.; Liu, Z.-P.; Li, C.; Lu, Z.; Fang, T.; Liu, X.; Zhou, J.; Lei, T.; Pei, J.; Bo, Z. Novel Isoindigo-Based Conjugated Polymers for Solar Cells and Field Effect Transistors. *Polym. Chem.* **2013**, *4*, 3563-3574.

(32) Sun, W.; Ma, Z.; Dang, D.; Zhu, W.; Andersson, M. R.; Zhang, F.; Wang, E. An Alternating D–A1–D–A2 Copolymer Containing Two Electron-Deficient Moieties for Efficient Polymer Solar Cells. *J. Mater. Chem. A* **2013**, *1*, 11141–11144.

(33) Grenier, F.; Berrouard, P.; Pouliot, J.-R.; Tseng, H.-R.; Heeger, A. J.; Leclerc, M. Synthesis of New n-Type Isoindigo Copolymers. *Polym. Chem.* **2013**, *4*, 1836-1841.

(34) Ying, W.; Guo, F.; Li, J.; Zhang, Q.; Wu, W.; Tian, H.; Hua, J. Series of New D-A-π-A Organic Broadly Absorbing Sensitizers Containing Isoindigo Unit for Highly Efficient Dye-Sensitized Solar Cells. *ACS Appl. Mater. Interfaces* **2012**, *4*, 4215–4224.

(35) Lei, T.; Dou, J.-H.; Ma, Z.-J.; Yao, C.-H.; Liu, C.-J.; Wang, J.-Y.; Pei, J. Ambipolar Polymer Field-Effect Transistors Based on Fluorinated Isoindigo: High Performance and Improved Ambient Stability. *J. Am. Chem. Soc.* **2012**, *134*, 20025–20028.

(36) Lei, T.; Dou, J.-H.; Ma, Z.-J.; Liu, C.-J.; Wang, J.-Y.; Pei, J. Chlorination as a Useful Method to Modulate Conjugated Polymers: Balanced and Ambient-Stable Ambipolar High-Performance Field-Effect Transistors and Inverters Based on Chlorinated Isoindigo Polymers. *Chem. Sci.* **2013**, *4*, 2447–2452.

(37) Deng, Y.; Liu, J.; Wang, J.; Liu, L.; Li, W.; Tian, H.; Zhang, X.; Xie, Z.; Geng, Y.; Wang, F. Dithienocarbazole and Isoindigo Based Amorphous Low Bandgap Conjugated Polymers for Efficient Polymer Solar Cells. *Adv. Mater.* **2013**, *26*, 471–476.

(38) Tatsugi, J.; Zhiwei, T.; Izawa, Y. An Improved Preparation of Isatins From Indoles. *Arkivoc* **2001**, *1*, 67–73.

(39) Wu, R.; Schumm, J. S.; Pearson, D. L.; Tour, J. M. Convergent Synthetic Routes to Orthogonally Fused Conjugated Oligomers Directed Toward Molecular Scale Electronic Device Applications. *J. Org. Chem.* **1997**, *61*, 6906–6921.

(40) Huang, J.; Miragliotta, J.; Becknell, A.; Katz, H. E. Hydroxy-Terminated Organic Semiconductor-Based Field-Effect Transistors for Phosphonate Vapor Detection. *J. Am. Chem. Soc.* **2007**, *129*, 9366–9376.

(41) Kritsanida, M.; Magiatis, P.; Skaltsounis, A.-L.; Peng, Y.; Li, P.; Wennogle, L. P. Synthesis and Antiproliferative Activity of 7-Azaindirubin-3′-Oxime, a 7-Aza Isostere of the Natural Indirubin Pharmacophore. *J. Nat. Prod.* **2009**, *72*, 2199–2202.

(42) Beaujuge, P. M.; Vasilyeva, S. V.; Liu, D. Y.; Ellinger, S.; McCarley, T. D.; Reynolds, J. R. Structure-Performance Correlations in Spray-Processable Green Dioxythiophene-Benzothiadiazole Donor–Acceptor Polymer Electrochromes. *Chem. Mater.* **2012**, *24*, 255–268.

(43) Blouin, N.; Michaud, A.; Gendron, D.; Wakim, S.; Blair, E.; Neagu-Plesu, R.; Belletête, M.; Durocher, G.; Tao, Y.; Leclerc, M. Toward a Rational Design of Poly(2,7-Carbazole) Derivatives for Solar Cells. *J. Am. Chem. Soc.* **2008**, *130*, 732–742.

(44) Steinberger, S.; Mishra, A.; Reinold, E.; Levichkov, J.; Uhrich, C.; Pfeiffer, M.; Bäuerle, P. Vacuum-Processed Small Molecule Solar Cells Based on Terminal Acceptor-Substituted Low-Band Gap Oligothiophenes. *Chem. Commun.* **2011**, *47*, 1982.

Chapter 3

Lewis Acid-Base Chemistry of 7-Azaisoindigo-Based Organic Semiconductors

Adapted with permission from

Randell, N. M.; Fransishyn, K. M.; Kelly, T. L.

ACS Applied Materials & Interfaces, **2017**, *9, 24788–24796. DOI: 10.1021/acsami.7b06335*

Consent was obtained from all co-authors to include this manuscript in the thesis. Unless otherwise noted, I performed all experimental work and wrote the first draft of the manuscript. K.F. Fransishyn performed the titration of **1** with trifluoroacetic acid, as well as titrations of **1** and **2** with BF_3•Et_2O. He also completed the ^1H NMR spectral titrations, and the thin film-vapor phase coordination experiment. These experiments were performed as a part of K.F. Fransishyn's Chemistry 483 project under my supervision. T.L. Kelly directed the study and revised the manuscript.

Transition

This chapter is a direct continuation of the work presented on azaisoindigo-based semiconductors in Chapter 2. While attempting to explain the poor OPV performance of the azaisoindigo-based semiconductors, I discovered that the pyridinic nitrogen of these molecules could be protonated resulting in a distinct colour change. This chapter presents the research on semiconductor Lewis acid-base adducts that followed.

Except for a brief overview of near-infrared absorbing semiconductors and a short overview of isoindigo-based materials, the introduction section of this chapter focuses primarily on new information revolving around Lewis acid-base chemistry in organic π-conjugated materials. Again, I feel that the repetitive information in the introduction section of this chapter is important for establishing the state of the art in organic semiconductor research at the time the original manuscript was written.

3.1 Introduction

Low band gap organic semiconductors are of great interest in a number of applications, from OPVs to near-infrared photodetectors and OFETs.[1-4] One of the most common methods for producing narrow band gap semiconductors is by juxtaposing electron-rich and electron-deficient aromatic groups. This synthetic design serves to partially isolate the HOMO and LUMO on the electron-rich donor and the electron-deficient acceptor, respectively.[5] This lowers the molecule's HOMO-LUMO gap and imparts some charge transfer character to the HOMO→LUMO transition, increasing its transition dipole moment. These materials are typically referred to as donor-acceptor materials. Adding additional electron-donating or electron-withdrawing groups to the donor and acceptor acts to further decrease the HOMO-LUMO gap and can shift the electronic absorption bands well into the near-infrared.

In recent years, isoindigo has gained popularity as the electron-deficient component of donor-acceptor materials for OPVs and OFETs.[6-11] By combining isoindigo with electron-rich groups, such as oligothiophenes, very low band gap materials can be synthesized.[12-16] While isoindigo has already been combined with a wide variety of electron rich groups, fewer alterations to the isoindigo core have been made. Adding more electron withdrawing groups to the isoindigo skeleton is one way to further red-shift the absorption spectrum of the resulting semiconductor. Halogenated derivatives, such as fluoro- and chloro-isoindigo, have been successfully incorporated into new organic semiconductors; they show improved ambipolar charge carrier mobility over non-halogenated derivatives.[17-20] Thienoisoindigo-based materials, which replace the benzo-fused pyrrolidone ring with the thieno-fused analogue, show similarly improved mobilities.[21-24] Ring-fused extensions of isoindigo, including thieno-substituted derivatives and dimerized isoindigo structures, also exhibit lower band gaps and higher carrier mobilities.[25-27]

Recently, a series of small-molecule organic semiconductors based on 7-azaisoindigo (**1** and **2**, Scheme 3.1) was reported; a nitrogen heteroatom was added to the isoindigo core with the goal of reducing the LUMO energy and increasing the molecule's electron affinity.[28] Shortly afterward, 7,7′-diazaisoindigo was synthesized by de Miguel *et al.*, and an in-depth study of its photophysical properties was carried out.[29] More recently, polymers incorporating 7,7′-diazaisoindigo into the repeat unit were shown to exhibit good ambipolar charge transport characteristics.[30-32]

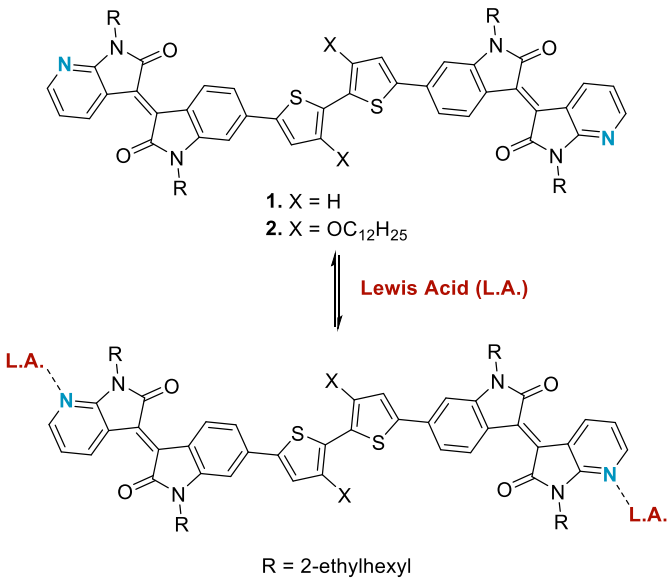

Scheme 3.1 Coordination of Lewis acids to compounds **1** and **2**.

The addition of nitrogen heteroatoms to the backbone of π-conjugated materials provides a unique opportunity to tune optoelectronic properties by the controlled addition of Lewis acids. Pioneering work by Bunz and co-workers was performed in this area in the early 2000's; they showed that the UV/vis absorption spectra of cruciform-shaped π-conjugated systems containing nitrogen heteroatoms could be tuned by the addition of a Lewis acid such as H^+ or Zn^{2+}.[33-36] In 2009, Welch *et al.* discovered that adding tris(pentafluorophenyl)borane to a solution of a

benzothiadiazole-based organic semiconductor induced a 200 nm red-shift in its HOMO to LUMO transition.[37] Two isosbestic points were observed, corresponding to the coordination of one $B(C_6F_5)_3$ molecule to the most sterically accessible azole nitrogen of each of two benzothiadiazoles. Following this work, Welch and Bazan developed a series of pyridalthiadiazole-bearing oligomers and polymers.[38] Comparative studies with the benzothiadiaozle analogues proved that the coordination of the Lewis acid was occurring at the more basic pyridine nitrogen, rather than the azole site. The coordination of $B(C_6F_5)_3$ to the pyridalthiadiazole was shown to lower both the HOMO and LUMO energies. The effect on the LUMO energy was more pronounced, leading to a decrease in the optical band gap. In 2012 Zalar *et al*. went on to show that the emission spectrum of organic light emitting diodes featuring pyridine-bearing conjugated polymers could be tuned by doping with $B(C_6F_5)_3$.[39] Following this, Zalar *et al.* demonstrated that doping the active layer of a hole-only device with 0.02 equivalents of $B(C_6F_5)_3$ increased the hole mobility of the organic layer by two orders of magnitude.[40] In addition to work with boron-based Lewis acids, Ratcliff *et al.* studied trap states in OPV active layers caused by the protonation of pyridine-containing organic semiconductors by acidic interlayers; it was demonstrated that coordination of H^+ at the interface had a negative impact on the efficiencies of the resulting OPVs.[41] In a recent work, Pingel *et al.* demonstrated that the well-studied polymer poly(3-hexylthiophene) could be p-doped with tris(pentafluorophenyl)borane, resulting in an increase in the hole mobility and conductivity of the polymer in hole-only diodes.[42]

Like pyridalthiadiazole, azaisoindigo also contains a pyridinic nitrogen. In a recent report on azaisoindigo-bearing organic semiconductors, the addition of an electronegative nitrogen atom did not substantially alter the position of the LUMO; however, the previous Lewis acid-base chemistry with pyridalthiadiazole semiconductors suggests that Lewis acids could be used to

further tune the energies of the frontier molecular orbitals. In this work, it is shown that the coordination of two different Lewis acids, trifluoroacetic acid (TFA) and $BF_3 \cdot Et_2O$, to organic semiconductors containing 7-azaisoindigo causes a large red-shift in their optical band gap. Using a combination of UV/vis and ^1H NMR spectroscopy, in tandem with TDDFT calculations, the Lewis adducts that are formed are identified. Finally, it is demonstrated that this Lewis acid-base interaction can also occur at the solid/vapor interface, suggesting that the chemistry could be used to alter the performance of a variety of organic electronic devices.

3.2 Experimental

3.2.1 Materials and methods

All chemicals were purchased from commercial suppliers and used as received. Compounds **1** and **2** were synthesized according to a previous literature report.[28] UV/vis spectroscopy was carried out using a Cary 6000i UV/vis spectrophotometer. NMR spectra were recorded using a Bruker Avance 600 MHz NMR spectrometer.

3.2.2 Density functional theory calculations

Calculations were carried out using the Gaussian 09 and Gaussview software suites.[43] All calculations were performed using the B3LYP exchange-correlation functional with the 6-31G(d,p) basis set. 2-Ethylhexyl and dodecyloxy groups were replaced with ethyl and methoxy groups respectively, in order to simplify the calculations. Geometry optimizations were first performed on all structures, after which frequency calculations were carried out to ensure that the optimization converged to a potential energy minimum. A polarizable continuum model (with a dielectric constant equal to that of chloroform) was used for the frequency calculations, from which

zero-point vibrational energies and thermal corrections to 298.15 K were determined. Single-point energy and TDDFT calculations (using the same basis set and solvent model) were used to determine frontier molecular orbital energies and isosurfaces, as well as the predicted electronic transitions. The predicted UV/vis spectra were generated using the SWizard program, revision 5.0, using the Gaussian/Lorentzian/pseudo-Voigt model.[44,45]

3.2.3 UV/vis spectroscopic titrations

Spectroscopic titrations were carried out on chloroform solutions of **1** and **2**. Concentrations were chosen such that the absorbance of the $S_0 \rightarrow S_1$ (HOMO-to-LUMO) transition was *ca.* 1. Actual concentrations were determined using published extinction coefficients.[28] For titrations with TFA, the titrant was dispensed as a neat liquid via syringe. For titrations with $BF_3 \cdot Et_2O$, a 0.01 mol/L chloroform solution was used initially, and the concentration was gradually increased over the course of the titration. After adding each aliquot of titrant, the sample was gently shaken and placed in the sample chamber. UV/vis spectra were acquired with a spectral window of 450 to 1400 nm, as it was found that the combination of a Lewis acid and UV light induced sample decomposition. Plotted titration spectra were corrected for volume change resulting from addition of Lewis acid.

3.2.4 ^{1}H NMR spectroscopic titrations

Due to the relatively insoluble nature of the Lewis adducts, the ^{1}H NMR titrations were performed in $CDCl_3$ at concentrations close to the detection limit of the spectrometer. Spectra were recorded first on the uncoordinated species, followed by the addition of aliquots of a solution of $BF_3 \cdot Et_2O$ in $CHCl_3$.

3.2.5 Thin film UV/vis spectroscopy

Glass slides were first cleaned by sonication in acetone and isopropanol for 20 min each, oven dried, and cleaned in a UV/ozone cleaner for 15 min before being placed in a N_2 atmosphere glove box. The substrates were immersed in a solution of trichlorooctadecylsilane (8.4 mmol/L in chlorobenzene) at 70 °C for 60 min. After 60 min the substrates were rinsed with chlorobenzene and dried at 130 °C for 10 min. Thin films of **1** and **2** were cast from chlorobenzene solutions (2-10 mg/ml) onto derivatized glass substrates at 1000 rpm. To perform vapor annealing studies, thin films of **1** and **2** were placed in a crystallizing dish flushed with argon along with a beaker of $BF_3{\cdot}Et_2O$. A cover was placed over the top. Samples were exposed for 30-120 min (as noted). The same procedure was used for the treatment of the **1** + BF_3 and **2** + BF_3 films with pyridine.

3.3 Results and discussion

3.3.1 UV/Vis spectroscopy and (TD)DFT results

In previous work, the synthesis of compounds **1** and **2** was reported and their performance as electron donors in bulk heterojunction OPVs was evaluated.[28] It was shown that the addition of nitrogen heteroatoms to the isoindigo structure had a relatively minor effect on the energy of the frontier molecular orbitals; however, the pyridine moieties provide lone pairs to which Lewis acids can be coordinated. Therefore, how the coordination of H^+ and BF_3 affects the optoelectronic properties of **1** and **2** became the goal of this study. The simplest of these properties to study is the $E_{g,opt}$, as determined by UV/vis absorbance spectroscopy.

Both **1** and **2** absorb light well into the near-infrared, with $E_{g,opt}$ values of 1.8 and 1.5 eV, as determined by solution-phase UV/vis spectroscopy. Addition of a large excess of TFA to chloroform solutions of **1** and **2** produced an immediate color change. Upon addition of TFA,

solutions of **1** turned from purple to blue, while solutions of **2** turned from blue to green. Addition of excess TFA to **1** and **2** produced a *ca*. 100 nm red-shift of the lowest-energy electronic transition (Figure 3.1). After this, the experiment was repeated with a different acid, $BF_3{\cdot}Et_2O$, again adding an excess of the acid. Again, the most distinct change in the absorption spectrum was the red-shift of the lowest-energy transition by *ca*. 100 nm. The effect of the two acids is similar; however, **1** displays a slightly larger (*ca*. 25 nm) red-shift when coordinated to TFA, while exactly the opposite behavior is observed for **2** (a larger red-shift is observed with $BF_3{\cdot}Et_2O$). The reversibility of this process was studied by adding pyridine to solutions containing **1** or **2** and an excess of $BF_3{\cdot}Et_2O$ (Figure 3.2). The adduct formation was fully reversible, with the addition of the stronger Lewis base regenerating the original UV/vis spectra.

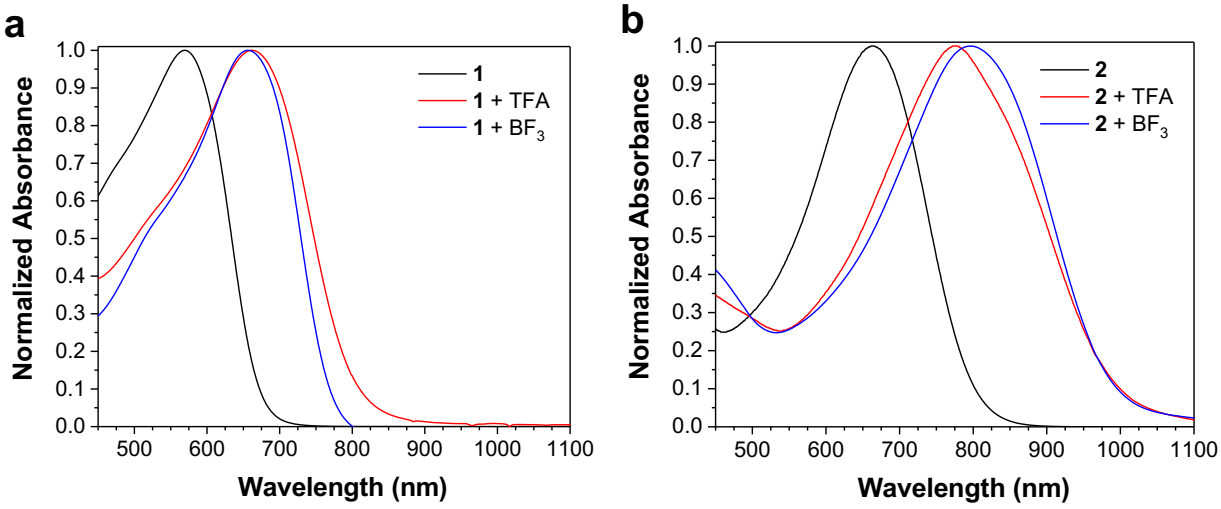

Figure 3.1 UV/vis spectra of chloroform solutions of: (a) **1**, and (b) **2**. Uncoordinated (black line), and with excess TFA (red line) or $BF_3{\cdot}Et_2O$ (blue line).

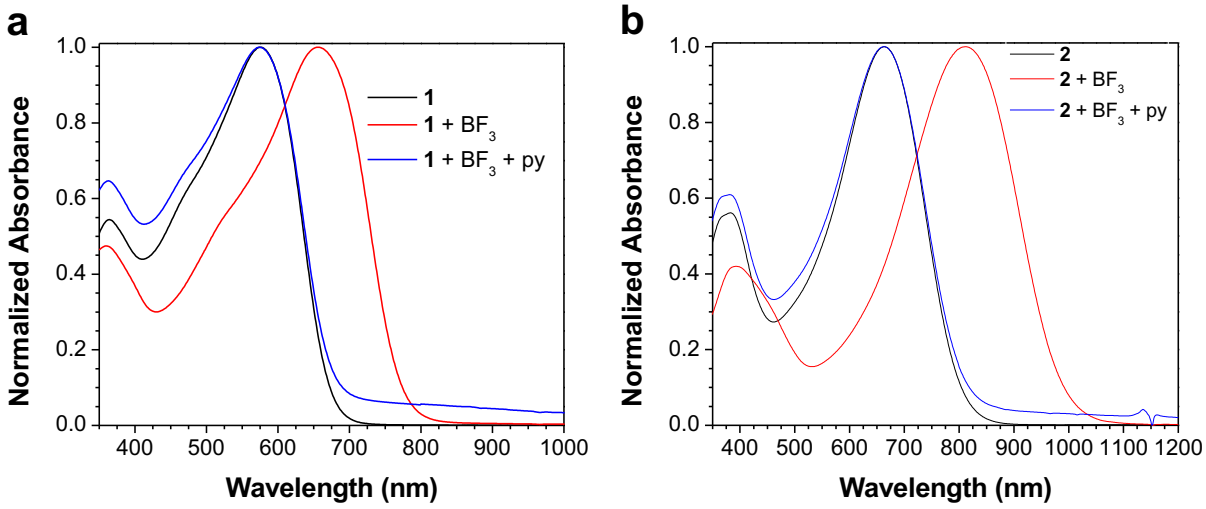

Figure 3.2 UV/vis spectra of chloroform solutions of (a) **1**, and (b) **2**. Uncoordinated (black line), with excess $BF_3 \cdot Et_2O$ (red line), with excess $BF_3 \cdot Et_2O$ and excess pyridine(blue line).

It is clear from Figure 3.1 that Lewis acids can coordinate to both **1** and **2**, resulting in a pronounced red-shift of the lowest-energy absorption band. However, the exact identity of the Lewis adduct is ambiguous. It is unclear whether both pyridine sites coordinate to Lewis acids, or whether the first coordination event adversely affects the basicity of the second nitrogen atom. In order to help identify the species present in solution, TDDFT calculations were used to predict the electronic absorption spectra of **1** and **2**, both before and after coordination to BF_3 (Figure 3.3). Coordination to both one and two BF_3 molecules was considered. The isosurfaces and energies of the frontier molecular orbitals for **1** and **2** after coordination to zero, one, or two BF_3 molecules are shown in Figure 3.4 and 3.5.

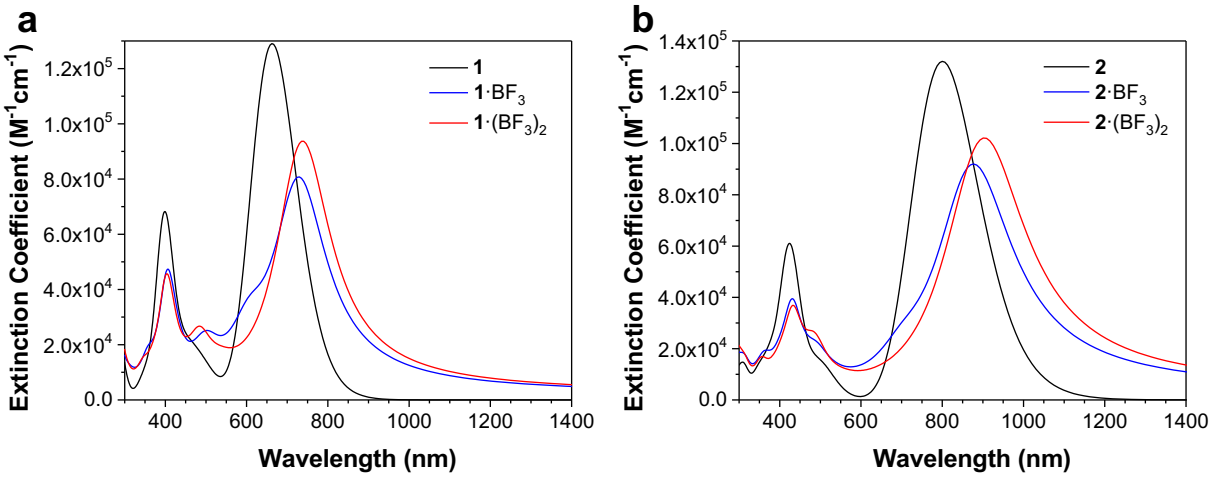

Figure 3.3 Electronic absorption spectra predicted by TDDFT for: (a) **1** and (b) **2**. Uncoordinated (black line), coordination to a single BF_3 molecule (blue line), coordination to two BF_3 molecules (red line).

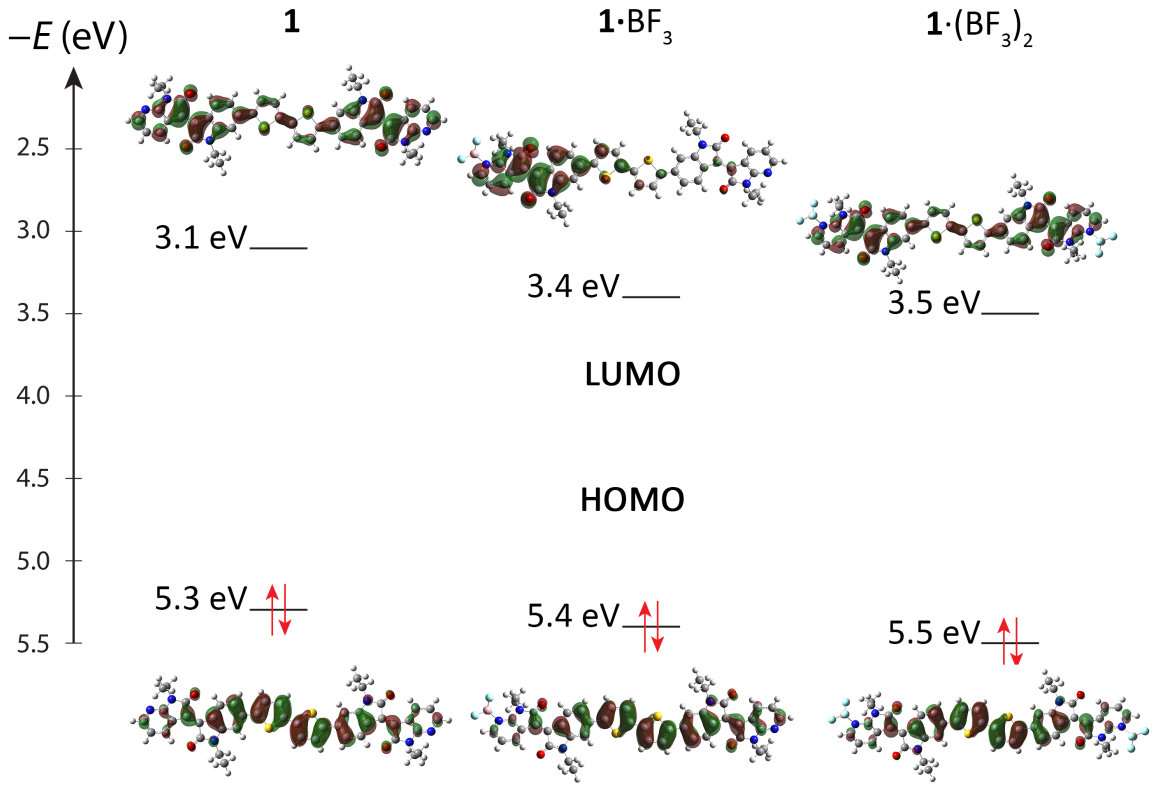

Figure 3.4 Frontier molecular orbitals of **1**, **1**·BF_3, and **1**·$(BF_3)_2$.

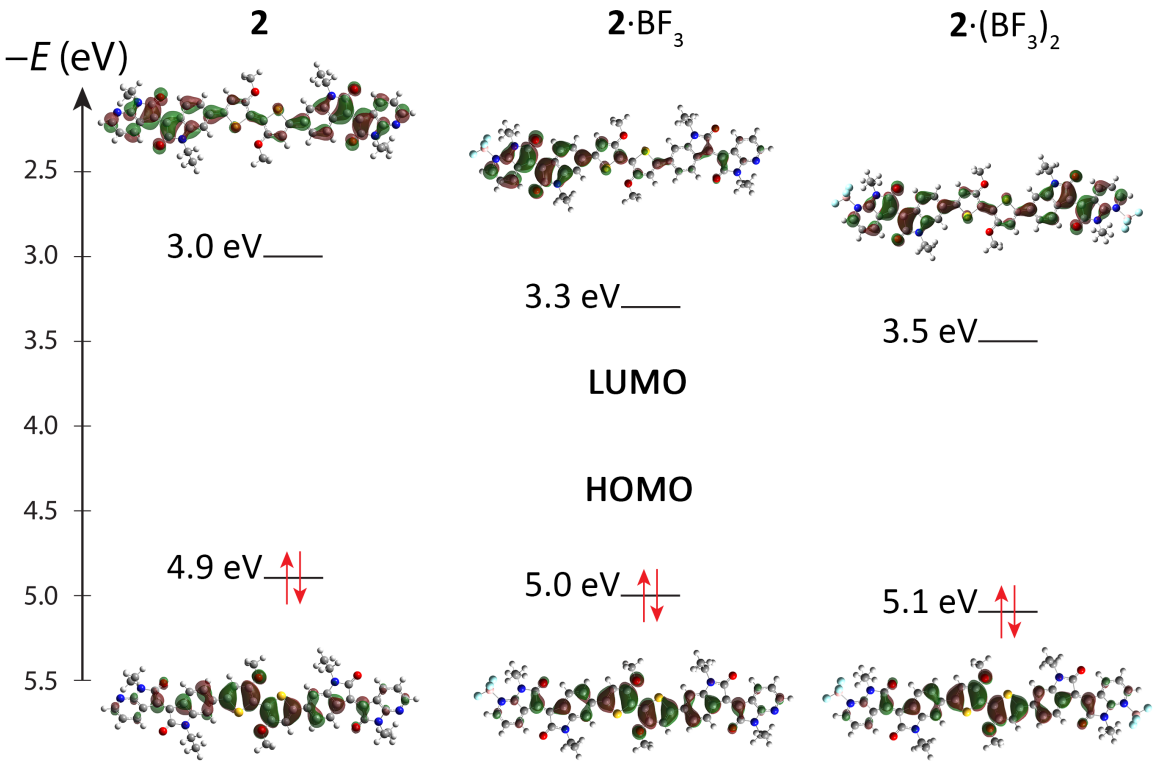

Figure 3.5 Frontier molecular orbitals of **2**, **2**·BF_3, and **2**·$(BF_3)_2$.

Based on the TDDFT analysis, in all cases the lowest-energy absorption band was assigned to the HOMO to LUMO transition. For both **1** and **2**, this transition has a great deal of π(bithiophene) to π*(isoindigo) character. The spectrum predicted for **1**·BF_3 shows a 70 nm red-shift in the HOMO→LUMO transition relative to **1**; addition of a second BF_3 red-shifts the transition slightly further, from 728 to 738 nm. Coordination of a single BF_3 molecule to **2** was calculated to induce a similar 76 nm red-shift in the HOMO→LUMO transition. In the case of **2**, the coordination of a second BF_3 has a slightly larger effect, red-shifting the absorption band a further 21 nm. The TDDFT-predicted UV/vis absorbance spectrum for **1**·BF_3 also features a shoulder at 605 nm, which is assigned to the HOMO to LUMO+1 transition. The oscillator strength

of this transition is two orders of magnitude greater in the spectrum of **1**·BF_3 than in the spectra of either **1** or **1**·$(BF_3)_2$. The LUMO+1 orbital of **1**·BF_3 lies primarily on the π* of the uncoordinated azaisoindigo moiety (Figure 3.6), while it is spread symmetrically across the molecule in **1** and **1**·$(BF_3)_2$. The intensity of the HOMO to LUMO+1 transition in the spectrum of **1**·BF_3 is likely due to the lack of symmetry in the LUMO+1, leading to a large transition dipole moment. The high energy transition at 400 nm present in all spectra (Figure 3.3) is attributed primarily to the HOMO to LUMO+2 transition. The LUMO+2 orbital is predominantly π*(bithiophene) in character (Figure 3.7); thus, this is primarily a localized π→π*(bithiophene) band. The electronic transitions predicted by TDDFT for **2**, **2**·BF_3, and **2**·$(BF_3)_2$ are all qualitatively similar to those for **1**, **1**·BF_3, and **1**·$(BF_3)_2$. The only major difference is that the HOMO→LUMO and HOMO→LUMO+1 transitions are found further into the near-infrared, owing to the higher-lying HOMO of **2** relative to **1**.

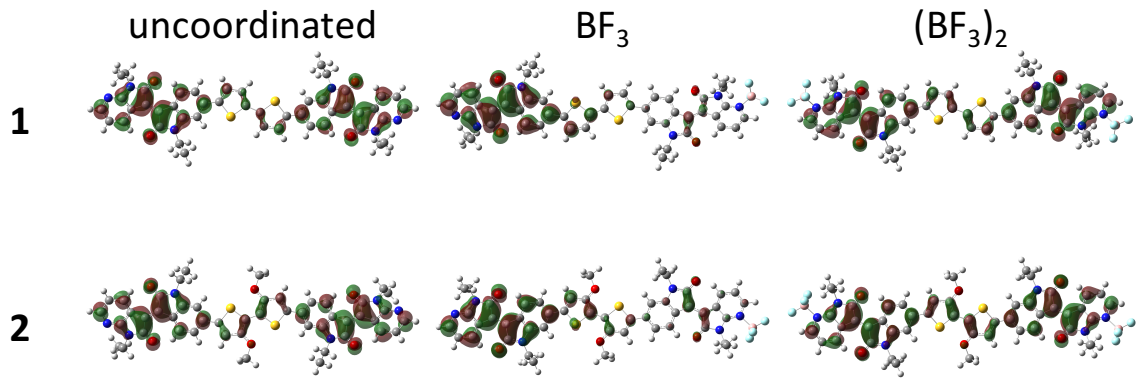

Figure 3.6 Orbital isosurfaces for the LUMO+1 of **1**, **1**·BF_3, **1**·$(BF_3)_2$, **2**, **2**·BF_3, and **2**·$(BF_3)_2$.

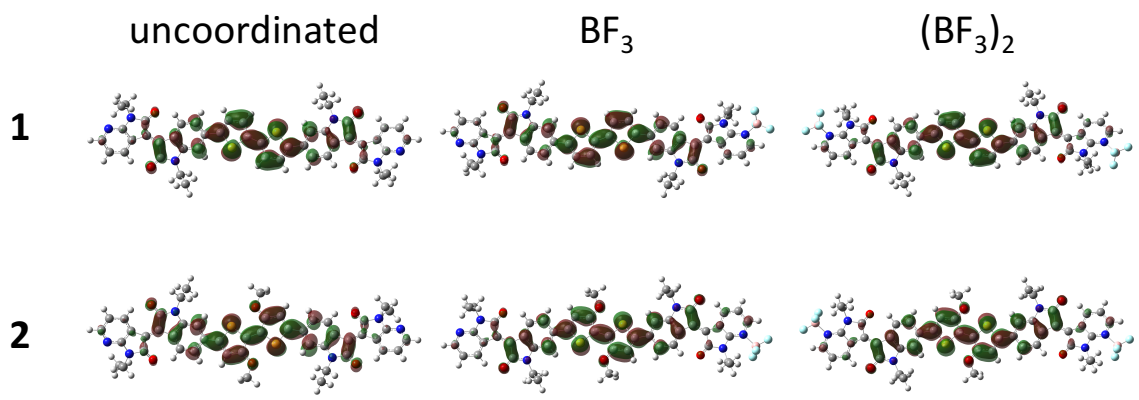

Figure 3.7 Orbital isosurfaces for the LUMO+2 of **1**, **1**·BF_3, **1**·$(BF_3)_2$, **2**, **2**·BF_3, and **2**·$(BF_3)_2$.

Coordination of BF_3 to **1** and **2** has a substantial impact on the frontier molecular orbitals (Figures 3.4 and 3.5). Prior to coordination, the HOMOs of **1** and **2** are primarily bithiophene in character, with a smaller contribution from the pendant isoindigo groups; conversely, the LUMOs are primarily centered on the peripheral isoindigo units. Coordination of the first BF_3 molecule to an azaisoindigo group serves to withdraw electron density from the azaisoindigo π-system, which lowers the LUMO energy by 0.3 eV. Since the HOMO is primarily bithiophene in character, the effect on the HOMO is less pronounced, and only a 0.1 eV shift in energy is calculated. The two azaisoindigo groups are now inequivalent, and the LUMO now resides almost exclusively on the azaisoindigo group bound to BF_3. This has the opposite effect on the HOMO, with the uncoordinated azaisoindigo group now making a larger overall contribution to the molecular orbital. The coordination of a second molecule of BF_3 to the other azaisoindigo group restores the original symmetry of the molecule. The frontier orbitals for **1**·$(BF_3)_2$ and **2**·$(BF_3)_2$ are very similar to those of **1** and **2**; however, the HOMO and LUMO energy continue to drop, with both the HOMO and LUMO decreasing by a further 0.1 – 0.2 eV relative to **1**·BF_3 and **2**·BF_3.

The calculated electronic absorption spectra and frontier molecular orbitals of **1** and **2,** before and after protonation, are shown in Figures 3.8-3.11. The trends exhibited in both the

molecular orbitals and absorption spectra are similar to those seen for the BF_3 adducts. Protonation of the azaisoindigo groups lowers the energy of the LUMO, leading to an overall red-shift in the energy of the HOMO→LUMO transition. The major difference between the H^+ and BF_3 adducts lies in the strength of the acid-base interaction. Structural optimizations performed on **1**·H^+ and **2**·H^+ in the presence of the trifluoroacetate counter-ion inevitably yielded free **1** and **2** and trifluoroacetic acid. This implies that the protonation of **1** and **2** with TFA is an energetically unfavorable process, and that an excess of acid is required to drive the equilibrium to the right. As a result, the calculations for **1**·H^+, **1**·$(H^+)_2$, **2**·H^+ and **2**·$(H^+)_2$ were all carried out in the absence of an explicit counter-ion. Therefore, while the experimental extinction coefficients of the H^+ and BF_3 adducts were found to be nearly identical, the TDDFT results predict oscillator strengths that are an order of magnitude higher for the H^+ adducts than the BF_3 adducts. The lack of explicit solvation of the protonated azaisoindigo group likely causes an overestimation of the transition dipole moment, and therefore an overestimation of the extinction coefficient. Similarly, the energies of the frontier molecular orbitals of **1**·H^+, **1**·$(H^+)_2$, **2**·H^+ and **2**·$(H^+)_2$ (Figures 3.10 and 3.11) are all likely artificially low.

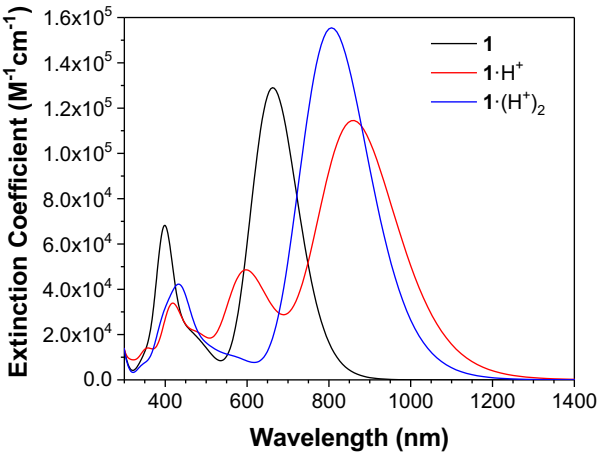

Figure 3.8 Electronic absorption spectra predicted by TDDFT for **1**, **1**·H^+, and **1**·$(H^+)_2$.

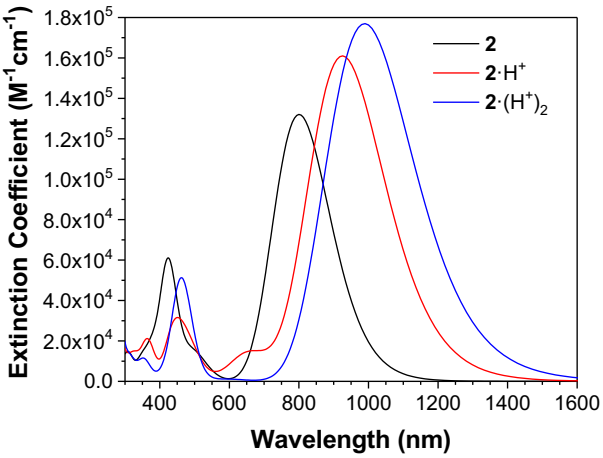

Figure 3.9 Electronic absorption spectra predicted by TDDFT for **2**, **2**·H^+, and **2**·$(H^+)_2$.

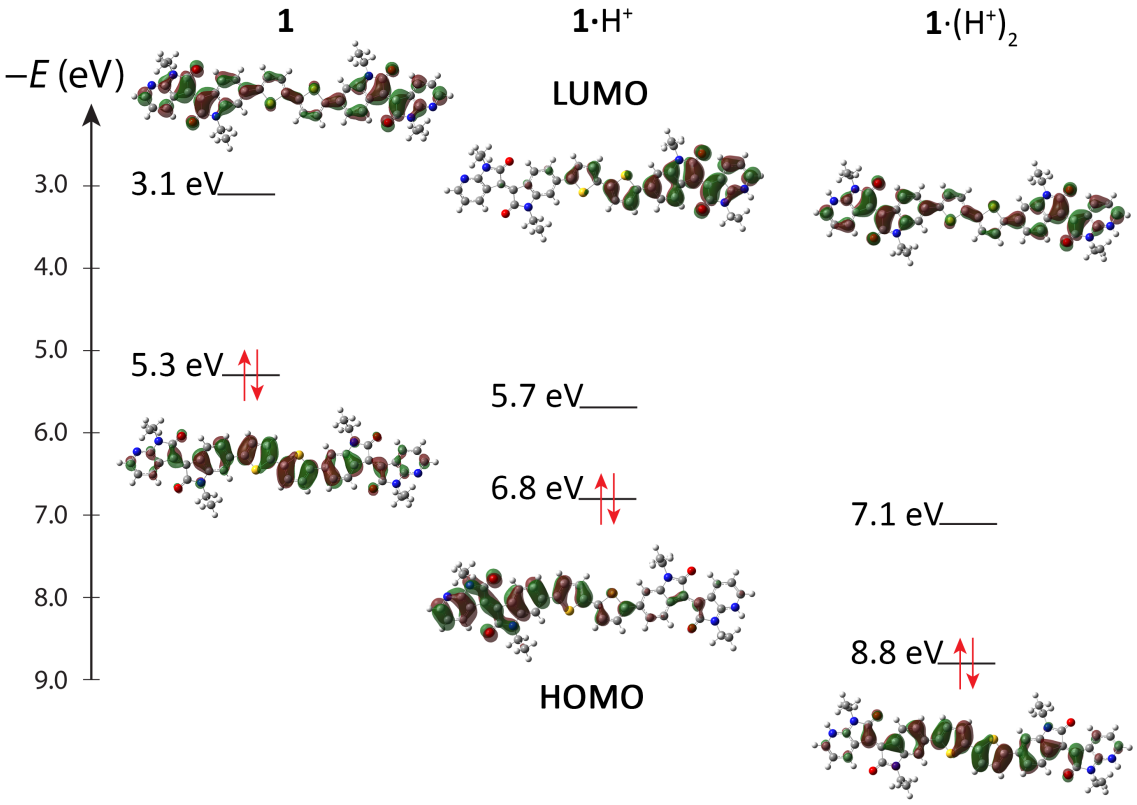

Figure 3.10 Frontier molecular orbitals of **1**, **1**·H^+, and **1**·$(H^+)_2$.

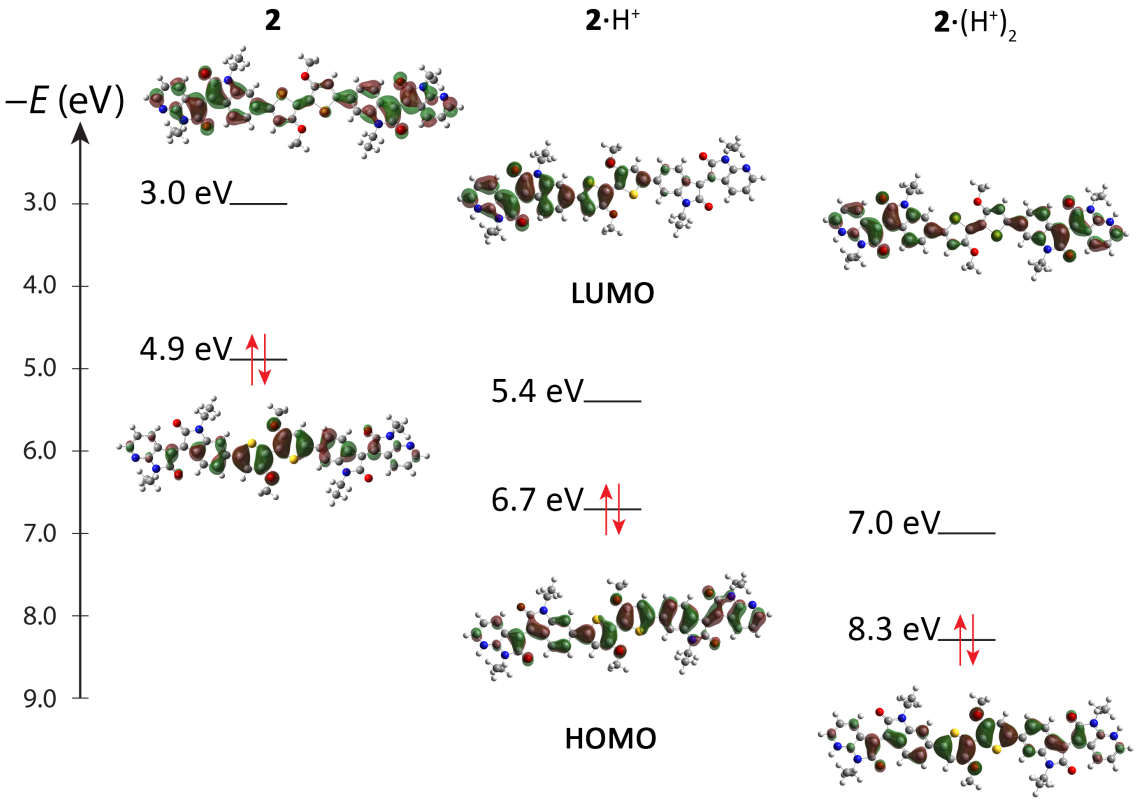

Figure 3.11 Frontier molecular orbitals of **2**, **2**·H^+, and **2**·$(H^+)_2$.

3.3.2 UV/Vis spectral titrations

The calculated spectra of the Lewis adducts revealed only a small red-shift between **1**·BF_3 and **1**·$(BF_3)_2$ and between **2**·BF_3 and **2**·$(BF_3)_2$. This was insufficient to determine whether the spectra in Figure 3.1 correspond to the single or double Lewis adducts. Therefore, UV/vis spectral titrations of **1** and **2** were performed. Chloroform solutions of **1** and **2** were each titrated with both BF_3·Et_2O and TFA. Titration of **1** with BF_3·Et_2O (Figure 3.12a) yielded a gradual red-shift of the λ_{max} from 575 to 657 nm. What appears to be a single isosbestic point is observed *ca*. 605 nm (Figure 3.12a); however, the overlap of the spectra is not perfect (Figure 3.13a), suggesting that this may not actually be a true isosbestic point and that the reaction may actually yield multiple products. Since the spectra of **1**·BF_3 and **1**·$(BF_3)_2$ are predicted to be quite similar (Figure 3.2), the

lack of a true isosbestic point may suggest an equilibrium between **1**, **1**·BF_3, and **1**·$(BF_3)_2$, which is driven further to the right as an excess of BF_3·Et_2O is added. The titration of **2** with BF_3·Et_2O yielded similar results (Figure 3.12b). The λ_{max} of the $S_0 \rightarrow S_1$ transition red-shifted from 660 to 795 nm, and again the overlap of the spectra at *ca*. 710 nm is not perfect (Figure 3.13b). This is consistent with an equilibrium between **2**, **2**·BF_3, and **2**·$(BF_3)_2$ that shifts to the right as the titration proceeds. In both cases, a substantial excess of BF_3·Et_2O is required to drive the reaction to completion.

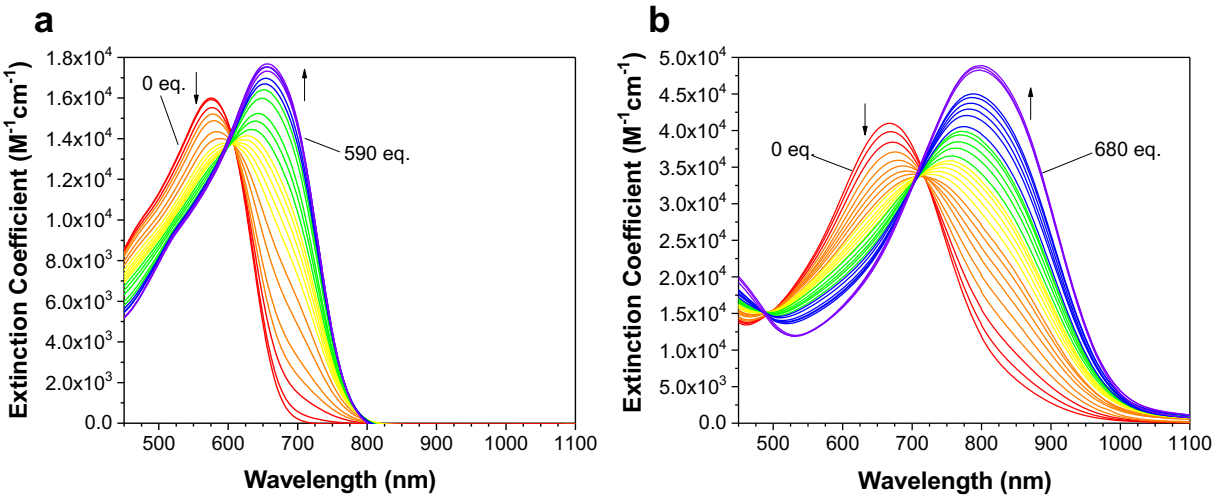

Figure 3.12 UV/vis absorbance spectra for the titration of (a) **1** and (b) **2** with BF_3·Et_2O in chloroform. The annotations indicate the number of equivalents of BF_3·Et_2O used.

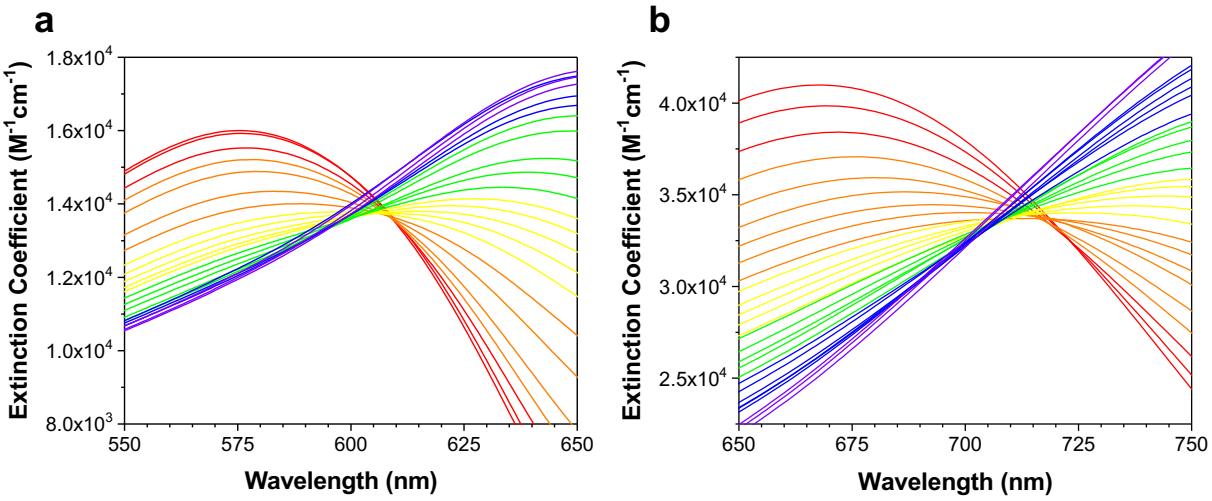

Figure 3.13 UV/vis absorbance spectra for the titration of (a) **1** and (b) **2** with $BF_3{\cdot}Et_2O$ in chloroform. Spectra are corrected for sample volume change to titrant addition.

Compounds **1** and **2** were also titrated with TFA (Figures 3.14 and 3.15), with similar results. Both titrations yielded a gradual red-shift of λ_{max} for the $S_0 \rightarrow S_1$ transition (570 – 660 nm and 660 – 775 nm for **1** and **2**, respectively); however, the major difference between the titrations with $BF_3{\cdot}Et_2O$ and TFA is the number of equivalents of acid required before no further change is observed in the UV/vis spectrum. With $BF_3{\cdot}Et_2O$, *ca*. 600 – 700 equivalents of acid are required to fully red-shift the $S_0 \rightarrow S_1$ absorption band; however, with TFA, an order of magnitude more acid is required (2.0×10^4 and 9.6×10^4 equivalents for **1** and **2**, respectively). The large excess of TFA required also supports the computational evidence that the trifluoroacetate anion is a stronger base than 7-azaisoindigo.

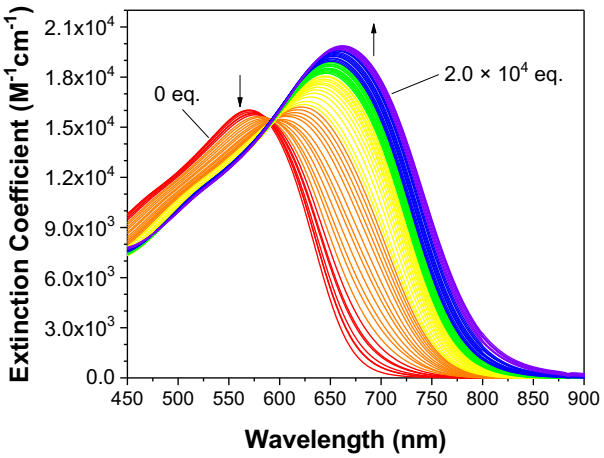

Figure 3.14 UV/vis absorbance spectra for the titration of **1** with TFA in chloroform. The annotations indicate the number of equivalents of TFA used.

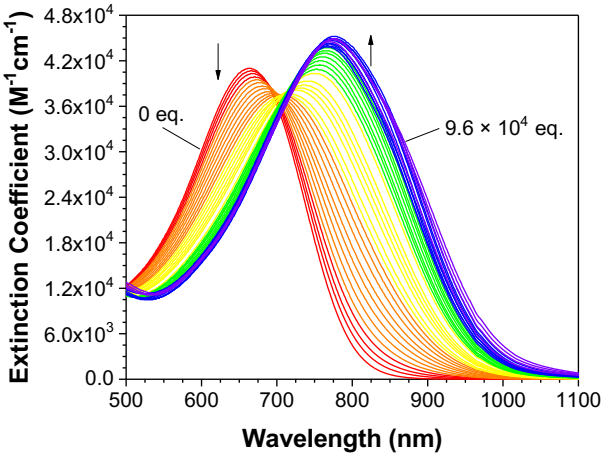

Figure 3.15 UV/vis absorbance spectra for the titration of **2** with TFA in chloroform. The annotations indicate the number of equivalents of TFA used.

3.3.3 ^{1}H NMR spectral titration

Although the lack of true isosbestic points in the UV/vis titrations is consistent with the sequential coordination of two Lewis acids, ultimately, UV/vis spectroscopy is not able to distinguish between the $\cdot BF_3$ and $\cdot(BF_3)_2$ Lewis adducts. The spectral differences between the mono- and di-coordinated species are too small, and the absorption bands too broad, to unambiguously determine

the exact species in solution. Therefore, **1** and **2** were titrated with $BF_3{\cdot}Et_2O$, and the titration followed by ^1H NMR (Figure 3.16). The greater acidity of $BF_3{\cdot}Et_2O$ relative to TFA meant that fewer equivalents of the acid were needed to fully convert the molecules to the Lewis adducts; for this reason, ^1H NMR titrations were only performed with $BF_3{\cdot}Et_2O$. Due to the limited solubility of the Lewis acid-base adducts, and the insensitivity of ^1H NMR relative to UV/vis spectroscopy (especially given the high optical extinction coefficients of **1** and **2**), the signal-to-noise ratio of all NMR spectra was relatively low.

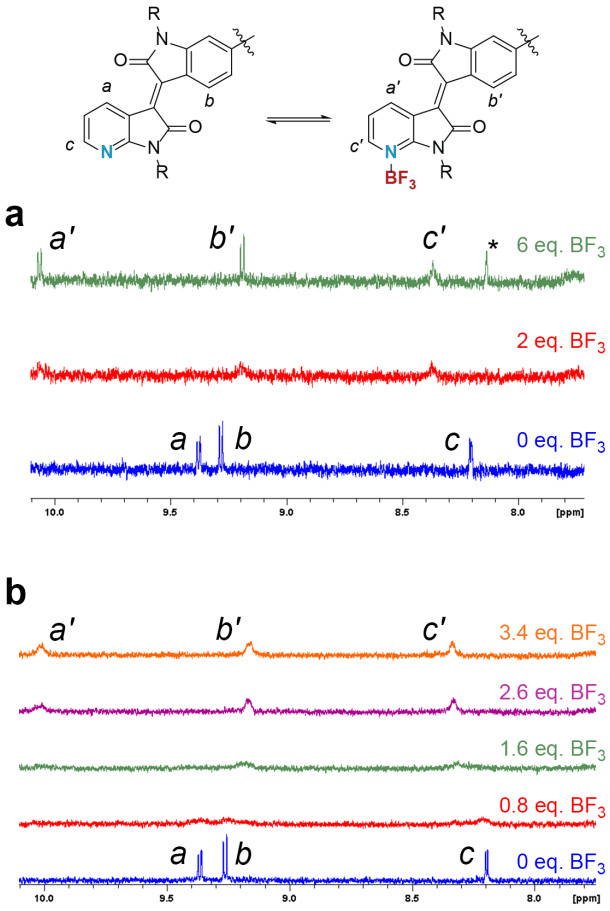

Figure 3.16 ^1H NMR spectroscopic titration of (a) **1** and (b) **2** with $BF_3{\cdot}Et_2O$. A small impurity introduced in the final aliquot of $BF_3{\cdot}Et_2O$ is denoted by an asterisk (*).

There are two main possibilities when monitoring a dynamic equilibrium process, such as that described in Figure 3.16, by ^{1}H NMR: (i) if BF_3 exchange is slow on the NMR timescale, then two distinct sets of peaks will be observed, one corresponding to the free base, and one corresponding to the Lewis adduct; (ii) if, however, BF_3 exchange is fast on the NMR timescale, then only one set of peaks will be observed, whose position shifts as the titration proceeds. Intermediate rates of exchange will yield similar behavior, only with highly broadened peak profiles. This behavior is commonly observed in labile complexes such as borane-imine and borane-acetonitrile Lewis adducts.[46,47] As $BF_3 \cdot Et_2O$ is added to a solution of **1**, the peak intensity decreases sharply, and the peaks develop a highly broadened profile, indicative of an intermediate rate of BF_3 exchange. The hydrogen atom *para* to the pyridinic nitrogen (a) displays a pronounced downfield shift ($\delta > 10$ ppm); smaller shifts are observed for the hydrogen atoms in the *ortho* position (c) and on the adjacent oxindole (b). As additional equivalents of $BF_3 \cdot Et_2O$ are added, the signals do not shift further, but increase in intensity and sharpness. The data indicate that the rate of BF_3 exchange is intermediate-to-slow, and since only one set of azaisoindigo signals is observed, it suggests that when an excess of BF_3 is present, both pyridinic nitrogens are bound to BF_3.

The results of the titration of **2** with $BF_3 \cdot Et_2O$ are qualitatively similar. As $BF_3 \cdot Et_2O$ is added to a solution of **2**, there is a decrease in signal intensity accompanied by substantial peak broadening, again indicative of an intermediate rate of BF_3 exchange. Critically, the position of the peaks does not change, they only become less intense; as more BF_3 is added, a new set of peaks grows in, corresponding to the $\mathbf{2} \cdot (BF_3)_2$ adduct. These new peaks grow in as an excess of BF_3 is added. Again, these data suggest that the rate of BF_3 exchange is intermediate-to-slow, and that

ultimately, both pyridinic nitrogens are bound to BF_3 molecules. As with the UV/vis titrations, an excess of $BF_3 \cdot Et_2O$ is required to form Lewis adducts with both **1** and **2**.

The ^1H NMR results suggest that coordination of the first BF_3 molecule does not adversely affect the basicity of the second nitrogen; however, in order to better quantify this, the DFT results were used to calculate $\Delta G°_{coord}$ at 298.15 K for the two coordination reactions (Scheme 3.2).

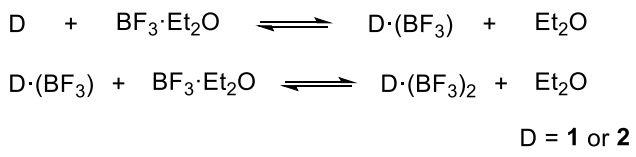

Scheme 3.2 Sequential reaction of **1** and **2** with two equivalents of $BF_3 \cdot Et_2O$.

Based on the calculated thermodynamic parameters, $\Delta G°_{coord}$ for the coordination of the first BF_3 molecule was determined to be –46 kJ mol^{-1} for compound **1**, and –50 kJ mol^{-1} for compound **2**. For the addition of a second BF_3 molecule, $\Delta G°_{coord}$ was calculated to be –47 kJ mol^{-1} and –45 kJ mol^{-1} for **1** and **2**, respectively. Although the computed values of $\Delta G°_{coord}$ are not likely to be quantitatively accurate (given the importance of solvation in correctly modeling this type of acid-base chemistry), the $\Delta G°_{coord}$ values for the addition of the first and second BF_3 groups should be directly comparable. In this case, there is little difference in $\Delta G°_{coord}$ for the first and second reactions: in compound **1**, $\Delta G°_{coord}$ is more negative by **1** kJ mol^{-1}, and in compound **2**, $\Delta G°_{coord}$ is more positive by 5 kJ mol^{-1}. Ultimately, such small differences are not likely to affect the ability of the second nitrogen to coordinate to BF_3, and further supports the conclusion that **1**$\cdot(BF_3)_2$ and **2**$\cdot(BF_3)_2$ are formed in the presence of excess $BF_3 \cdot Et_2O$.

3.3.4 Solid-vapor interface Lewis adduct formation

Although the solution acid-base chemistry of **1** and **2** is of interest, ultimately, these materials are of importance for applications in organic electronics. Therefore, the processing of the Lewis adducts into thin films was of interest; however, they proved to be too insoluble to spin coat from solution. The addition of a droplet of neat $BF_3{\cdot}Et_2O$ onto films of **1** and **2** led to immediate bleaching of the films; however, it was noted that nearby portions of the film (that were not directly exposed to $BF_3{\cdot}Et_2O$) underwent the same color change that was observed in solution. The films visibly changed color in the presence of $BF_3{\cdot}Et_2O$ vapor alone. Therefore, films of **1** and **2** were spin coated onto glass slides and placed inside a sealed jar containing an open beaker of $BF_3{\cdot}Et_2O$. Films were exposed to the $BF_3{\cdot}Et_2O$ vapor for either 30 or 60 min, after which their UV/vis spectra were measured (Figure 3.17). The spectra of both **1** and **2** exhibit a large red-shift in their absorption edge upon exposure to $BF_3{\cdot}Et_2O$. In the case of **1**, the full 60 min is required to complete the reaction, whereas with **2** the reaction is complete in < 30 min. As in solution, the adduct formation in the solid state is reversible; exposure of the films to pyridine vapor (Figure 3.18) yields the spectra of uncoordinated **1** and **2**. Since boron trihalides such as BF_3 are known to hydrolyze when exposed to moisture, the stability of the Lewis adducts was evaluated. Under ambient conditions, thin films of **1** and **2** revert back to their initial uncoordinated state overnight (Figure 3.19).

The red-shift observed in Figure 3.17 suggests that thin films of **1** and **2** can be converted into the corresponding Lewis adducts, thereby altering not just the optical band gap, but other optoelectronic properties. For instance, Zalar *et al.*, and more recently Han *et al.*, have shown that the charge carrier mobilities of organic semiconductors can be improved by coordination to Lewis acids; Lewis acid-base interactions such as these have been exploited in OFET-based sensors.

[40,48,49] The fact that **1** and **2** can be converted into their Lewis adducts by a vapor-phase reaction with $BF_3 \cdot Et_2O$ suggests that it might be used as a way of improving the performance of azaisoindigo-based thin film transistors.

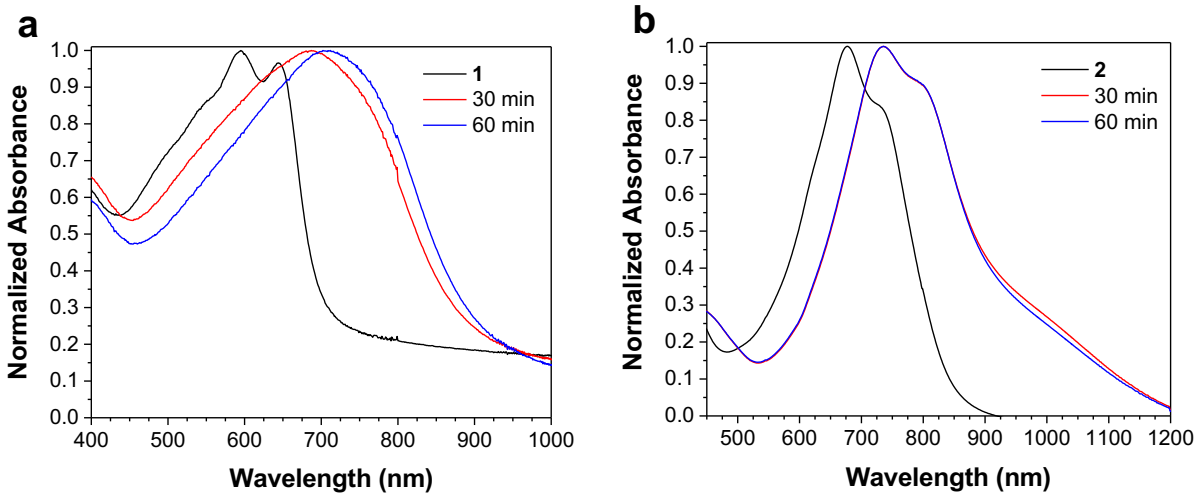

Figure 3.17 Thin film UV/vis absorbance spectra of (a) **1** and (b) **2**, before and after exposure to $BF_3 \cdot Et_2O$ vapor for 30 min (red line) or 60 min (blue line).

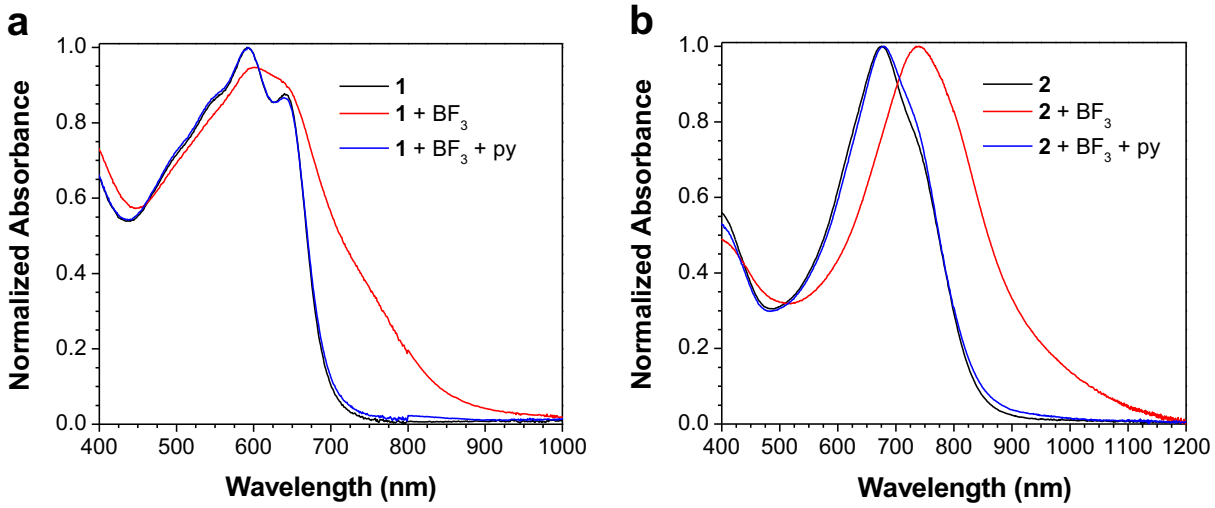

Figure 3.18 Thin film UV/vis spectra of (a) **1** and (b) **2**: as-cast (black line), after exposure to $BF_3 \cdot Et_2O$ vapor (red line), and after exposure of the resulting Lewis adducts to pyridine vapor (blue line).

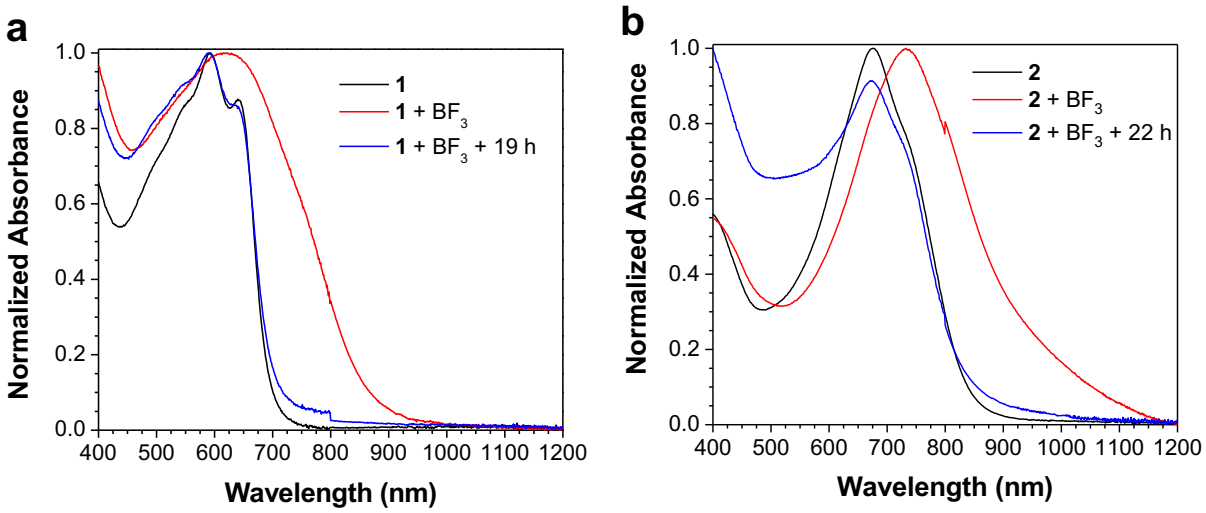

Figure 3.19 Thin film UV/vis spectra of (a) **1** and (b) **2**: as-cast (black line), after exposure to $BF_3 \cdot Et_2O$ vapor (red line), and after exposure of the resulting Lewis adducts to ambient atmosphere overnight (blue line).

3.4 Conclusion

In summary, it has been shown that Lewis acids induce a major red-shift in 7-azaisoindigo-based donor-acceptor organic semiconductors. A combination of TDDFT calculations, UV/vis spectroscopy, and ^{1}H NMR spectroscopy were used to determine the structure and optical properties of the subsequent Lewis adducts. Finally, it has been proven that this same acid-base chemistry can be carried out at the solid-gas interface by the reaction of thin films with $BF_3 \cdot Et_2O$ vapor. The ability to manipulate the band gap of thin film organic semiconductors through the use of Lewis acid-base chemistry at the solid-gas interface is an important first step toward the tailored doping of organic semiconductors, with direct application to thin film devices such as OFETs and OPVs.

3.5 Acknowledgements

Prof. R.P. Steer is gratefully acknowledged for many helpful discussions during the interpretation of the TDDFT and UV/vis spectroscopic results. The Natural Sciences and Engineering Research Council of Canada (NSERC) and the University of Saskatchewan are acknowledged for financial support. T.L.K. is a Canada Research Chair in Photovoltaics. This research was undertaken, in part, thanks to funding from the Canada Research Chairs Program. N.M.R. thanks NSERC for CGS-D scholarship funding.

3.6 References

(1) Meerheim, R.; Körner, C.; Oesen, B.; Leo, K. 10.4% Efficient Triple Organic Solar Cells Containing Near Infrared Absorbers. *Appl. Phys. Lett.* **2016**, *108*, No. 103302.

(2) Hasegawa, T.; Ashizawa, M.; Hiyoshi, J.; Kawauchi, S.; Mei, J.; Bao, Z.; Matsumoto, H. An Ultra-Narrow Bandgap Derived From Thienoisoindigo Polymers: Structural Influence on Reducing the Bandgap and Self-Organization. *Polym. Chem.* **2016**, *7*, 1181–1190.

(3) Zhang, B.; Trinh, M. T.; Fowler, B.; Ball, M.; Xu, Q.; Ng, F.; Steigerwald, M. L.; Zhu, X. Y.; Nuckolls, C.; Zhong, Y. Rigid, Conjugated Macrocycles for High Performance Organic Photodetectors. *J. Am. Chem. Soc.* **2016**, *138*, 16426–16431.

(4) Dou, L.; Liu, Y.; Hong, Z.; Li, G.; Yang, Y. Low-Bandgap Near-IR Conjugated Polymers/Molecules for Organic Electronics. *Chem. Rev.* **2015**, *115*, 12633–12665.

(5) Heeger, A. J. Semiconducting Polymers: the Third Generation. *Chem. Soc. Rev.* **2010**, *39*, 2354–2371.

(6) Mei, J.; Graham, K. R.; Stalder, R.; Reynolds, J. R. Synthesis of Isoindigo-Based Oligothiophenes for Molecular Bulk Heterojunction Solar Cells. *Org. Lett.* **2010**, *12*, 660–663.

(7) Stalder, R.; Mei, J.; Graham, K. R.; Estrada, L. A.; Reynolds, J. R. Isoindigo, a Versatile Electron-Deficient Unit for High-Performance Organic Electronics. *Chem. Mater.* **2014**, *26*, 664–678.

(8) Wang, E.; Mammo, W.; Andersson, M. R. 25th Anniversary Article: Isoindigo-Based Polymers and Small Molecules for Bulk Heterojunction Solar Cells and Field Effect Transistors. *Adv. Mater.* **2014**, *26*, 1801–1826.

(9) Guo, X.; Facchetti, A.; Marks, T. J. Imide- and Amide-Functionalized Polymer Semiconductors. *Chem. Rev.* **2014**, *114*, 8943–9021.

(10) Grenier, F.; Aïch, B. R.; Lai, Y.-Y.; Guérette, M.; Holmes, A. B.; Tao, Y.; Wong, W. W. H.; Leclerc, M. Electroactive and Photoactive Poly[Isoindigo-Alt-EDOT] Synthesized Using Direct (Hetero)Arylation Polymerization in Batch and in Continuous Flow. *Chem. Mater.* **2015**, *27*, 2137–2143.

(11) Goswami, S.; Gish, M. K.; Wang, J.; Winkel, R. W.; Papanikolas, J. M.; Schanze, K. S. π-Conjugated Organometallic Isoindigo Oligomer and Polymer Chromophores: Singlet and Triplet Excited State Dynamics and Application in Polymer Solar Cells. *ACS Appl. Mater. Interfaces* **2015**, *7*, 26828–26838.

(12) Ho, C.-C.; Chen, C.-A.; Chang, C.-Y.; Darling, S. B.; Su, W.-F. Isoindigo-Based Copolymers for Polymer Solar Cells with Efficiency Over 7%. *J. Mater. Chem. A.* **2014**, *2*, 8026–8032.

(13) Stalder, R.; Puniredd, S. R.; Hansen, M. R.; Koldemir, U.; Grand, C.; Zajaczkowski, W.; Müllen, K.; Pisula, W.; Reynolds, J. R. Ambipolar Charge Transport in Isoindigo-Based Donor–Acceptor Polymers. *Chem. Mater.* **2016**, *28*, 1286–1297.

(14) Stalder, R.; Grand, C.; Subbiah, J.; So, F.; Reynolds, J. R. An Isoindigo and Dithieno[3,2-b:2′,3′-d]Silole Copolymer for Polymer Solar Cells. *Polym. Chem.* **2012**, *3*, 89–92.

(15) Stalder, R.; Mei, J.; Reynolds, J. R. Isoindigo-Based Donor−Acceptor Conjugated Polymers. *Macromolecules* **2010**, *43*, 8348–8352.

(16) Dong, X.; Deng, Y.; Tian, H.; Xie, Z.; Geng, Y.; Wang, F. Isoindigo-Based Low Bandgap Conjugated Polymer for *o*-Xylene Processed Efficient Polymer Solar Cells with Thick Active Layers. *J. Mater. Chem. A.* **2015**, *3*, 19928–19935.

(17) Lei, T.; Dou, J.-H.; Ma, Z.-J.; Yao, C.-H.; Liu, C.-J.; Wang, J.-Y.; Pei, J. Ambipolar Polymer Field-Effect Transistors Based on Fluorinated Isoindigo: High Performance and Improved Ambient Stability. *J. Am. Chem. Soc.* **2012**, *134*, 20025–20028.

(18) Lei, T.; Dou, J.-H.; Ma, Z.-J.; Liu, C.-J.; Wang, J.-Y.; Pei, J. Chlorination as a Useful Method to Modulate Conjugated Polymers: Balanced and Ambient-Stable Ambipolar High-Performance Field-Effect Transistors and Inverters Based on Chlorinated Isoindigo Polymers. *Chem. Sci.* **2013**, *4*, 2447–2452.

(19) Deng, Y.; Li, W.; Liu, L.; Tian, H.; Xie, Z.; Geng, Y.; Wang, F. Low Bandgap Conjugated Polymers Based on Mono-Fluorinated Isoindigo for Efficient Bulk Heterojunction Polymer Solar Cells Processed with Non-Chlorinated Solvents. *Energy Environ. Sci.* **2015**, *8*, 585–591.

(20) Yang, Y.; Wu, R.; Wang, X.; Xu, X.; Li, Z.; Li, K.; Peng, Q. Isoindigo Fluorination to Enhance Photovoltaic Performance of Donor–Acceptor Conjugated Copolymers. *Chem. Commun.* **2014**, *50*, 439–441.

(21) Koizumi, Y.; Ide, M.; Saeki, A.; Vijayakumar, C.; Balan, B.; Kawamoto, M.; Seki, S. Thienoisoindigo-Based Low-Band Gap Polymers for Organic Electronic Devices. *Polym. Chem.* **2013**, *4*, 484–494.

(22) Zhang, G.; Ye, Z.; Li, P.; Guo, J.; Wang, Q.; Tang, L.; Lu, H.; Qiu, L. A New Thieno-Isoindigo Derivative-Based D–A Polymer with Very Low Bandgap for High-Performance Ambipolar Organic Thin-Film Transistors. *Polym. Chem.* **2015**, *6*, 3970–3978.

(23) Meager, I.; Nikolka, M.; Schroeder, B. C.; Nielsen, C. B.; Planells, M.; Bronstein, H.; Rumer, J. W.; James, D. I.; Ashraf, R. S.; Sadhanala, A.; Hayoz, P.; Flores, J.C.; Sirringhaus, H.; McCulloch, I. Thieno[3,2-b]Thiophene Flanked Isoindigo Polymers for High Performance Ambipolar OFET Applications. *Adv. Funct. Mater.* **2014**, *24*, 7109–7115.

(24) Kim, G.; Kang, S.-J.; Dutta, G. K.; Han, Y.-K.; Shin, T. J.; Noh, Y.-Y.; Yang, C. A Thienoisoindigo-Naphthalene Polymer with Ultrahigh Mobility of 14.4 $cm^2/v{\cdot}s$ That Substantially Exceeds Benchmark Values for Amorphous Silicon Semiconductors. *J. Am. Chem. Soc.* **2014**, *136*, 9477–9483.

(25) Randell, N. M.; Boutin, P. C.; Kelly, T. L. Bisisoindigo: Using a Ring-Fusion Approach to Extend the Conjugation Length of Isoindigo. *J. Mater. Chem. A.* **2016**, *4*, 6940–6945.

(26) Jiang, Y.; Gao, Y.; Tian, H.; Ding, J.; Yan, D.; Geng, Y.; Wang, F. Synthesis and Characterization of Isoindigo[7,6-g]Isoindigo-Based Donor–Acceptor Conjugated Polymers. *Macromolecules* **2016**, *49*, 2135–2144.

(27) Yue, W.; Ashraf, R. S.; Nielsen, C. B.; Collado-Fregoso, E.; Niazi, M. R.; Yousaf, S. A.; Kirkus, M.; Chen, H.-Y.; Amassian, A.; Durrant, J. R.; McCulloch, I. A Thieno[3,2-b][1]Benzothiophene Isoindigo Building Block for Additive- and Annealing-Free High-Performance Polymer Solar Cells. *Adv. Mater.* **2015**, *27*, 4702–4707.

(28) Randell, N. M.; Douglas, A. F.; Kelly, T. L. 7-Azaisoindigo as a New Electron Deficient Component of Small Molecule Chromophores for Organic Solar Cells. *J. Mater. Chem. A.* **2014**, *2*, 1085–1092.

(29) de Miguel, G.; Camacho, L.; a-Frutos, E. M. G. 7,7′-Diazaisoindigo: a Novel Building Block for Organic Electronics. *J. Mater. Chem. C.* **2016**, *4*, 1208–1214.

(30) Huang, J.; Mao, Z.; Chen, Z.; Gao, D.; Wei, C.; Zhang, W.; Yu, G. Diazaisoindigo-Based Polymers with High-Performance Charge-Transport Properties: From Computational Screening to Experimental Characterization. *Chem. Mater.* **2016**, *28*, 2209–2218.

(31) Yue, W.; Nikolka, M.; Xiao, M.; Sadhanala, A.; Nielsen, C. B.; White, A. J. P.; Chen, H.-Y.; Onwubiko, A.; Sirringhaus, H.; McCulloch, I. Azaisoindigo Conjugated Polymers for High Performance n-Type and Ambipolar Thin Film Transistor Applications. *J. Mater. Chem. C.* **2016**, *4*, 9704–9710.

(32) Huang, J.; Chen, Z.; Mao, Z.; Gao, D.; Wei, C.; Lin, Z.; Li, H.; Wang, L.; Zhang, W.; Yu, G. Tuning Frontier Orbital Energetics of Azaisoindigo-Based Polymeric Semiconductors to Enhance the Charge-Transport Properties. *Adv. Electron. Mater.* **2017**, No. 1700078.

(33) Wilson, J. N.; Bunz, U. H. F. Switching of Intramolecular Charge Transfer in Cruciforms: Metal Ion Sensing. *J. Am. Chem. Soc.* **2005**, *127*, 4124–4125.

(34) Zucchero, A. J.; McGrier, P. L.; Bunz, U. H. F. Cross-Conjugated Cruciform Fluorophores. *Acc. Chem. Res.* **2010**, *43*, 397–408.

(35) Zucchero, A. J.; Wilson, J. N.; Bunz, U. H. F. Cruciforms as Functional Fluorophores: Response to Protons and Selected Metal Ions. *J. Am. Chem. Soc.* **2006**, *128*, 11872–11881.

(36) Tolosa, J.; Zucchero, A. J.; Bunz, U. H. F. Water-Soluble Cruciforms: Response to Protons and Selected Metal Ions. *J. Am. Chem. Soc.* **2008**, *130*, 6498–6506.

(37) Welch, G. C.; Coffin, R.; Peet, J.; Bazan, G. C. Band Gap Control in Conjugated Oligomers via Lewis Acids. *J. Am. Chem. Soc.* **2009**, *131*, 10802–10803.

(38) Welch, G. C.; Bazan, G. C. Lewis Acid Adducts of Narrow Band Gap Conjugated Polymers. *J. Am. Chem. Soc.* **2011**, *133*, 4632–4644.

(39) Zalar, P.; Henson, Z. B.; Welch, G. C.; Bazan, G. C.; Nguyen, T.-Q. Color Tuning in Polymer Light-Emitting Diodes with Lewis Acids. *Angew. Chem. Int. Ed.* **2012**, *51*, 7495–7498.

(40) Zalar, P.; Kuik, M.; Henson, Z. B.; Woellner, C.; Zhang, Y.; Sharenko, A.; Bazan, G. C.; Nguyen, T.-Q. Increased Mobility Induced by Addition of a Lewis Acid to a Lewis Basic Conjugated Polymer. *Adv. Mater.* **2013**, *26*, 724–727.

(41) Ratcliff, E. L.; Bakus, R. C., II; Welch, G. C.; van der Poll, T. S.; Garcia, A.; Cowan, S. R.; MacLeod, B. A.; Ginley, D. S.; Bazan, G. C.; Olson, D. C. Formation of Interfacial Traps Upon Surface Protonation in Small Molecule Solution Processed Bulk Heterojunctions Probed by Photoelectron Spectroscopy. *J. Mater. Chem. C.* **2013**, *1*, 6223-6234.

(42) Pingel, P.; Arvind, M.; K lln, L.; Steyrleuthner, R.; Kraffert, F.; Behrends, J.; Janietz, S.; Neher, D. p-Type Doping of Poly(3-Hexylthiophene) with the Strong Lewis Acid Tris(Pentafluorophenyl)Borane. *Adv. Electron. Mater.* **2016**, *2*, No. 1600204.

(43) Gaussian 09, Revision D.01, Frisch, M. J.; Trucks, G. W.; Schlegel, H. B.; Scuseria, G. E.; Robb, M. A.; Cheeseman, J. R.; Scalmani, G.; Barone, V.; Petersson, G. A.; Nakatsuji, H.; Li, X.; Caricato, M.; Marenich, A.; Bloino, J.; Janesko, B. G.; Gomperts, R.; Mennucci, B.; Hratchian, H. P.; Ortiz, J. V.; Izmaylov, A. F.; Sonnenberg, J. L.; Williams-Young, D.; Ding, F.; Lipparini, F.; Egidi, F.; Goings, J.; Peng, B.; Petrone, A.; Henderson, T.; Ranasinghe, D.; Zakrzewski, V. G.; Gao, J.; Rega, N.; Zheng, G.; Liang, W.; Hada, M.; Ehara, M.; Toyota, K.; Fukuda, R.; Hasegawa, J.; Ishida, M.; Nakajima, T.; Honda, Y.; Kitao, O.; Nakai, H.; Vreven, T.; Throssell, K.; Montgomery, J. A., Jr.; Peralta, J. E.; Ogliaro, F.; Bearpark, M.; Heyd, J. J.; Brothers, E.; Kudin, K. N.; Staroverov, V. N.; Keith, T.; Kobayashi, R.; Normand, J.; Raghavachari, K.; Rendell, A.; Burant, J. C.; Iyengar, S. S.; Tomasi, J.; Cossi, M.; Millam, J. M.; Klene, M.; Adamo, C.; Cammi, R.; Ochterski, J. W.; Martin, R. L.; Morokuma, K.; Farkas, O.; Foresman, J. B.; Fox, D. J. Gaussian, Inc., Wallingford CT, **2016**.

(44) Gorelsky, S. I. SWizard Program, Http://Www.Sg-Chemistry.Net/, University of Ottawa, Canada, 2013.

(45) Gorelsky, S. I.; Lever, A. B. P. Electronic Structure and Spectra of Ruthenium Diimine Complexes by Density Functional Theory and INDO/S. Comparison of the Two Methods. *J. Organomet. Chem.* **2001**, *635*, 187–196.

(46) Parks, D. J.; Piers, W. E.; Parvez, M.; Atencio, R.; Zaworotko, M.J. Synthesis and Solution and Solid-State Structures of Tris (Pentafluorophenyl) Borane Adducts of PhC (O) X (X= H, Me, OEt, NPr^{i}_{2}). *Organometallics* **1998**, *17*, 1369–1377.

(47) Li, L.; Marks, T. J. New Organo-Lewis Acids. Tris (β-Perfluoronaphthyl) Borane (PNB) as a Highly Active Cocatalyst for Metallocene-Mediated Ziegler−Natta α-Olefin Polymerization. *Organometallics* **1998**, *17*, 3996–4003.

(48) Huang, W.; Besar, K.; LeCover, R.; Rule, A. M. A.; Breysse, P. N.; Katz, H. E. Highly Sensitive NH_3 Detection Based on Organic Field-Effect Transistors with Tris(Pentafluorophenyl)Borane as Receptor. *J. Am. Chem. Soc.* **2012**, *134*, 14650–14653.

(49) Han, Y.; Barnes, G.; Lin, Y.-H.; Martin, J.; Al-Hashimi, M.; AlQaradawi, S. Y.; Anthopoulos, T. D.; Heeney, M. Doping of Large Ionization Potential Indenopyrazine Polymers via Lewis Acid Complexation with Tris(Pentafluorophenyl)Borane: a Simple Method for Improving the Performance of Organic Thin-Film Transistors. *Chem. Mater.* **2016**, *28*, 8016–8024.

Chapter 4

Bisisoindigo: Using a Ring-Fusion Approach to Extend the Conjugation Length of Isoindigo

Reproduced from

Randell, N. M., Boutin, P. C., & Kelly, T. L.

J. Mater. Chem. A, **2016**, *4*, 6940–6945. DOI: 10.1039/c5ta07511d

with permission of the Royal Society of Chemistry.

Consent was obtained from all co-authors to include this manuscript in the thesis. Unless otherwise noted, I performed all experimental work and the writing of the manuscript. P.C. Boutin performed the fluorescence quenching experiments. T.L. Kelly directed the study and revised the manuscript.

Transition

The work described in this chapter marked a significant departure from the study of azaisoindigo. Since nitrogen substitution had proved to be ineffective in altering the frontier orbitals of isoindigo in Chapter 2, and the Lewis adducts presented in Chapter 3 could not be incorporated into OPVs, it was decided that a new direction for studying the optoelectronic properties of isoindigo-based semiconductors was required. This chapter introduces a second modification of isoindigo, the fusion of two isoindigo units in a coplanar dimer structure. While this is markedly different from heteroatom substitution, the goal of studying the effects of this structural change on the optoelectronic properties of the resulting semiconductors, particularly their frontier orbital energies, remained the same.

While there is some overlap in introductory material between this chapter and Chapter 1, the introduction here focuses on the use of expanded isoindigo structures as they existed in 2015. Particular attention is paid to the, at the time, emerging trend of using expanded isoindigo structures with emphasis placed on those synthesized by double cross aldol reactions.

.

4.1 Introduction

In the last several years, there have been significant advances in the field of organic semiconductor design that have produced substantial increases in the efficiency of OPV devices and the performance of OFETs. One of the chief reasons behind these advances has been the rise of new organic semiconductors characterized by their use of alternating electron donor and acceptor units.[1] Juxtaposition of these units leads to materials with substantially reduced bandgaps and good charge carrier mobilities. Common electron donors are often thiophene based (e.g., benzodithiophene,[2,3] thieno[3,2-b]thiophene[4-6]), due to the electron-rich nature of the thiophene ring. In contrast, electron-withdrawing imide and amide groups are prevalent in common acceptor units such as diketopyrrolopyrrole and isoindigo.

Isoindigo was first incorporated into organic semiconductors by Mei *et al*.,[7] and has since become ubiquitous throughout the field of organic electronics as an electron accepting unit in both polymers and small molecules.[8-15] Many studies have varied the identity of donor groups and alkyl chains, but relatively few variations of isoindigo itself have been reported.[16-21] Among the few reported modifications to isoindigo are the 7-haloisoindigos (both chloro and fluoro derivatives),[16,17,22] and thienoisoindigo, where the benzene ring is replaced with thiophene.[18-20] In recent work, the conjugation length of thienoisoindigo has been extended by the fusion of additional aromatic rings to the molecular structure. Both thienothiophene and benzothienothiophene have been used in this fashion to extend the planarity and conjugation length of isoindigos in organic electronics. [23,24]

More recently, the concept of using crossed aldol reactions to form expanded isoindigo units has been reported. The reaction of an isatin with benzodifurandione has been shown to produce an expanded, lactone-containing isoindigo system,[25,26] and the same type of crossed aldol

reaction between benzodifurandione and a thienoisatin yields the thienoisoindigo analogue.[27] A second example of an expanded isoindigo system is prepared from the condensation of 2,2′-bithiophene-5,5′-dicarboxyaldehyde with an isatin to form an isoindigo-like motif containing an interior bithiophene group.[28] Most recently, two groups independently synthesized an expanded isoindigo structure in which one phenyl ring bears two lactam moieties oriented *para*- to one another.[29,30] this work has been inspired by the idea of exploiting crossed aldol chemistry to expand the isoindigo core unit, as well as using ring fusion to further extend the conjugation length of the system.

Herein, the synthesis of bisisoindigo, an expanded isoindigo structure that consists of two isoindigo moieties fused across the 6 and 7 positions is reported. The bisisoindigo building block features a highly extended conjugation length, having an optical band gap well into the near-infrared. The dibromobisisoindigo derivative was coupled to a 2,2′-bithiophene moiety to create an organic semiconductor with a donor-acceptor motif. Thin films of this material absorb across the entire visible region, with an absorption edge of nearly 1000 nm. Both bisisoindigo and the donor-acceptor compound were incorporated into the active layers of OPVs. While device performance was modest, both bisisoindigo-based compounds were able to function as electron donors. Bisisoindigo is an exciting new electron-deficient building block in the synthesis of organic semiconductors, and it is anticipated that through judicious choice of both donor sub-unit and alkyl chain length, it will lead to a number of new, high-performance organic semiconductors.

4.2 Experimental

4.2.1 Materials and characterization

Prior to use DMF and toluene were dried over activated 3 Å molecular sieves and stored under nitrogen. $Pd(PPh_3)_4$ was stored in an inert atmosphere N_2 glove box when not in use. All other solvents and reagents were used as received. NMR spectra were obtained using a Bruker Avance 500 MHz spectrometer. UV/vis spectroscopy measurements were performed in $CHCl_3$ or as thin films on glass substrates using a Cary 6000i UV/vis spectrophotometer. AFM measurements were performed using a Dimensions Hybrid Nanoscope system (Veeco Metrology Group). Cyclic voltammetry was carried out in 0.05 mol L^{-1} tetrabutylammonium hexafluorophosphate dissolved in dry, degassed CH_2Cl_2. The working electrode was glassy carbon, the counter electrode was a Pt wire, and the reference electrode was a Ag wire. Voltammograms were referenced to an internal Fc/Fc^+ standard. Mass spectra were acquired on a JEOL AccuToF 4G GCv mass spectrometer with an EiFi Field desorption ionization source. Melting points were measured using a DigiMelt MPA160 (Stanford Research Systems) melting point analyser. Elemental analysis was carried out on a 2400 CHN Elemental analyser (Perkin Elmer).

Fluorescence spectra for quenching and quantum yield experiments were measured using a Photon Technology International QuantaMaster spectrofluorometer. Data were smoothed by a Savitzky-Golay algorithm. Fluorescence-quenching experiments were performed by titrating solutions of P3HT or PTB7-Th with either **6** or **8**. In all cases the donor concentration was held fixed at 45 μg/mL while the acceptor concentration was increased from 0 to ~45 μg/mL. Fluorescence quantum yields of P3HT and PTB7-Th in chloroform were calculated via the comparative method,[31] taking

$$\Phi_F^x = \Phi_F^s \frac{1 - 10^{A_{\lambda ex}^s}}{1 - 10^{A_{\lambda ex}^x}} \frac{\int F^x(\lambda_{em})}{\int F^s(\lambda_{em})} \frac{n_x^2}{n_s^2}$$

where x is the compound under study, s is the reference standard, and Φ_F, A, $F(\lambda_{em})$, and n are the fluorescence quantum yield, absorption, fluorescence spectrum, and solvent refractive index, respectively. The sample and reference standard were excited at the same wavelength, far removed from any fluorescence features. Fluorescence spectra were corrected for reabsorption. Rhodamine 6G in chloroform, which has a fluorescence quantum yield of 0.75,[32] was used as the reference standard for P3HT. Chlorophyll a in methanol ($\Phi_F = 0.15$)[33] was used as the reference standard for PTB7-Th. Stern-Volmer constants (K_{sv}) for donor-acceptor pairs were determined from the slope of the Stern-Volmer plots. DFT and TDDFT calculations were carried out, using the Gaussian 09 and Gaussview suites of software, at a B3LYP/6-31G(d,p) level of theory using a chloroform dielectric continuum model. Alkyl substituents on **6** and **8** were replaced with methyl groups in order to simplify the calculations.[34] The UV/vis spectra were calculated using the SWizard program, revision 5.0, using the (Gaussian/Lorentzian/pseudo-Voigt) model.[35,36]

4.2.2 OPV fabrication and testing

ITO-coated glass substrates (Delta Technologies, R_s = 15-25 Ω/□) were cleaned by sequential sonication in: Extran detergent (10% v/v in Millipore H_2O), Millipore H_2O, acetone and isopropanol. Cleaned substrates were stored under isopropanol until use. Substrates were blown dry with compressed air and UV/ozone cleaned for 15 min immediately prior to use. Poly(3,4-ethylenedioxythiophene:polystyrene sulfonate (Clevios P VP AI 4083) solutions were mixed with 0.5% v/v Zonyl F-300 fluoro-surfactant (40% solids in H_2O) and filtered through a 0.45 μm syringe

filter. The solution was then spin cast onto the ITO substrates and annealed at 125 °C for 10 min before being placed in a nitrogen atmosphere glove box. Active layer solutions were prepared at a 1:1 donor:acceptor ratio (by mass), and were stirred overnight and syringe filtered using a 0.45 μm filter before use. DIO was added after filtration. Active layers were spin cast at either 5000 rpm ($CHCl_3$) or 1000 rpm (*o*-dichlorobenzene and chlorobenzene). Residual solvent was allowed to evaporate at room temperature for 1 hour before electrode deposition. LiF (0.8 nm) and Al (100 nm) were then thermally evaporated onto the substrates at a base pressure of 3×10^{-6} mbar.

Current-voltage measurements were made inside a nitrogen atmosphere glove box using a Keithley 2400 source-measure unit. The cells were illuminated by a 450 W Class AAA solar simulator equipped with an AM1.5G filter (Sol3A, Oriel instruments) at a calibrated intensity of 100 mW cm^{-2}, as determined by a standard silicon reference cell (91150V, Oriel Instruments). The cell area was defined by a non-reflective anodized aluminium mask to be 0.0708 cm^2. Incident photon-to-current efficiency (IPCE) measurements were performed on the highest efficiency devices in a nitrogen atmosphere using a QE-PV-SI system (Oriel Instruments) consisting of a 300 W Xe arc lamp, monochromator, chopper, lock-in amplifier, and certified silicon reference cell. Measurements were made using a 30 Hz chop frequency.

4.2.3 Detailed synthetic procedures

2-Ethylhexyl iodide and 5-hexyl-5′-tertbutylstannyl-2,2′-bithiophene were synthesized according to previously reported methods.[37,38]

1-(2-Ethylhexyl)isatin[39]

Isatin (2.00 g, 13.6 mmol) and K_2CO_3 (2.25 g, 16.3 mmol) were dissolved in 50 mL of DMF and the mixture was heated to 100 °C. 2-Ethylhexyl bromide (3.0 mL, 16.8 mmol) was added via syringe and the resulting mixture was stirred at 100 °C for 18 hours. The reaction mixture was poured over ice and extracted with CH_2Cl_2. The combined organic layers were washed with brine, dried over $MgSO_4$ and concentrated. The resulting orange solid was heated to 90 °C *in vacuo* to remove excess 2-ethylhexyl bromide, yielding 1-(2-ethylhexyl)isatin as an orange oil (3.11 g, 88%). ^{1}H NMR (500 MHz, $CDCl_3$, ppm) δ: 7.55-7.62 (m, 2H), 7.11 (t, J = 7.5 Hz, 1H), 6.87 (d, J = 7.9 Hz, 1H), 3.56-3.65 (m, 2H), 1.78-1.85 (m, 1H), 1.24-1.42 (m, 8H), 0.94 (t, J = 7.5 Hz, 3H), 0.89 (t, J = 7.1 Hz, 3H). ^{13}C NMR (125 MHz, $CDCl_3$) δ: 183.82, 158.68, 151.69, 138.45, 125.59, 123.75, 117.83, 110.57, 44.57, 37.54, 30.81, 28.81, 24.16, 23.21, 14.23, 10.76. HRMS (*m/z*) ($M^{\bullet+}$): Calc ($C_{16}H_{21}NO_2$): 259.15723 Found: 259.15691. Anal. Calcd for $C_{16}H_{21}NO_2$: C, 74.10; H, 8.16; N, 5.40; Found: C, 73.86; H, 7.91; N, 5.38.

6-Bromo-1-(2-ethylhexyl)isatin[39]

6-Bromoisatin was reacted with 2-ethylhexyl bromide following the same procedure as for the synthesis of 1-(2-ethylhexyl)isatin, yielding 6-bromo-1-(2-ethylhexyl)isatin as an orange solid (1.38 g, 46%). m.p. 62-64 °C. ^{1}H NMR (500 MHz, $CDCl_3$, ppm) δ: 7.46 (d, J = 8.0 Hz, 1H), 7.27 (d, 8.0 Hz, 1H), 7.03 (s, 1H), 3.54-3.63 (m, 2H), 1.77-1.82 (m, 1H), 1.29-1.41 (m, 9H), 0.94 (t, J

= 7.5 Hz, 3H), 0.90 (t, J = 7.0 Hz, 3H). ^{13}C NMR (125 MHz, $CDCl_3$) δ: 182.4, 158.4, 152.4, 133.6, 126.9, 126.5, 116.4, 114.1, 44.7, 37.3, 30.6, 28.5, 24.0, 23.1, 14.1, 10.6. HRMS (*m/z*) ($M^{\bullet+}$): Calc ($C_{16}H_{20}NO_2Br$): 337.06774 Found: 337.06652. Anal. Calcd for $C_{16}H_{20}NO_2Br$: C, 56.82; H, 5.96; N, 4.14; Found: C, 57.39; H, 5.97; N, 4.23.

Bisisatin (**2**)

1,5-Diaminonaphthalene (2.01 g, 12.7 mmol) was dissolved in 20 mL of glacial acetic acid and heated to reflux. To the resulting purple solution, was added a solution of diethylketomalonate (8.0 mL, 52 mmol) in glacial acetic acid (23 mL) dropwise over 0.75 hours. The resulting red-brown suspension was heated at reflux for 18 hours. The acetic acid was removed *in vacuo* and the resulting red solid was dissolved in 1 mol L^{-1} NaOH to a final solution pH of 11-12. The resulting dark brown solution was heated at reflux with sparging air for 5 hours. The solution was then poured onto ice and acidified to pH 0 with aqueous 6 mol L^{-1} HCl. The resulting red-purple solid was collected by suction filtration, washed with H_2O and dried *in vacuo* to yield the crude product as a black-purple solid (3.28 g, 97%). The crude product was determined to be approximately 75% pure by ^{1}H NMR spectroscopy; however, due to its extremely low solubility, the product was carried forward without further purification. ^{1}H NMR (500 MHz, DMSO-d_6, ppm) δ: 11.78 (s, 2H), 7.79 (d, J = 8.3 Hz, 2H), 7.61 (d, J = 8.3 Hz, 2H).

1,1′-Bis(2-ethylhexyl)bisisatin (**3**)

In an oven dried Schlenk flask, crude **2** (2.42 g, 9.08 mmol) and freshly dried K_2CO_3 (3.16 g, 22.9 mmol) were dissolved in 50 mL of dry DMF. The reaction mixture was heated to 70 °C, 2-ethylhexyliodide (8.60 g, 35.8 mmol) was added via syringe, and the temperature was increased

to 100 °C for a further 5.5 hours. The reaction mixture was poured over 200 mL H_2O and acidified to pH 7 with aqueous 1 mol L^{-1} HCl. The aqueous layer was extracted with CH_2Cl_2. The organic layers were dried over $MgSO_4$ and concentrated to yield the crude product as a viscous black oil. The crude product was purified by column chromatography on silica gel (eluent: 1:3 ethyl acetate (EtOAc):hexanes) followed by recrystallization from 1:3 EtOAc:hexanes. The resulting blue solid was isolated by suction filtration and dried *in vacuo*. Total yield **3**: 984 mg (30% yield, assuming 75% pure **1**). m.p. 175 °C (decomp.). ^{1}H NMR (500 MHz, $CDCl_3$, ppm) δ: 8.00 (d, J = 8.7 Hz, 2H), 7.67 (d, J = 8.6 Hz, 2H), 4.11-4.24 (m, 5H), 1.85-1.91 (m, 2H), 1.23-1.45 (m, 16H), 0.93 (t, J = 7.5 Hz, 6H), 0.87 (t, J = 6.6 Hz, 6H). ^{13}C NMR (125 MHz, $CDCl_3$) δ: 182.7, 159.3, 152.3, 127.4, 120.1, 120.0, 116.447.2, 38.7, 30.1, 28.4, 28.3, 23.5, 23.0, 14.0, 10.35, 10.33. HRMS (*m/z*): ($M^{\bullet+}$) Calc ($C_{30}H_{38}N_2O_4$): 490.28316 Found: 490.28261. Anal. Calcd for $C_{30}H_{38}N_2O_4$: C, 73.44; H, 7.81; N, 5.71; Found: C, 73.43; H, 7.70; N, 5.64.

1-(2-Ethylhexyl)-2-oxindole **(4)**[16,40]

1-(2-ethylhexyl)isatin (3.11 g, 12.0 mmol) was suspended in 20 mL of hydrazine hydrate and the reaction mixture was heated at reflux for 4 hours. The reaction mixture was cooled and extracted with EtOAc. The combined organic layers were dried over $MgSO_4$ and concentrated to yield a yellow solid. Metallic sodium (0.86 g) was dissolved in 40 mL of anhydrous EtOH. The yellow solid was transferred into the EtOH/NaOEt solution using anhydrous EtOH and the reaction mixture was heated at reflux for 2 hours. The resulting brown solution was poured over ice and acidified with aqueous 1 mol L^{-1} HCl. The suspension was extracted with EtOAc and the combined organic layers were washed with brine, dried over $MgSO_4$, and concentrated to yield pure 1-(2-ethylhexyl)-2-oxindole as a yellow-orange oil (2.51 g, 85%). ^{1}H NMR (500 MHz, $CDCl_3$, ppm) δ:

7.22-7.28 (m, 3H), 7.02 (t, J = 7.5 Hz, 1H), 6.81 (t, J = 7.5 Hz, 1H), 3.54-2.64 (m, 2H), 3.53 (s, 1H), 1.79-1.84 (m, 1H), 1.23-1.40 (m, 13H), 0.92 (t, J = 7.5 Hz, 3H), 0.88 (t, J = 7.0 Hz, 3H). ^{13}C NMR (125 MHz, $CDCl_3$) δ:175.4, 145.1, 127.8, 124.7, 124.4, 122.0, 108.6, 44.1, 37.4, 35.8, 30.7, 28.7, 24.0, 23.1, 14.1, 10.7. HRMS (*m/z*) ($M^{\bullet+}$): Calc ($C_{16}H_{23}NO$): 245.17796 Found: 245.17699. Anal. Calcd for $C_{16}H_{23}NO$: C, 78.32; H, 9.45; N, 5.71; Found: C, 77.98; H, 9.61; N, 5.95.

6-Bromo-1-(2-ethylhexyl)-2-oxindole **(5)**[16,40]

6-bromo-1-(2-ethylhexyl)isatin was reacted with hydrazine hydrate and NaOEt/EtOH following the same procedure as **4** to yield an orange-red solid (1.33 g, quantitative yield). m.p. 46-48 °C. ^{1}H NMR (500 MHz, $CDCl_3$, ppm) δ:7.15 (d, J = 7.80 Hz, 1H), 7.09 (d, J = 7.85 Hz, 1H), 6.93 (s, 1H), 3.51-3.58 (m, 2H), 3.46 (s, 2H), 1.77-1.82 (m, 1H), 1.24-1.34 (m, 12H), 0.88-0.94 (m, 7H). ^{13}C NMR (125 MHz, $CDCl_3$) δ: 175.2, 146.5, 125.7, 125.0, 123.5, 121.4, 112.1, 44.4, 37.3, 35.5, 30.6, 28.7, 24.0, 23.2, 14.2, 10.7. HRMS (*m/z*) ($M^{\bullet+}$) Calc ($C_{16}H_{22}NOBr$): 323.08848, Found: 323.08762. Anal. Calcd for $C_{16}H_{22}NOBr$: C, 59.27; H, 6.84; N, 4.32; Found: C, 59.45; H, 6.81; N, 5.19.

Bisisoindigo (**6**)

Compounds **3** (399 mg, 0.812 mmol) and **4** (478 mg, 1.95 mmol) were dissolved in 15 mL of glacial acetic acid. Concentrated HCl (100 μL) was added and the reaction mixture was heated at reflux for 14 hours. After 14 hours, the reaction mixture was poured over a mixture of ice and brine, and extracted with CH_2Cl_2. The combined organic layers were washed with brine, dried over $MgSO_4$, and concentrated to yield the crude product as a black solid. The crude product was purified by column chromatography (silica gel, eluent: 3:2 CH_2Cl_2:hexanes) and concentrated *in*

vacuo to yield a dark brown-black solid (347 mg, 45%). m.p. 250-252 °C. ^{1}H NMR (500 MHz, CD_2Cl_2, ppm) δ: 9.06 (d, *J* = 7.9 Hz, 2H), 9.00 (d, *J* = 9.3 Hz, 2H), 7.87 (d, *J* = 9.36, 2H), 7.37 (t, *J*= 8.2, 2H), 7.03 (t, *J* = 7.4 Hz, 2H), 6.82 (d, *J* = 7.8 Hz, 2H), 4.20-4.35 (m, 4H), 3.62-3.73 (m, 4H), 1.98-2.07 (m, 2H), 1.84-1.92 (m, 2H), 1.22-1.48 (m, 37 H), 0.84-0.99 (m, 26H). ^{13}C NMR (125 MHz, $CDCl_3$) δ:169.9, 168.1, 145.4, 143.2, 134.0, 132.9, 132.4, 129.2, 124.3, 123.4, 122.3, 122.1, 120.1, 117.2, 108.4, 47.0, 44.3, 38.5, 37.7, 30.8, 30.2, 28.8, 28.3, 24.1, 23.5, 23.1, 14.1, 14.0, 10.7, 10.5. HRMS. (*m/z*): ($M^{\bullet+}$) Calc ($C_{62}H_{80}N_4O_4$): 944.61795 Found: 944.62061. Anal. Calcd for $C_{62}H_{80}N_4O_4$: C, 78.77; H, 8.53; N, 5.93; Found: C, 77.79; H, 8.60; N, 5.78.

Dibromo-bisisoindigo (**7**)

Compounds **3** (462.6 mg, 0.9433 mmol) and **5** (827.6 mg, 2.55 mmol) were dissolved in 20 mL of glacial acetic acid. Concentrated HCl (100 µL) was added and the reaction mixture was heated at reflux for 18 hours. The reaction mixture was poured over H_2O and extracted with CH_2Cl_2. The combined organic layers were washed with brine, dried over $MgSO_4$, and concentrated to yield the crude product. The crude product was purified by column chromatography (silica gel, eluent: 7:3 CH_2Cl_2:hexanes, gradient to 10:1 CH_2Cl_2:MeOH). The combined fractions were concentrated *in vacuo* to yield a brown-black solid; the solid was washed with acetone and dried on high vacuum to yield the pure product as a black/brown solid (235 mg, 23%). m.p. 237-252 °C (decomp.). ^{1}H NMR (500 MHz, $CDCl_3$, ppm) δ: 8.95 (dd, J_1 = 2.4 Hz, J_2 = 9.0 Hz, 4H), 7.84 (d, *J* = 9.4 Hz, 2H), 7.17 (d, *J* = 8.6 Hz, 2H), 6.90 (s, 2H), 4.18-4.30 (m, 4H), 3.58-3.71 (m, 4H), 1.95-2.04 (m, 2H), 1.80-1.90 (m, 2H), 1.21-1.47 (m, 34 H), 0.83-0.98 (m, 25H).^{13}C NMR (125 MHz, $CDCl_3$) δ: 169.9, 168.0, 143.4, 132.6, 132.6, 130.3, 126.9, 125.2, 120.8, 117.3, 111.7, 47.0, 44.4, 38.5, 37.5, 30.6, 30.2, 28.6, 28.3, 24.0, 23.5, 23.1, 14.1, 14.0, 10.7, 10.5, 7.8. HRMS (*m/z*) ($M^{\bullet+}$) Calc

($C_{62}H_{78}Br_2N_2O_4$): 1102.43693 Found: 1102.43715. Anal. Calcd for $C_{62}H_{78}Br_2N_2O_4$: C, 67.51; H, 7.13; N, 5.08; Found: C, 67.15; H, 7.45; N, 5.91.

Bis-bithiophene-bisisoindigo (**8**)

Compound **7** (145 mg, 0.132 mmol), $Pd(PPh_3)_4$ (11.1 mg, 9.6 μmol), and 5′-hexyl-5-tributylstannyl-2,2′-bithiophene (315 mg, 0.584 mmol) were added sequentially to 15 mL dry, degassed toluene. The reaction mixture was heated to reflux for 15 hours. The reaction mixture was concentrated *in vacuo*, purified by column chromatography (silica gel, eluent 70:30 toluene:hexanes, gradient to 3% methanol in toluene). The combined fractions were concentrated *in* vacuo; the resulting solid was recrystallized from CH_2Cl_2/acetone, filters, and dried on high vacuum to yield a blue-black solid (151 mg, 80%). m.p. 237-245 °C. ^{1}H NMR (500 MHz, CD_2Cl_2, ppm) δ: 9.02 (d, *J* = 8.4 Hz, 2H), 8.90 (d, *J* = 9.2 Hz, 2H), 7.78 (d, *J* = 9.6 Hz, 2H), 7.31 (d, *J* = 3.8 Hz, 2H), 7.21 (d, *J* = 8.7 Hz, 2H) 7.05 (q, *J* = 5.8 Hz, 4H), 6.71 (d, *J* = 3.6 Hz), 4.19-4.34 (m, 5H), 3.60-3.78 (m 5H), 2.80 (t, *J* = 7.6 Hz, 3H), 1.97-2.04 (m, 3H), 1.82-1.91 (m, 2H), 1.65-1.73 (m, 4H), 1.53-1.63 (m, 6H), 1.21-1.49 (m, 39H), 0.82-1.00 (m, 24H). ^{13}C NMR 125 MHz, $CDCl_3$) δ: 169.8, 168.3, 146.2, 145.8, 142.6, 141.8, 138.9, 137.8, 134.5, 132.5, 130.6, 129.9, 125.2, 125.0, 124.1, 124.0, 123.8, 122.9, 121.1, 119.9, 118.5, 117.0, 104.5, 46.9, 44.0, 38.5, 37.8, 31.6, 31.56, 30.9, 30.3, 30.2, 29.7, 28.0, 28.8, 28.8, 28.4, 28.3, 24.2, 23.5, 23.2, 23.2, 23.1, 22.6, 14.2, 14.1, 10.9, 10.6, 10.6, 10.5. HRMS (*m/z*) ($M^{\bullet+}$) Calc ($C_{90}H_{112}N_4O_4S_4$): 1440.75664 Found: 1440.75420. Anal. Calcd for $C_{90}H_{112}N_4O_4S_4$: C, 74.96; H, 7.83; N, 3.88; Found: C, 74.78; H, 8.49; N, 3.29.

4.3 Results and discussion

4.3.1 Synthesis of bisisoindigo (6) and donor-acceptor molecular semiconductor (8)

The preparation of bisisoindigo presented several distinct synthetic challenges. Isatins are often synthesized by the Sandmeyer isatin synthesis.[41] Attempts to perform the Sandmeyer isatin synthesis using 1,5-diaminonaphthalene (**1**) as described by Kossmehl and Manecke[42] yielded the desired bisisatin (**2**) as a minor product and aminobenzoisatin as the major product (Scheme 4.1). The ring-closing step of the Sandmeyer isatin synthesis requires the electrophillic aromatic substitution of a hydroxyimine group onto a benzene ring.[43] When attempting to perform this reaction twice on a single ring system, the formation of the first isatin withdraws much of the electron density from the ring, preventing the second ring closure. Therefore, in order to synthesize bisisatin (**2**), the Martinet isatin synthesis (Scheme 4.1) was employed.[44] In this reaction, the ring closing step produces a 3-hydroxy-2-oxindole intermediate. This group is much less electron withdrawing than an isatin, and therefore the aromatic ring is not deactivated towards the second ring closure. Bubbling air is sufficient to oxidize both 3-hydroxy-2-oxindole groups to the corresponding isatins, producing bisisatin as the major product.

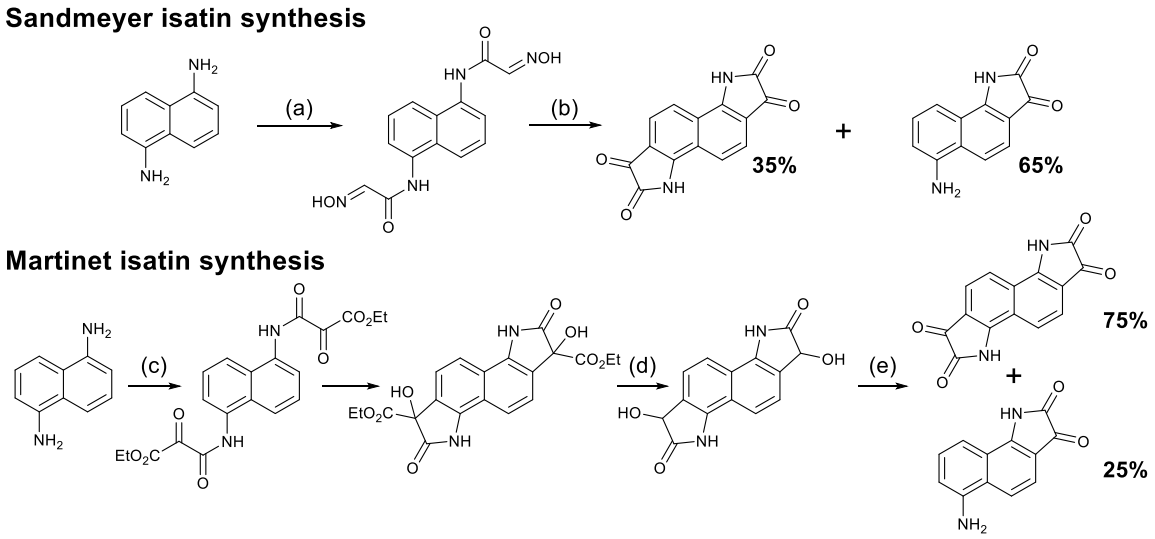

Scheme 4.1 Sandmeyer and Martinet isatin syntheses. (a) $C(OH)_2CCl_3$, NH_3OHCl, (b) H_2SO_4, (c) diethylketomalonate, glacial acetic acid, (d) NaOH, H_2O, (e) sparging air.

The synthesis of compounds **6** and **8** using this Martinet isatin synthesis is shown in Scheme 4.2. The electron deficient nature of **2** stabilizes the anion formed by deprotonation of the amide, making it a poor nucleophile, and alkyl iodides were required to alkylate the heterocyclic *N*-atom to form **3**. An acid-catalysed double crossed aldol reaction of **3** and the appropriate 2-oxindole derivatives (**4** or **5**) was then used to complete the synthesis of **6** and **7**. The dibrominated derivative was subsequently used in a Stille cross-coupling reaction with 5-tributylstannyl-5'-hexyl-2,2'-bithiophene to form a donor-acceptor-donor molecule, **8.** Significant colour changes were noted with each subsequent extension of the conjugation; **3** is a blue solid, **6** is a brown-black solid, and **8** is a dark blue-black solid.

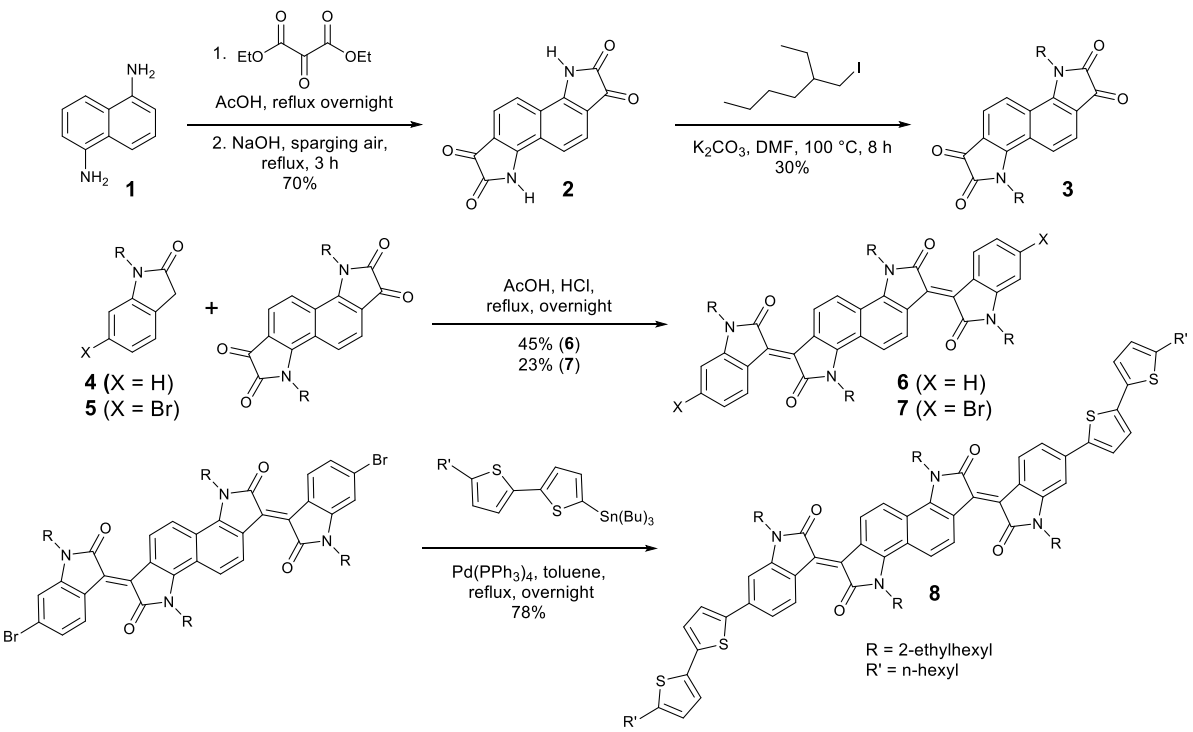

Scheme 4.2 Synthesis of bisisoindigo (**6**) and bis(5′-hexyl-2,2′-bithienyl)-bisisoindigo (**8**).

4.3.2 Frontier orbital energies and absorption spectroscopy

Solution and solid-state UV/vis spectroscopy was performed on **6** and **8** (Figure 4.1a,b). Using TDDFT calculations (Figure 4.2 and 4.1c), the lowest energy peak in the spectra of both **6** and **8** can be assigned to the HOMO to LUMO transition; the additional peak at 625 nm in the spectrum of **8** is assigned to a transition from a bithiophene-based π-orbital to the LUMO. As a result of the extended conjugation in bisisoindigo, both molecules absorb well into the near-infrared. The effect of the donor bithiophene group is immediately apparent when the spectra of **6** and **8** are compared. While the HOMO to LUMO transition in **6** has a relatively low oscillator strength, the HOMO to LUMO transition in **8** is much more intense. This increase in oscillator strength is also predicted by the TDDFT calculations. Calculation of the frontier orbital geometries of both **6** and **8** (Figure 4.2) reveals a higher degree of orbital localization in the LUMO of the

donor-acceptor compound. While both the HOMO and LUMO of **6** are delocalized across the entire molecule, the LUMO of **8** is isolated almost entirely on the bisisoindigo core. This localization leads to an increase in the transition dipole moment of the HOMO to LUMO transition, greatly increasing its extinction coefficient. The large extinction coefficient and small band gap (Table 4.1) of **8** are ideal characteristics for application in organic photovoltaic devices.

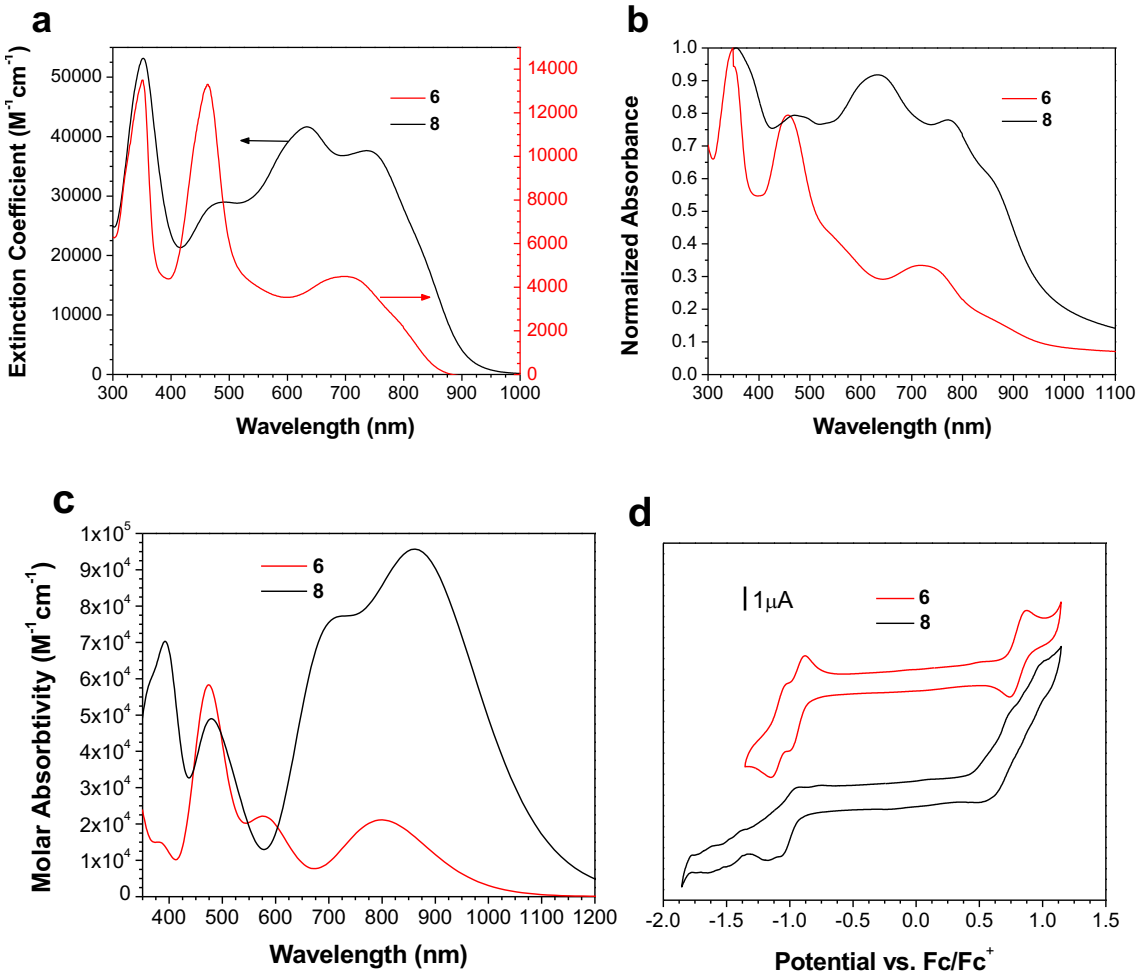

Figure 4.1 UV/vis absorption spectra of **6** and **8** in (a) $CHCl_3$ and (b) as a thin film on glass. (c) Theoretical UV/vis spectra of **6** and **8**. (d) Cyclic voltammagrams of **6** and **8**.

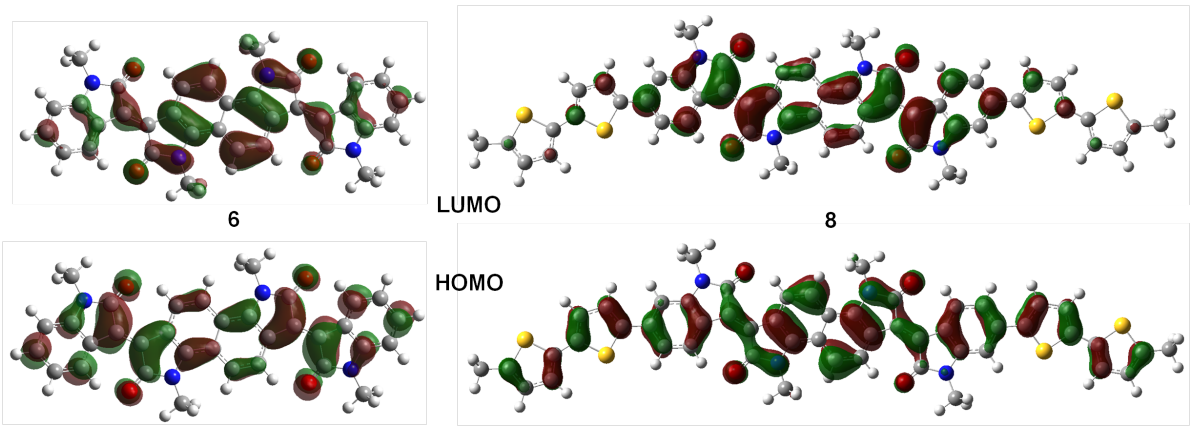

Figure 4.2 Frontier molecular orbitals of **6** and **8**.

Cyclic voltammetry (Figure 4.1d) was used to determine the absolute energy levels of **6** and **8** (Table 4.1). Consistent with the addition of electron donating bithiophene groups, the HOMO of **8** lies 0.2 eV higher in energy than that of **6**; however, the energy of the LUMO is unchanged, providing further evidence that the bithiophene groups do not appreciably contribute to the LUMO. Compound **6** exhibits a quasi-reversible oxidation wave, as well as two independent quasi-reversible reduction peaks. Conversely, neither the oxidation nor reduction of **8** was reversible. Upon oxidation and reduction, a solid film was noted on the surface of the glassy carbon electrode. The onset of oxidation and reduction were used to estimate the HOMO and LUMO levels of **6** and **8**, and are listed in Table 4.1.

Table 4.1 Calculated and experimental frontier orbital energy levels and band gaps of **6** and **8**.

Compound	E_{HOMO}[a] (eV)	E_{LUMO}[a] (eV)	$E_{g,elec}$ (eV)	$E_{g,calc}$ (eV)	$E_{g,opt}$ (eV)
6	5.8	4.2	1.6	1.55	1.44
8	5.6	4.2	1.4	1.42	1.27

[a]Voltammagrams were referenced to the Fc/Fc^+ redox couple (5.1 eV *vs.* vacuum) and subsequently referenced to vacuum. HOMO and LUMO values were taken from the onset of oxidation and reduction respectively.

4.3.3 Organic solar cell performance of compounds 6 and 8

The cyclic voltammetry results indicated that the frontier orbital energies of both **6** and **8** lay in between those of OPV donor materials such as PTB7-Th,[3] and fullerene-based acceptors such as $PC_{71}BM$. This suggested that **6** and **8** could be used as either the electron donor or the electron acceptor in an OPV device. Therefore, **6** and **8** were tested in both roles: as the electron acceptor (blended with PTB7-Th), and as the electron donor (blended with $PC_{71}BM$).

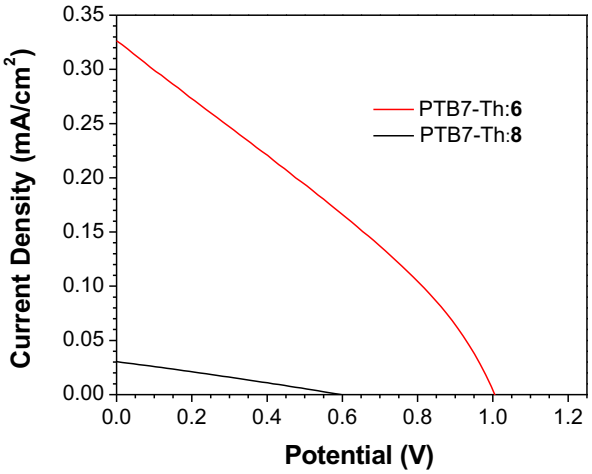

Figure 4.3 Current-voltage curves of the best devices fabricated with PTB7-Th:**6** and PTB7-Th:**8** active layers.

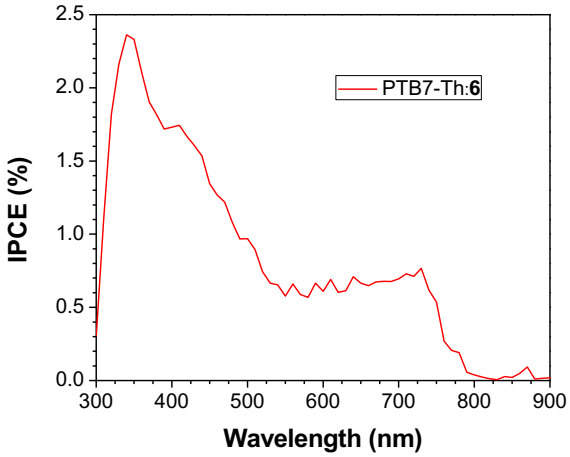

Figure 4.4 IPCE spectrum of a representative OPV device fabricated with a PTB7-Th:**6** active layer.

Table 4.2 Champion photovoltaic device performance of ITO/PEDOT:PSS/Active layer/LiF/Al bulk heterojunction solar cells.

Active Layer	V_{OC} **(V)**	J_{SC} **(mA·cm^{-2})**	**Fill Factor (%)**	**Efficiency (%)**
PTB7-Th:**6**	1.0	0.33	31	0.10
6:$PC_{71}BM$	0.68	0.92	45	0.28
PTB7-Th:**8**	0.60	0.030	27	0.0048
8:$PC_{71}BM$	0.59	1.28	30	0.23

OPVs were first fabricated using an active layer blend of PTB7-Th:**6** (Table 4.2, Figure 4.3-4.4). Device performance was modest, but improved greatly with the addition of DIO. AFM images of PTB7-Th:**6** blends (Figure 4.5) suggests that the addition of DIO decreases the domain size from ~1 μm to <100 nm. Unfortunately, even upon addition of DIO, some large crystallites were still visible. However, although the overall efficiency was low, the devices did nonetheless display very high V_{OC} values (up to 1.0 V). OPVs fabricated with PTB7-Th:**8** active layers also performed relatively poorly. This is likely because **8** was insufficiently soluble in chlorobenzene and *o*-dichlorobenzene, the ideal solvents for processing PTB7-Th. The films cast from chloroform

exhibited poor film morphologies and large domain sizes, which greatly reduced device performance (Figure 4.3 and Figure 4.6).

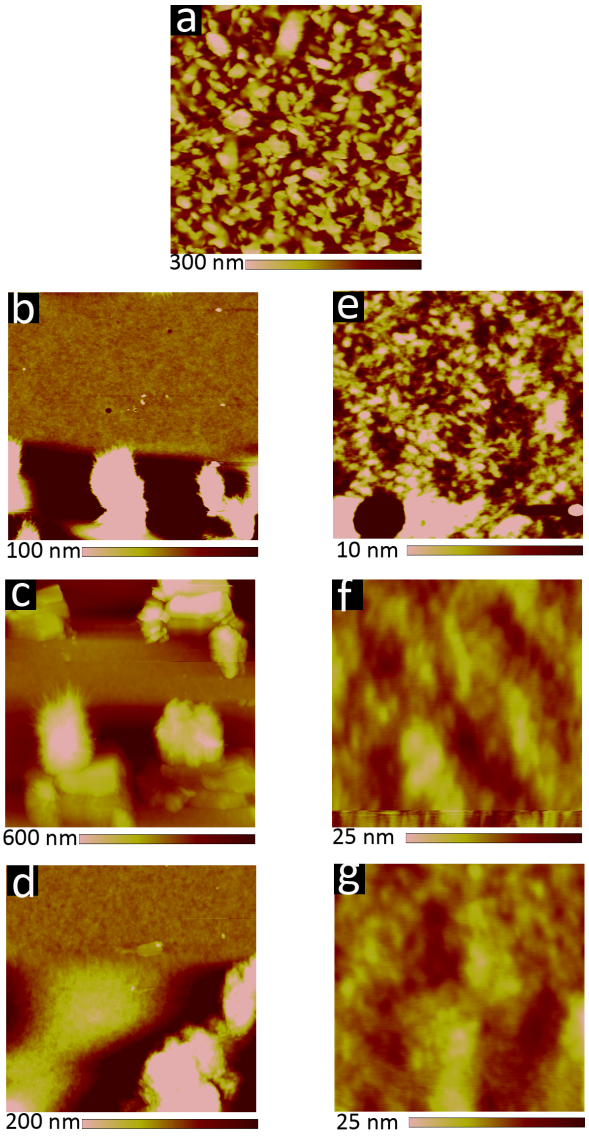

Figure 4.5 AFM images of PTB7-Th:**6** active layer blends cast from 20 mg/mL solutions containing: (a) 0%, (b,e) 1% , (c,f) 2%, (d,g) 3% DIO.
Images (a-d) are 10 µm × 10 µm, images (e-g) are 1 µm × 1 µm.

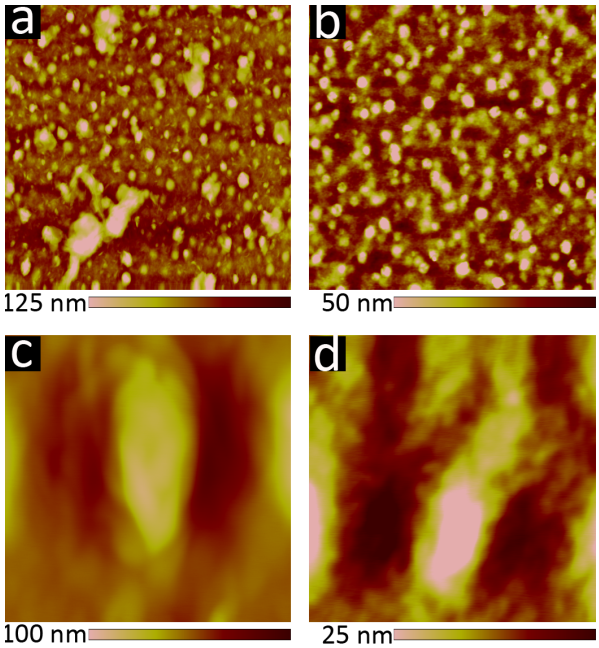

Figure 4.6 AFM images of PTB7-Th:**8** active layer blends cast from 20 mg/mL solutions containing:(a,c) 0%, (b,d) 1% DIO.
Images (a-b) are 10 μm × 10 μm, images (c-d) are 1 μm × 1 μm.

Although poor film morphology is likely the cause of the poor photovoltaic performance, one alternative is a lack of energetic driving force for electron transfer at the donor/acceptor interface. Electron transfer between the donor (PTB7-Th) and acceptor (**6**/**8**) was therefore evaluated using solution phase fluorescence spectroscopy (Figure 4.7-4.8); a decrease in donor fluorescence in the presence of **6** or **8** is indicative of electron transfer. The fluorescence quantum yield of P3HT in chloroform was measured as 0.22, which is comparable to the previously reported value of 0.33 ± 0.07 in chlorobenzene.[45] The fluorescence quantum yield of PTB7-Th in chloroform was measured as 0.042, which is comparable to the previously recorded value of 0.02 for PTB7 in chlorobenzene.[46] In order to extract quantitative information regarding fluorescence quenching, a Stern-Volmer analysis was performed (Figure 4.9). The fluorescence quenching of PTB7-Th yielded Stern-Volmer constants of (1.5 ± 0.4) × 10^4 mol^{-1} L when quenched by **6**, and

$(4.8 \pm 0.8) \times 10^4$ mol^{-1} L when quenched by **8**. These values are similar to the Stern-Volmer quenching constant obtained when P3HT emission is quenched by $PC_{61}BM$ (1.6×10^4 mol^{-1} L).[47] This suggests that there is a sufficiently large energy level offset to split the exciton at the donor/acceptor interface, and that either the morphology or the electron mobility limit the performance of these devices.

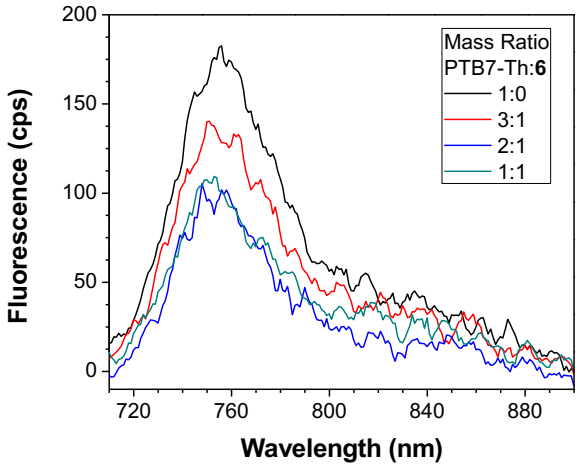

Figure 4.7 Emission spectra of PTB7-Th at various concentrations of **6**.

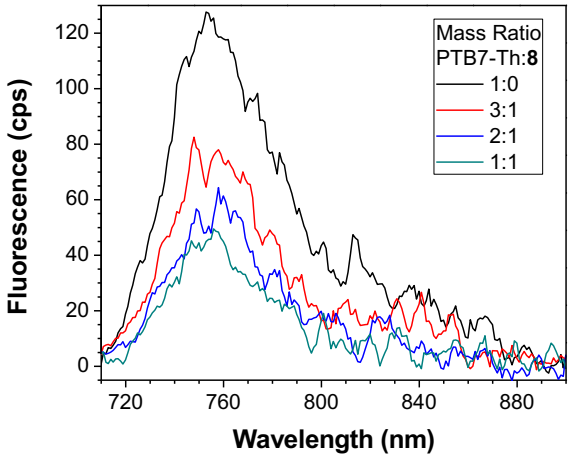

Figure 4.8 Emission spectra of PTB7-Th at various concentrations of **8**.

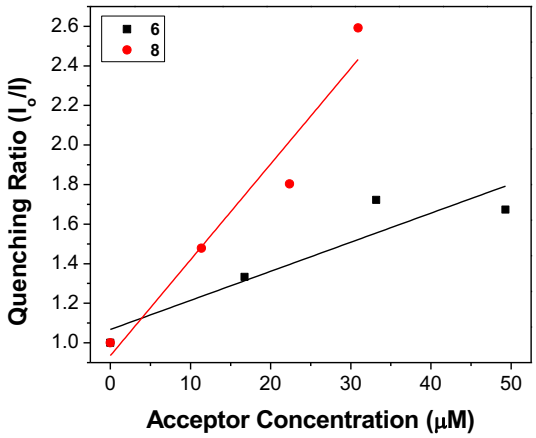

Figure 4.9 Stern-Volmer plot of PTB7-Th fluorescence quenching as a function of acceptor concentration.

Both **6** and **8** were then evaluated as electron donors alongside $PC_{71}BM$ (Table 4.2, Figure 4.10). DIO loadings between 0% and 3% were investigated and the champion device using **6**:$PC_{71}BM$ and 1% DIO produced an efficiency of 0.28%. The current densities produced by these cells were 3× greater than those of the PTB7-Th containing cells. Similarly, devices with an active layer of **8**:$PC_{71}BM$ performed much better than the analogous PTB7-Th:**8** devices. However, these devices suffered from a much lower fill factor than those using **6**:$PC_{71}BM$ active layers (Figure 4.10a). This is likely due to the poor blend morphology, which again results from the use of chloroform as the casting solvent. Optical microscopy revealed cracks in the **8**:$PC_{71}BM$ films, which would be expected to lead to microshorts and carrier recombination, decreasing the fill factor. The larger extinction coefficient of **8** relative to **6** is reflected in a higher incident photon-to-current efficiency (IPCE) (Figure 4.10b).

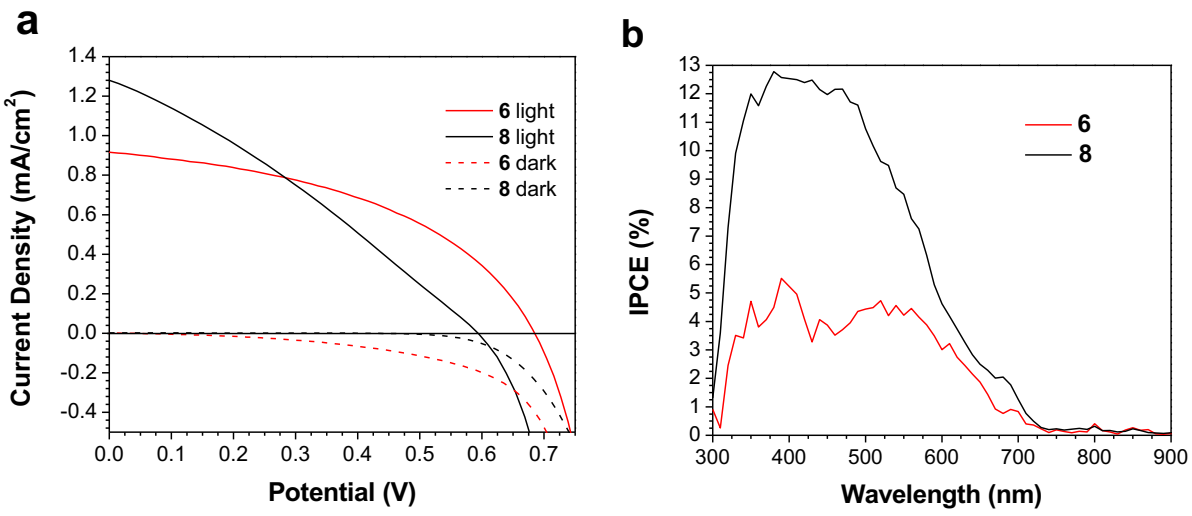

Figure 4.10 (a) *J*–*V* curves for champion devices, and (b) IPCE spectra for devices based on active layers of **6** or **8** and $PC_{71}BM$.

As in the PTB7-Th based OPVs, the addition of DIO was required to optimize the performance of the **6**/**8**:$PC_{71}BM$ devices; however, instead of seeing a decrease in domain size, the formation of larger domains is observed (Figure 4.11). The addition of 1% DIO to **6**:$PC_{71}BM$ blends greatly increased the device performance, while a 3% loading led to domains that were too large, leading to a decrease in device efficiency.

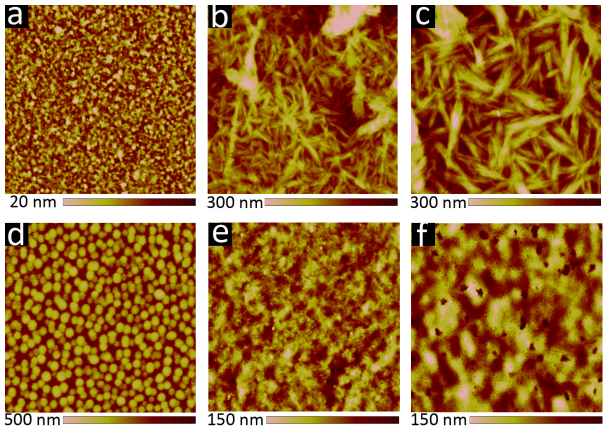

Figure 4.11 10 × 10 μm AFM images of active layer blends cast from 20 mg/mL solutions; (a-c) **6**:$PC_{71}BM$ active layers with (a) 0%, (b) 1%, (c) 3% DIO (v/v) (d-f) **8:**$PC_{71}BM$ active layers with (d) 0%, (e) 1%, (f) 3% DIO (v/v).

4.4 Conclusions

In conclusion, the synthesis of a unique electron acceptor sub-unit incorporating two isoindigo units fused along the 6 and 7 positions (**6**) has been reported. This acceptor sub-unit was then coupled to 2,2′-bithiophene donor groups to form a donor-acceptor compound (**8**). Both **6** and **8** absorb light well into the near-infrared, with **8** exhibiting a large extinction coefficient due to a higher degree of intramolecular charge transfer character in the HOMO to LUMO transition. **6** and **8** were incorporated into OPV active layers (paired with either PTB7-Th or $PC_{71}BM$). Although the PCEs were modest, bisisoindigo (**6**) features the deep energy levels desired in an electron acceptor, and **8** absorbs strongly throughout the visible and into the near-infrared, demonstrating the utility of the bisisoindigo building block. The incorporation of **6** into new donor-acceptor compounds (both polymers and small molecules) may therefore yield a variety of new, high-performance organic semiconductors.

4.5 Acknowledgements

The Natural Science and Engineering Research Council of Canada (NSERC) and the University of Saskatchewan are acknowledged for financial support. T.L.K. is a Canada Research Chair in Photovoltaics. This research was undertaken in part, thanks to funding from the Canada Research Chairs Program. N.M.R. and P.C.B. thank NSERC for scholarship funding; P.C.B. also thanks the Government of Saskatchewan for the Queen Elizabeth II Centennial Aboriginal Scholarship.

4.6 References

(1) Heeger, A. J. Semiconducting Polymers: The Third Generation. *Chem. Soc. Rev.* **2010**, *39*, 2354–2371.

(2) Mei, C.-Y.; Liang, L.; Zhao, F.-G.; Wang, J.-T.; Yu, L.-F.; Li, Y.-X.; Li, W.-S. A Family of Donor–Acceptor Photovoltaic Polymers with Fused 4,7-Dithienyl-2,1,3-Benzothiadiazole Units: Effect of Structural Fusion and Side Chains. *Macromolecules* **2013**, *46*, 7920–7931.

(3) Liao, S.-H.; Jhuo, H.-J.; Cheng, Y.-S.; Chen, S.-A. Fullerene Derivative-Doped Zinc Oxide Nanofilm as the Cathode of Inverted Polymer Solar Cells with Low-Bandgap Polymer (PTB7-Th) for High Performance. *Adv. Mater.* **2013**, *25*, 4766–4771.

(4) McCulloch, I.; Heeney, M.; Chabinyc, M. L.; DeLongchamp, D.; Kline, R. J.; Cölle, M.; Duffy, W.; Fischer, D.; Gundlach, D.; Hamadani, B.; Hamilton, R.; Richter, L.; Salleo, A.; Shkunov, M.; Sparrowe, D.; Tierney, S.; Zhang, W. Semiconducting Thienothiophene Copolymers: Design, Synthesis, Morphology, and Performance in Thin-Film Organic Transistors. *Adv. Mater.* **2009**, *21*, 1091–1109.

(5) Bijleveld, J. C.; Verstrijden, R. A. M.; Wienk, M. M.; Janssen, R. A. J. Copolymers of Diketopyrrolopyrrole and Thienothiophene for Photovoltaic Cells. *J. Mater. Chem.* **2011**, *21*, 9224-9231.

(6) Schneider, J. A.; Black, H.; Lin, H.-P.; Perepichka, D. F. Polymorphism in New Thienothiophene-Thiazolothiazole Organic Semiconductors. *ChemPhysChem* **2015**, *16*, 1173–1178.

(7) Mei, J.; Graham, K. R.; Stalder, R.; Reynolds, J. R. Synthesis of Isoindigo-Based Oligothiophenes for Molecular Bulk Heterojunction Solar Cells. *Org. Lett.* **2010**, *12*, 660–663.

(8) Wang, E.; Mammo, W.; Andersson, M. R. 25th Anniversary Article: Isoindigo-Based Polymers and Small Molecules for Bulk Heterojunction Solar Cells and Field Effect Transistors. *Adv. Mater.* **2014**, *26*, 1801–1826.

(9) Stalder, R.; Mei, J.; Graham, K. R.; Estrada, L. A.; Reynolds, J. R. Isoindigo, a Versatile Electron-Deficient Unit for High-Performance Organic Electronics. *Chem. Mater.* **2014**, *26*, 664–678.

(10) Ho, C.-C.; Chen, C.-A.; Chang, C.-Y.; Darling, S. B.; Su, W.-F. Isoindigo-Based Copolymers for Polymer Solar Cells with Efficiency Over 7%. *J. Mater Chem. A* **2014**, *2*, 8026–8032.

(11) Wang, Z.; Zhao, J.; Li, Y.; Peng, Q. Low Band-Gap Copolymers Derived From Fluorinated Isoindigo and Dithienosilole: Synthesis, Properties and Photovoltaic Applications. *Polym. Chem.* **2014**, *5*, 4984-4922.

(12) Głowacki, E. D.; Voss, G.; Sariciftci, N. S. 25th Anniversary Article: Progress in Chemistry and Applications of Functional Indigos for Organic Electronics. *Adv. Mater.* **2013**, *25*, 6783–6800.

(13) Guo, X.; Facchetti, A.; Marks, T. J. Imide- and Amide-Functionalized Polymer Semiconductors. *Chem. Rev.* **2014**, *114*, 8943–9021.

(14) Stalder, R.; Mei, J.; Subbiah, J.; Grand, C.; Estrada, L. A.; So, F.; Reynolds, J. R. N-Type Conjugated Polyisoindigos. *Macromolecules* **2011**, *44*, 6303–6310.

(15) Grenier, F.; Berrouard, P.; Pouliot, J.-R.; Tseng, H.-R.; Heeger, A. J.; Leclerc, M. Synthesis of New n-Type Isoindigo Copolymers. *Polym. Chem.* **2013**, *4*, 1836-1841.

(16) Lei, T.; Dou, J.-H.; Ma, Z.-J.; Yao, C.-H.; Liu, C.-J.; Wang, J.-Y.; Pei, J. Ambipolar Polymer Field-Effect Transistors Based on Fluorinated Isoindigo: High Performance and Improved Ambient Stability. *J. Am. Chem. Soc.* **2012**, *134*, 20025–20028.

(17) Lei, T.; Dou, J.-H.; Ma, Z.-J.; Liu, C.-J.; Wang, J.-Y.; Pei, J. Chlorination as a Useful Method to Modulate Conjugated Polymers: Balanced and Ambient-Stable Ambipolar High-Performance Field-Effect Transistors and Inverters Based on Chlorinated Isoindigo Polymers. *Chem. Sci.* **2013**, *4*, 2447–2452.

(18) Koizumi, Y.; Ide, M.; Saeki, A.; Vijayakumar, C.; Balan, B.; Kawamoto, M.; Seki, S. Thienoisoindigo-Based Low-Band Gap Polymers for Organic Electronic Devices. *Polym. Chem.* **2013**, *4*, 484–494.

(19) Dutta, G. K.; Han, A.-R.; Lee, J.; Kim, Y.; Oh, J. H.; Yang, C. Visible-Near-infrared Absorbing Polymers Containing Thienoisoindigo and Electron-Rich Units for Organic Transistors with Tunable Polarity. *Adv. Funct. Mater.* **2013**, *23*, 5317–5325.

(20) Kim, G.; Kang, S.-J.; Dutta, G. K.; Han, Y.-K.; Shin, T. J.; Noh, Y.-Y.; Yang, C. A Thienoisoindigo-Naphthalene Polymer with Ultrahigh Mobility of 14.4 $cm^2 v^{-1} s^{-1}$ That Substantially Exceeds Benchmark Values for Amorphous Silicon Semiconductors. *J. Am. Chem. Soc.* **2014**, *136*, 9477–9483.

(21) Randell, N. M.; Douglas, A. F.; Kelly, T. L. 7-Azaisoindigo as a New Electron Deficient Component of Small Molecule Chromophores for Organic Solar Cells. *J. Mater Chem. A* **2014**, *2*, 1085–1092.

(22) Deng, Y.; Liu, J.; Wang, J.; Liu, L.; Li, W.; Tian, H.; Zhang, X.; Xie, Z.; Geng, Y.; Wang, F. Dithienocarbazole and Isoindigo Based Amorphous Low Bandgap Conjugated Polymers for Efficient Polymer Solar Cells. *Adv. Mater.* **2013**, *26*, 471–476.

(23) Meager, I.; Nikolka, M.; Schroeder, B. C.; Nielsen, C. B.; Planells, M.; Bronstein, H.; Rumer, J. W.; James, D. I.; Ashraf, R. S.; Sadhanala, A.; Hayoz, P.; Flores, J.-C.; Sirringhaus, H.; McCulloch, I. Thieno[3,2-b]Thiophene Flanked Isoindigo Polymers for High Performance Ambipolar OFET Applications. *Adv. Funct. Mater.* **2014**, *24*, 7109–7115.

(24) Yue, W.; Ashraf, R. S.; Nielsen, C. B.; Collado-Fregoso, E.; Niazi, M. R.; Yousaf, S. A.; Kirkus, M.; Chen, H.-Y.; Amassian, A.; Durrant, J. R.; McCulloch, I. A Thieno[3,2-b][1]Benzothiophene Isoindigo Building Block for Additive- and Annealing-Free High-Performance Polymer Solar Cells. *Adv. Mater.* **2015**, *27*, 4702–4707.

(25) Lei, T.; Dou, J.-H.; Cao, X.-Y.; Wang, J.-Y.; Pei, J. A BDOPV-Based Donor-Acceptor Polymer for High-Performance n-Type and Oxygen-Doped Ambipolar Field-Effect Transistors. *Adv. Mater.* **2013**, *25*, 6589–6593.

(26) Zhou, X.; Ai, N.; Guo, Z.-H.; Zhuang, F.-D.; Jiang, Y.-S.; Wang, J.-Y.; Pei, J. Balanced Ambipolar Organic Thin-Film Transistors Operated Under Ambient Conditions: Role of the Donor Moiety in BDOPV-Based Conjugated Copolymers. *Chem. Mater.* **2015**, *27*, 1815–1820.

(27) Zhang, G.; Ye, Z.; Li, P.; Guo, J.; Wang, Q.; Tang, L.; Lu, H.; Qiu, L. A New Thieno-Isoindigo Derivative-Based D-A Polymer with Very Low Bandgap for High-Performance Ambipolar Organic Thin-Film Transistors. *Polym. Chem.* **2015**, *6*, 3970–3978.

(28) Li, S.; Yuan, Z.; Yuan, J.; Deng, P.; Zhang, Q.; Sun, B. An Expanded Isoindigo Unit as a New Building Block for a Conjugated Polymer Leading to High-Performance Solar Cells. *J. Mater Chem. A* **2014**, *2*, 5427-5433.

(29) Cao, Y.; Yuan, J.-S.; Zhou, X.; Wang, X.-Y.; Zhuang, F.-D.; Wang, J.-Y.; Pei, J. N-Fused BDOPV: a Tetralactam Derivative as a Building Block for Polymer Field-Effect Transistors. *Chem. Commun.* **2015**, *51*, 10514–10516.

(30) He, Y.; Guo, C.; Bin Sun; Quinn, J.; Li, Y. (3*E*,7*E*)-3,7-Bis(2-Oxoindolin-3-Ylidene)-5,7- Dihydropyrrolo[2,3-*f*]Indole-2,6(1*H*,3*H*)-Dione Based Polymers for Ambipolar Organic Thin Film Transistors. *Chem. Commun.* **2015**, *51*, 8093–8096.

(31) Rurack, K.; Spieles, M. Fluorescence Quantum Yields of a Series of Red and Near-Infrared Dyes Emitting at 600−1000 nm. *Anal. Chem.* **2011**, *83*, 1232–1242.

(32) Reisfeld, R.; Zusman, R.; Cohen, Y.; Eyal, M. The Spectroscopic Behaviour of Rhodamine 6G in Polar and Non-Polar Solvents and in Thin Glass and PMMA Films. *Chem. Phys. Lett.* **1988**, *147*, 142–147.

(33) Forster, L. S.; Livingston, R. The Absolute Quantum Yields of the Fluorescence of Chlorophyll Solutions. *J. Chem. Phys.* **1952**, *20*, 1315–1320.

(34) Gaussian 09, Revision D.01, Frisch, M. J.; Trucks, G. W.; Schlegel, H. B.; Scuseria, G. E.; Robb, M. A.; Cheeseman, J. R.; Scalmani, G.; Barone, V.; Petersson, G. A.; Nakatsuji, H.; Li, X.; Caricato, M.; Marenich, A.; Bloino, J.; Janesko, B. G.; Gomperts, R.; Mennucci, B.; Hratchian, H. P.; Ortiz, J. V.; Izmaylov, A. F.; Sonnenberg, J. L.; Williams-Young, D.; Ding, F.; Lipparini, F.; Egidi, F.; Goings, J.; Peng, B.; Petrone, A.; Henderson, T.; Ranasinghe, D.; Zakrzewski, V. G.; Gao, J.; Rega, N.; Zheng, G.; Liang, W.; Hada, M.; Ehara, M.; Toyota, K.; Fukuda, R.; Hasegawa, J.; Ishida, M.; Nakajima, T.; Honda, Y.; Kitao, O.; Nakai, H.; Vreven, T.; Throssell, K.; Montgomery, J. A., Jr.; Peralta, J. E.; Ogliaro, F.; Bearpark, M.; Heyd, J. J.; Brothers, E.; Kudin, K. N.; Staroverov, V. N.; Keith, T.; Kobayashi, R.; Normand, J.; Raghavachari, K.; Rendell, A.; Burant, J. C.; Iyengar, S. S.; Tomasi, J.; Cossi, M.; Millam, J. M.; Klene, M.; Adamo, C.; Cammi, R.; Ochterski, J. W.; Martin, R. L.; Morokuma, K.; Farkas, O.; Foresman, J. B.; Fox, D. J. Gaussian, Inc., Wallingford CT, **2016**.

(35) Gorelsky, S. I. *SWizard Program, Http://Www.Sg-Chemistry.Net/, University of Ottawa, Canada, 2013*.

(36) Gorelsky, S. I.; Lever, A. B. P. Electronic Structure and Spectra of Ruthenium Diimine Complexes by Density Functional Theory and INDO/S. Comparison of the Two Methods. *J. Organomet. Chem.* **2001**, *635*, 187–196.

(37) Jones, L. R.; Schumm, J. S.; Tour, J. M. Rapid Solution and Solid Phase Syntheses of Oligo(1,4-phenylene ethynylene)s with Thioester Termini: Molecular Scale Wires with Alligator Clips. Derivation of Iterative Reaction Efficiencies on a Polymer Support. *J. Org. Chem.* **1997**, *62*, 1388-1410

(38) Sotgiu, G.; Zambianchi, M.; Barbarella, G.; Botta, C. Synthesis and Optical Properties of Soluble Sexithiophenes with One Central Head-to-Head Junction. *Tetrahedron* **2002**, *58*, 2245–2251.

(39) Shmidt, M. S.; Reverdito, A. M.; Kremenchuzky, L.; Perillo, I. A.; Blanco, M. M. Simple and Efficient Microwave Assisted *N*-Alkylation of Isatin. *Molecules* **2008**, *13*, 831–840.

(40) Soriano, D. S. Example of the Wolff-Kishner Reduction Procedure Suitable for an Undergraduate Organic Lab Experiment: Preparation of Oxindole. *J. Chem. Ed.* **1993**, ***70***, 332.

(41) Da Silva, J.; Garden, S. J.; Pinto, A. C. The Chemistry of Isatins: a Review From 1975 to 1999. *J. Braz. Chem. Soc.* **2001**, *12*, 273-324.

(42) Kossmehl, G.; Manecke, G. Synthese, Charakterisierung Und Halbleitereigenschaften Eines Polymeren Indopheninhomologen. *Die Makromolekulare Chemie,* **1975,** *176,* 333-340.

(43) Silva, B. V.; Violante, F. A.; Pinto, A. C.; Santos, L. S. The Mechanism of Sandmeyer's Cyclization Reaction by Electrospray Ionization Mass Spectrometry. *Rapid Commun. Mass Spectrom.* **2011**, *25*, 423–428.

(44) Rice, K. C.; Boone, B. J.; Rubin, A. B.; Rauls, T. J. Synthesis, Antimalarial Activity, and Phototoxicity of Some Benzo(H)Quinoline-4-Methanols. *J. Med. Chem.* **1976**, *19*, 887–892.

(45) Banerji, N.; Cowan, S.; Vauthey, E.; Heeger, A. J. Ultrafast Relaxation of the Poly(3-Hexylthiophene) Emission Spectrum. *J. Phys. Chem. C* **2011**, *115*, 9726–9739.

(46) Hedley, G. J.; Ward, A. J.; Alekseev, A.; Howells, C. T.; Martins, E. R.; Serrano, L. A.; Cooke, G.; Ruseckas, A.; Samuel, I. D. W. Determining the Optimum Morphology in High-Performance Polymer-Fullerene Organic Photovoltaic Cells. *Nat. Commun.* **2013**, *4*, No. 2867.

(47) Senevirathna, W.; Sauvé, G. Introducing 3D Conjugated Acceptors with Intense Red Absorption: Homoleptic Metal(II) Complexes of Di(Phenylacetylene) Azadipyrromethene. *J. Mater Chem. C* **2013**, *1*, 6684-6694.

Chapter 5

Effect of Acceptor Unit Length and Planarity on the Optoelectronic Properties of Isoindigo-Thiophene Donor-Acceptor Polymers

This chapter is based on the manuscript

Randell, N.M.; Radford, C.L.; Yang, J.; Quinn, J.; Hou, D.; Li, Y.; Kelly, T.L.

2017, *in preparation*

Consent was obtained from all co-authors to include this manuscript in the thesis. Unless otherwise noted, I performed all experimental work and wrote the first draft of the manuscript. During the project, C.L. Radford developed the new synthesis of bisisatin (**8**). J. Yang performed the initial solar cell fabrication using the isoindigo/diisoindigo polymers and helped to optimize fabrication conditions. J. Quinn, and D. Hou fabricated and tested the thin film transistors, processed the results, and calculated the charge carrier mobilities. Prof. Y. Li directed the fabrication, testing, and reporting of the transistor results. T.L. Kelly directed the study and revised the manuscript.

Transition

The content of this chapter is very much a successor to the bisisoindigo work presented in Chapter 4. While performing the experiments in Chapter 4, I discovered the propensity for the flat bisisoindigo-based molecular semiconductors to aggregate and crystallize in the solid state. This, combined with an overall shift in the field of organic semiconductors, inspired the move to polymeric semiconductors in this project. Additionally, the synthetic strategy developed in Chapter 4, in which I synthesized the isoindigo dimer by first making an isatin dimer structure, was key in the successful synthesis of the freely rotating diisoindigo dimer presented in this chapter. Finally,

the bisisoindigo unit developed in Chapter 4 was used to make two of the six polymers presented herein and allowed me to study the effects of enforced planarity *vs.* free rotation in the acceptor dimers.

Naturally, there is some overlap between the material discussed in the introduction of this Chapter and Chapter 1. Where the two diverge is that there is a focus on the study of donor length in isoindigo-based semiconductors in the introductory section of this chapter that is not present in Chapter 1. Additionally, the material presented here includes studies of extending donor number in donor-acceptor polymers with acceptor units other than isoindigo, which were not discussed in Chapter 1.

5.1 Introduction

Organic electronic devices, such as OPVs and organic thin film transistors (OTFTs), have made great strides in performance over the last two decades due to advances in the design and synthesis of donor-acceptor semiconductors.[1-3] DA semiconductors are composed of alternating electron-rich (donor) and electron-poor (acceptor) units.[4] This results in the partial isolation of the frontier molecular orbitals; the HOMO typically resembles that of the donor material, while the LUMO is largely isolated on the acceptor unit, resulting in low band gap, near-infrared absorbing materials.[5] Common donor units include oligothiophenes, thienothiophenes, and benzodithiophene; typical acceptor units incorporate electron withdrawing functional groups (e.g. amides and imides) or electronegative halogen atoms.[6-11]

Conventional DA polymers have a repeat unit consisting of a donor and acceptor pair. Recently, multiple research groups have investigated the effects of increasing the number of donor units in DA copolymers, often by varying the number of thiophenes in an oligothiophene donor. Zhou *et al.* investigated the effects of thiophene donor number in a series of DA polymers with two acceptor units, thieno[3,4-c]pyrrole-4,6-dione (TPD) and bithiopheneimide (BTI).[12] Using Raman spectroscopy, they discovered that for one to three thiophene units, the conjugation length of the polymers was proportional to the number of thiophenes; however, a fourth thiophene did not increase the conjugation length. They also found that increasing the length of the oligothiophene increased the polymers' HOMO energy. Both the TPD and BTI-based polymers were used in OPVs, and the maximum PCE was achieved with the terthiophene containing polymers.

The effects of increasing donor number have also been studied in DA polymers using the acceptor unit isoindigo.[13,14] Ma *et al.* synthesized isoindigo-oligothiophene polymers containing

one, three, five and six thiophenes in the repeat unit.[13] The LUMO level was constant for all four polymers, while the HOMO energy increased with increasing number of thiophene rings. The isoindigo-terthiophene copolymer had the lowest $E_{g,opt}$, and longer donor units did not red shift the absorbance further; this implies that the effective conjugation length stops increasing after three thiophene units. The highest OPV efficiency was also achieved with the isoindigo-terthiophene polymer. TEM and GIWAXS measurements showed that donor units larger than terthiophene caused aggregation in the OPV active layer, leading to decreased efficiencies. Following this, Reynolds and coworkers investigated the disparate OPV performance of isoindigo-thiophene (**iI-T**) and isoindigo-terthiophene (**iI-3T**) polymers.[15-17] Despite similar optoelectronic properties, OPVs fabricated with **iI-3T** were more than twice as efficient as OPVs fabricated with **iI-T**. They discovered that the dielectric constant of an **iI-3T:**$PC_{71}BM$ blend was greater than that of **iI-T**:$PC_{71}BM$; this implies better electronic coupling between **iI-3T** and $PC_{71}BM$. The improved electronic coupling between **iI-3T** and $PC_{71}BM$ promoted faster exciton dissociation, leading to the increase in PCE.[16]

A significant amount of research has now been performed that examined how increasing donor number affects the optoelectronic properties of DA polymers; conversely, relatively little research has been performed on increasing the number of acceptors. This lack of study is likely because the synthesis of acceptor oligomers is significantly more difficult than the synthesis of donor oligomers. One potential acceptor unit for studying increased acceptor number in DA semiconductors is isoindigo. Isoindigo (**iI**) (Chart 5.1) was first used as the acceptor unit in DA semiconductors in 2010 by Mei *et al.,* and has since become a common acceptor unit in organic semiconductors.[18-27] Modified isoindigo structures, such as thienoisoindigo and various extended isoindigos, have recently became a popular motif in new DA semiconductors.[28-35] The electron-

poor nature of these semiconductors has made them useful components in OTFTs with high n-type or ambipolar charge carrier mobility.

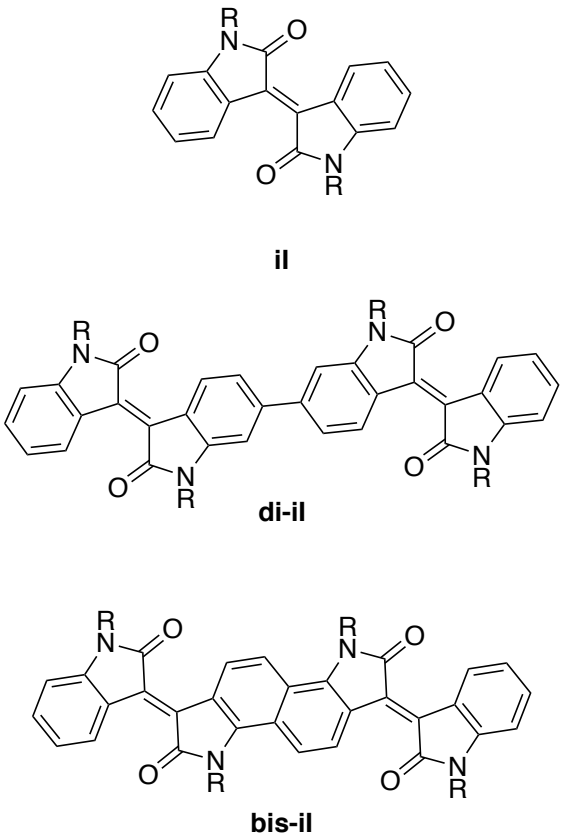

Chart 5.1 Isoindigo (**iI**) and isoindigo dimers, diisoindigo (**di-iI**) and bisisoindigo (**bis-iI**).

One particularly useful variant of isoindigo is thienoisoindigo, which replaces the benzene rings of isoindigo with thiophenes. Thienoisoindigo and its derivatives can be brominated, making the synthesis of acceptor unit dimers simple.[28,29,36] James *et al.* used this approach to synthesize a thieno-benzoisoindigo dimer and incorporate it into polymers.[37] These DAA polymers featured a repeat structure of one donor unit and two acceptor units. They were incorporated into OTFTs which displayed high hole mobility (1.1 $cm^2\ V^{-1}\ s^{-1}$) and ambipolar charge transport behavior (μ_e = 6.6 $\times 10^{-3}\ cm^2\ V^{-1}\ s^{-1}$).[37] In 2016, a molecular semiconductor using bisisoindigo (**bis-iI**) (Chart

5.1), an isoindigo dimer in which the two monomer units were ring-fused at the 6 and 7 positions, was reported.[38] This planarity lowered the frontier orbital energies and reduced the $E_{g,opt}$ relative to isoindigo. Following this, Jiang *et al.* incorporated **bis-iI** into a series of DAA polymers which exhibited similar optoelectronic properties to the **bis-iI** molecular semiconductor, and had balanced charge carrier mobilities (μ_h = 1.79 cm^2 V^{-1} s^{-1}, μ_e = 0.087 cm^2 V^{-1} s^{-1}).[39]

Herein, the synthesis of a second isoindigo dimer, diisoindigo (**di-iI)** (Chart 5.1) is described; in this case, two isoindigos are joined by a single bond at the 6-position, allowing free rotation between the acceptor units. Using **iI**, **di-iI**, and **bis-iI** four DAA copolymers and two DA copolymers featuring either a thiophene or terthiophene donor unit have been synthesized. The objective of this work is to compare the optoelectronic properties of conventional DA copolymers with DAA copolymers that feature an additional acceptor in their structural repeat unit. Using the four DAA copolymers, the effects of increasing the number and planarity of acceptor units on the optoelectronic properties, and device performance, of organic semiconductors are determined. By comparing the **iI** and **di-iI**-based polymers, the effects of adding a second acceptor monomer to the repeat unit of a DA copolymer were studied. Additionally, comparison of the **di-iI** and **bis-iI** polymers allowed us to explore the effect of planarizing the two acceptor units. It is demonstrated that increasing the number of acceptor units in a DA copolymer lowers the energy of the frontier molecular orbitals and increases the electron mobility.

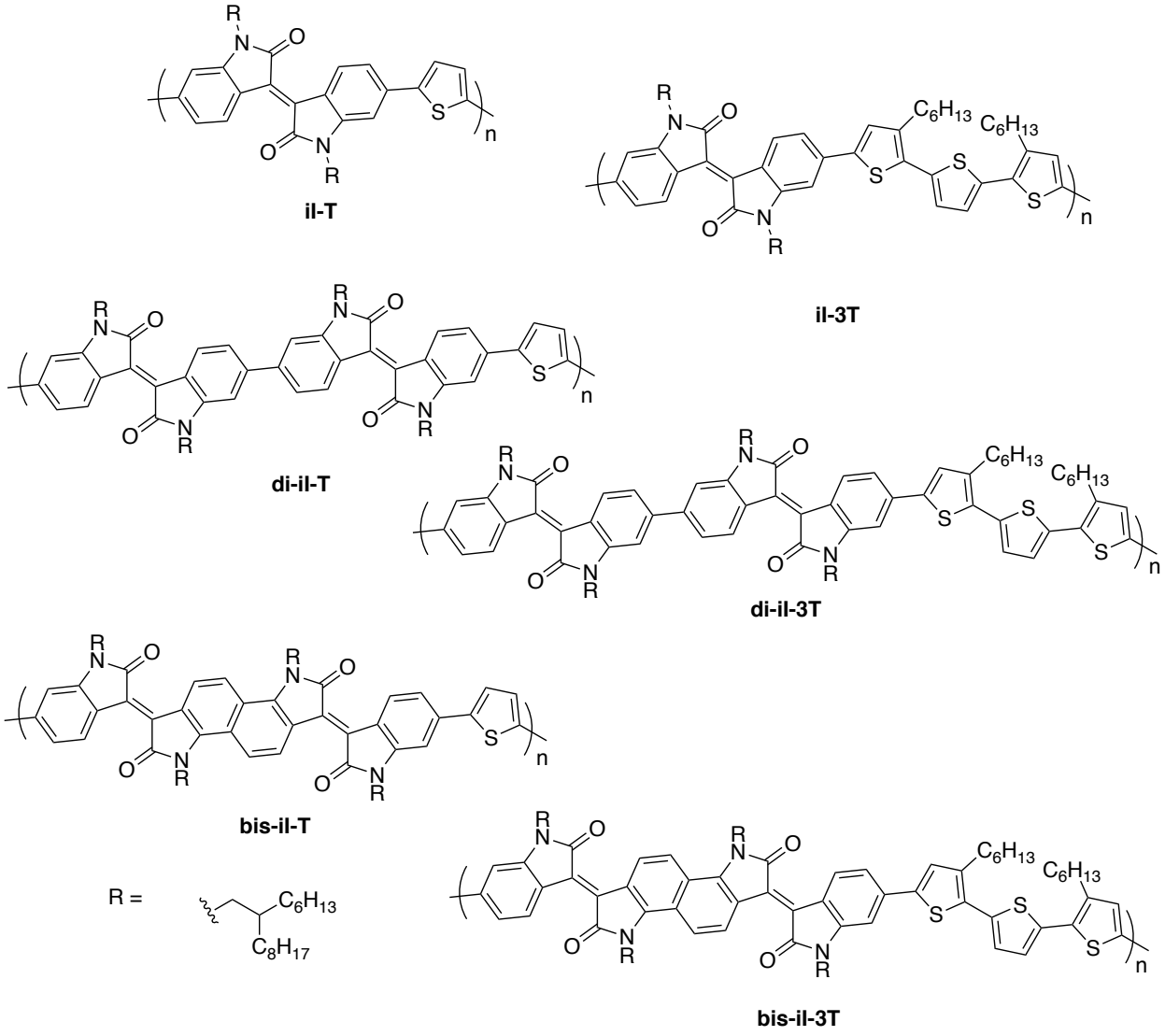

Chart 5.2 Structures of DAA copolymers using **di-iI**, and **bis-iI**, and DA copolymers using **iI**.

5.2 Experimental

5.2.1 Materials

Solvents were dried over activated 3Å molecular sieves and stored under argon. All reactions were performed under argon, unless otherwise noted. $Pd_2(dba)_3$ and P(*o*-tolyl)$_3$ were purchased from Strem Chemicals Inc., and stored in a nitrogen atmosphere glove box when not in use. *p*-Toluenesulfonic acid monohydrate was purchased from Millipore Sigma, and dried under high vacuum at 50 °C. All other reagents were used as received.

5.2.2 Characterization

NMR spectra were obtained using a Bruker Avance 500 or 600 MHz spectrometer. UV/vis spectroscopy measurements were performed on polymer thin films on ZnO coated glass substrates using a Cary 6000i UV/vis spectrophotometer. AFM measurements were performed using a Dimensions Hybrid Nanoscope system (Veeco Metrology Group). Cyclic voltammetry was carried out in 0.05 mol L^{-1} tetrabutylammonium hexafluorophosphate dissolved in dry, degassed acetonitrile. The working electrode was glassy carbon, the counter electrode was a Pt wire, and the reference electrode was a Ag wire; polymer films were drop cast from chloroform solutions onto the working electrode. Voltammograms were referenced to a Fc/Fc^+, which was estimated to be 5.1 V *vs.* vacuum.[15] Mass spectra were acquired on a JEOL AccuToF 4G GCv mass spectrometer with an EiFi Field desorption ionization source. Size exclusion chromatography (SEC) was performed with 1,3,5-trichlorobenzene (TCB) at an elution rate of 1.0 mL min^{-1} (injection volume: 200 µL) through a PL gel MIXED-B column (10µm) (+PL gel guard), at 130 °C. The SEC system consisted of an Alliance 2000 separation module equipped with RI detector. The apparent molecular weights and dispersities ($Đ$) (M_w/M_n) were determined with a calibration based on linear

polystyrene (PS) standards. The polymers were dissolved in hot TCB (100 °C) and filtered hot using Millex – SV (5 μm) filters before the injection.

DFT Calculations were performed using the Gaussian 09/Gaussview suite of software.[40] All calculations were performed using the B3LYP exchange-correlation functional with the 6-31G(d,p) basis set. 2-Hexyldecyl, and *n*-hexyl groups were replaced with methyl groups to simplify the calculations. Geometry optimizations were first performed on all structures and frequency analyses were performed to ensure that the optimizations had converged to a potential energy minimum. Single point energy calculations were performed using a solvent continuum model with a dielectric constant equal to that of chloroform. From the single point energy calculations, frontier orbital energies and orbital isosurfaces were obtained.

GIWAXS measurements on thin films were performed at the Hard X-ray Microanalysis (HXMA) beamline of the Canadian Light Source (CLS). A photon energy of 12.658 keV was selected using a Si monochromator. GIWAXS patterns were collected on a SX165 CCD camera (Rayonix), with a sample to detector distance of 159 mm (determined using a silver behenate thin film standard), and a lead beam stop was used to block the direct path of the beam. Polymer thin films were cast from 8 mg mL^{-1} solutions in either dichlorobenzene (**iI-T**, **iI-3T**) or chlorobenzene (**di-iI-T**, **di-iI-3T**, **bis-iI-T**, and **bis-iI-3T**) onto ZnO coated glass substrates prepared via the same method as the ZnO layer used in OPV fabrication. Polymer:fullerene blend films were prepared using the same methodology as in OPV fabrication, on ZnO coated glass substrates.

5.2.3 OTFT fabrication and testing

The bottom-contact bottom-gate configuration was used for all OTFT devices. The preparation procedure of the substrate and devices are as follows. A heavily n^{++}-doped SiO_2/Si wafer with ~300 nm-thick SiO_2 was patterned with gold source and drain pairs by conventional photolithography, and thermal deposition. The substrate was treated with air plasma, followed by cleaning with acetone and isopropanol in an ultra-sonication bath. Subsequently, the substrate was placed in a solution of dodecyltrichlorosilane (3% in toluene) at room temperature for 20 min, washed with toluene, and dried under a nitrogen flow. Then a polymer solution in chloroform (5 mg mL^{-1}) was spin-coated onto the substrate at 3000 rpm for 60 s to give the polymer film, which was further subject to thermal annealing at different temperatures for 20 min in a glove box. All the OTFT devices had a channel length (L) of 30 μm and a channel width (W) of 1000 μm, and were characterized in the same glove box using an Agilent B2912A Precision Source/Measure Unit.

5.2.4 OPV fabrication

ITO coated glass substrates with (20 Ω/□ sheet resistance, Xin Yan Technology Ltd.) were cleaned by sequential sonication in Extran detergent (10% v/v in Millipore H_2O), Millipore H_2O, acetone, and isopropanol for 20 min each, and stored under fresh isopropanol. Prior to use, substrates were blown dry with filtered nitrogen (0.45 μm poly(trifluoroethylene) (PTFE) syringe filter) and UV/ozone cleaned for 15 min. ZnO sol-gel precursor solution was prepared by dissolving $ZnOAc{\cdot}2H_2O$ (0.108 g) and ethanolamine (30 μL) in methoxyethanol (1.0 mL) overnight with vigorous stirring.[41,42] The ZnO precursor solution was filtered through a 0.45 μm PTFE syringe filter and spin cast onto the cleaned ITO/glass substrates and annealed at 180 °C for

15 min; the substrates were placed into a nitrogen atmosphere glove box while still hot. Polymer:$PC_{71}BM$ active layer solutions (1:1.5 polymer:$PC_{71}BM$ by weight) were prepared by dissolving the polymer and $PC_{71}BM$ in either dichlorobenzene (**iI-T**, **iI-3T**) or chlorobenzene **(di-iI-T**, **di-iI-3T**, **bis-iI-T**, and **bis-iI-3T**) to a total solid concentration of 20 mg mL^{-1}, and diiodooctane (DIO) was added to a concentration of 2.5% v/v. The active layer solution was stirred overnight at 60 °C, cooled, and filtered through a 0.45 μm PTFE syringe filter prior to deposition. Active layers were spin cast at 1000 rpm for either 60 s (chlorobenzene solutions) or 120 s (dichlorobenzene solutions). After active layer deposition, MoO_x (5 nm, 0.1 Å s^{-1}) and Ag (70 nm, 0.1-0.3 Å s^{-1}) were thermally evaporated at a base pressure of 3×10^{-6} mbar.

5.2.5 OPV characterization

Current voltage measurements were performed inside a nitrogen atmosphere glove box using a Keithley 2400 source-measure unit. The cells were illuminated by a 450 W Class AAA solar simulator equipped with an AM1.5G filter (Sol3A, Oriel instruments) at a calibrated intensity of 100 mW cm^{-2}, as determined by a standard silicon reference cell (91150V, Oriel Instruments). The cell area was defined as 0.0708 cm^2 by a non-reflective anodized aluminium mask. Incident photon to current (IPCE) measurements were performed in air on the best-performing devices using a QE-PV-SI system (Oriel Instruments) consisting of a 300 W Xe arc lamp, monochromator, chopper, lock-in amplifier, and certified silicon reference cell, operating at a 30 Hz beam-chopping frequency.

5.2.6 Detailed synthetic procedures for di-iI-T and di-iI-3T

2-Hexyldecylbromide (**1**)[45]

2-Hexyldecanol (20.0 mL, 69.0 mmol) and CBr_4 (23.0 g, 69.4 mmol) were dissolved in dry CH_2Cl_2 (100 mL) and degassed with sparging argon for 20 min. The solution was cooled to 0 °C and PPh_3 (18.6 g, 70.9 mmol) was added slowly over 20 min. The solution was warmed to room temperature and stirred overnight. The reaction mixture was concentrated under vacuum and poured over hexanes (300 mL). The resulting precipitate was removed by suction filtration and the crude product was filtered through a silica gel plug. The product was concentrated on high vacuum to yield a clear colorless liquid (19.8 g, 95.3%). ^{1}H NMR (500 MHz, $CDCl_3$, ppm) δ: 3.45 (d, J = 4.8 Hz, 2H), 1.56-1.63 (m, 1H) 1.19-1.43 (m, 24H) 0.88 (t, J = 3.5 H, 6H).

N-(2-hexyldecyl)-6-bromoisatin (**2**)

6-Bromoisatin (10.0 g, 44.2 mmol) and dry K_2CO_3 (7.41 g, 53.6 mmol) were dissolved in dry DMF (150 mL) and stirred at room temperature for 0.5 h. KI (1.52 g, 9.16 mmol) and 2-hexyldecylbromide (**1**) (16.2 g, 53.1 mmol) were added and the reaction mixture was stirred at 80 °C for 18 h. The reaction mixture was poured over H_2O, acidified with a small amount of dilute HCl (aq) (~1-5 mL, 1 mol L^{-1}), and extracted with ethyl acetate. The combined organic layers were washed with H_2O and brine, dried over Na_2SO_4, and concentrated to yield the crude product as a dark red/orange oil. The crude product was recrystallized from hexanes/isopropanol at -20 °C. The resulting orange solid was collected by suction filtration and dried on high vacuum to yield the desired product as a bright orange solid (6.83 g, 34.3%). ^{1}H NMR (500 MHz, $CDCl_3$, ppm) δ: 7.46 (d, J = 8.0 Hz, 1H), 7.27 (d, J = 8.0 Hz, 1H), 7.02 (s, 1H), 3.57 (d, J = 3.57, 2H), 1.80-1.88 (m, 1H), 1.52-1.61 (m, 1H), 1.20-1.40 (m, 25H), 0.87 (t, J = 6.9 Hz, 6H). ^{13}C NMR (126 MHz, $CDCl_3$)

δ: 182.47, 158.46, 152.46, 133.63, 126.92, 126.47, 116.42, 114.14, 45.06, 36.11, 32.00, 31.91, 31.57, 30.07, 29.74, 29.66, 29.41, 26.43, 26.39, 22.81, 22.78, 14.25, 14.22. HRMS (*m/z*) ($M^{\bullet+}$): calc ($C_{24}H_{36}BrNO_2$): 449.19294 found: 449.19246.

N-(2-hexyldecyl)-6-bromo-2-oxindole (**3**)[38]

N-(2-hexyldecyl)-6-bromoisatin (**2**) (2.51 g, 5.57 mmol) was suspended in hydrazine monohydrate (20 mL, 0.41 mol) and stirred at reflux for 18 h. The reaction mixture was poured over H_2O and extracted with ethyl acetate. The combined organic layers were washed with H_2O and brine, dried over $MgSO_4$, and concentrated to yield the desired product as a viscous red oil in quantitative yield (2.09 g). ^{1}H NMR (500 MHz, $CDCl_3$, ppm) δ: 7.15 (d, *J* = 7.8 Hz, 1H), 7.09 (d, *J* = 7.8 Hz, 1H), 6.92 (s, 1H), 3.55 (d, *J* = 7.5 Hz, 2H), 3.46 (s, 2H), 1.80-1.88 (m, 1H), 1.20-1.44 (m, 34H), 0.88 (t, *J* = 7.2 Hz, 8H). ^{13}C NMR (126 MHz, $CDCl_3$) δ: 175.19, 171.31, 146.62, 125.71, 124.93, 123.53, 121.43, 112.43, 65.91, 60.54, 44.78, 40.69, 36.03, 35.46, 32.02, 31.94, 31.09, 30.12, 29.79, 29.67, 29.43, 26.51, 26.47, 14.25. HRMS (*m/z*) ($M^{\bullet+}$): calc ($C_{24}H_{38}BrNO$): 435.21368 found: 435.21485.

N-(2-hexyldecyl)-6-boroisatin pinacolate ester (**4**)

N-(2-hexyldecyl)-6-bromoisatin (**2**) (1.99 g, 4.44 mmol), bispinacolatodiboron (B_2Pin_2) (1.35 g, 5.32 mmol) and potassium acetate (1.34 g, 13.6 mmol) were suspended in 1,4-dioxane (4 mL) and degassed for 15 min with sparging argon. [Pd(dppf)Cl_2] • CH_2Cl_2 (0.243 g, 0.271 mmol) was added and the reaction mixture was stirred at 80 ºC for 4 h. The reaction mixture was poured over H_2O and extracted with ethyl acetate. The combined organic layers were washed with H_2O and brine, dried over $MgSO_4$, and concentrated to yield the crude product as a red oil. The crude product was

dissolved in CH_2Cl_2 and filtered through a short silica plug. The CH_2Cl_2 was removed under reduced pressure and the pure product was dried on high vacuum to yield an orange solid (1.60 g, 72.8%). ^{1}H NMR (500 MHz, $CDCl_3$, ppm) δ: 7.55 (q, *J* = 6.7 Hz, 2H), 7.24 (s, 1H), 3.61 (d, *J* = 7.4 Hz, 2H), 1.85-1.93 (m, 1H), 1.56-1.60 (m, 1H), 1.18-1.43 (m, 40H), 0.87 (t, *J* = 6.8Hz, 8H). ^{13}C NMR (126 MHz, $CDCl_3$) δ: 184.36, 158.54, 150.59, 130.15, 124.20, 119.47, 115.72, 84.76, 83.60, 44.75, 36.01, 31.99, 31.90, 31.64, 31.62, 30.03, 24.98, 14.20. HRMS (*m/z*) ($M^{\bullet+}$): calc ($C_{30}H_{48}BNO_4$): 497.36764 found: 497.36780.

<u>*N,N′*-bis(2-hexyldecyl)-6,6′-disisatin (**5**)</u>

N-(2-Hexyldecyl)-6-bromoisatin (**2**) (775 mg, 1.72 mmol) and *N*-(2-hexyldecyl)-6-boroisatin pinacolate ester (**4**) (968 mg, 1.95 mmol) were dissolved in acetonitrile (40 mL). K_2CO_3 (555 mg, 4.01 mmol) was dissolved in a minimum of H_2O and added to the reaction mixture; the suspension was degassed with argon for 0.5 h. $[Pd(dppf)Cl_2] \bullet CH_2Cl_2$ (0.085 g, 0.10 mmol) was added and the reaction mixture was heated to reflux for 1 h. The mixture was diluted with ethyl acetate and washed with H_2O and brine. The organic layers were dried over Na_2SO_4 and concentrated to yield the crude product. The crude product was purified by column chromatography (silica gel, 4:1 ethyl acetate:hexanes); the combined fractions were concentrated under reduced pressure and dried on high vacuum to yield the desired product as a bright red solid (913 mg, 71.5%). ^{1}H NMR (500 MHz, $CDCl_3$, ppm) δ: 7.72 (d, *J* = 7.7 Hz, 2H,), 7.30 (d, *J* = 7.7 Hz, 2H), 7.00 (s, 2H), 3.66 (d, *J* = 7.4 Hz, 4H), 1.84-1.93 (m, 2H), 1.18-1.42 (m, 57 H), 0.81-0.90, (m, 14 H). ^{13}C NMR (126 MHz, $CDCl_3$) δ: 182.93, 158.59, 152.22, 149.65, 126.09, 122.78, 117.68, 109.20, 77.42, 77.16, 76.91, 44.90, 36.34, 31.96, 31.89, 31.87, 31.63, 30.10, 29.76, 29.66, 29.41, 26.55, 26.51, 22.80, 22.75, 22.72, 14.21, 14.18. HRMS (*m/z*) ($M^{\bullet+}$): calc ($C_{48}H_{72}N_2O_4$): 740.54921 found: 740.55050.

Dibromodiisoindigo **Br_2-di-iI**

N-(2-hexyldecyl)-6-bromo-2-oxindole (**3**) (0.984 g, 2.25 mmol), *N,N′*-bis(2-hexyldecyl)-6,6′-diisatin (**5**) (661 mg, 0.892 mmol) and *p*-TsOH (62 mg, 0.36 mmol) were dissolved in glacial acetic acid (25 mL) and the solution was stirred at 80 ºC for 18 h. The reaction mixture was poured over 100 mL of ice water and collected by suction filtration. The crude product was purified by trituration in acetone three times to yield pure **Br_2-di-iI** as a red-black solid (0.810 g, 57.6%). ^{1}H NMR (500 MHz, $CDCl_3$, ppm) δ: 9.26 (d, *J* = 8.4 Hz, 2H), 9.10 (d, J = 8.6 Hz, 2H), 7.30 (d, *J* = 8.4 Hz, 2H), 7.18 (d, *J* = 8.6 Hz, 2H), 7.00 (s, 2H), 6.92 (s, 2H) 3.73 (d, *J* = 7.5 Hz, 4H), 3.65 (d, *J* = 7.5 Hz, 4H), 1.86-2.00 (m, 2H), 1.18-1.43 (m, 49H), 0.80-0.89 (m, 12H). ^{13}C NMR (126 MHz, $CDCl_3$) δ: 168.65, 168.32, 146.38, 146.20, 144.63, 133.27, 132.33, 131.16, 130.52, 126.63, 125.18, 121.78, 120.99, 120.70, 111.66, 106.67, 44.89, 36.59, 36.29, 32.01, 31.96, 31.82, 31.70, 30.21, 30.13, 298.88, 29.81, 29.71, 29.69, 29.46, 29.43, 26.66, 26.56, 26.51, 22.80, 14.23. HRMS (*m/z*) ($M^{\bullet+}$): calc ($C_{96}H_{144}Br_2N_4O_4$): 1574.95543 found: 1574.96001.

2-Trimethylstannyl-4-hexylthiophene (**14**)[22]

3-Hexylthiophene (3.20 g, 0.0190 mol) was dissolved in dry THF (50 mL) and cooled to -78 °C. *n*-BuLi (2.5 mol L^{-1} in hexanes) (8.0 mL, 0.020 mol) was added and the reaction mixture was stirred at -78 °C for 0.5 h before being warmed to room temperature and stirred for a further 1 h. The mixture was cooled to -78 °C and trimethyltin chloride (1.0 mol L^{-1} in hexanes) (21 mL 0.021 mol) was added. The reaction mixture was warmed to room temperature and stirred for 4 h. The reaction mixture was poured over H_2O and extracted with Et_2O. The combined organic layers were washed with H_2O and brine, dried over Na_2SO_4, concentrated under reduced pressure and dried on high vacuum to yield the desired product as a clear colorless oil (6.02 g, 95.9%). 1H NMR (500

MHz, $CDCl_3$, ppm) δ: 7.22 (s, 1H), 7.04 (s, 1H), 2.63-2.71 (m, 2H), 1.62-1.69 (m, 2H), 1.30-1.42 (m, 8H), 0.92 (t, *J* = 6.6 Hz, 4H), 0.77, (s, 11H).

Ditheinyldiisoindigo **T_2-di-iI**

Br_2-di-iI (1.21 g, 0.767 mmol) and 2-trimethylstannyl-4-hexylthiophene (**14**) (0.714 g, 2.16 mmol) were dissolved in dry THF (20 mL) in a flame dried two-neck flask and degassed for 0.5 h with sparging argon. $Pd_2(dba)_3$ (11 mg, 0.012 mmol) and P(*o*-tolyl)$_3$ (15 mg, 0.049 mmol) were added and the reaction mixture was stirred at 75 °C for 18 h. The reaction mixture was poured over H_2O, and extracted with Et_2O. The organic phase was washed with H_2O, dried over Na_2SO_4, and concentrated to yield the crude product. The crude product was purified by column chromatography (silica gel, 2:3 CH_2Cl_2:hexanes gradient to 3:2 CH_2Cl_2:hexanes). The collected fractions were concentrated under reduced pressure, and dried on high vacuum to yield the desired product as a black solid (0.924 g, 68.7%). ^{1}H NMR (500 MHz, $CDCl_3$, ppm) δ: 9.25 (d, *J* = 8.4 Hz, 2H), 9.19 (d, *J* = 8.4 Hz, 2H), 7.33 (d, *J* = 8.4 Hz, 2H), 7.30, (s, 2H), 7.27 (d, *J* = 8.4 Hz, 2H), 7.06 (s, 2H), 7.00 (s, 2H), 6.98 (s, 2H), 3.76 (d, *J* = 7.45 Hz, 4H), 3.72 (d, *J* = 7.25 Hz, 4H), 2.63 (t, *J* = 7.7 Hz, 4H), 1.92-2.04 (m, 4H), 1.66 (quint, *J* = 7.5 Hz, 2H), 1.18-1.48 (m, 113H), 0.91 (t, *J* = 7.0 Hz, 6H), 0.81-0.88 (m, 24H). ^{13}C NMR (126 MHz, CD_2Cl_2) δ: 169.02, 146.59, 146.35, 145.46, 144.26, 144.00, 138.71, 133.14, 132.19, 130.88, 130.58, 126.30, 122.39, 121.58, 121.47, 120.79, 119.18, 106.86, 105.36, 45.08, 44.93, 37.02, 36.97, 32.47, 32.45, 32.37, 32.30, 32.27, 31.11, 31.01, 30.69, 30.59, 30.36, 30.28, 30.17, 29.93, 29.89, 29.61, 27.20, 27.17, 27.10, 23.30, 23.25, 14.44. HRMS (*m/z*) ($M^{\bullet+}$): calc ($C_{116}H_{174}N_4O_4S_2$): 1751.29765 found: 1751.29073.

Dibromodithineyldiisoindigo **Br_2-T_2-di-iI**

T_2-di-iI (201 mg, 0.114 mmol) was dissolved in chloroform (13 mL) and acetic acid (5 mL). *N*-bromosuccinimide (NBS) (45 mg, 0.25 mmol) was added portion-wise and the reaction mixture was heated to reflux for 5 h. The solution was cooled to room temperature and concentrated undr reduced pressure to yield the crude product. The crude product was dissolved in Et_2O, washed with 5% v/v $NaHCO_3$ (aq) and H_2O, dried over Na_2SO_4, and concentrated on high vacuum to yield the desired product as a black solid (187 mg, 85.7%). ^{1}H NMR (500 MHz, $CDCl_3$, ppm) δ: 9.22 (d, *J* = 8.4 Hz, 2H), 9.27 (d, *J* = 8.4 Hz, 2H), 7.29 (d, J = 8.4 Hz, 2H), 7.18 (d, *J* = 8.3 Hz, 2H), 7.09 (s, 2H), 7.00 (s, 2H), 6.86 (s, 2H), 3.75 (d, *J* = 7.5 Hz, 4H), 3.71 (d, *J* = 7.3 Hz, 4H), 2.57 (t, *J* = 7.7 Hz, 4H), 1.88-2.02 (m, 4H), 1.62 (quint, *J* = 7.5 Hz, 4H), 1.19-1.50 (m, 101 H), 0.91 (t, *J* = 6.9 HZ, 6H), 0.82-0.88 (m, 22H). ^{13}C NMR (126 MHz, $CDCl_3$) δ: 168.55, 168.50, 145.92, 145.72, 143.95, 143.61, 143.25, 137.22, 132.48, 130.44, 130.13, 125.03, 121.77, 121.17, 120.51, 118.62, 109.97, 106.40, 104.58, 44.67, 44.53, 36.49, 36.43, 31.90, 31.86, 31.82, 31.71, 31.64, 30.12, 30.03, 29.79, 29.72, 29.63, 29.60, 29.35, 29.33, 28.97, 26.69, 26.66, 26.55, 22.68, 22.63, 14.1. HRMS (*m/z*) ($M^{\bullet+}$): calc ($C_{116}H_{172}Br_2N_4O_4S_2$): 1907.11868 found: 1907.11699.

2,5-Bis(trimethylstannyl)thiophene (**11**)[15]

2,5-Dibromothiophene (2.0 mL, 0.018 mol) was dissolved in dry THF (180 mL) and cooled to -85 °C. *n*-BuLi (2.5 mol L^{-1} in hexanes) (15.0 mL, 0.0375 mol) was added and the reaction mixture was stirred at -85 °C for 1 h. Trimethyltin chloride (1 mol L^{-1} in hexanes) (40 mL, 0.04 mol) was added and the reaction mixture was brought to room temperature and stirred for 18 h. The reaction mixture was poured over 0.5 mol L^{-1} NH_4Cl (aq) and extracted with Et_2O. The combined organic layers were washed with H_2O and brine, dried over Na_2SO_4, and concentrated to yield the crude

product. The crude product was purified by recrystallization, first in hot EtOH, and again in hot isopropanol, to yield the pure product as an off-white solid (2.68 g, 36.8%). ^{1}H NMR (500 MHz, $CDCl_3$, ppm) δ: 7.37 (s, 2H), 0.36 (s, 17H).

Poly(diisoindigo-thiophene) **di-iI-T**

Br_2-di-iI (379 mg, 0.240 mmol) and 2,5-bis(trimethylstannyl)thiophene (**11**) (98 mg, 0.24 mmol) were dissolved in dry toluene (40 mL) in a flame dried schlenk flask and the solution was degassed with argon for 0.5 h. $Pd_2(dba)_3$ (14 mg, 0.015 mmol) and P(*o*-tolyl)$_3$ (12 mg, 0.039 mmol) were added and the reaction mixture was heated to 95 ºC for 48 hours. The reaction mixture was cooled to room temperature, a spatula tip of diethyldithiocarbamic acid diethyl ammonium salt was added, and the solution was stirred for 3 h. The mixture was poured over methanol and the resulting black solid was collected by suction filtration. The crude product was purified by Soxhlet extraction with methanol, acetone, hexanes and chloroform for 24 h each. The chloroform fraction was concentrated, poured over methanol, and collected by centrifugation to yield a black-green solid (264 mg 73.3%). ^{1}H NMR (500 MHz, $CDCl_3$, ppm) δ: 8.75-9.20 (br), 6.50-7.30 (br), 3.60-4.40 (br), 1.8-2.2 (br), 0.54-1.80 (br). M_w 55.4 kDa, M_n 17.1 kDa, $Đ$ 3.2.

Poly(diisoindigo-terthiophene) **di-iI-3T**

Br_2-T_2-di-iI (180 mg, 0.0941 mmol) and 2,5-bis(trimethylstannyl)thiophene (**11**) (38 mg, 0.093 mmol) were dissolved in toluene (10 mL) in a flame dried two-neck flask and degassed with argon for 0.5 h. $Pd_2(dba)_3$ (7 mg, 0.007 mmol) and P(*o*-tolyl)$_3$ (9 mg, 0.03 mmol) were added and the reaction mixture was stirred at 100 °C for 44 h. The reaction mixture was cooled to room temperature and a small amount of diethyldithiocarbamic acid diethylammonium salt was added.

The mixture was stirred for 2 h, poured over MeOH, acidified with a small amount of dilute HCl (aq) (~5 mL, 1 mol L^{-1}), and suction filtered. The resulting black solid was purified by Soxhlet extraction with methanol, acetone, hexanes and chloroform for 24 h each. The chloroform fraction was concentrated and poured over methanol, the resulting black solid was collected by centrifugation and dried on high vacuum to yield the desired polymer (115 mg, 66.7%). ^{1}H NMR (500 MHz, $CDCl_3$, ppm) δ: 8.74-9.28 (br), 6.81-7.36 (br), 6.49-6.72 (br), 3.59-4.27 (br), 2.42-2.93 (br), 0.64-2.11 (br). M_w 51.4 kDa, M_n 21.2 kDa, $Đ$ 2.4.

5.2.7 Detailed synthetic procedures for bis-iI-T and bis-iI-3T

N,N′-(naphthalene-1,5-diyl)bis(2-hexyldecanamide) (**6**)[39]

In a flame dried, 100 mL 2-neck round bottom flask, 2-hexyldecanoic acid (5.0 mL, 17 mmol) and thionyl chloride (15 mL) were stirred at reflux for 2.5 h. The mixture was cooled and the thionyl chloride was removed under high vacuum. In a flame dried, 250 mL schlenk flask, 1,5-diaminonapthalene (1.33 g, 8.44 mmol) and triethylamine (2.59 mL, 18.6 mmol) were suspended in dry CH_2Cl_2 (90 mL) under argon and cooled to 0 °C. A solution of the isolated 2-hexyldecanoyl chloride in dry CH_2Cl_2 (20 mL) was added dropwise to the cooled reaction mixture under argon. The mixture was slowly brought to room temperature and stirred for 18 h. The resulting solid was isolated by suction filtration, washed with water and minimal ethanol, and dried under high vacuum to obtain the desired product as a white powder (5.09 g, 95.0%). ^{1}H NMR (500 MHz, $CDCl_3$, ppm) δ: 7.88 (d, J = 6.85 Hz, 2H), 7.68 (s, 2H), 7.57 (d, J = 8.15 Hz, 2H), 7.38 (t, J = 7.60 Hz, 2H), 2.35-2.45 (m, 2H), 1.74-1.85 (m, 4H), 1.19-1.50 (m, 48H), 0.82-0.93 (m, 12H). ^{13}C NMR (126 MHz, $CDCl_3$) δ: 175.22, 132.96, 128.00, 126.04, 121.41, 118.04, 49.18, 33.57, 32.02, 31.93,

29.93, 29.69, 29.59, 29.45, 28.03, 28.00, 22.81, 22.78, 14.24. HRMS (m/z): ($M^{\bullet+}$) calc ($C_{42}H_{70}N_2O_2$): 634.54373 found: 634.54256.

N,N′-bis(2-hexyldecyl)naphthalene-1,5-diamine (**7**)[39]

In a flame dried 250 mL 2-neck round bottom flask, *N,N′*-(naphthalene-1,5-diyl)bis(2-hexyldecanamide) (**6**) (5.00 g, 7.87 mmol) was suspended in dry THF (80 mL). The mixture was cooled to 0 °C and lithium aluminum hydride solution (2 mol L^{-1} in THF) (16.1 mL, 32.3 mmol) was added dropwise to the mixture. The mixture was slowly brought to room temperature, and stirred at reflux for 90 h. The mixture was then cooled to 0 °C and 0.33 mol L^{-1} aqueous NaOH (50 mL) was added dropwise to the solution. The crude product was collected by suction filtration and washed with water. The solid was dissolved in CH_2Cl_2, washed with 5% HCl, dried over $MgSO_4$, and concentrated under reduced pressure to yield the crude product. The crude product was purified by chromatography (silica gel, 3:7 ethyl acetate:hexanes). The combined fractions were concentrated under reduced pressure and dried on high vacuum to yield the desired product as a pale red oil (3.44 g, 5.65 mmol, 72%). ^{1}H NMR (500 MHz, $CDCl_3$, ppm) δ: 7.30 (t, J = 8.0 Hz, 2H), 7.12 (d, J = 8.4 Hz, 2H), 6.59 (d, J = 7.6 Hz, 2H), 4.39 (br, 2H), 3.16 (d, J = 6.1 Hz, 4H), 1.77 (sep, J = 6.0 Hz, 2H), 1.39-1.46 (m, 8H), 1.34-1.39 (m, 8H), 1.21-1.33 (m, 32H), 0.85-0.90 (m, 12H). ^{13}C NMR (126 MHz, $CDCl_3$) δ:144.56, 125.58, 124.09, 108.37, 104.20, 47.90, 37.75, 32.62, 32.05, 32.02, 30.22, 29.89, 29.75, 29.48, 26.95, 26.93, 22.83, 14.25. HRMS (m/z): ($M^{\bullet+}$) calc ($C_{42}H_{74}N_2$): 606.58520 found: 606.58473.

N,N′-bis(2-hexyldecyl)bisisatin (**8**)

In a 2-neck round bottom flask, *N,N′*-bis(2-hexyldecyl)naphthalene-1,5-diamine (**7**) (1.93 g, 3.17 mmol) was suspended in glacial acetic acid (10 mL), degassed with argon, then heated to reflux. To the reaction mixture, a solution of diethylketomalonate (2.18 mL, 14.3 mmol) in acetic acid (7 mL) was added dropwise under argon. The mixture was stirred at reflux for 18 h. The solvent was then removed via rotary evaporation, the mixture was dissolved in ethyl acetate and filtered through a silica plug. The filtrate was collected in a round bottom flask and the solvent was removed under reduced pressure. 1,4-Dioxane (80 mL) was added to the mixture, and it was stirred vigorously in air. To the solution, 1.5 M tetraethylammonium hydroxide solution in methanol (10.6 mL, 15.9 mmol) was added rapidly and the mixture was quickly placed in an 80 °C oil bath. The reaction was monitored by TLC (3:7 ethyl acetate:hexanes) to observe the complete consumption of the isolated intermediate (~1 minute), after which time the reaction was quickly quenched with cold HCl (10% v/v, 100 mL). The product is not stable in basic conditions, and must not be exposed to base longer than necessary. The mixture was then separated with brine and ethyl acetate and the combined organic layers were concentrated under reduced pressure. Water was added to the concentrated organic layer, and the mixture was stirred for 18 h in air to allow completion of the oxidation. The mixture was then separated with brine and ethyl acetate; the combined organic layers were dried over $MgSO_4$ and concentrated under reduced pressure. The crude product was purified by chromatography (silica gel, 3:7 ethyl acetate:hexanes). The collected fractions were concentrated under reduced pressure and dried on high vacuum to yield the desired product as a dark blue solid (1.02 g, 45.0%). ^{1}H NMR (500 MHz, $CDCl_3$, ppm) δ: 7.99 (d, J = 8.66 Hz, 2H), 7.66 (d, J = 8.66 Hz, 2H), 4.16 (d, J = 7.40 Hz, 4H), 1.87-1.94 (m, 2H), 1.31-142 (m, 8H), 1.16-1.31 (m, 40H), 0.80-0.92 (m, 12H). ^{13}C NMR (126 MHz, $CDCl_3$) δ: 182.89, 159.41, 152.50,

127.55, 120.22, 120.10, 116.45, 47.70, 37.68, 31.98, 31.84, 31.17, 30.09, 29.85, 29.75, 29.61, 29.39, 26.31, 26.26, 22.80, 22.74, 14.26, 14.21. HRMS (m/z): ($M^{\bullet+}$) calc ($C_{46}H_{70}N_2O_4$): 714.53356 found: 714.53246.

Dibromobisisoindigo (**Br_2-bis-iI)**

In a two-neck round bottom flask, *N*-(2-hexyldecyl)-6-bromo-2-oxindole (**3**) (1.37 g, 3.14 mmol) was dissolved in glacial acetic acid (35 mL) and degassed with argon. *N,N′*-bis(2-hexyldecyl)bisisatin (**8**) (1.02 g, 1.43 mmol) and *p*-toluenesulfonic acid monohydrate (0.0679 g, 0.357 mmol) were added to the mixture and heated to 80 ºC for 18 h. The mixture was cooled and poured into water (100 mL). The resulting solid was collected by suction filtration, washed with water and acetone, and dried on high vacuum to yield the desired product as a brown waxy solid (0.91 g, 41%). ^{1}H NMR (500 MHz, $CDCl_3$, ppm) δ: 8.94-9.01 (m, 4H) 7.84 (d, *J* = 9.3 Hz, 2H), 7.17 (d, *J* = 8.5 Hz, 2H), 6.91 (s, 2H), 4.23 (d, *J* = 7.20 Hz, 4H), 3.65 (d, *J* = 7.40 Hz, 4H), 1.99-2.09 (m, 2H), 1.86-1.96 (m, 2H), 1.08-1.45 (m, 96H), 0.77-0.93 (m, 24H). ^{13}C NMR (126 MHz, $CDCl_3$) δ: 170.03, 168.06, 146.47, 143.53, 132.73, 132.70, 130.50, 127.03, 125.23, 124.51, 123.51, 120.97, 120.24, 117.41, 111.80, 47.47, 44.93, 37.50, 36.29, 32.02, 31.95, 31.90, 31.70, 31.19, 30.22, 30.14, 29.86, 29.80, 29.70, 29.65, 29.43, 26.59, 26.53, 26.24, 22.81, 22.78, 22.74, 14.23. HRMS (m/z): ($M^{\bullet+}$) calc ($C_{94}H_{142}Br_2N_4O_4$): 1548.93978 found: 1548.94600.

Dithienylbisisoindigo **T_2-bis-iI**

Br_2-bis-iI (221 mg, 0.143 mmol) and 2-trimethylstannyl-4-hexylthiophene (**14**) (141 mg, 0.426 mmol) were dissolved in dry THF (5 mL) in a flame dried two-neck flask and degassed with argon for 30 min. $Pd_2(dba)_3$ (4.7 mg, 0.0051 mmol) and P(*o*-tolyl)$_3$ (4.5 mg, 0.015 mmol) were added

and the reaction mixture was heated to 75 °C for 18 h. The reaction mixture was poured over H_2O and extracted with Et_2O. The combined organic layers were washed with H_2O, dried over Na_2SO_4 and concentrated to yield the crude product as a black solid. The crude product was purified by column chromatography (silica gel, 1:1 CH_2Cl_2:hexanes); the combined fractions were concentrated under reduced pressure, and the solid was dried high vacuum to yield the desired product as a black solid (225 mg, 90.5%). 1H NMR (500 MHz, CD_2Cl_2, ppm) δ: 9.06 (d, *J* = 6.4 Hz, 2H), 8.96 (d, *J* = 9.3 Hz, 2H), 7.80 (d, *J* = 9.1 Hz, 2H), 7.29 (s, 2H), 7.26 (d, *J* = 8.4 Hz, 2H), 6.99 (s, 2H), 6.93 (s, 2H), 4.25 (d, *J* = 6.8 Hz, 4H), 3.66 (d, *J* = 7.3 Hz, 4H), 2.64 (t, *J* = 7.7 Hz, 4H), 2.01-2.11 (m, 2H), 1.87-1.97 (m, 2H), 1.67 (quint, *J* = 7.5 Hz, 2H), 1.32-1.45 (m, 43H), 1.16-1.31 (m, 75 H), 0.91 (q, *J* = 4.6 Hz, 6H), 0.82-0.87 (m, 25H). ^{13}C NMR (126 MHz, CD_2Cl_2) δ: 170.43, 168.70, 146.71, 145.50, 144.03, 143.40, 139.03, 133.48, 131.48, 130.43, 126.39, 124.90, 123.48, 121.76, 120.62, 119.13, 117.41, 105.36, 47.73, 44.94, 37.97, 36.97, 32.48, 32.44, 32.38, 31.65, 31.13, 31.03, 30.68, 30.59, 30.32, 30.26, 30.18, 30.11, 29.90, 29.63, 27.24, 27.19, 26.68, 23.26, 23.23, 23.20, 14.46, 14.44. HRMS (*m/z*) ($M^{\bullet+}$): calc ($C_{114}H_{172}N_4O_4S_2$): 1725.28200 found: 1725.28903.

Dibromodithienylbisisoindigo **Br_2-T_2-bis-iI**

T_2-bis-iI (190 mg, 0.110 mmol) was dissolved in dry THF (5 mL), cooled to -80 °C, and dibromantin (37.8 mg, 0.132 mmol) was added. The reaction mixture was stirred at -80 °C for 0.5 h before being brought to room temperature and stirred for a further 2 h. The mixture was diluted with Et_2O and washed with H_2O (50 mL). The organic layer was dried over $MgSO_4$ and concentrated to yield the crude product. To remove excess grease, the crude product was dissolved in hexanes and loaded onto a short silica plug. The column was washed with hexanes and the

product was removed from the silica with CH_2Cl_2. The CH_2Cl_2 was removed under reduced pressure and the pure product was dried on high vacuum to yield a black solid (193 mg, 93.1%). ^{1}H NMR (500 MHz, $CDCl_3$, ppm) δ: 9.05 (d, *J* = 8.4 Hz, 2H), 8.94 (d, *J* = 9.4 Hz, 2H), 7.80 (d, *J* = 9.5 Hz, 2H), 7.16 (d, *J* = 8.5 Hz, 2H) 7.09 (s, 2H), 6.81 (s, 2H), 4.24 (d, *J* = 7.3 Hz, 4H), 3.67 (d, *J* = 7.3 Hz, 4H) 2.58 (t, *J* = 7.8 Hz, 4H), 2.0-2.09 (m, 2H), 1.86-1.94 (m, 2H), 1.63 (quint, *J* = 7.5 Hz, 2H), 0.91 (t, *J* = 7.0 Hz, 7H), 1.31-1.45 (m, 42H), 1.17-1.31 (m, 74H), 0.78-0.89 (m, 26H). ^{13}C NMR (126 MHz, $CDCl_3$) δ: 170.04, 168.40, 146.15, 143.79, 143.36, 143.14, 137.66, 132.90, 131.51, 129.99, 125.22, 124.40, 123.25, 121.60, 120.25, 118.73, 117.23, 110.31, 104.73, 47.41, 44.67, 37.51, 36.53, 32.02, 31.91, 31.76, 31.18, 30.24, 30.14, 29.85, 29.81, 29.75, 29.67, 29.45, 29.43, 29.10, 26.84, 26.79, 26.24, 22.80, 22.75, 14.22. HRMS (*m/z*) ($M^{\bullet+}$): calc ($C_{114}H_{170}Br_2N_4O_4S_2$): 1881.10303 found: 1881.09955.

Poly(bisisoindigo-thiophene) **Bis-iI-T**[39]

Br_2-bis-iI (201 mg, 0.130 mmol) and 2,5-bis(trimethylstannyl)thiophene (**11**) (54 mg, 0.13 mmol) were dissolved in dry toluene (15 mL) in a flame dried two-neck flask and degassed for 0.5 h with sparging argon. $Pd_2(dba)_3$ (15 mg, 0.016 mmol) and P(*o*-tolyl)$_3$ (6 mg, 0.02 mmol) were added and the reaction mixture was stirred at 100 °C for 24 h. The reaction mixture was cooled to room temperature, a spatula tip of diethyldithiocarbamic acid diethylammonium salt was added, and the mixture was stirred for 0.5 h. The mixture was poured over methanol (acidified with ~5 mL 1 mol L^{-1} HCl (aq)) and the crude product was collected by suction filtration. The crude product was purified by Soxhlet extraction using methanol, acetone, hexanes and chloroform for 24 h each. The chloroform fraction was concentrated under reduced pressure and poured over methanol. The resulting precipitate was collected by centrifugation and dried on high vacuum to yield the desired

polymer as a black solid (102 mg, 53.2%). ^{1}H NMR (600 MHz, $CDCl_3$, ppm) δ: 8.80-9.20 (br), 7.54-7.83 (br), 6.89-7.16 (br), 6.54-6.86 (br), 3.15-4.71 (br), 1.79-2.17 (br), 0.62-1.76 (br). M_w 51.9 kDa, M_n 19.9 kDa, $Đ$ 2.6.

Poly(bisisoindigo-terthiophene) **Bis-iI-3T**

Br_2-T_2-bis-iI (120 mg, 0.0638 mmol) and 2,5-bis(trimethylstannyl)thiophene (**11**) (26 mg, 0.064 mmol) were dissolved in dry toluene (10 mL) in a flame dried two-neck flask and degassed for 0.5 h with sparging argon. $Pd_2(dba)_3$ (6.0 mg, 0.0066 mmol) and P(*o*-tolyl)$_3$ (6.6 mg, 0.022 mmol) were added and the reaction mixture was stirred at 100 °C for 18 h. The reaction mixture was cooled to room temperature, a spatula tip of diethyldithiocarbamic acid diethylammonium salt was added, and the mixture was stirred for 0.5 h. The mixture was poured over methanol and the crude product was collected by suction filtration. The crude product was purified by Soxhlet extraction using methanol, acetone, hexanes and chloroform for 24 h each. The chloroform fraction was concentrated under reduced pressure and poured over methanol. The resulting precipitate was collected by suction filtration and dried on high vacuum to yield the desired polymer as a black solid (84 mg, 73%). ^{1}H NMR (500 MHz, $CDCl_3$, ppm) δ: 8.42-9.17 (br), 6.87-7.78 (br), 6.38-6.77 (br), 3.83-4.72 (br), 2.45-3.18 (br), 0.61-2.15 (br). M_w 69.2 kDa, M_n 25.1 kDa, $Đ$ 2.8.

5.2.8 Detailed synthetic procedures for iI-T and iI-3T

6-Bromo-2-oxindole (**9**)[43,44]

6-Bromoisatin (2.50 g, 11.0 mmol) was dissolved in methanol (20 mL). Hydrazine monohydrate (1.5 mL, 31 mmol) was added and the reaction mixture was stirred at reflux for 1 h. The reaction mixture was cooled to 0 °C and suction filtered, to yield a bright yellow solid. The yellow solid

was added to a solution of EtONa in EtOH (sodium metal (0.97 g, 42 mmol) dissolved in absolute ethanol (25 mL)). The reaction mixture was stirred at reflux in air for 0.5 h. The reaction mixture was poured over ice and acidified to pH 1 with dilute HCl (aq). The resulting solid was collected by suction filtration and dried under high vacuum to yield 6-bromo-2-oxindole as a beige solid (1.84 g, 78.4%). ^{1}H NMR (500 MHz, D_6-DMSO, ppm) δ: 10.48 (s, 1H), 7.15 (d, J = 7.9 Hz, 1H), 7.10 (d, 7.9 Hz, 1H), 6.94 (s, 1H), 3.44 (s, 2H).

6,6′-Dibromoisoindigo (**10**)[18]

6-Bromoisatin (1.23 g, 5.44 mmol) and 6-bromo-2-oxindole (**9**) (1.16 g, 5.47 mmol) were suspended in glacial acetic acid (35 mL); concentrated HCl (0.25 mL) was added, and the reaction mixture was stirred at reflux for 18 h. The reaction mixture was cooled to room temperature and suction filtered. The solid was washed with H_2O, EtOH, and ethyl acetate, and dried on high vacuum to yield a black/red solid (1.98 g, 86.7%) ^{1}H NMR (500 MHz, D_6-DMSO, ppm) δ: 11.11, (s, 2H), 8.99 (d, J = 8.6 Hz, 2H), 7.19 (d, J = 8.6 Hz, 2H), 7.00 (s, 2H).

N,N′-(2-hexyldecyl),6,6′-dibromoisoindigo (**Br_2-iI**)[25]

6,6′-Dibromoisoindigo (**10**) (2.10 g, 5.00 mmol) and K_2CO_3 (6.91 g, 52.2 mmol) were suspended in dry DMF (100 mL). 2-Hexyldecylbromide (**1**) (3.34 g, 10.9 mmol) was added and the reaction mixture was stirred at 100 °C for 20 h. The reaction mixture was poured over ice and extracted with Et_2O. The combined organic layers were washed with H_2O and brine, dried over Na_2SO_4 and concentrated under reduced pressure to yield the crude product. The crude product was purified by column chromatography (silica gel, 3:5 CH_2Cl_2:hexanes); the combined fractions were concentrated under reduced pressure, and the solid was dried on high vacuum to yield the desired

product as a red solid (1.37 g, 31.3%). ^{1}H NMR (500 MHz, $CDCl_3$, ppm) δ: 9.06 (d, *J* = 8.6 Hz, 2H), 7.16 (d, *J* = 8.7 Hz, 2H), 6.90 (s, 1H), 3.62 (d, *J* = 7.5 Hz, 4H), 1.84-1.92 (m, 2H), 1.17-1.42 (m, 46 H), 0.85 (t, *J* = 3.6 Hz, 12H).

3,3′′-Dihexyl-2,2′:5′,2′′-terthiophene (**12**)[46]

To a suspension of Mg turnings (380 mg, 15.6 mmol) and a small amount of I_2 in dry THF, 2-bromo-3-hexylthiophene (2.20 mL, 11.3 mmol) was added slowly. The exothermic reaction was stirred at reflux for 1 h. The reaction mixture was cooled to room temperature and added slowly to a solution of Ni(dppp)Cl_2 (0.128 g, 0.236 mmol) and 2,5-dibromothiophene (0.50 mL, 4.5 mmol) in THF. The reaction mixture was heated to reflux for 18 h. The reaction mixture was poured over ice, and extracted with ethyl acetate. The combined organic layers were washed with H_2O and brine, dried over Na_2SO_4, and concentrated under reduced pressure to yield the crude product. The crude product was purified by column chromatography (silica gel, hexanes). The combined fractions were concentrated under reduced pressure, and the product was dried on high vacuum to yield a yellow oil (739 mg, 40%). ^{1}H NMR (500 MHz, $CDCl_3$, ppm) δ: 7.18 (d, *J* = 5.2 Hz, 2H), 7.05 (s, 2H), 6.94 (d, *J* = 5.3 Hz, 2H) 2.78 (t, *J* = 7.9 Hz, 4H), 1.60-1.69 (m, 4.5H), 1.25-1.42 (m, 14 H), 0.86-0.90 (m, 7H).

2,5-Bis(trimethylstannyl)-3,3′′-dihexyl-2,2′:5′,2′′-terthiophene (**13**)[15]

3,3′′-Dihexyl-2,2′:5′,2′′-terthiophene (**12**) (687 mg, 1.65 mmol) was dissolved in dry Et_2O (16 mL) and cooled to 0 °C. *n*-BuLi (2.5 mol L^{-1} in hexanes) (0.70 mL, 1.8 mmol) was added and the reaction mixture was warmed to room temperature for 1 h. After 1 h the reaction mixture was cooled to 0 °C and *n*-BuLi (2.5 mol L^{-1} in hexanes) (0.75 mL, 1.9 mmol) was added. The mixture

was stirred at 0 °C for 0.5 h and room temperature for 0.5 h. The mixture was cooled to 0 °C and trimethyltin chloride (1 mol L^{-1} in hexanes) (4.0 mL, 4.0 mmol) was added. The mixture was warmed to room temperature and stirred for 18 h. The reaction mixture was poured over H_2O and extracted with Et_2O. The combined organic layers were washed with brine, dried over Na_2SO_4, and concentrated under reduced pressure. The product was dissolved in ethyl acetate, and washed with 1 mol L^{-1} NaOH (aq) and brine to remove excess trimethyltin chloride. The resulting organic layer was dried over Na_2SO_4, concentrated under reduced pressure, and dried on high vacuum to yield a pale orange oil (1.21 g, 92%). ^{1}H NMR (500 MHz, $CDCl_3$, ppm) δ: 7.04 (s, 2H), 7.00 (s, 2H), 2.79 (t, J = 7.98 Hz, 4H), 1.66 (quint, J = 7.72 Hz, 5H), 1.35-1.44 (m, 5H), 1.25-1.35 (m, 11H), 0.86-0.92 (m, 7H), 0.38 (s, 19H).

Poly(isoindigo-thiophene) **iI-T**[15]

Br_2-iI (435 mg, 0.501 mmol) and 2,5-bis(trimethylstannyl)thiophene (**11**) (205 mg, 0.501 mmol) were dissolved in dry toluene (100 mL) in a flame dried schlenk flask and the solution was degassed with argon for 0.5 h. $Pd_2(dba)_3$ (16 mg, 0.018 mmol) and P(*o*-tolyl)$_3$ (10 mg, 0.033 mmol) were added and the reaction mixture was heated to 95 °C for 18 h. The reaction mixture was poured over methanol and acidified with HCl (aq) (~5 mL, 1 mol L^{-1}). The crude product was collected by suction filtration and purified by Soxhlet extraction in methanol, acetone, hexanes, and chloroform for 24 h each. The chloroform fraction was concentrated and poured over methanol; the resulting black solid was collected by suction filtration, and dried on high vacuum to yield the pure product (334 mg, 84.4%). ^{1}H NMR (500 MHz, $CDCl_3$, ppm) δ: 8.81-9.27 (br), 6.87-7.50 (br), 6.38-6.85 (br), 3.20-4.22 (br), 0.52-2.18 (br). M_w 93.2 kDa, M_n 36.7 kDa, $Đ$ 2.5.

Poly(isoindigo-terthiophene) **iI-3T**[15]

Br_2-iI (255 mg, 0.294 mmol) and 3,3′′-dihexyl-2,2′:5′,2′′-terthiophene (**13**) (242 mg, 0.327 mmol) were placed in a flame dried 3-neck round bottom flask. The flask was evacuated, and filled with argon three times; toluene (15 mL) was added and the solution was degassed with argon for 0.5 h. $Pd_2(dba)_3$ (10.4 mg, 0.0114 mmol) and P(*o*-tolyl)$_3$ (7.8 mg, 0.026 mmol) were added and the reaction mixture was heated to 95 °C for 44 h. The reaction mixture was cooled to room temperature and a small amount of diethyldithiocarbamic acid diethylammonium salt was added. The mixture was stirred for 2 h, poured over methanol, and acidified with a small amount of dilute HCl (aq) (~5 mL, 1 mol L^{-1}). The crude product was collected by suction filtration and purified by Soxhlet extraction in methanol, acetone, hexanes and chloroform for 24 hours each. The chloroform fraction was concentrated and poured over methanol; the resulting black solid was collected by suction filtration and dried on high vacuum to yield the desired polymer (299 mg, 87.2%). ^{1}H NMR (500 MHz, $CDCl_3$, ppm) δ: 8.92-9.22 (br), 6.91-7.34 (br), 6.49-6.71 (br), 3.31-3.78 (br), 2.67-2.99 (br), 1.63-1.96 (br), 1.03-1.63 (br), 0.72-1.03 (br). M_w 79.5 kDa, M_n 26.6 kDa, $Đ$ 3.0.

5.3 Results and discussion

5.3.1 Synthesis of DAA polymers

The synthesis of both **bis-iI** and **di-iI** involves first synthesizing a dimer of isatin, followed by two concurrent crossed aldol condensations with 6-bromo-2-oxindole to form the desired dihalogenated isoindigo dimer; the synthesis of the dibrominated monomer **Br_2-di-iI** is shown in Scheme 5.1. First, the 6-bromoisatin is alkylated (**2**), and then a Miayura coupling is used to generate the boronic ester-functionalized isatin (**4**). The 6-isatinboronate ester and an equivalent of the 6-bromoisatin are combined in a Suzuki coupling to form the 6,6′-diisatin (**5**) dimer in moderate yield. Finally, the dihalogenated **Br_2-di-iI** dimer (Scheme 5.1) is synthesized by a double cross aldol reaction.

In the previous report of **bis-iI**, the central ring-fused isatin dimer was first synthesized by the Martinet isatin synthesis and subsequently alkylated using 2-ethylhexyl iodide, to produce a soluble product.[38] However, in this work, longer 2-hexyldecyl alkyl groups were required to solubilize the DAA polymers. It was found that the size of these bulkier alkyl chains prevented the alkylation of the lactam nitrogens; therefore, a new synthetic method to produce the dibrominated monomer **Br_2-bis-iI** (Scheme 5.2) was employed. In this synthesis, 1,5-diaminonaphthalene is first alkylated before being subjected to the Martinet isatin synthesis and subsequent aldol condensations, producing **Br_2-bis-iI**.[39]

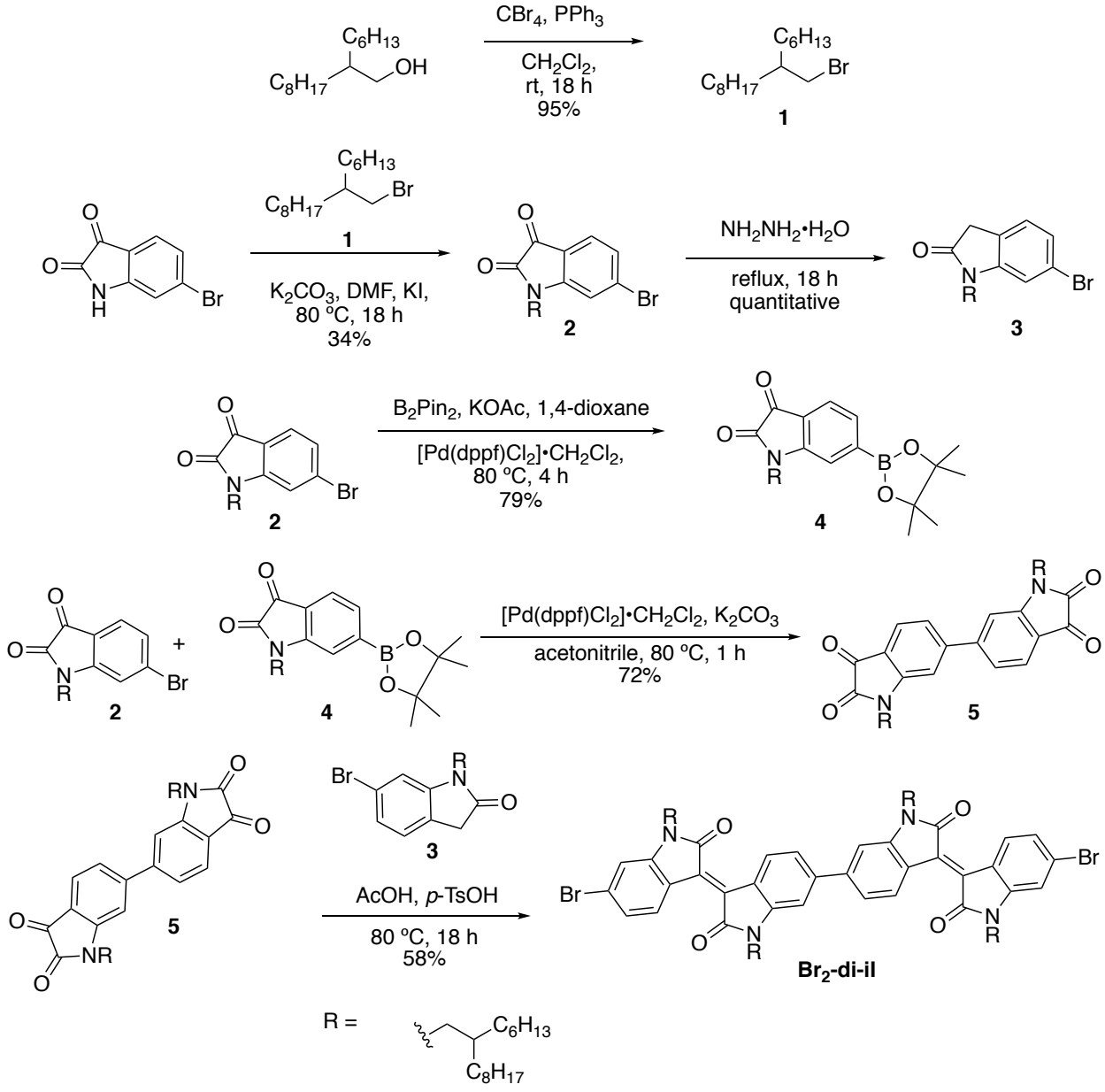

Scheme 5.1 Synthesis of dibromodiisoindigo (**Br_2-di-iI**).

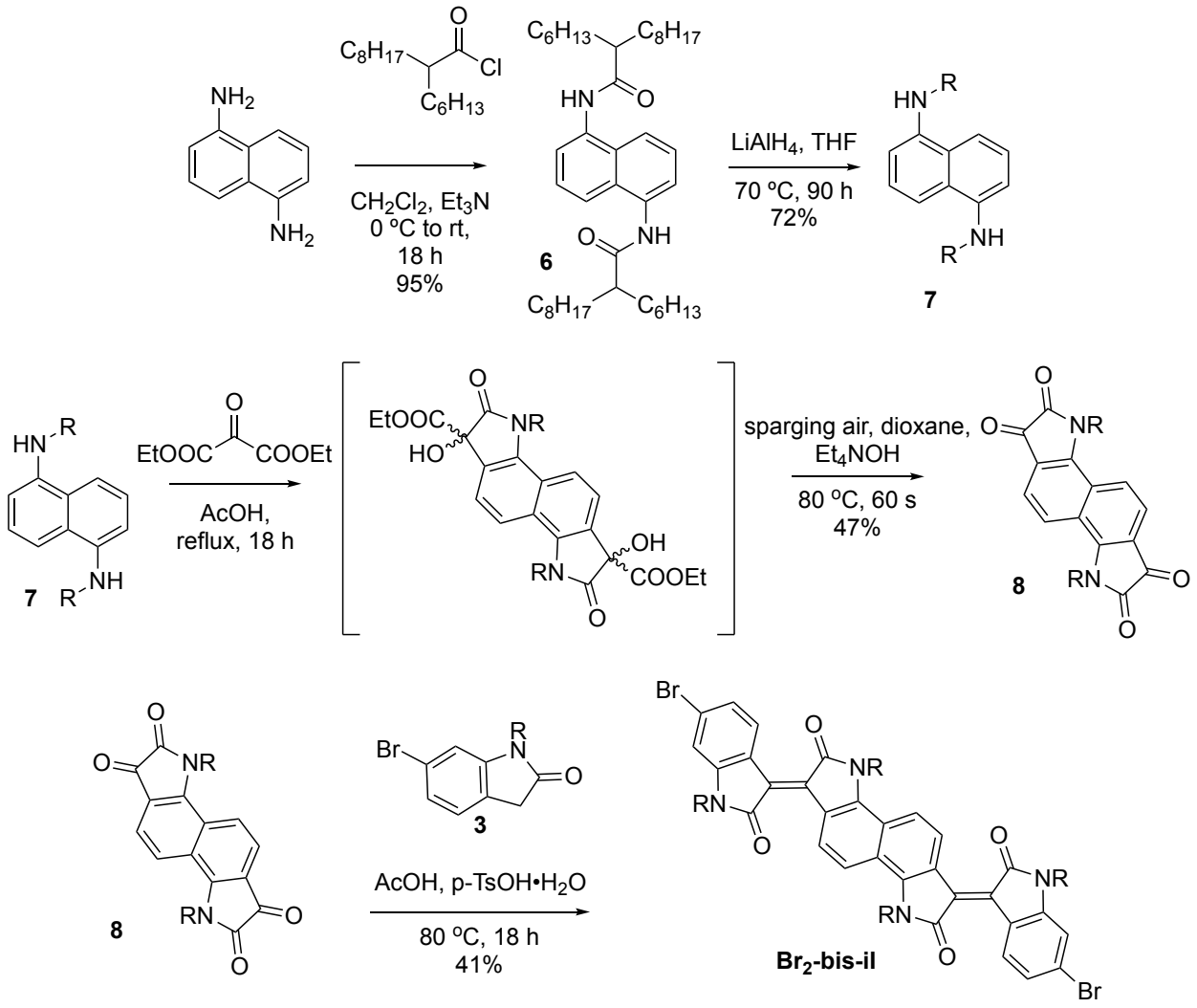

Scheme 5.2 Synthesis of dibromobisisoindigo (**Br_2-bis-iI**).

All six polymers (Chart 5.2) were synthesized by palladium catalyzed Stille polymerizations. **iI-T** and **iI-3T** were synthesized according to procedures reported by Stalder *et al* (Scheme 5.3).[15] Similarly, **di-iI-T** and **bis-iI-T** were synthesized by polymerization of the extended isoindigo monomer (**Br_2-di-iI** and **Br_2-bis-iI**) with 2,5-bis(trimethylstannyl)thiophene (Scheme 5.4). Owing to difficulty in purification of the bis(trimethylstannyl)terthiophene co-monomer used by Stalder *et al.*, both **di-iI-3T** and **bis-iI-3T** were synthesized by methods analogous to those used by Wang *et al.* to synthesize **iI-3T** (Scheme 5.5 and 5.6).[22] First, the

extended isoindigo (**Br_2-di-iI** or **Br_2-bis-iI**) was coupled to two equivalents of 2-trimethylstannyl-4-hexylthiophene (**T_2-di-iI** or **T_2-bis-iI**); the product was dibrominated (**T_2-Br_2-di-iI** or **T_2-Br_2-bis-iI**), and a Stille polycondensation with 2,5-bis(trimethylstannyl)thiophene was used to produce polymers **di-iI-3T** and **bis-iI-3T** (Scheme 5.3 and 5.4). All six polymers had weight average molecular weights (M_w) between 51 and 93 kDa, and number average molecular weights (M_n) between 17 kDa and 37 kDa (Table 5.1) as determined by size exclusion chromatography. The M_n values of the DAA polymers are all lower than their DA counterparts, possibly due to lower solubility. The molecular weights of **iI-T** and **iI-3T** are lower than those reported by Stalder *et al*.[17] The dispersity ($Đ$) of all of the polymers synthesized is between 2.4 and 3.2; $Đ \geq 2$ is expected for step growth polymerizations.

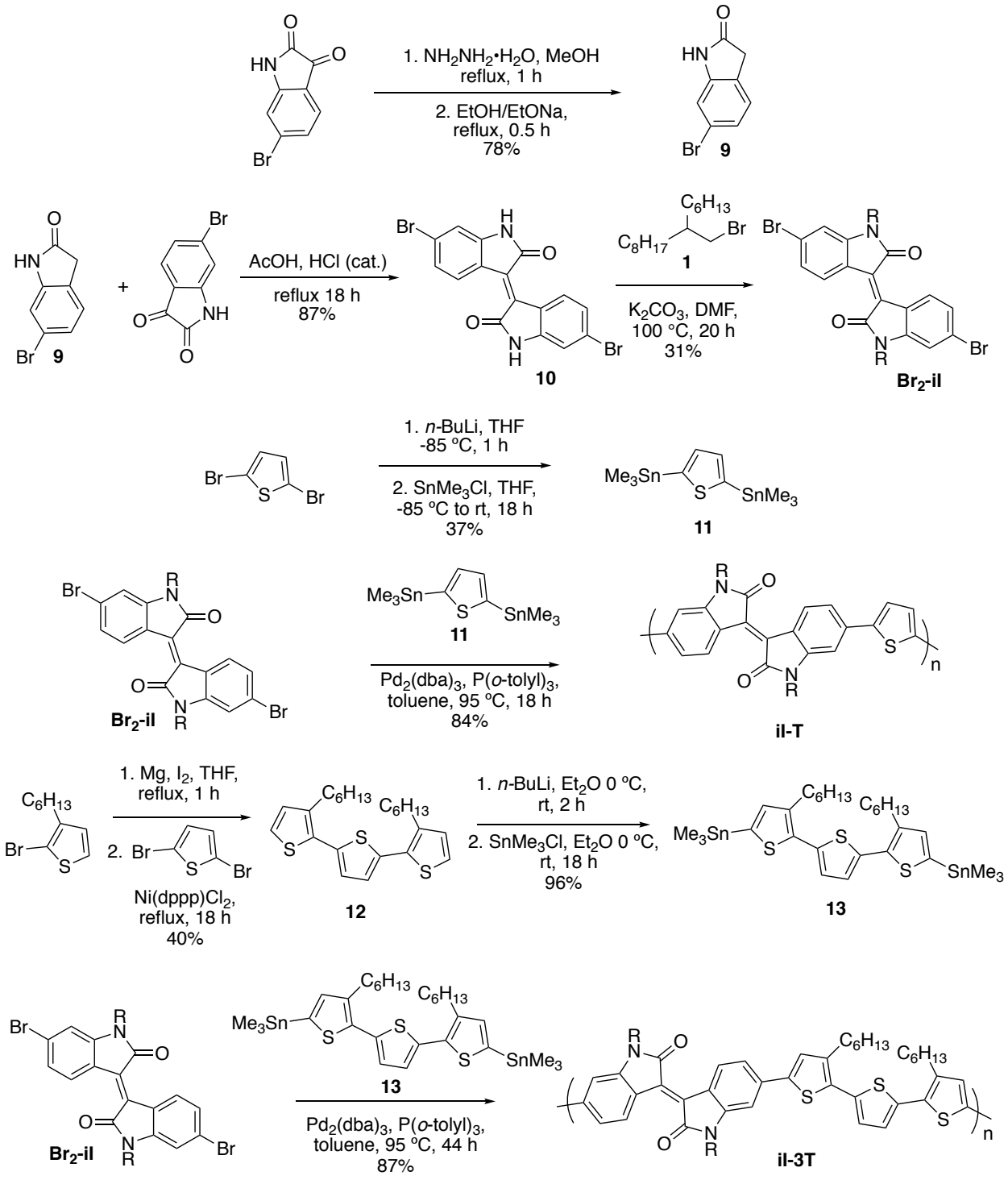

Scheme 5.3 Synthesis of **iI-T** and **iI-3T**.

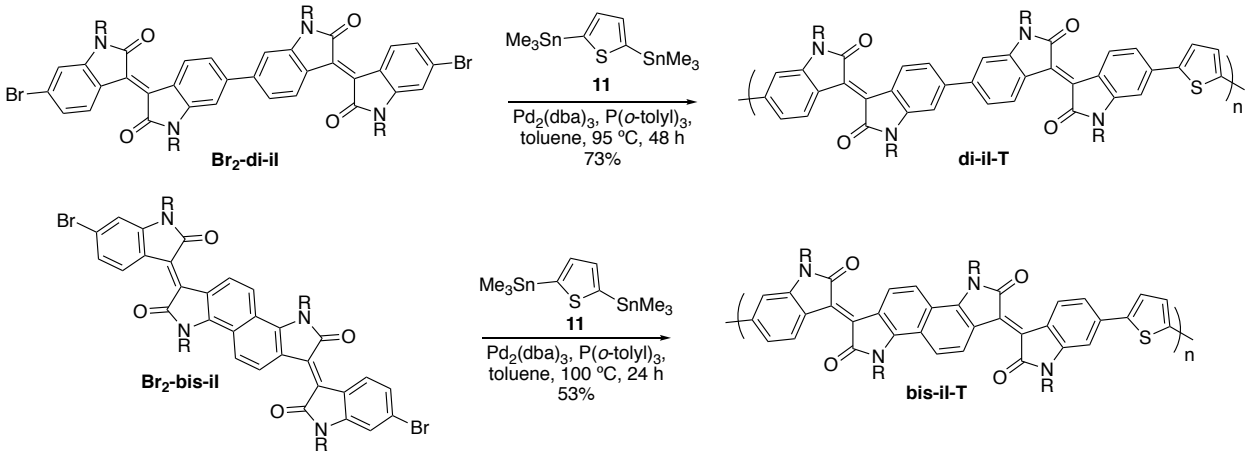

Scheme 5.4 Synthesis of **di-iI-T** and **bis-iI-T**.

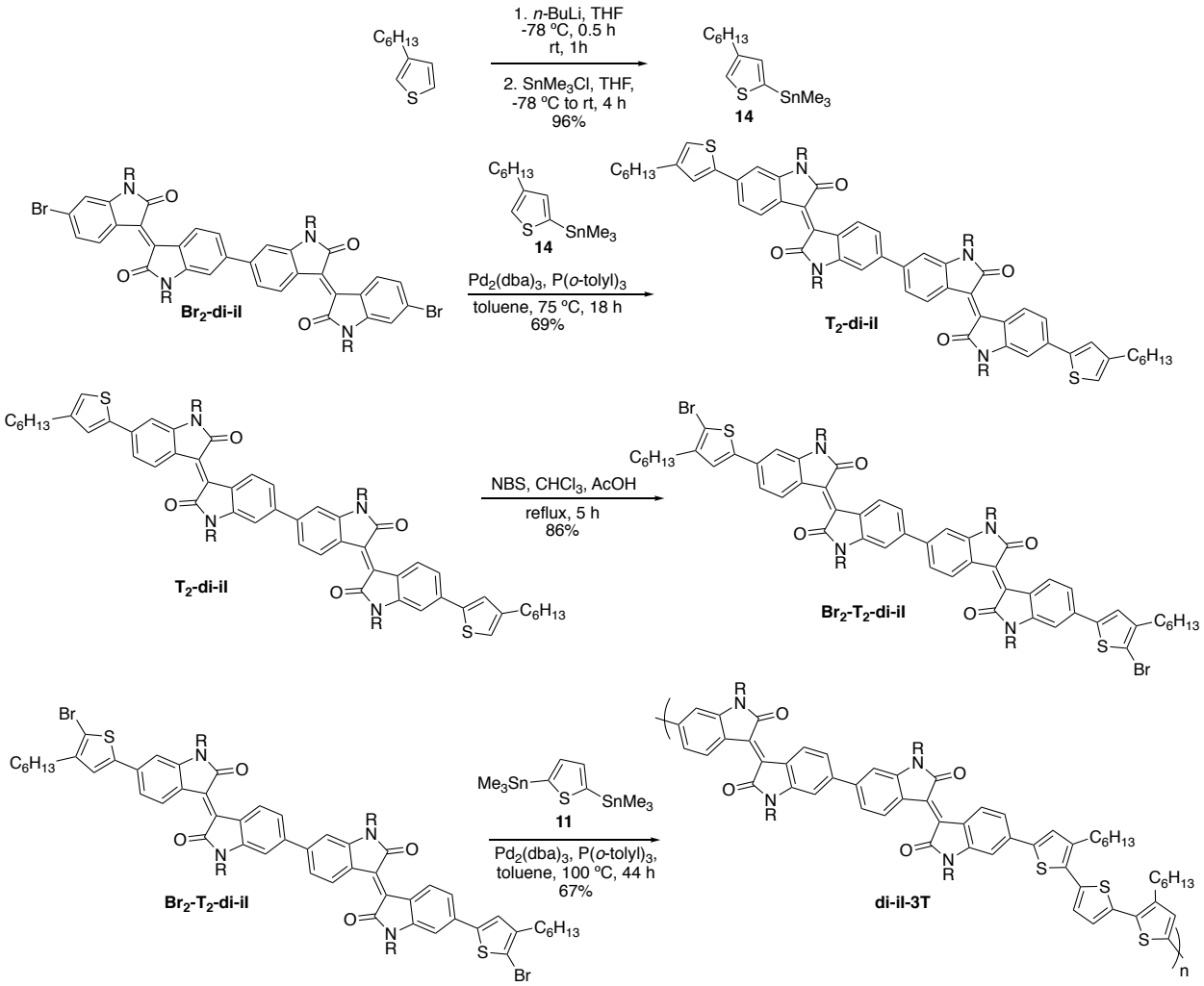

Scheme 5.5 Synthesis of **di-iI-3T**.

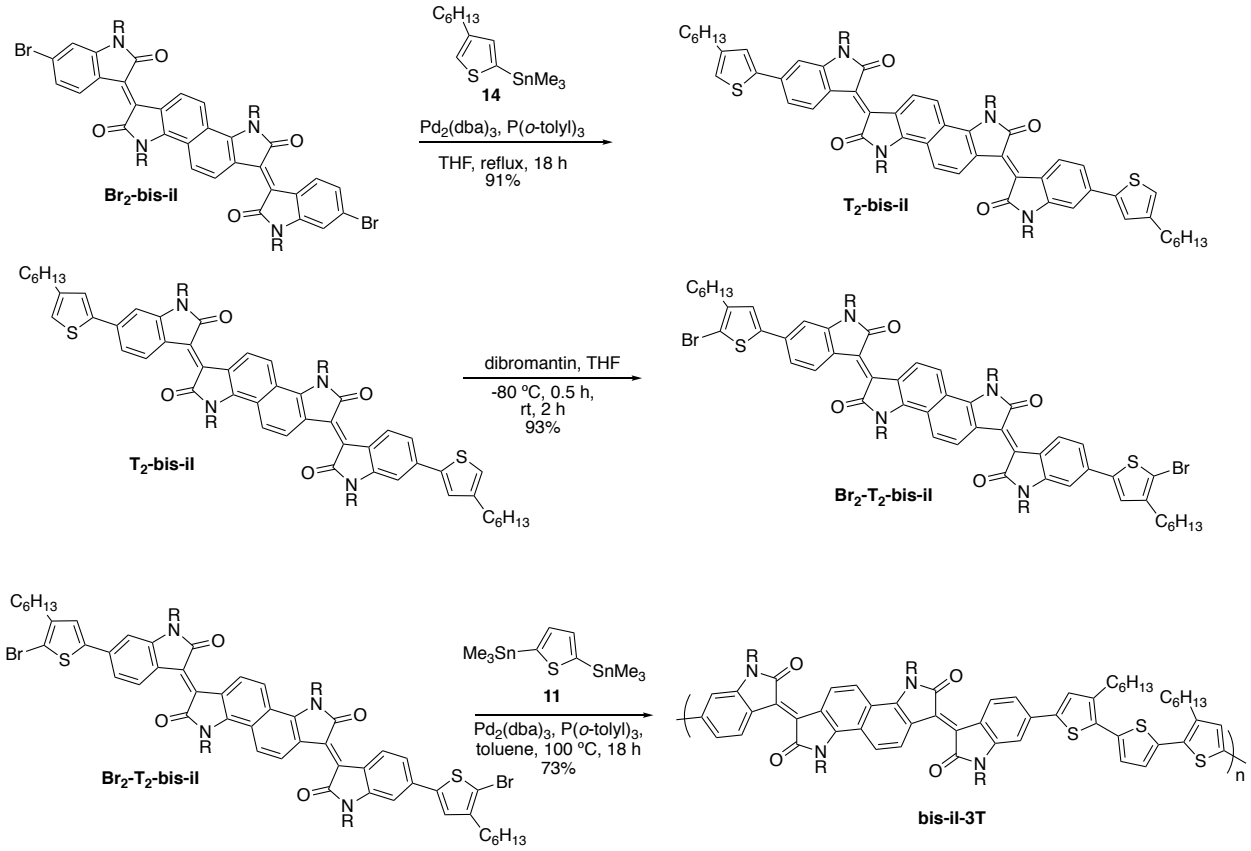

Scheme 5.6 Synthesis of **bis-iI-3T**.

Table 5.1 Molecular weight, dispersity, and optoelectronic properties of **iI**, **di-iI** and **bis-iI** polymers.

Polymer	M_w (kDa)	M_n (kDa)	$Đ$	$E_{g,elec}$[a] (eV)	$E_{g,opt}$ (eV)	E_{bind} (eV)	μ_h ($cm^2 V^{-1} s^{-1}$)	μ_e ($cm^2 V^{-1} s^{-1}$)
iI-T	93	37	2.5	2.04	1.61	0.4	$9 \pm 1 \times 10^{-4}$	$5.1 \pm 0.9 \times 10^{-4}$
iI-3T	80	27	3.0	1.96	1.57	0.4	$4.1 \pm 0.4 \times 10^{-3}$	n/a
di-iI-T	55	17	3.2	1.99	1.60	0.5	$1.6 \pm 0.2 \times 10^{-3}$	$1.3 \pm 0.5 \times 10^{-3}$
di-iI-3T	51	21	2.4	1.83	1.54	0.3	$9 \pm 4 \times 10^{-4}$	$2.3 \pm 0.3 \times 10^{-3}$
bis-iI-T	52	20	2.6	1.86	1.30	0.6	$1.5 \pm 0.1 \times 10^{-3}$	$1.7 \pm 0.6 \times 10^{-3}$
bis-iI-3T	69	25	2.8	1.69	1.31	0.4	$2.6 \pm 0.3 \times 10^{-3}$	$6 \pm 1 \times 10^{-4}$

[a] $E_{g,elec} = E_{LUMO} - E_{HOMO}$.

5.3.2 UV/vis spectroscopy, DFT calculations, and voltammetry

Increasing the number of acceptors in the polymer repeat unit was expected to lower the LUMO energy of the resulting semiconductors; this lower LUMO energy should result in a lower $E_{g,opt}$ for **di-iI** and **bis-iI**-based polymers than for their **iI** counterparts. However, the UV/vis spectra of thin films of the polymers (Figure 5.1) show that the **iI** and **di-iI** polymers have similar $E_{g,opt}$, while only the **bis-iI** polymers exhibit the expected red shift in absorbance (Table 5.1).

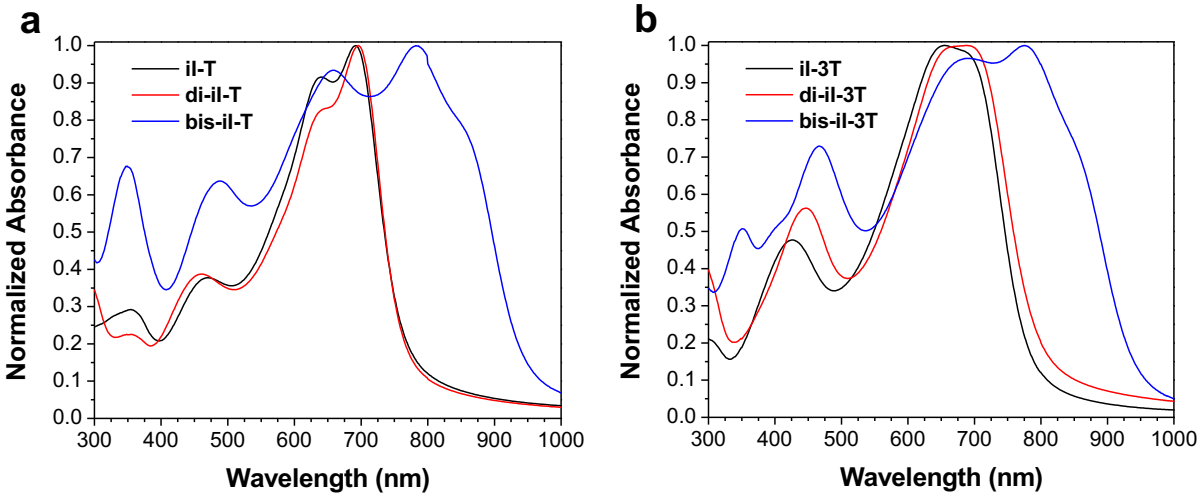

Figure 5.1 Thin film UV/vis spectra of (a) **iI-T**, **di-iI-T**, and **bis-iI-T** and (b) **iI-3T**, **di-iI-3T**, and **bis-iI-3T**.

The low band gap of the **bis-iI** polymers is due to the coplanar nature of the two isoindigo units in this dimer (Figure 5.2). When there is free rotation between the acceptor units, as in the **di-iI**-containing polymers, the UV/vis spectra are much more similar to the **iI**-based polymers. This is likely due to steric repulsion causing a large dihedral angle between the isoindigo units of **di-iI**; this twisting lowers the degree of conjugation between the adjacent isoindigo units, diminishing the effect of having two acceptors in the polymer repeat unit. This is especially clear in the spectra of **iI-T** and **di-iI-T**; in this case the $E_{g,opt}$ of **di-iI-T** is only red shifted by 5 nm

relative to **iI-T**. While the red shift is slightly more pronounced between **iI-3T** and **di-iI-3T**, the $E_{g,opt}$ of **di-iI-3T** is still much larger than that of the more coplanar **bis-iI-3T**.

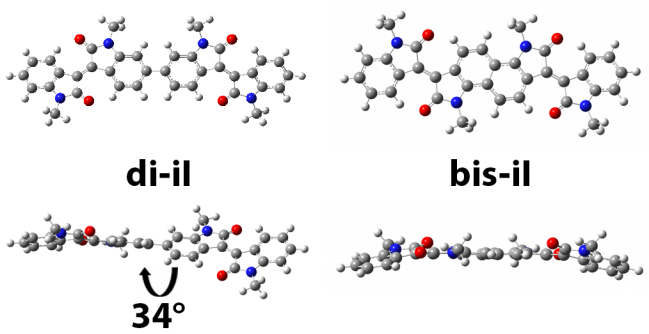

Figure 5.2 DFT optimized geometries of **di-iI** and **bis-iI**.

DFT calculations were performed on **di-iI** and **bis-iI** to determine optimized geometries, frontier MO isosurfaces, and orbital energies. The optimized geometry of **di-iI** exhibits the expected large dihedral angle (34°) between the isoindigo groups (Figure 5.2). This supports the theory that backbone twisting was responsible for the relatively small change in $E_{g,opt}$ of the **di-iI** polymers compared to the **iI** analogues; the enforced planarity in **bis-iI** results in a flatter structure (Figure 5.2). Additionally, optimized geometries, frontier MO isosurfaces, and orbital energies of oligomers of **iI**, **di-iI** and **bis-iI** with thiophene and terthiophene were calculated to approximate the results expected in the longer repeating polymers. In all three thiophene copolymers the frontier molecular orbitals are delocalized across the entire repeat unit (Figure 5.3-5.5); however, the effects of increasing acceptor length can be seen more clearly in the frontier orbitals of terthiophene copolymers (Figure 5.6-5.8). In the LUMO of **iI-3T**, there is still significant electron density on the central terthiophene; in the LUMOs of **di-iI-3T** and **bis-iI-3T**, there is almost no

electron density remaining on the terthiophene unit, as the increased acceptor strength of the **di-iI** and **bis-iI** units results in less orbital mixing.

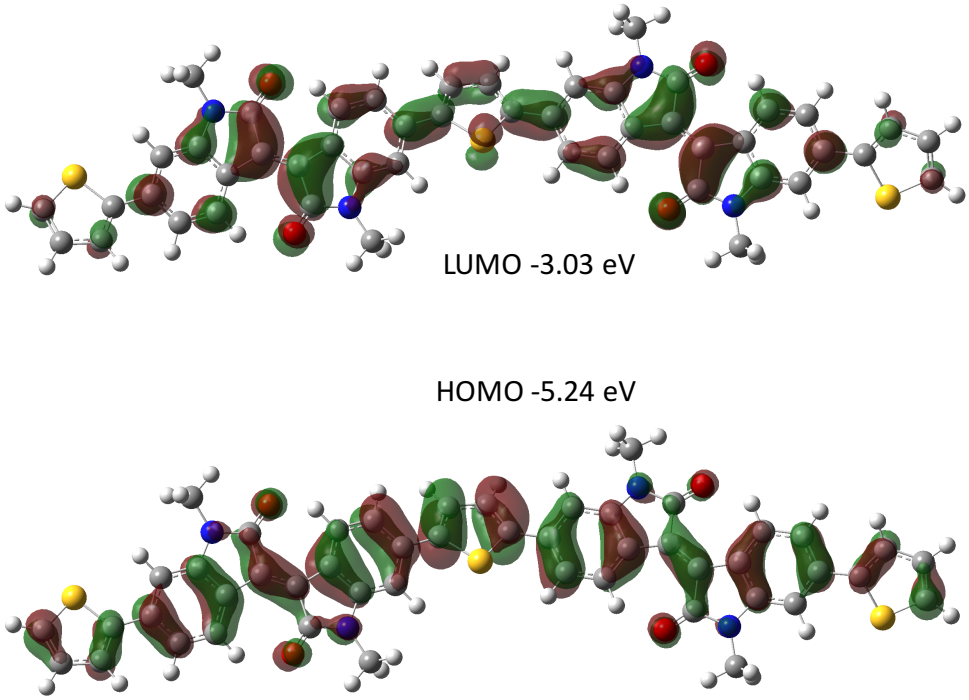

Figure 5.3 HOMO and LUMO isosurfaces and calculated orbital energies of **iI-T**.

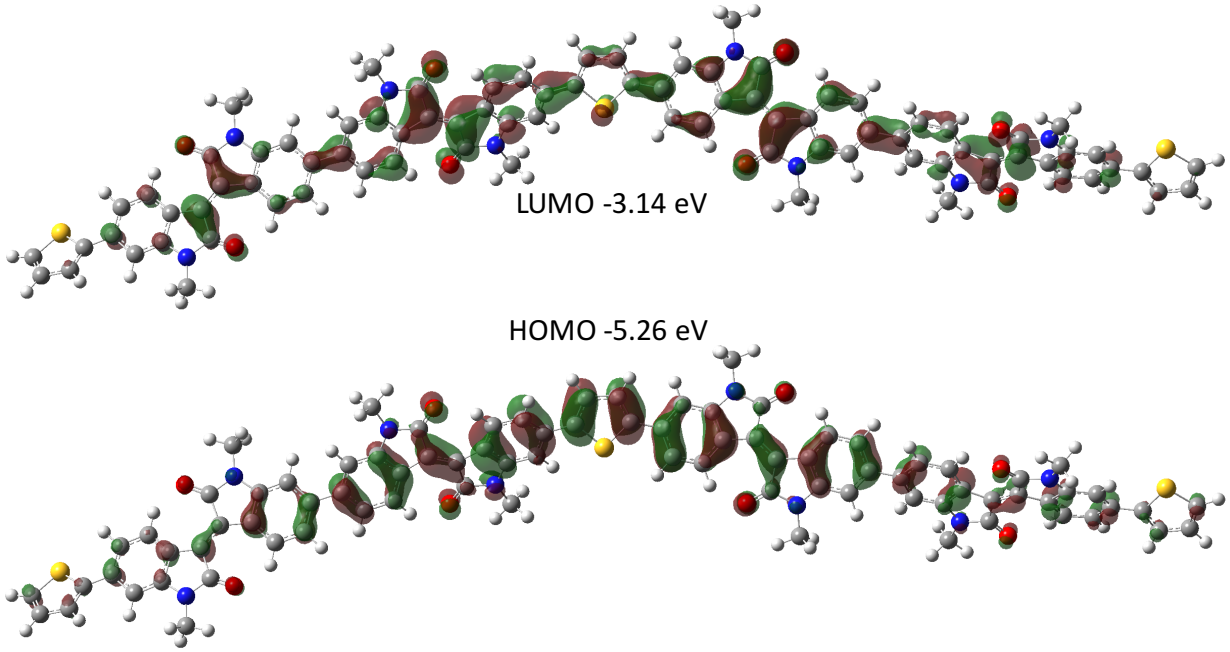

Figure 5.4 HOMO and LUMO isosurfaces and calculated orbital energies of **di-iI-T**.

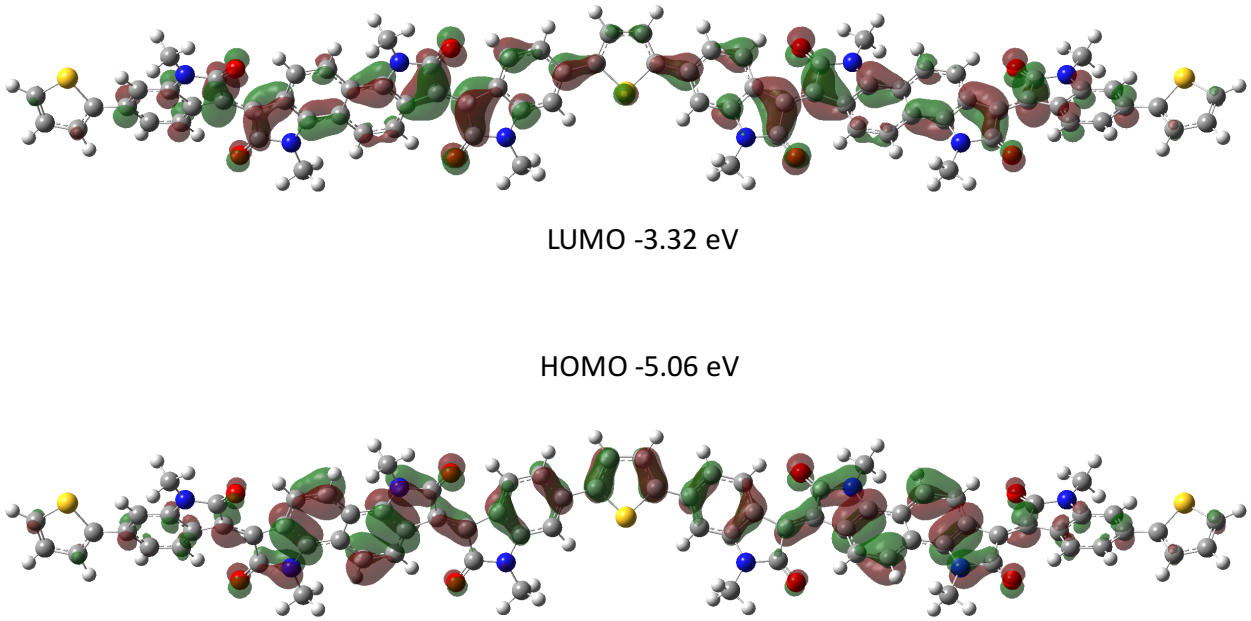

Figure 5.5 HOMO and LUMO isosurfaces and calculated orbital energies of **bis-iI-T**.

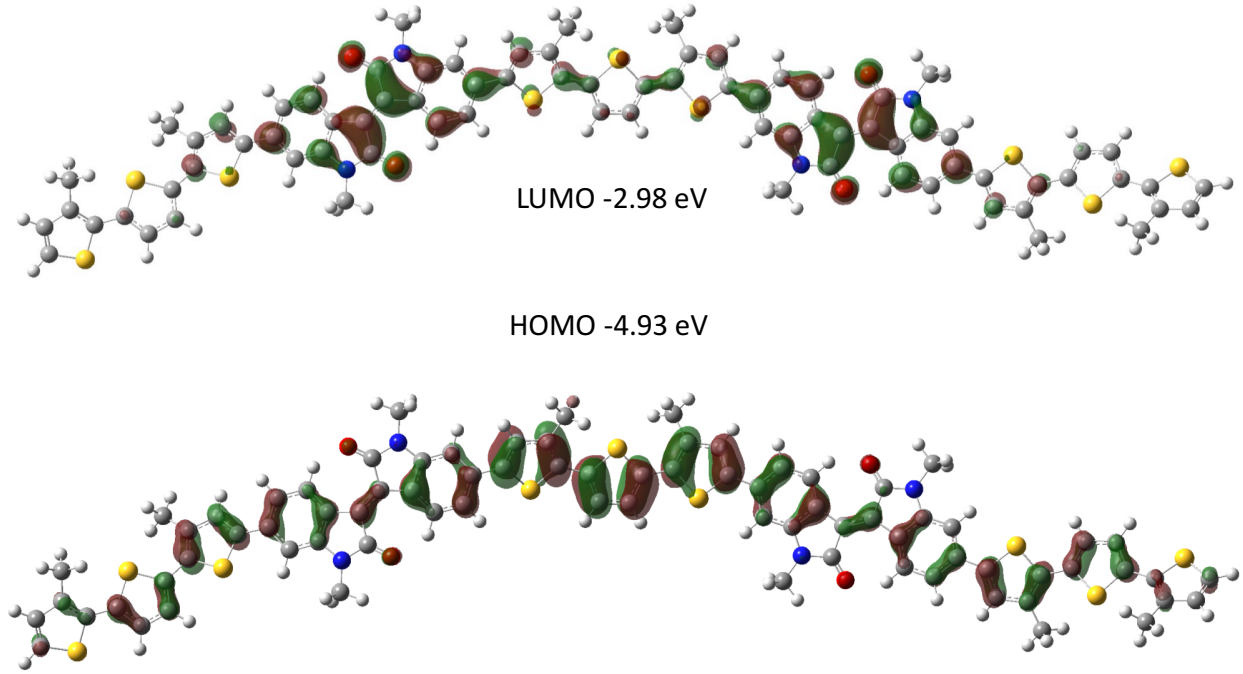

Figure 5.6 HOMO and LUMO isosurfaces and calculated orbital energies of **iI-3T**.

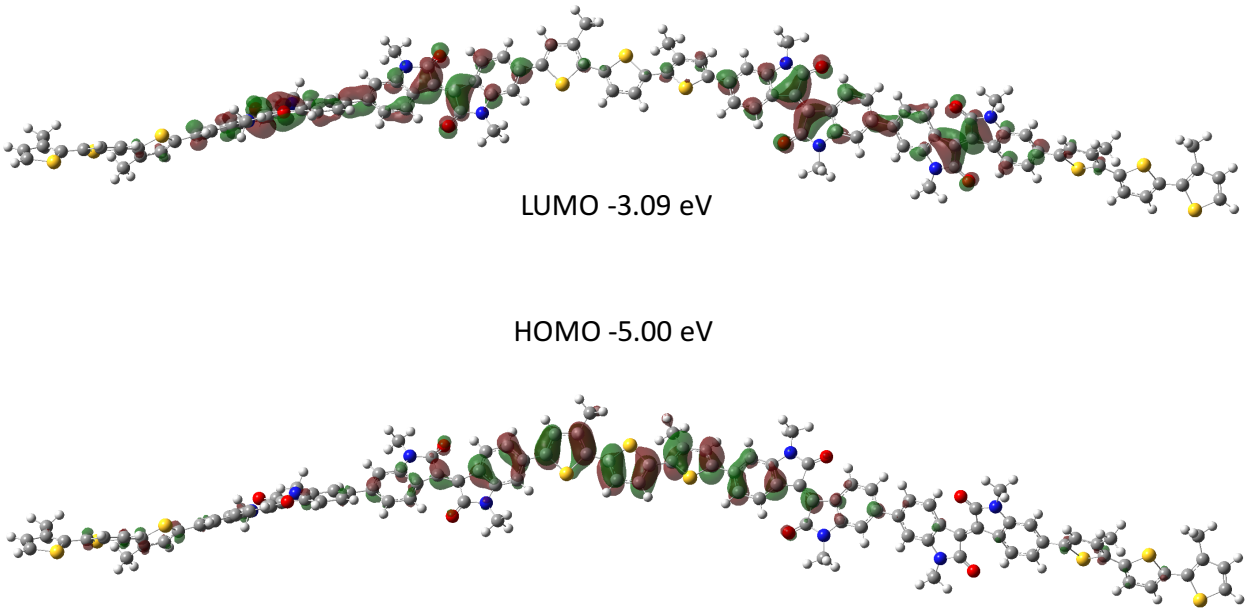

Figure 5.7 HOMO and LUMO isosurfaces and calculated orbital energies of **di-iI-3T**.

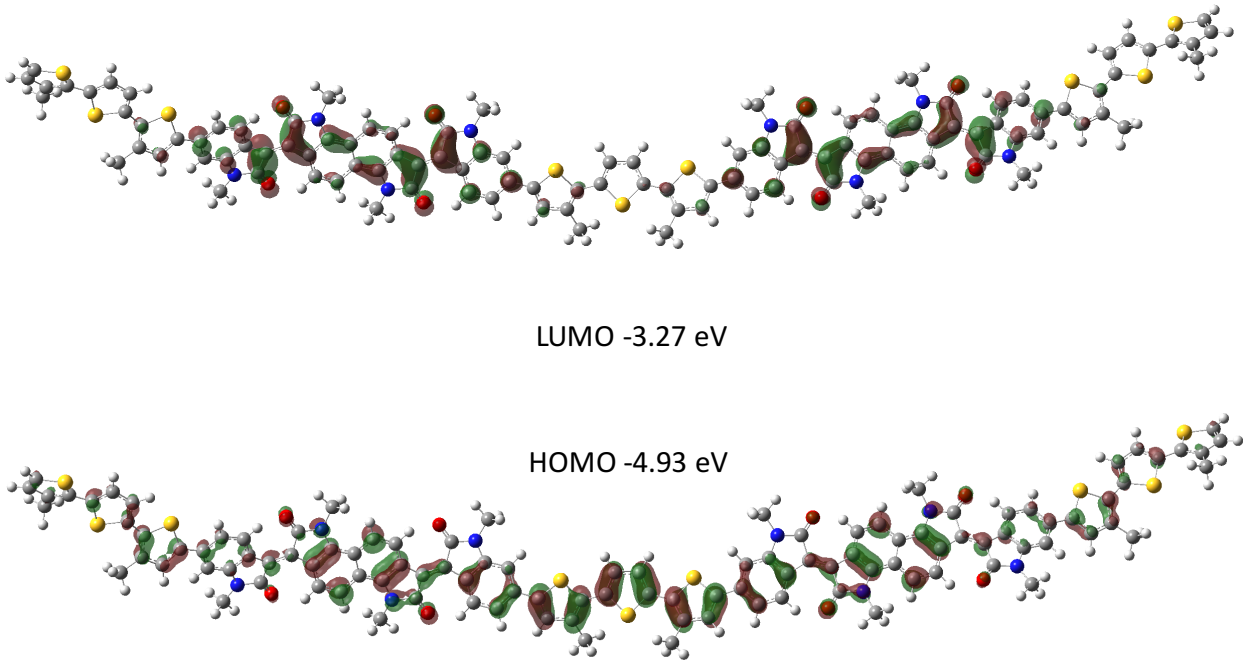

Figure 5.8 HOMO and LUMO isosurfaces and calculated orbital energies of **bis-iI-3T**.

Cyclic voltammetry was used to study the electrochemical behavior of the polymers and estimate their frontier orbital energies. The oxidation of the polymers is largely governed by the identity of the donor unit (Figure 5.9 and 5.10). All six polymers exhibit irreversible oxidation; this process happens at a lower potential vs Fc/Fc^{+} for the polymers containing terthiophene than those containing the weaker thiophene donor group. The decrease in oxidation potential is consistent with observations of **iI-T** and **iI-3T** from other research groups.[13,17] The behavior of the polymers at negative potential is much more dependent on the identity of the acceptor unit. Both of the DA polymers exhibit a single reduction peak; for **iI-T** this peak is sharp and quasi-reversible, while in **iI-3T** it is much broader and irreversible. The DAA polymers have more complex reduction behavior; **di-iI-T** exhibits one quasi-reversible reduction, followed by two irreversible reductions at lower potentials, while **di-iI-3T** can be quasi-reversibly reduced twice. Both **bis-iI**

polymers show two peaks at negative potentials; however, only in **bis-iI-3T** were both reductions quasi-reversible.

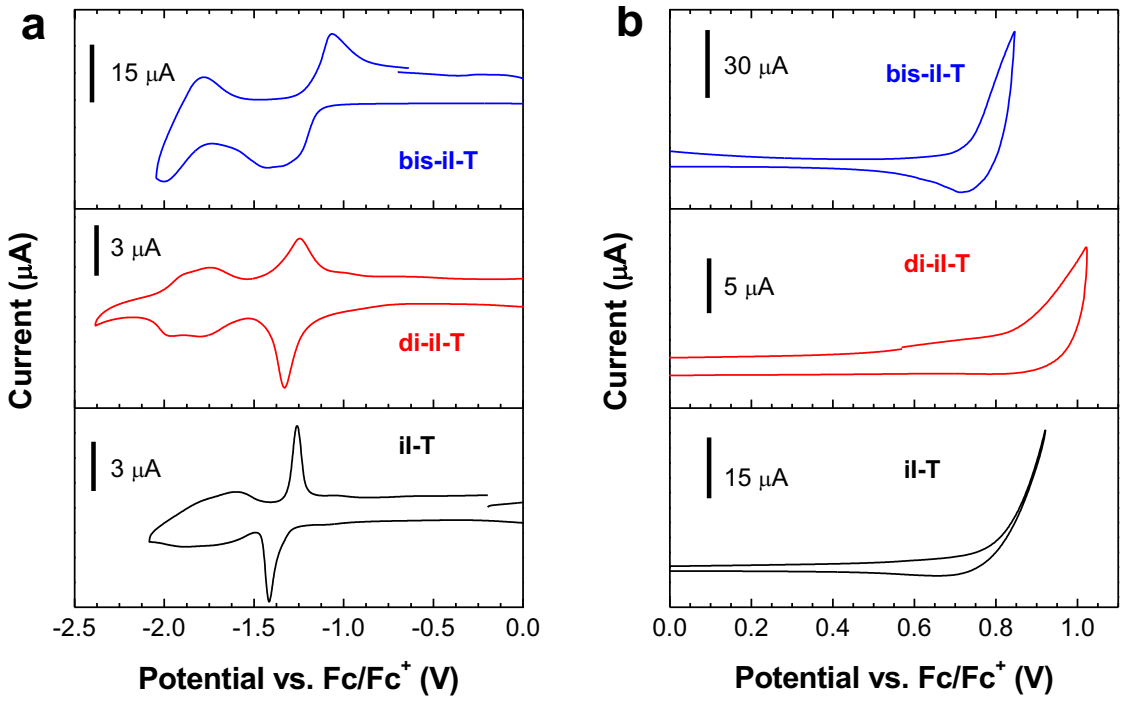

Figure 5.9 Cyclic voltammograms of **iI-T**, **di-iI-T**, and **bis-iI-T** at (a) negative potentials, and (b) positive potentials.

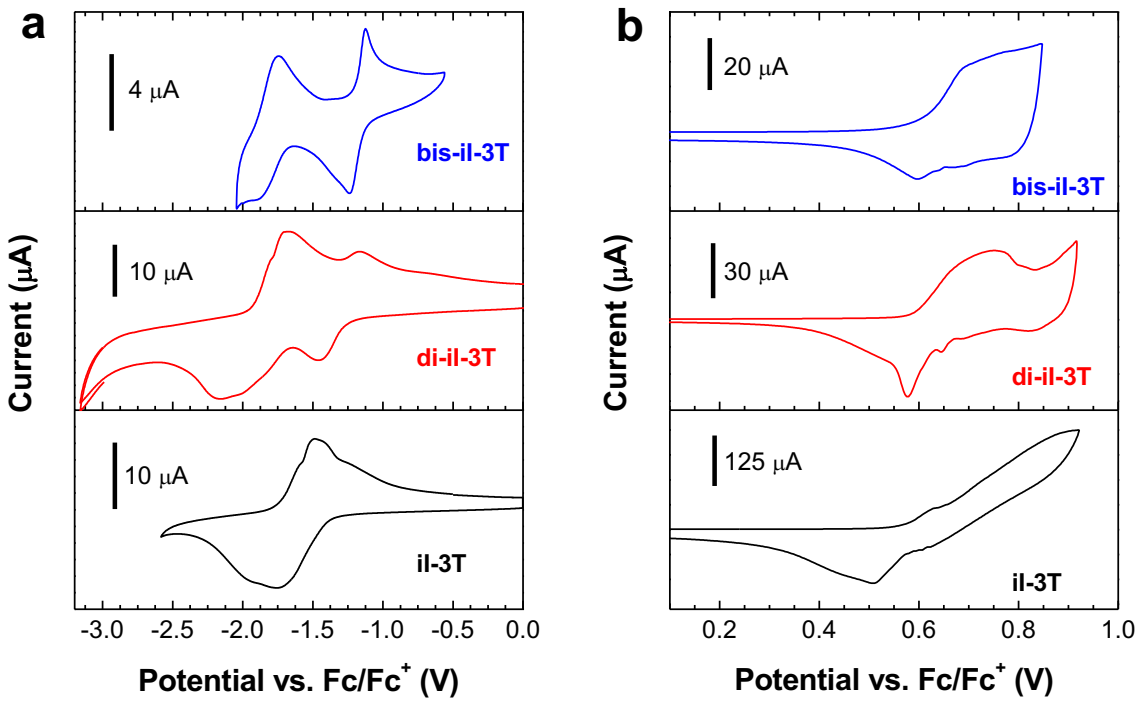

Figure 5.10 Cyclic voltammograms of **iI-3T**, **di-iI-3T**, and **bis-iI-3T** copolymers at (a) negative potentials, and (b) positive potentials.

The polymers' HOMO and LUMO energies were estimated from the onset of oxidation and reduction respectively (Figure 5.11), and the $E_{g,elec}$ are summarized in Table 5.2. The HOMO levels are largely determined by the identity of the donor unit; in general the terthiophene-containing polymers have HOMO levels approximately 0.2 eV higher in energy than the thiophene-containing polymers. The LUMO energy is much more dependent on the identity of the acceptor unit. The LUMO energies of the **di-iI** polymers are slightly lower than those of the **iI** polymers due to the electron withdrawing influence of the additional acceptor unit. The decrease in LUMO energy upon addition of a second acceptor is 0.05 eV for the thiophene copolymers (**iI-T** to **di-iI-T)** and 0.14 eV for the terthiophene copolymers (**iI-3T** to **di-iI-3T)**. In both the thiophene and terthiophene cases, this is a smaller change than was observed for increasing the number of donor units, and may reflect the lack of effective conjugation through the two acceptor units. The

coplanar **bis-iI** is the strongest acceptor unit of the three; this lowers the LUMO energy of **bis-iI-T** and **bis-iI-3T** below that of either the **iI** or **di-iI** polymers. These low LUMO levels contribute to the low $E_{g,opt}$ of the **bis-iI** polymers, which is important in creating OPVs that efficiently harvest near-infrared light.

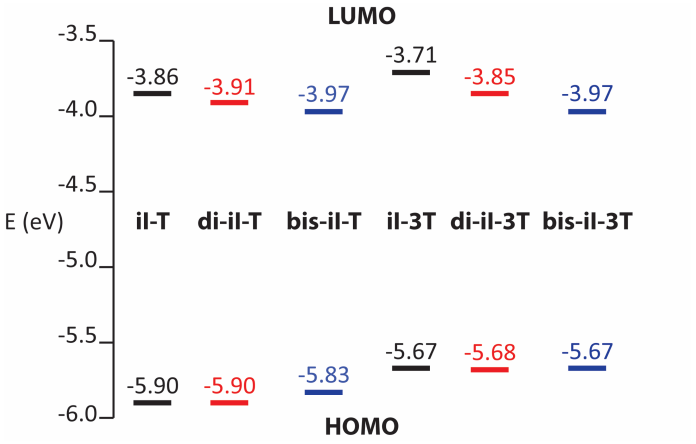

Figure 5.11 HOMO and LUMO energies of polymers *vs.* vacuum as estimated from the onset of oxidation and reduction in cyclic voltammetry; Fc/Fc^{+} was estimated at -5.1 eV *vs.* vacuum.

The difference between the $E_{g,elec}$ and the $E_{g,opt}$ is an estimate of the exciton binding energy (E_{bind}); this is the energy required to split an exciton into free charge carriers.[47] Polymers with a high E_{bind} require a larger LUMO-LUMO offset between p-type and n-type semiconductors to facilitate efficient exciton splitting. The E_{bind} of the DA polymers **iI-T** and **iI-3T** is approximately the same (0.4 eV); conversely, the DAA polymers **di-iI-3T** (0.3 eV) and **bis-iI-3T** (0.4 eV) have lower E_{bind} than **di-iI-T** (0.5 eV) and **bis-iI-T** (0.6 eV). The difference between the E_{bind} in the thiophene and terthiophene DAA copolymers may be due to their greater degree of orbital localization compared to the DA copolymers. Of note, **bis-iI-T** has an E_{bind} of 0.6 eV; the low LUMO energy and large E_{bind} of this polymer suggest that a n-type semiconductor with a very low LUMO energy would be required for efficient exciton dissociation.

5.3.3 OTFT performance and charge carrier mobilities

To test the effect of the additional acceptor units on the charge carrier mobilities of the DAA semiconductors, the polymers were used as the active material in bottom-gate bottom-contact OTFTs; Figure 5.12 compares the average charge carrier mobilities of the six polymers. With the exception of **iI-3T** (which is already known to be a p-type semiconductor),[15] the polymers demonstrated ambipolar charge transport behavior (Table 5.1). In all cases the DAA polymers exhibited improved electron mobilities over the DA analogues. This result demonstrates that the μ_e of a DA polymer can be systematically tuned by inserting additional acceptor units into the polymer repeat unit. In addition to improved electron transport, both **di-iI-T** and **bis-iI-T** also exhibited better hole mobility than **iI-T**; this improvement may be due to changes in the polymer packing induced by the presence of the extended isoindigo units. Of all six polymers, **iI-3T** showed the highest hole mobility ($4.1 \pm 0.4 \times 10^{-3}$ cm^2 V^{-1} s^{-1}); this is unsurprising given that it also has the highest HOMO level of all six polymers. The charge carrier mobility of **bis-iI-T** is similar to that reported by Jiang *et al.*; the small difference is likely due to changes in interchain packing resulting from the different alkyl substituent used. The polymer with the highest electron mobility ($2.3 \pm 0.3 \times 10^{-3}$ cm^2 V^{-1} s^{-1}) was **di-iI-3T**; the output and transfer curves of OTFTs fabricated using all six polymers are shown in Figures 5.13-5.18.

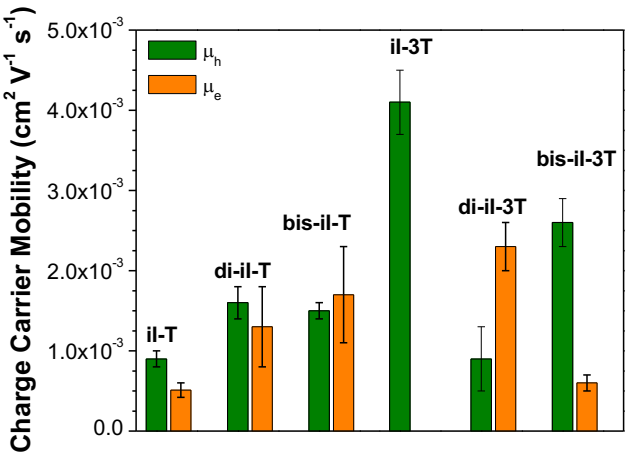

Figure 5.12 Average charge carrier mobilities of the polymers as measured using bottom-gate bottom-contact OTFTs. Error bars = ± 1σ.

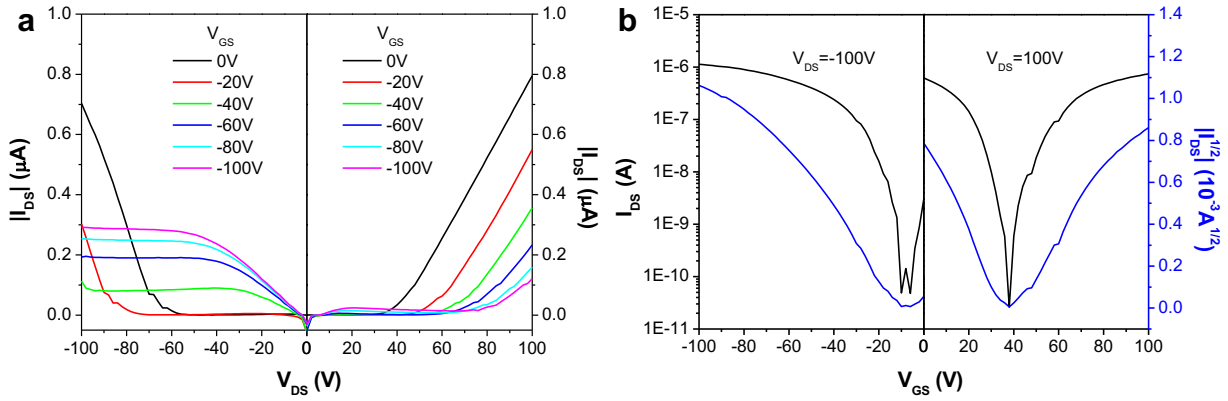

Figure 5.13 (a) Output and (b) transfer curves of bottom-gate bottom-contact OTFTs using **di-iI-3T**, annealed at 50 °C.

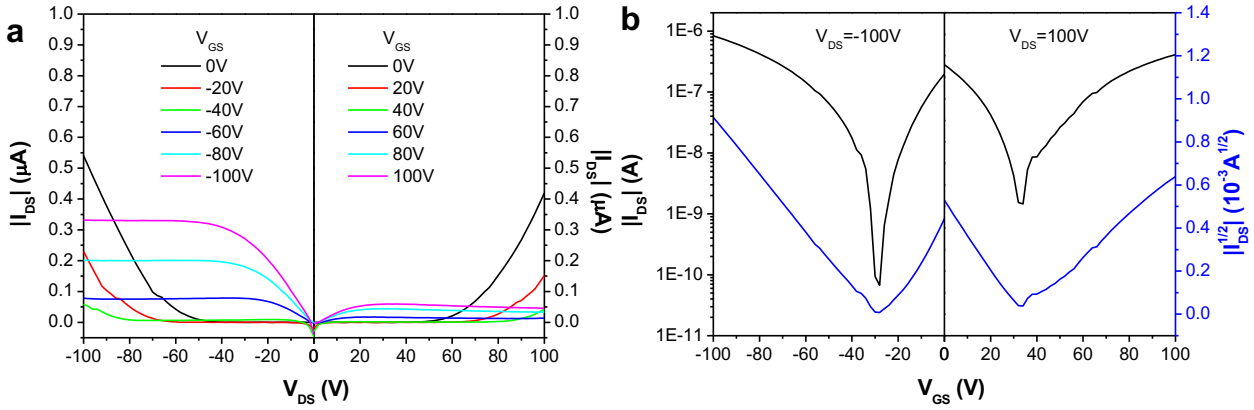

Figure 5.14 (a) Output and (b) transfer curves of bottom-gate bottom-contact OTFTs using **iI-T**, annealed at 100 °C.

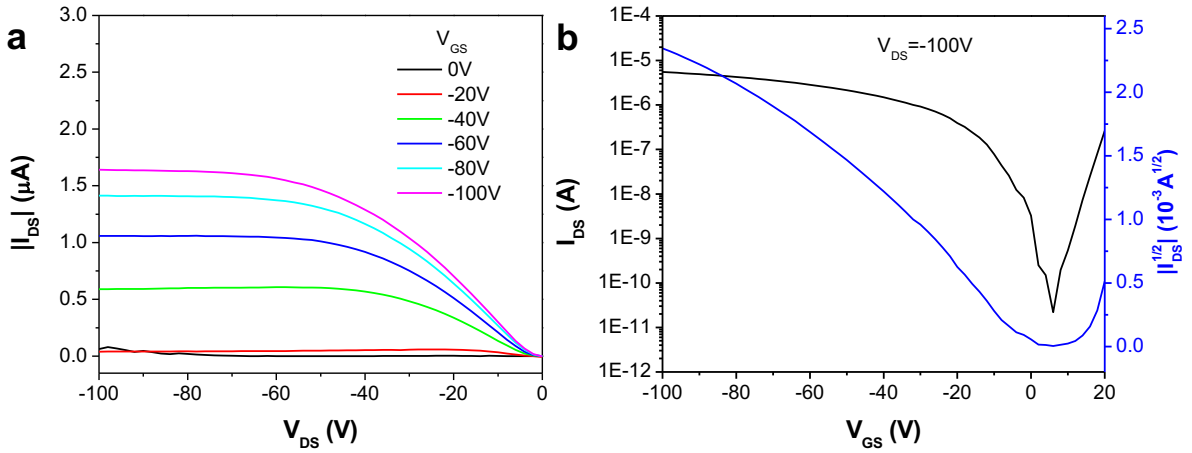

Figure 5.15 (a) Output and (b) transfer curves of bottom-gate bottom-contact OTFTs using **iI-3T**, annealed at 50 °C.

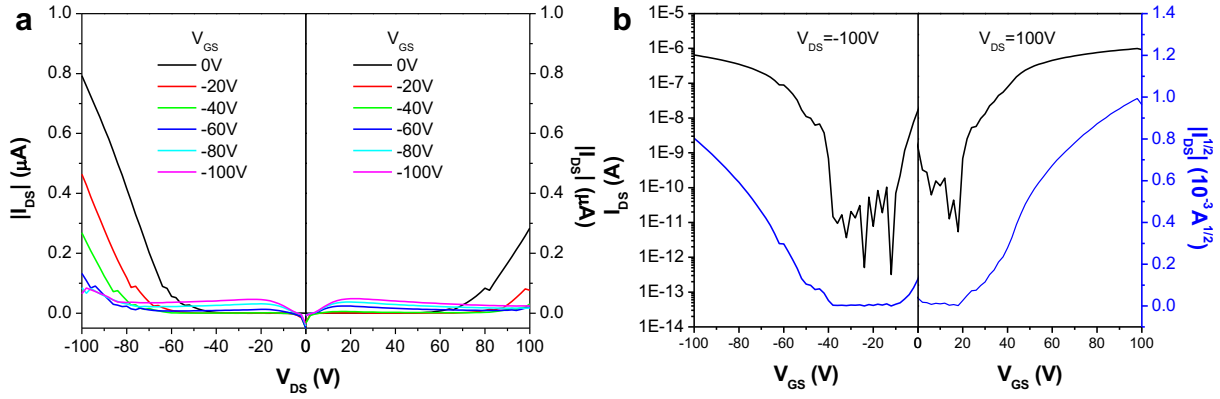

Figure 5.16 (a) Output and (b) transfer curves of bottom-gate bottom-contact OTFTs using **di-iI-T**, annealed at 50 °C.

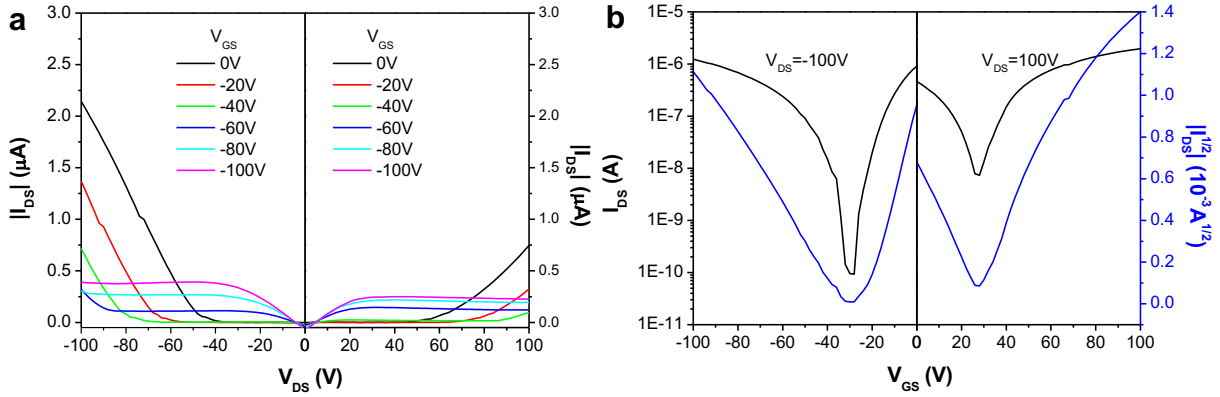

Figure 5.17 (a) Output and (b) transfer curves of bottom-gate bottom-contact OTFTs using **bis-iI-T**, annealed at 50 °C.

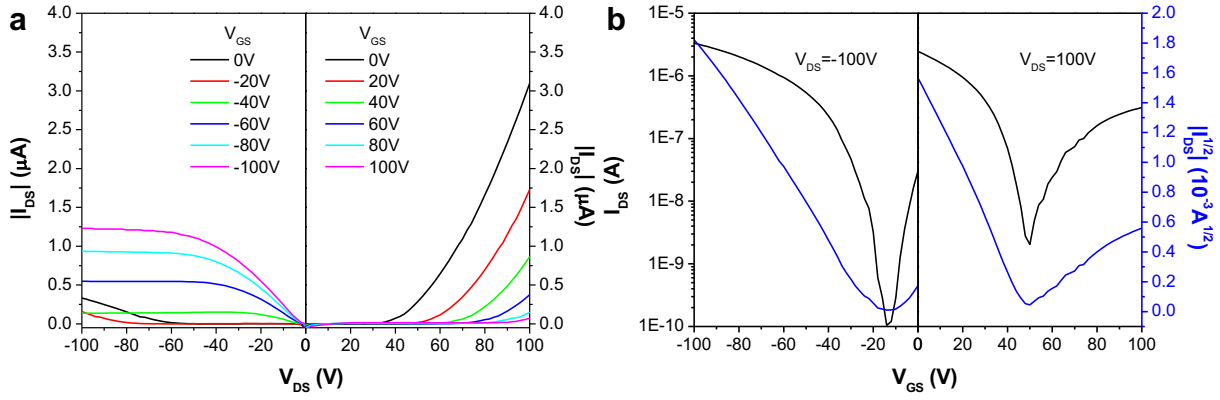

Figure 5.18 (a) Output and (b) transfer curves of bottom-gate bottom-contact OTFTs using **bis-iI-3T**, annealed at 50 °C.

5.3.4 OPV performance of DA and DAA copolymers

The solar cell performance of the polymers was evaluated by incorporating them into OPVs as the p-type semiconductor in a BHJ active layer with $PC_{71}BM$. The results are summarized in Table 5.2, and *J-V* curves of the best devices for each polymer are shown in Figure 5.19. Both **iI-T** and **iI-3T** have been used in OPVs before and are well studied. The performance of the **iI-T**:$PC_{71}BM$ OPVs is consistent with published results; however, the average PCE of the **iI-3T**:$PC_{71}BM$ based devices reported here (4.2 ± 0.3%) is slightly lower than that reported by others (6.5 ± 0.2%).[17] This is likely due to the relatively low molecular weight of the **iI-3T** used in this work (M_n 27 kDa); previous studies by Ma *et al*. found an improvement from 6.3%-6.9% in maximum PCE of **iI-3T**-based OPVs when M_n improved from 43 kDa to 100 kDa.[13] The molecular weight dependence of the PCE may be amplified for the lower molecular weight polymers.

Di-iI and **bis-iI**-based polymers have not been previously used in OPVs; in this work, they have been used as the p-type semiconductor in OPV active layers with $PC_{71}BM$, and compared the results to those of **iI** polymers. The V_{OC} and *FF* are similar for all polymers that have the same donor unit. In all cases the V_{OC} decreases when the donor unit changes from thiophene to terthiophene, due to the increased HOMO energy; this decrease in V_{OC} is offset by an increase in the *FF* and J_{SC}. The largest difference in performance between the **iI**-based DA polymers and the **di-iI** and **bis-iI** DAA polymers is a decrease in J_{SC}. Both **di-iI-T** and **di-iI-3T** have lower PCEs than the isoindigo analogues, owing chiefly to lower J_{SC}; the **bis-iI** polymers had the lowest PCE due to very low J_{SC}.

Table 5.2 Performance of BHJ OPVs with ITO/ZnO/Polymer:$PC_{71}BM$/MoO_x/Ag architecture. Numbers in brackets represent the best performing device. Average calculated using a minimum of 17 devices.

Polymer	V_{OC} (V)	J_{SC} (mA cm^{-2})	Fill Factor (%)	PCE (%)	J_{SC} [a] (mA cm^{-2})
iI-T	0.85 ± 0.02 (0.87)	6.3 ± 0.2 (6.51)	58 ± 1 (58)	3.1 ± 0.1 (3.28)	6.10
iI-3T	0.72 ± 0.01 (0.72)	8.7 ± 0.5 (9.78)	66.8 ± 0.6 (67)	4.2 ± 0.3 (4.73)	9.47
di-iI-T	0.86 ± 0.03 (0.91)	4.2 ± 0.1 (4.55)	50 ± 3 (51)	1.8 ± 0.2 (2.12)	4.68
di-iI-3T	0.77 ± 0.01 (0.79)	5.9 ± 0.3 (6.54)	61 ± 2 (58)	2.8 ± 0.1 (3.04)	6.58
bis-iI-T	0.8 ± 0.1 (0.78)	0.8 ± 0.1 (0.89)	54 ± 8 (59)	0.3 ± 0.1 (0.42)	0.82
bis-iI-3T	0.66 ± 0.01 (0.66)	2.4 ± 0.2 (2.61)	58 ± 4 (62)	0.9 ±0.1 (1.07)	2.29

[a] J_{SC} calculated from the IPCE spectrum of the best device.

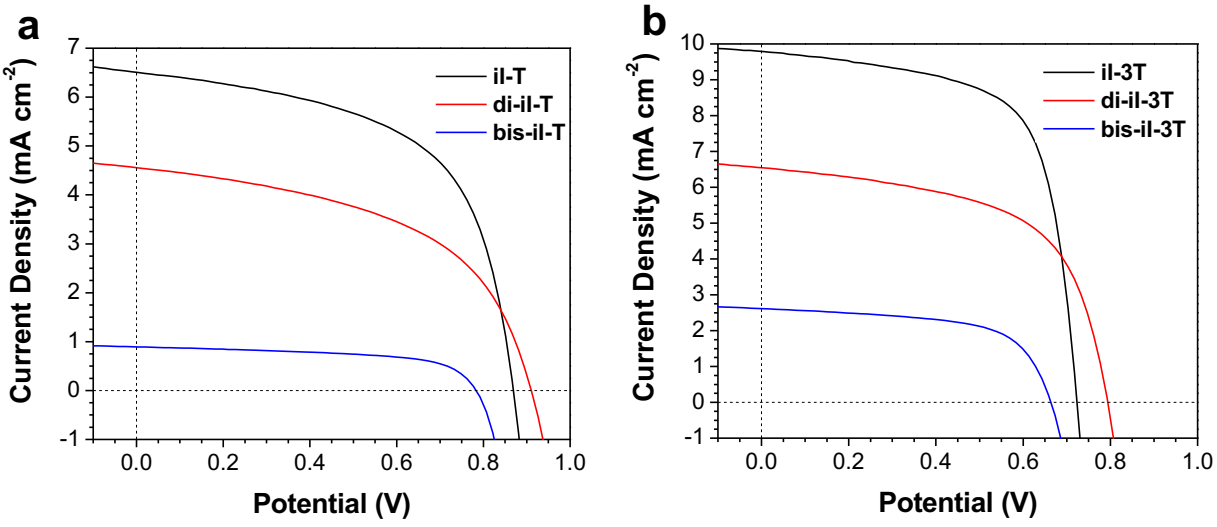

Figure 5.19 *J-V* curves of highest performing BHJ OPVs with ITO/ZnO/polymer:$PC_{71}BM$/MoO_x/Ag architecture. (a) **iI-T**, **di-iI-T**, and **bis-iI-T** and (b) **iI-3T, di-iI-3T**, and **bis-iI-3T**.

Two factors could cause the lower J_{SC} in the **di-iI** and **bis-iI**-based polymers relative to their **iI** counterparts: low charge carrier mobility, or inefficient exciton dissociation. The difference between the hole mobilites of **di-iI-3T** and **bis-iI-3T** compared to **iI-3T** is relatively small and unlikely to account for the difference in J_{SC}. In fact, the hole mobilities of **di-iI-T** and **bis-iI-T** were slightly higher than **iI-T**, but their OPV performance was worse. This makes it likely that poor charge carrier mobility is not the reason for the diminished performance of the DAA polymers.

The other possibility is that inefficient exciton dissociation in the OPV active layer resulted in a lack of free charge carriers, causing a low J_{SC}. This can be caused either by poor exciton diffusion to the p/n semiconductor junction, or by poor rates of dissociation once the exciton has reached this interface. Exciton diffusion length in organic semiconductors is typically ~10 nm; therefore, the domain size in a BHJ must be on a similar length scale for efficient exciton seperation.[48] Changes in active layer morphology caused by the **di-iI** and **bis-iI** units could cause decreases in J_{SC}.

AFM and GIWAXS were used to assess the morphology and crystallinity of the OPV active layers. AFM was used to investigate the morphology of the polymer:$PC_{71}BM$ OPV active layers; 1 μm × 1 μm height images were recorded of the active layer, and the R_q was calculated (Figure 5.20). The morphologies of the **iI-T**:$PC_{71}BM$ and **iI-3T**:$PC_{71}BM$ active layers were similar to those reported by others.[17] With the exception of **bis-iI-T** (Figure 5.20c), all of the active layers had roughness values between 3 and 9 nm, and featured similar domain sizes. The R_q of the **bis-iI-T**:$PC_{71}BM$ active layer (23 nm) is much higher than the others; this is a possible explanation as to why these devices performed worse than those fabricated with the other polymers. However, while both **bis-iI-T** and **bis-iI-3T** exhibited poor photovoltaic performance, only **bis-iI-T** had any

noticeable difference in film morphology. Additionally, the domain sizes of the **di-iI** polymers were similar to those of the **iI** polymers, while their OPV performance was worse. Therefore, it is unlikely that changes in active layer morphology between the DA and DAA polymers are the sole cause of the decrease in OPV efficiency.

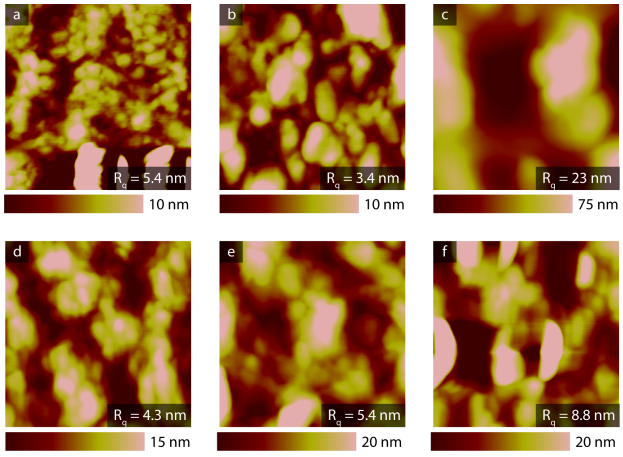

Figure 5.20 1 × 1 μm AFM height images of polymer:$PC_{71}BM$ OPV active layer blends. (a) **iI-T,** (b) **di-iI-T**, (c) **bis-iI-T,** (d) **iI-3T**, (e) **di-iI-3T**, and (f) **bis-iI-3T**.

The crystallinity of the polymers in pristine thin films as well as in thin film blends with $PC_{71}BM$ was evaluated by GIWAXS (Figure 5.21-5.23). GIWAXS patterns of **iI-T** and **iI-3T** have previously been reported by Grand *et al*.; the principal peaks at 0.3 $Å^{-1}$ and 1.6 $Å^{-1}$ were assigned to the (100) and (010) reflections respectively.[15,17] The (100) and (010) planes represent the interchain lamellar packing, and π stacking interactions. The GIWAXS patterns of all six polymers in this study were found to be similar to those previously reported for **iI-T** and **iI-3T**. With the exception of **iI-3T**, the polymers show preferential face-on orientation to the surface (in both the as-cast (Figure 5.21) and annealed (Figure 5.22) films), as evidenced by the greater intensity of the (010) peak along the q_z axis and the (100) peak along the q_r axis. Conversely, **iI-3T** appears to

exhibit edge-on orientation with a (100) maximum along the q_z axis; unfortunately, the (010) signal along the q_r axis was obscured by shadowing from the sample stage. The d-spacing of the (100) and (010) planes has been reported to be approximately 20-22 Å for the lamellar packing (100) and 3.7-3.8 Å for the π stacking (010) in **iI-T** and **iI-3T**;[17] this is similar to the d-spacing distance found for **di-iI-3T** and **bis-iI-3T** (Table 5.3). However, **di-iI-T** and **bis-iI-T** both had a π-stacking distance of 4.0 Å, 0.2 Å longer than **iI-T**. The increased π-π distance for **di-iI-T** and **bis-iI-T** may be due to the difference in the relative size of the donor and acceptor units. The GIWAXS patterns of the OPV active layer blends are shown in Figure 5.23; in addition to the (100) plane for each polymer, an isotropic peak attributed to $PC_{71}BM$ is seen at ~1.3 $Å^{-1}$.[49] The similarity of the patterns for all six blends suggests that there are no drastic differences in the crystallinity of the films which can account for the variation in OPV performance.

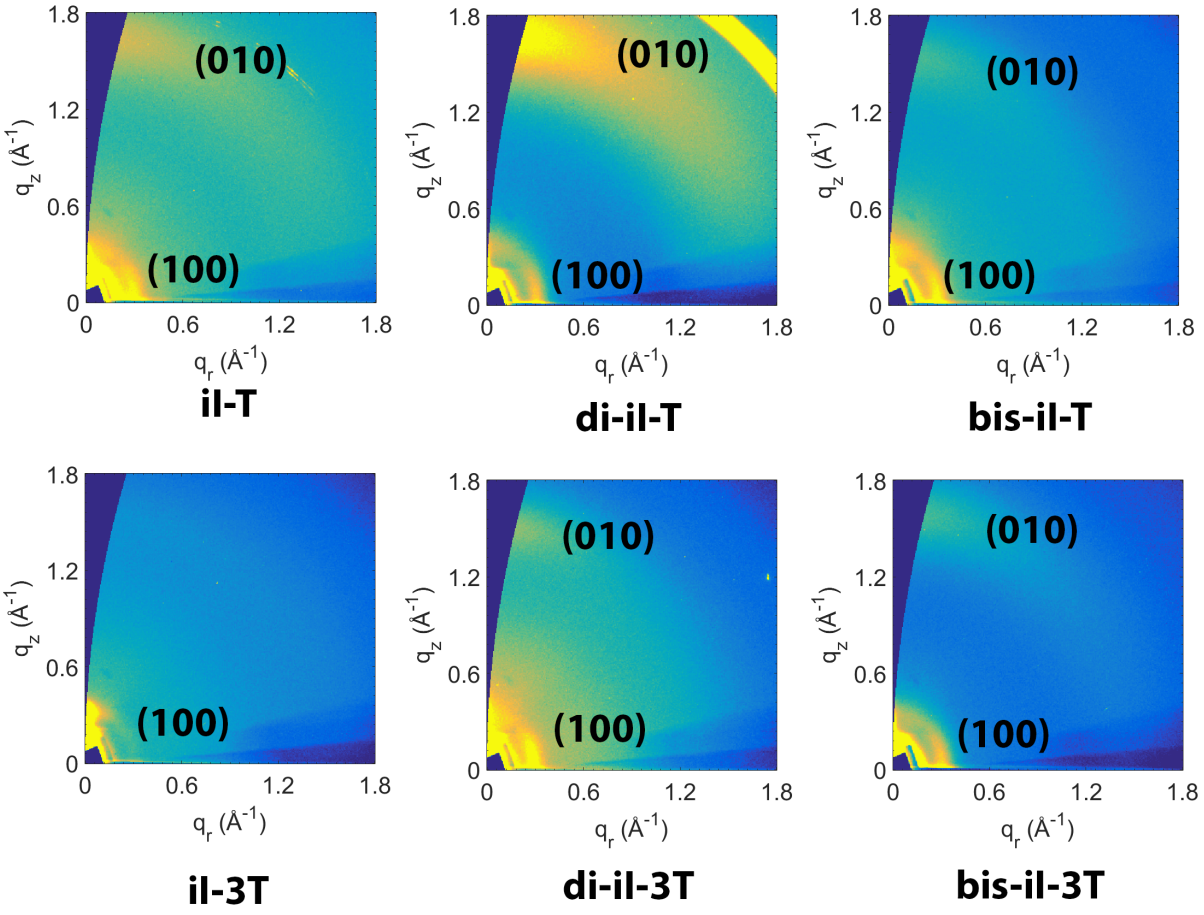

Figure 5.21 GIWAXS patterns of as-cast polymer thin films on ZnO/glass substrates.

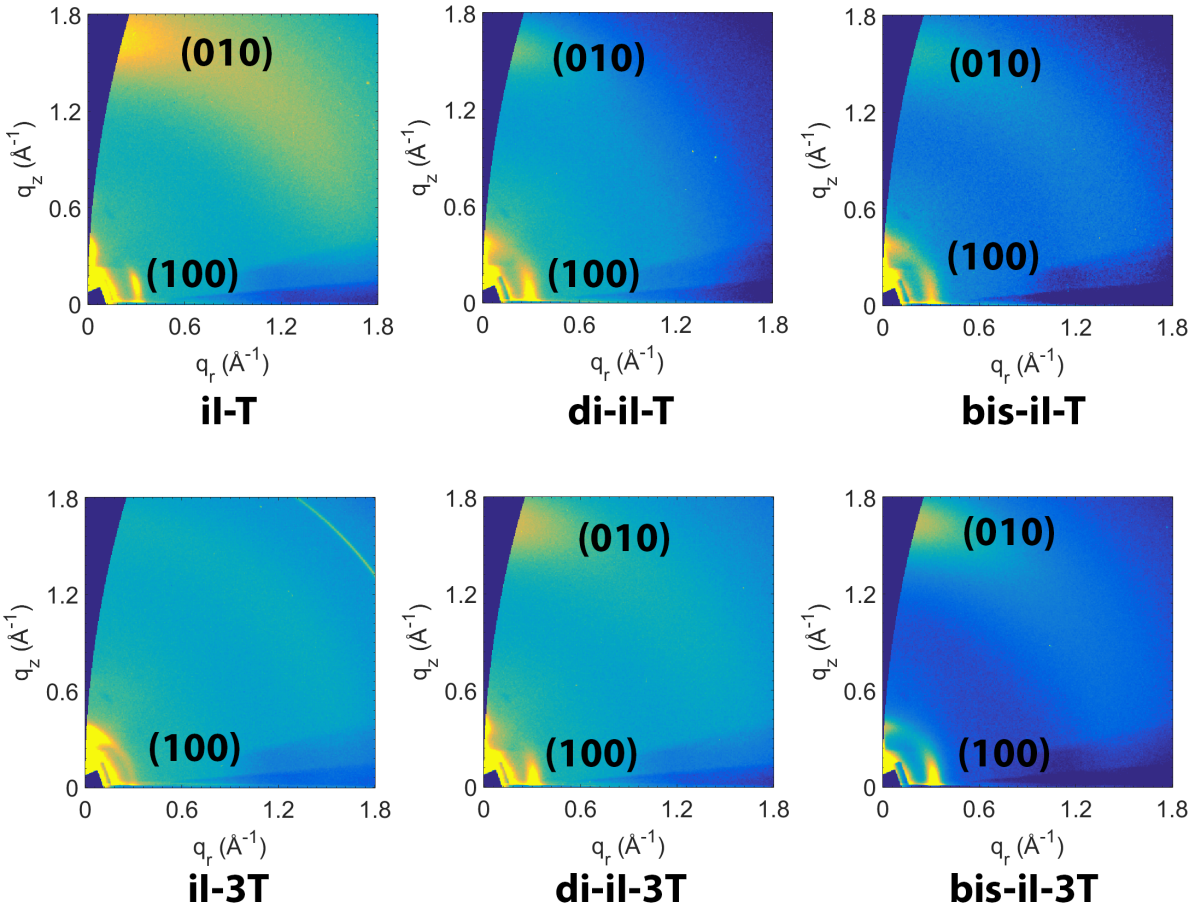

Figure 5.22 GIWAXS patterns of polymer films on ZnO/glass substrates, annealed at 200 °C for 30 min.

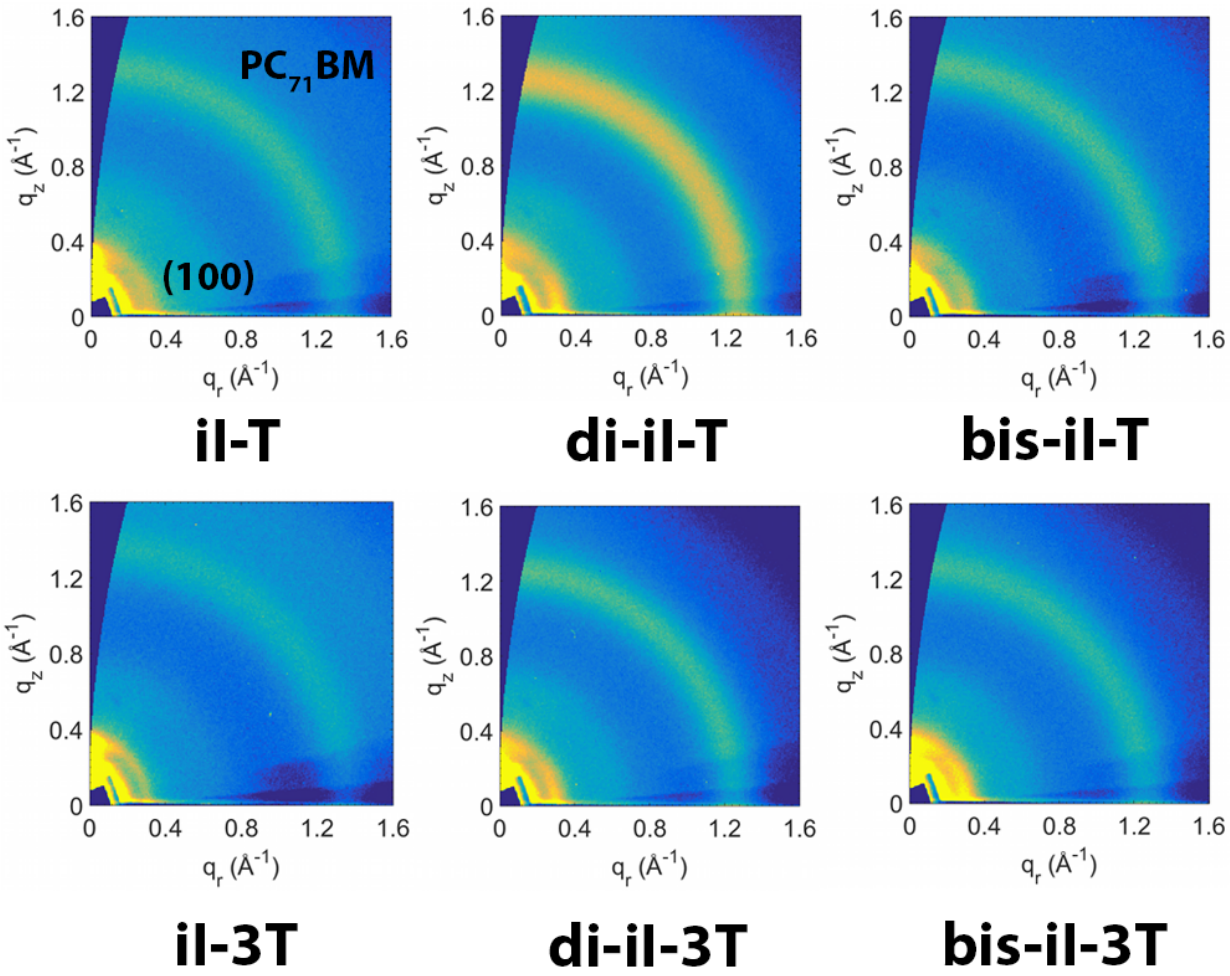

Figure 5.23 GIWAXS patterns of as-cast polymer:$PC_{71}BM$ blends (with 2.5% (v/v) DIO).

Table 5.3 d-Spacing of (100) (lamellar stacking) and (010) (π-π stacking) planes determined by GIWAXS on polymer thin films, annealed at 200 ºC for approximately 0.5 h.

Polymer	Lamellar distance (Å)	π-π distance (Å)
il-T	20	3.8
il-3T	20	3.8
di-il-T	21	4.0
di-il-3T	20	3.8
bis-il-T	21	4.0
bis-il-3T	20	3.8

Since the crystallinity and active layer morphology of the polymers are largely similar it is most likely that poor active layer morphology is not the cause of the poor OPV performance of the **di-iI** and **bis-iI** polymers. Another possible cause of the low J_{SC} is a low energetic driving force for exciton dissociation. Because excitons in organic semiconductors are relatively tightly bound, an energetic driving force must be present to promote electron transfer from the LUMO of the p-type semiconductor to that of the n-type semiconductor. From Figure 5.11, it is obvious that the polymer LUMO energies decrease from **iI**, to **di-iI**, to **bis-iI**-based polymers; this decrease in LUMO energy correlates very well with the decreasing J_{SC} of the OPVs. When designing p-type semiconductors for OPVs, the LUMO level must remain above that of the n-type semiconductor to provide an energetic driving force for electron transfer between the two. The LUMO level of $PC_{71}BM$ has been measured to be between -4.0 and -4.2 eV *vs.* vacuum.[12,50] A minimum LUMO-LUMO offset of 0.1-0.5 eV is often used as an estimate of whether efficient electron transfer will occur between two organic semiconductors.[1] Since the LUMO levels of **bis-iI-T** and **bis-iI-3T** approach -4.0 eV *vs.* vacuum, inefficient exciton dissociation is a likely cause of the low J_{SC}.

The incident photon to current efficiency (IPCE) spectra (Figure 5.24a-b) support this possibility, especially for **bis-iI-T** and **bis-iI-3T**. The IPCE spectra of OPVs based on the **iI** and **di-iI** polymers closely match the UV/vis spectra of the polymer films, and the onset of photocurrent production is at the $E_{g,opt}$ of the polymer. The IPCE spectra of OPVs made using **bis-iI-T** and **bis-iI-3T** are distinctly different; despite the $E_{g,opt}$ of these polymers being 950 nm, negligible photocurrent is produced beyond 700 nm. While these IPCE spectra do not match the UV/vis absorbance of the polymers, Figure 5.24c overlays the normalized IPCE spectrum of a **bis-iI-3T**:$PC_{71}BM$-based OPV with the normalized thin film absorbance spectrum of $PC_{71}BM$. These spectra match very well, and the onset of photocurrent production is at the HOMO-LUMO gap of

the fullerene. This implies that excitons generated in the **bis-iI** polymers are not dissociating and that the majority of photocurrent in these OPVs is generated by fullerene-based excitons. In this case, the driving force for exciton dissociation is governed not by the LUMO-LUMO offset, but by the offset of the HOMO levels of the two semiconductors. The HOMO level of $PC_{71}BM$ is approximately -6.10 eV *vs.* vacuum;[12] this is a substantial enough HOMO-HOMO offset with **bis-iI-3T** (-5.67 eV *vs.* vacuum) to provide the energetic driving force for exciton dissociation. The IPCE spectra combined with the measurements of LUMO level demonstrate that as the acceptor strength of the polymers is increased, the energetic driving force for exciton dissociation decreases. As this process becomes less energetically favorable, the J_{SC} decreases. In the extreme case of the **bis-iI** polymers, there is no longer sufficient driving force for electron transfer between the p- and n-type semiconductors, and the efficiency of the OPV decreases dramatically.

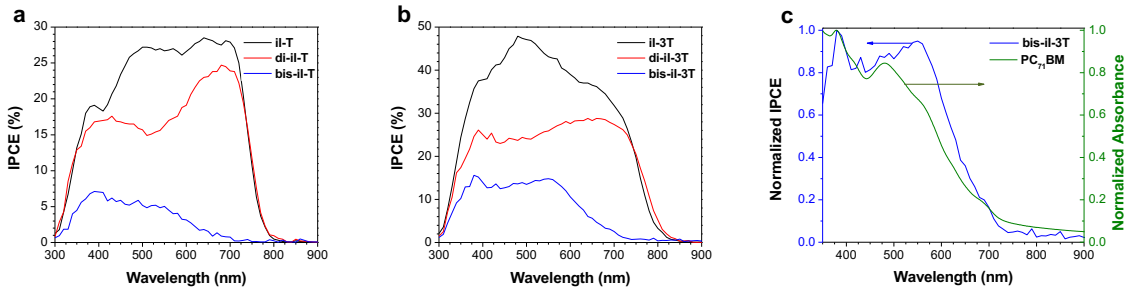

Figure 5.24 IPCE spectra of best performing polymer:$PC_{71}BM$ active layer OPVs (a) **iI-T**, **di-iI-T**, and **bis-iI-T** and (b) **iI-3T**, **di-iI-3T**, and **bis-iI-3T**. (c) Normalized IPCE spectrum of the best performing **bis-iI-3T**:$PC_{71}BM$ OPV and the normalized thin film absorbance spectrum of $PC_{71}BM$.

5.4 Conclusion

In conclusion, a series of four DAA copolymers using thiophene donor units and isoindigo dimers as the acceptor units: one with free rotation, and one with enforced planarity have been synthesized. The optoelectronic properties of these four polymers were compared to analogous, well studied, DA copolymers of isoindigo. It was found that increasing the number of acceptors in the polymer repeat unit lowered the LUMO energy of the polymer, and increased the electron mobility; this effect was amplified when the two acceptor units were fused together in a coplanar fashion. These changes can have a pronounced effect on the performance of optoelectronic devices, as illustrated here with OPVs. It is believed that increasing the number of acceptors in the polymer repeat unit is a general strategy that could be used to fine-tune the properties of donor-acceptor systems, leading to better materials with precisely-tailored frontier orbital energies or more balanced charge carrier mobilities.

5.5 Acknowledgements

The Natural Science and Engineering Research Council of Canada (NSERC) and the University of Saskatchewan are acknowledged for financial support. T.L.K. is a Canada Research Chair in Photovoltaics. This research was undertaken in part, thanks to funding from the Canada Research Chairs Program. N.M.R. and C.L.R. thank NSERC for scholarship funding. The GIWAXS experiments described in this paper were performed at the Canadian Light Source, which is supported by the Canada Foundation for Innovation, the Natural Sciences and Engineering Research Council of Canada (NSERC), the University of Saskatchewan, the Government of Saskatchewan, Western Economic Diversification Canada, the National Research Council Canada, and the Canadian Institutes of Health Research. Technical support from HXMA beamline scientist Dr. Chang-Yong Kim is gratefully acknowledged. Federico Cruciani, and Prof.

Pierre Beaujuge are gratefully acknowledged for performing the size exclusion chromatography analysis.

5.6 References

(1) Brabec, C. J.; Gowrisanker, S.; Halls, J. J. M.; Laird, D.; Jia, S.; Williams, S. P. Polymer-Fullerene Bulk-Heterojunction Solar Cells. *Adv. Mater.* **2010**, *22*, 3839–3856.

(2) Scharber, M. C.; Mühlbacher, D.; Koppe, M.; Denk, P.; Waldauf, C.; Heeger, A. J.; Brabec, C. J. Design Rules for Donors in Bulk-Heterojunction Solar Cells—Towards 10 % Energy-Conversion Efficiency. *Adv. Mater.* **2006**, *18*, 789–794.

(3) Heeger, A. J. Semiconducting Polymers: the Third Generation. *Chem. Soc. Rev.* **2010**, *39*, 2354–2371.

(4) Zhang, Q. T.; Tour, J. M. Alternating Donor/Acceptor Repeat Units in Polythiophenes. Intramolecular Charge Transfer for Reducing Band Gaps in Fully Substituted Conjugated Polymers. *J. Am. Chem. Soc.* **1998**, *120*, 5355-5362.

(5) Dou, L.; Liu, Y.; Hong, Z.; Li, G.; Yang, Y. Low-Bandgap Near-IR Conjugated Polymers/Molecules for Organic Electronics. *Chem. Rev.* **2015**, *115*, 12633–12665.

(6) Blouin, N.; Michaud, A.; Leclerc, M. A Low-Bandgap Poly(2,7-Carbazole) Derivative for Use in High-Performance Solar Cells. *Adv. Mater.* **2007**, *19*, 2295–2300.

(7) Blouin, N.; Michaud, A.; Gendron, D.; Wakim, S.; Blair, E.; Neagu-Plesu, R.; Belletête, M.; Durocher, G.; Tao, Y.; Leclerc, M. Toward a Rational Design of Poly(2,7-Carbazole) Derivatives for Solar Cells. *J. Am. Chem. Soc.* **2008**, *130*, 732–742.

(8) Qu, S.; Tian, H. Diketopyrrolopyrrole (DPP)-Based Materials for Organic Photovoltaics. *Chem. Commun.* **2012**, *48*, 3039-3051.

(9) Zheng, Y.-Q.; Wang, Z.; Dou, J.-H.; Zhang, S.-D.; Luo, X.-Y.; Yao, Z.-F.; Wang, J.-Y.; Pei, J. Effect of Halogenation in Isoindigo-Based Polymers on the Phase Separation and Molecular Orientation of Bulk Heterojunction Solar Cells. *Macromolecules* **2015**, *48*, 5570–5577.

(10) Lei, T.; Dou, J.H.; Ma, Z.J.; Liu, C.J.; Wang, J.Y.; Pei, J. Chlorination as a Useful Method to Modulate Conjugated Polymers: Balanced and Ambient-Stable Ambipolar High-Performance Field-Effect Transistors and Inverters Based on Chlorinated Isoindigo Polymers. *Chem. Sci.* **2013**, *4*, 2447–2452.

(11) Lei, T.; Dou, J.H.; Ma, Z.J.; Yao, C.H.; Liu, C.J.; Wang, J.Y.; Pei, J. Ambipolar Polymer Field-Effect Transistors Based on Fluorinated Isoindigo: High Performance and Improved Ambient Stability. *J. Am. Chem. Soc.* **2012**, *134*, 20025–20028.

(12) Zhou, N.; Guo, X.; Ortiz, R. P.; Harschneck, T.; Manley, E. F.; Lou, S. J.; Hartnett, P. E.; Yu, X.; Horwitz, N. E.; Burrezo, P. M.; Aldrich, T. J.; López Navarrete, J. T.; Wasielewski, M. R.; Chen, L. X.; Chang, R. P. H.; Facchetti, A.; Marks, T. J. Marked Consequences of Systematic Oligothiophene Catenation in Thieno[3,4-c]Pyrrole-4,6-Dione and Bithiopheneimide Photovoltaic Copolymers. *J. Am. Chem. Soc.* **2015**, *137*, 12565–12579.

(13) Ma, Z.; Sun, W.; Himmelberger, S.; Vandewal, K.; Tang, Z.; Bergqvist, J.; Salleo, A.; Andreasen, J. W.; Inganäs, O.; Andersson, M. R.; Muller, C.; Zhang, F.; Wang, E. Structure–Property Relationships of Oligothiophene–Isoindigo Polymers for Efficient Bulk-Heterojunction Solar Cells. *Energy Environ. Sci.* **2014**, *7*, 361–369.

(14) Ho, C.-C.; Chen, C.-A.; Chang, C.-Y.; Darling, S. B.; Su, W.-F. Isoindigo-Based Copolymers for Polymer Solar Cells with Efficiency Over 7%. *J. Mater. Chem. A* **2014**, *2*, 8026–8032.

(15) Stalder, R.; Puniredd, S. R.; Hansen, M. R.; Koldemir, U.; Grand, C.; Zajaczkowski, W.; Müllen, K.; Pisula, W.; Reynolds, J. R. Ambipolar Charge Transport in Isoindigo-Based Donor–Acceptor Polymers. *Chem. Mater.* **2016**, *28*, 1286–1297.

(16) Lai, T.-H.; Constantinou, I.; Grand, C. M.; Klump, E. D.; Baek, S.; Hsu, H.-Y.; Tsang, S.-W.; Schanze, K. S.; Reynolds, J. R.; So, F. Evidence of Molecular Structure Dependent Charge Transfer Between Isoindigo-Based Polymers and Fullerene. *Chem. Mater.* **2016**, *28*, 2433–2440.

(17) Grand, C.; Baek, S.; Lai, T.-H.; Deb, N.; Zajaczkowski, W.; Stalder, R.; Müllen, K.; Pisula, W.; Bucknall, D. G.; So, F.; Reynolds, J. R. Structure–Property Relationships Directing Transport and Charge Separation in Isoindigo Polymers. *Macromolecules* **2016**, *49*, 4008–4022.

(18) Mei, J.; Graham, K. R.; Stalder, R.; Reynolds, J. R. Synthesis of Isoindigo-Based Oligothiophenes for Molecular Bulk Heterojunction Solar Cells. *Org. Lett.* **2010**, *12*, 660–663.

(19) Stalder, R.; Mei, J.; Graham, K. R.; Estrada, L. A.; Reynolds, J. R. Isoindigo, a Versatile Electron-Deficient Unit for High-Performance Organic Electronics. *Chem. Mater.* **2014**, *26*, 664–678.

(20) Wang, E.; Mammo, W.; Andersson, M. R. 25th Anniversary Article: Isoindigo-Based Polymers and Small Molecules for Bulk Heterojunction Solar Cells and Field Effect Transistors. *Adv. Mater.* **2014**, *26*, 1801–1826.

(21) Stalder, R.; Mei, J.; Reynolds, J. R. Isoindigo-Based Donor−Acceptor Conjugated Polymers. *Macromolecules* **2010**, *43*, 8348–8352.

(22) Wang, E.; Ma, Z.; Zhang, Z.; Vandewal, K.; Henriksson, P.; Inganäs, O.; Zhang, F.; Andersson, M. R. An Easily Accessible Isoindigo-Based Polymer for High-Performance Polymer Solar Cells. *J. Am. Chem. Soc.* **2011**, *133*, 14244–14247.

(23) Wang, E.; Ma, Z.; Zhang, Z.; Henriksson, P.; Inganäs, O.; Zhang, F.; Andersson, M. R. An Isoindigo-Based Low Band Gap Polymer for Efficient Polymer Solar Cells with High Photo-Voltage. *Chem. Commun.* **2011**, *47*, 4908–4910.

(24) Deng, P.; Zhang, Q. Recent Developments on Isoindigo-Based Conjugated Polymers. *Polym. Chem.* **2014**, *5*, 3298-3305.

(25) Stalder, R.; Mei, J.; Subbiah, J.; Grand, C.; Estrada, L. A.; So, F.; Reynolds, J. R. n-Type Conjugated Polyisoindigos. *Macromolecules* **2011**, *44*, 6303–6310.

(26) Grenier, F.; Aïch, B. R.; Lai, Y.-Y.; Guérette, M.; Holmes, A. B.; Tao, Y.; Wong, W. W. H.; Leclerc, M. Electroactive and Photoactive Poly[Isoindigo -Alt-EDOT] Synthesized Using Direct (Hetero)Arylation Polymerization in Batch and in Continuous Flow. *Chem. Mater.* **2015**, *27*, 2137–2143.

(27) Grenier, F.; Berrouard, P.; Pouliot, J.-R.; Tseng, H.-R.; Heeger, A. J.; Leclerc, M. Synthesis of New n-Type Isoindigo Copolymers. *Polym. Chem.* **2013**, *4*, 1836-1841.

(28) Ashraf, R. S.; Kronemeijer, A. J.; James, D. I.; Sirringhaus, H.; McCulloch, I. A New Thiophene Substituted Isoindigo Based Copolymer for High Performance Ambipolar Transistors. *Chem. Commun.* **2012**, *48*, 3939-3941.

(29) Koizumi, Y.; Ide, M.; Saeki, A.; Vijayakumar, C.; Balan, B.; Kawamoto, M.; Seki, S. Thienoisoindigo-Based Low-Band Gap Polymers for Organic Electronic Devices. *Polym. Chem.* **2013**, *4*, 484–494.

(30) Li, S.; Yuan, Z.; Yuan, J.; Deng, P.; Zhang, Q.; Sun, B. An Expanded Isoindigo Unit as a New Building Block for a Conjugated Polymer Leading to High-Performance Solar Cells. *J. Mater. Chem. A* **2014**, *2*, 5427-5433.

(31) Lei, T.; Dou, J.H.; Cao, X.Y.; Wang, J.Y.; Pei, J. A BDOPV-Based Donor-Acceptor Polymer for High-Performance n-Type and Oxygen-Doped Ambipolar Field-Effect Transistors. *Adv. Mater.* **2013**, *25*, 6589–6593.

(32) Dou, J.H.; Zheng, Y.Q.; Yao, Z.F.; Yu, Z.A.; Lei, T.; Shen, X.; Luo, X.Y.; Sun, J.; Zhang, S.D.; Ding, Y.F.; Han, G.; Yi, Y.; Wang, J.Y.; Pei, J. Fine-Tuning of Crystal Packing and Charge Transport Properties of BDOPV Derivatives Through Fluorine Substitution. *J. Am. Chem. Soc.* **2015**, *137*, 15947–15956.

(33) Lei, T.; Dou, J.H.; Cao, X.Y.; Wang, J.Y.; Pei, J. Electron-Deficient Poly(*p*-Phenylene Vinylene) Provides Electron Mobility Over 1 $cm^2 V^{-1} s^{-1}$ under Ambient Conditions. *J. Am. Chem. Soc.* **2013**, *135*, 12168–12171.

(34) Cao, Y.; Yuan, J.-S.; Zhou, X.; Wang, X.-Y.; Zhuang, F.-D.; Wang, J.-Y.; Pei, J. N-Fused BDOPV: a Tetralactam Derivative as a Building Block for Polymer Field-Effect Transistors. *Chem. Commun.* **2015**, *51*, 10514–10516.

(35) He, Y.; Guo, C.; Bin Sun; Quinn, J.; Li, Y. (3*E*,7*E*)-3,7-Bis(2-oxoindolin-3-ylidene)-5,7-Dihydropyrrolo[2,3-*f*]Indole-2,6(1*H*,3*H*)-Dione Based Polymers for Ambipolar Organic Thin Film Transistors. *Chem. Commun.* **2015**, *51*, 8093–8096.

(36) Chen, M. S.; Niskala, J. R.; Unruh, D. A.; Chu, C. K.; Lee, O. P.; Fréchet, J. M. J. Control of Polymer-Packing Orientation in Thin Films Through Synthetic Tailoring of Backbone Coplanarity. *Chem. Mater.* **2013**, *25*, 4088–4096.

(37) James, D. I.; Wang, S.; Ma, W.; Hedström, S.; Meng, X.; Persson, P.; Fabiano, S.; Crispin, X.; Andersson, M. R.; Berggren, M.; Wang, E. High-Performance Hole Transport and Quasi-Balanced Ambipolar OFETs Based on D-A-A Thieno-Benzo-Isoindigo Polymers. *Adv. Electron. Mater.* **2016**, *2*, No. 1500313.

(38) Randell, N. M.; Boutin, P. C.; Kelly, T. L. Bisisoindigo: Using a Ring-Fusion Approach to Extend the Conjugation Length of Isoindigo. *J. Mater. Chem. A* **2016**, *4*, 6940–6945.

(39) Jiang, Y.; Gao, Y.; Tian, H.; Ding, J.; Yan, D.; Geng, Y.; Wang, F. Synthesis and Characterization of Isoindigo[7,6-g]Isoindigo-Based Donor–Acceptor Conjugated Polymers. *Macromolecules* **2016**, *49*, 2135–2144.

(40) Gaussian 09, Revision D.01, Frisch, M. J.; Trucks, G. W.; Schlegel, H. B.; Scuseria, G. E.; Robb, M. A.; Cheeseman, J. R.; Scalmani, G.; Barone, V.; Petersson, G. A.; Nakatsuji, H.; Li, X.; Caricato, M.; Marenich, A.; Bloino, J.; Janesko, B. G.; Gomperts, R.; Mennucci, B.; Hratchian, H. P.; Ortiz, J. V.; Izmaylov, A. F.; Sonnenberg, J. L.; Williams-Young, D.; Ding, F.; Lipparini, F.; Egidi, F.; Goings, J.; Peng, B.; Petrone, A.; Henderson, T.; Ranasinghe, D.; Zakrzewski, V. G.; Gao, J.; Rega, N.; Zheng, G.; Liang, W.; Hada, M.; Ehara, M.; Toyota, K.; Fukuda, R.; Hasegawa, J.; Ishida, M.; Nakajima, T.; Honda, Y.; Kitao, O.; Nakai, H.; Vreven, T.; Throssell, K.; Montgomery, J. A., Jr.; Peralta, J. E.; Ogliaro, F.; Bearpark, M.; Heyd, J. J.; Brothers, E.; Kudin, K. N.; Staroverov, V. N.; Keith, T.; Kobayashi, R.; Normand, J.; Raghavachari, K.; Rendell, A.; Burant, J. C.; Iyengar, S. S.; Tomasi, J.; Cossi, M.; Millam, J. M.; Klene, M.; Adamo, C.; Cammi, R.; Ochterski, J. W.; Martin, R. L.; Morokuma, K.; Farkas, O.; Foresman, J. B.; Fox, D. J. Gaussian, Inc., Wallingford CT, **2016**.

(41) Holliday, S.; Ashraf, R. S.; Wadsworth, A.; Baran, D.; Yousaf, S. A.; Nielsen, C. B.; Tan, C.-H.; Dimitrov, S. D.; Shang, Z.; Gasparini, N.; Alamoudi, M.; Laquai, F.; Brabec, C. J.; Salleo, A.; Durrant, J. R.; McCulloch, I. High-Efficiency and Air-Stable P3HT-Based Polymer Solar Cells with a New Non-Fullerene Acceptor. *Nat. Commun.* **2016**, *7*, No. 11585.

(42) Baran, D.; Ashraf, R. S.; Hanifi, D. A.; Abdelsamie, M.; Gasparini, N.; Röhr, J. A.; Holliday, S.; Wadsworth, A.; Lockett, S.; Neophytou, M.; Emmott, C. J. M.; Nelson, J.; Brabec, C. J.; Amassian, A.; Salleo, A.; Kirchartz, T.; Durrant, J. R.; McCulloch, I. Reducing the Efficiency–Stability–Cost Gap of Organic Photovoltaics with Highly Efficient and Stable Small Molecule Acceptor Ternary Solar Cells. *Nat. Mater.* **2017**, *16*, 363–369.

(43) Soriano, D. S. Example of the Wolff-Kishner Reduction Procedure Suitable for an Undergraduate Organic Lab Experiment: Preparation of Oxindole. *J Chem. Educ.* **1993**, 332.

(44) Ganguly, A.; Zhu, J.; Kelly, T. L. Effect of Cross-Conjugation on Derivatives of Benzoisoindigo, an Isoindigo Analogue with an Extended π-System. *J. Phys. Chem. C* **2017**, *121*, 9110-9119.

(45) Guo, X.; Ortiz, R. P.; Zheng, Y.; Kim, M.-G.; Zhang, S.; Hu, Y.; Lu, G.; Facchetti, A.; Marks, T. J. Thieno[3,4-c]Pyrrole-4,6-Dione-Based Polymer Semiconductors: Toward High-Performance, Air-Stable Organic Thin-Film Transistors. *J. Am. Chem. Soc.* **2011**, *133*, 13685–13697.

(46) Saravanan, C.; Liu, C.-L.; Chang, Y.-M.; Lu, J.-D.; Hsieh, Y.-J.; Rwei, S.-P.; Wang, L. [60]Fulleropyrrolidines Bearing π-Conjugated Moiety for Polymer Solar Cells: Contribution of the Chromophoric Substituent on C_{60} to the Photocurrent. *ACS Appl. Mater. Interfaces* **2012**, *4*, 6133–6141.

(47) Savoie, B. M.; Jackson, N. E.; Marks, T. J.; Ratner, M. A. Reassessing the Use of One-Electron Energetics in the Design and Characterization of Organic Photovoltaics. *Phys. Chem. Chem. Phys.* **2013**, *15*, 4538–4547.

(48) Mikhnenko, O. V.; Blom, P. W. M.; Nguyen, T.-Q. Exciton Diffusion in Organic Semiconductors. *Energy Environ. Sci.* **2015**, *8*, 1867–1888.

(49) Xiao, T.; Xu, H.; Grancini, G.; Mai, J.; Petrozza, A.; Jeng, U.-S.; Wang, Y.; Xin, X.; Lu, Y.; Choon, N. S.; Xiao, H.; Ong, B. S.; Lu, X.; Zhao, N. Molecular Packing and Electronic Processes in Amorphous-Like Polymer Bulk Heterojunction Solar Cells with Fullerene Intercalation. *Sci. Rep.* **2014**, *4*, No. 5211.

(50) Liao, S.-H.; Jhuo, H.-J.; Cheng, Y.-S.; Chen, S.-A. Fullerene Derivative-Doped Zinc Oxide Nanofilm as the Cathode of Inverted Polymer Solar Cells with Low-Bandgap Polymer (PTB7-Th) for High Performance. *Adv. Mater.* **2013**, *25*, 4766–4771.

Chapter 6

Conclusion and outlook

6.1 Summary and conclusions

The overarching goal of this thesis was to provide insight into the relationship between changes in the molecular structure of isoindigo-based organic semiconductors and the optoelectronic properties of the resulting materials. This was accomplished by synthesizing several modified versions of the π-conjugated building block isoindigo and incorporating these modified isoindigo structures into a variety of donor-acceptor organic semiconductors. The optoelectronic properties of the resulting materials, as well as their performance in organic electronic devices, was studied and compared to analogous isoindigo semiconductors in order to assess the effects of the structural modifications. In the four main projects detailed in Chapters 2-5 the effects of structural changes such as the inclusion of electronegative heteroatoms, the planarization of multiple isoindigo units, and of altering the repeating structure in donor-acceptor polymers were studied.

The first two projects in this thesis examined the effects of incorporating electronegative nitrogen atoms into the backbone of isoindigo-based donor acceptor semiconductors. It was hypothesized that by incorporating additional electronegative atoms into the isoindigo acceptor unit, the LUMO energy of the resulting semiconductors would be lowered, resulting in low band gap, near-infrared absorbing materials. However, it was discovered that the use of azaisoindigo did not substantially affect the semiconductor's frontier orbital energy levels, and it had a negative impact on the material's performance in solar cells.

While this result limited its utility in OPVs, the pyridine nitrogen in azaisoindigo did present an opportunity to study interesting Lewis acid-base interactions between the semiconductors and common Lewis acids. It was discovered that coordination of a Lewis acid to the pyridinic nitrogen of azaisoindigo greatly decreased the LUMO energy of the semiconductor, causing a large red-shift in the molecule's HOMO-LUMO transition. This result demonstrated that while electronegative heteroatoms may not have the desired effect on the electronic structure of the molecule, they do provide the opportunity for other interesting chemistry as a site for further tuning of its optoelectronic properties.

In order to produce low band gap semiconductors based on modified isoindigos, another design strategy was required. The third major project in this thesis focused on extending conjugation in isoindigo-based semiconductors by fusing together two isoindigo units in a coplanar dimer. Here it was theorized that extending the conjugation between two electron-withdrawing acceptor units would lower the energy of the LUMO, producing low optical band gap materials for use in OPVs. While isoindigo itself is not typically used as an organic semiconductor, it was hypothesized that the large dimer, bisisoindigo, could be used as a component in OPV active layers without necessarily extending the conjugation further. To test this, both bisisoindigo and a donor-acceptor molecule based on bisisoindigo and bithiophene were synthesized, characterized and incorporated into solar cells.

Unlike the previous azaisoindigo-based materials, the bisisoindigo semiconductors did have the desired optical band gap, much lower than that of isoindigo. Both bisisoindigo and the donor-acceptor molecule had frontier orbital energy levels intermediate between those of typical p and n-type materials, but performed better in OPVs as the p-type material. Unfortunately, the device performance was modest; examination of the active layer morphology showed that the

semiconductor domain size was much too large for efficient exciton diffusion to the heterojunction. At the time, the poor performance of these OPVs was attributed to this over-crystallization in the active layer. In response to the tendency of these highly planar molecular to aggregate and crystallize, further research in modified isoindigo structures focused on the synthesis and characterization of polymer organic semiconductors.

Having already studied a ring-fused dimer of isoindigo, the natural progression was to compare it to a dimer in which the isoindigo units were joined by a single bond. At the time, a number of groups had published research on extending the number and size of donor units in donor-acceptor polymer semiconductors, but similar research on extending acceptor units was limited. Using the two isoindigo dimers, the final project in this thesis focused on the study of acceptor unit number and planarity in the repeat structure of donor-acceptor copolymers. To accomplish this, six copolymers were synthesized, combining the donor monomers thiophene and terthiophene with the acceptor monomers isoindigo, bisisoindigo (a planar dimer), and diisoindigo (a dimer with free rotation about a single bond).

Extending the number of isoindigo units in the repeat structure led to the predicted lowering of the frontier molecular orbital energies; this effect was greatest when the two isoindigo units were locked in a coplanar geometry. It was also discovered that increasing the number of acceptor units improved electron mobility in the resulting polymers. OPVs mere made using all six polymers, and the device performance correlated directly with the LUMO energy of the resulting polymers. The highest LUMO energy polymers based on isoindigo performed the best; the semiconductors featuring the freely rotating isoindigo dimers performed slightly worse than the isoindigo analogues, while the low LUMO energy bisisoindigo polymers performed very poorly. It was determined that lowering the LUMO energies of the polymers decreased the energetic

driving force for exciton dissociation. This was an important lesson in semiconductor design as the drive to produce low band gap materials often leads to semiconductors with low LUMO energy. Care must be taken to avoid lowering this energy to such an extent that there is no longer energetically favorable exciton dissociation with common n-type semiconductors such as $PC_{71}BM$. The OPV performance of the bisisoindigo-based polymers in this chapter prompted re-examining of the previous bisisoindigo-based molecular semiconductors. In hindsight, it is likely that the problem of insufficient driving force for exciton dissociation was also present in these systems.

All three modifications of isoindigo chiefly manipulated the LUMO energy of the resulting semiconductor, with wide ranging consequences. On its own, heteroatom substitution was shown not to have a significant effect on LUMO energy, but opened the possibility of Lewis acid coordination which could dramatically alter the semiconductor's optical band gap. By dimerizing isoindigo in a ring-fused fashion, the LUMO energy of the resulting donor-acceptor semiconductor was significantly lowered, and incorporating extended isoindigo units into donor-acceptor polymers allowed for incremental tuning of the frontier orbital levels. Band gap engineering such as this is an essential tool in semiconductor design; it allows researchers to control important device performance parameters such as solar cell voltage, and photocurrent, as well as aesthetic qualities such as device color and transparency.

6.2 Outlook and future work

While band gap engineering is an important facet of semiconductor design, there are many other optoelectronic properties that can be tuned by the rational design of molecular structure. In particular, designing materials that optimize the interactions between p-type and n-type semiconductors is important to improving OPV performance, and is an area that is relatively poorly understood. The electronic coupling between the p and n-type semiconductors at the interface of a bulk heterojunction is crucial to photovoltaic performance. This has been shown for isoindigo-oligothiophene copolymers, in which increased electronic coupling between the polymer and $PC_{71}BM$ led to a two-fold increase in device efficiency for an isoindigo-terthiophene polymer compared to the isoindigo-thiophene copolymer.[1] It has also been shown that moving the steric bulk of solubilizing alkyl chains from the acceptor unit to the donor unit, in order to promote acceptor-fullerene interactions, also dramatically improves device performance.[2]

With the goal of studying polymer-fullerene interactions, a series of modified isoindigo structures are proposed for future study; the proposed expanded isoindigo units incorporate large planar aromatic structures to promote polymer-fullerene π-π interactions. Chart 6.1 depicts two proposed polymers featuring polycyclic aromatic cores in expanded isoindigo units. Each polymer contains a common polycyclic aromatic hydrocarbon, either anthracene or pyrene; the same methodology used to produce bisisoindigo in Chapter 5 could be employed to produce the expanded isatin units from 1,5-diaminoanthracene and 1,7-diaminopyrene. Two concurrent aldol reactions with 6-bromo-2-oxindole would then be used to yield the dihalogenated monomers **ant-iI** and **pyr-iI**. It is possible that these extended isoindigo units may suffer from the low LUMO levels that impaired the performance of bisisoindigo. However, synthetic methodology exists to install electron-donating alkoxy groups on the pyrene and anthracene units if required.

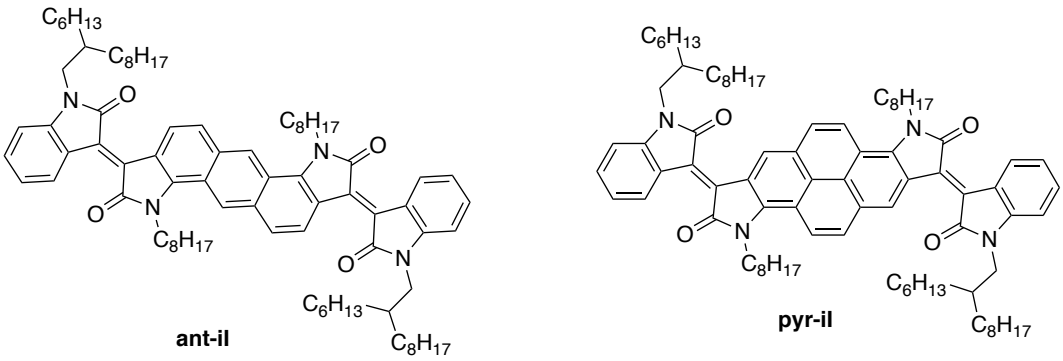

Chart 6.1 Expanded isoindigo units **ant-iI** and **pyr-iI**.

Alternatively, the planar nature of these extended isoindigo units would likely make them very useful in n-type polymers for OFETs. In Chart 6.1 the core lactam units fused directly to the polycyclic aromatic structure have linear octyl chains to reduce steric bulk and promote fullerene docking; the peripheral isatin units have larger branched alkyl substituents to promote solubility and prevent aggregation in solution. The expanded isoindigo units are depicted as copolymers with terthiophene as the analogous isoindigo-terthiophene copolymer is well known and exhibits good electronic coupling with fullerene.

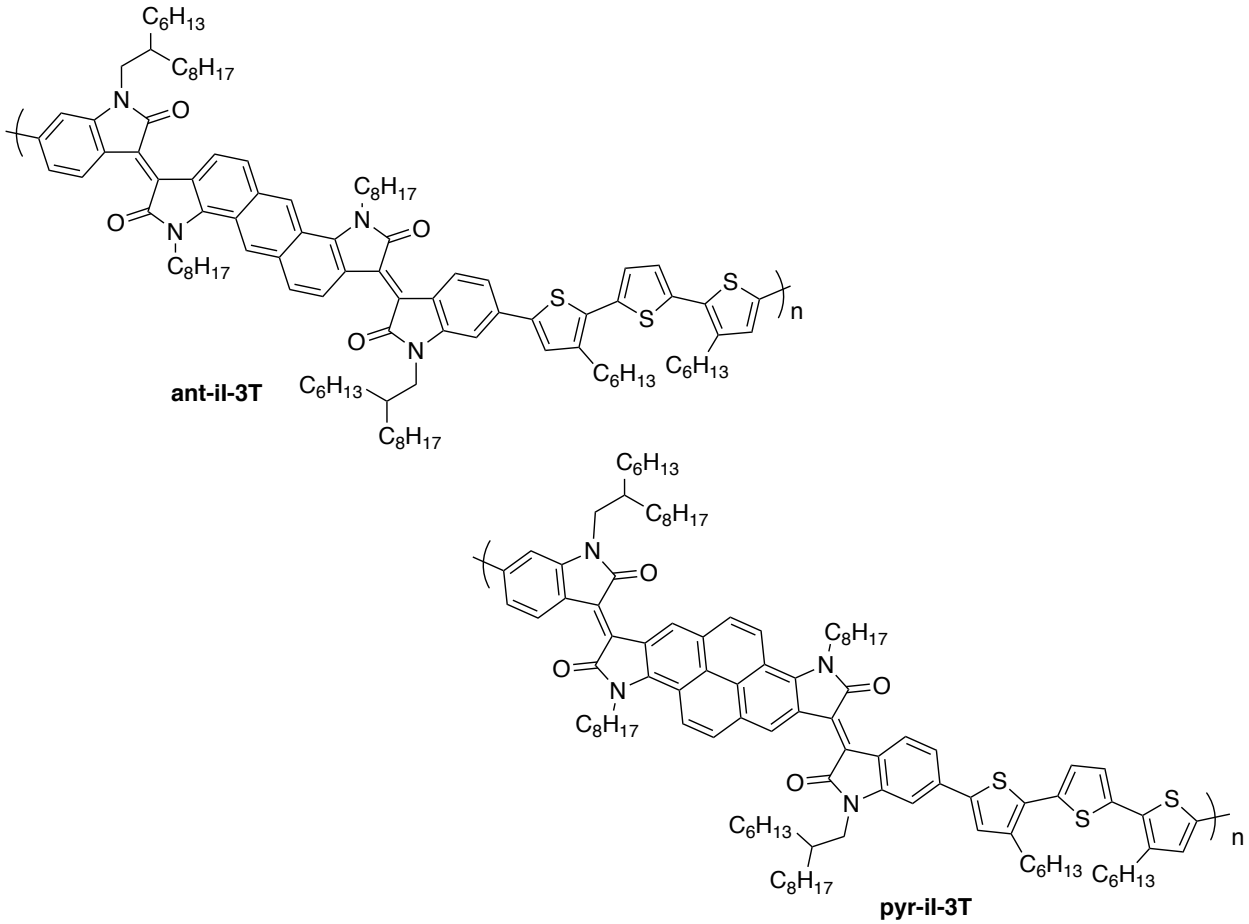

Chart 6.2 Structures of proposed isoindigo-inspired polymers **ant-iI-3T**, and **pyr-iI-3T**.

While OPV performance would be an important parameter for these semiconductors, several characterization methods not used in this thesis could be used to study the electronic coupling between the polymers and fullerene. Transient photoluminescence quenching as well as photoluminescence decay can determine how fast the polymer excited state is quenched by electron transfer to fullerene.[1,3,4] Electroluminescence spectroscopy and Fourier transform photocurrent spectroscopy could measure the energy of the charge transfer state between the polymer and fullerene, further elucidating the electronic coupling between the two semiconductors.[1,5] Shedding light on the importance of electronic coupling between semiconductors in a bulk heterojunction would influence future iterations of material design.

Fullerene derivatives have been the dominant n-type semiconductor in BHJ OPVs since the field's beginnings. Recently n-type molecular semiconductors combining central indacenodithieno[3,2-b]thiophene (IT) cores with a variety of peripheral electron acceptors, such as **ITIC** (Chart 6.2), have produced high efficiencies when used in OPVs. [6-10] Here again, the possibility exists to improve electronic coupling at the BHJ interface by synthesizing molecules designed to promote intermolecular interactions between the p and n-type semiconductor. Inclusion of an isoindigo-based unit as the peripheral electron acceptor group in such a non-fullerene electron acceptor could promote such interactions. The proposed structure, **iI-ITIC** (Chart 6.2), features the isoindigo dimer bisisoindigo discussed in this thesis; in this case it has been condensed onto the thiophene-carboxyaldehyde group of the **ITIC** core. Hypothetically, this structure would have a very low energy LUMO which would likely reside primarily on the peripheral isoindigo moieties. In OPVs, **iI-ITIC** would be combined with p-type isoindigo-based polymers on the theory that the similar acceptor units would promote favorable interactions between the semiconductors; this strong electronic coupling between the two would promote exciton dissociation and lead to devices with high J_{SC}. The same optoelectronic characterization proposed for the study of polymer-fullerene interactions would be performed to quantify the degree of electronic coupling seen here. By providing insight into the electronic interactions between this new generation of n-type semiconductors and p-type polymers, device performance can be improved through enhanced electronic coupling leading to higher J_{SC}.

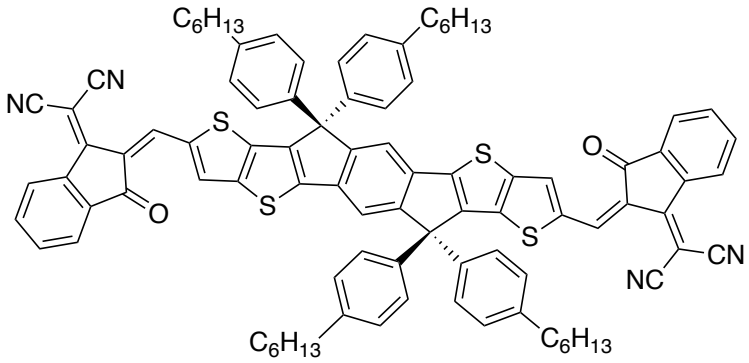

ITIC

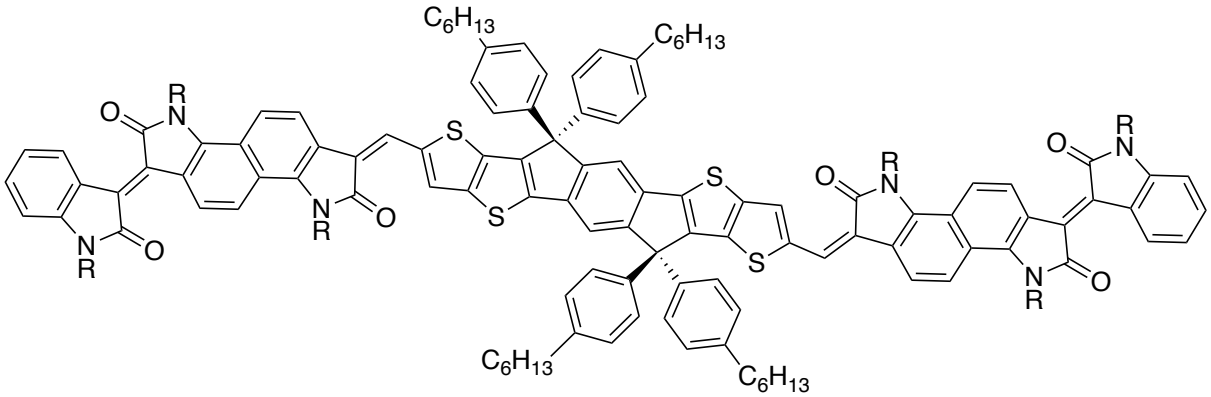

iI-ITIC

Chart 6.3 Non-fullerene n-type semiconductor **ITIC** and proposed **iI-ITIC** structure.

In summary, the work in this thesis focused primarily on using modifications of isoindigo to manipulate frontier orbital energy levels and study the effect on the optoelectronic properties and device performance of organic semiconductors. Moving forward, it is hoped that the same rational design approach that motivated this thesis can be applied to the electronic coupling between semiconductors in OPVs; this is an area in which increased knowledge could dramatically improve the ability of researchers to design future generations of organic semiconductors.

6.3 References

(1) Lai, T.-H.; Constantinou, I.; Grand, C. M.; Klump, E. D.; Baek, S.; Hsu, H.-Y.; Tsang, S.-W.; Schanze, K. S.; Reynolds, J. R.; So, F. Evidence of Molecular Structure Dependent Charge Transfer Between Isoindigo-Based Polymers and Fullerene. *Chem. Mater.* **2016**, *28*, 2433–2440.

(2) Graham, K. R.; Cabanetos, C.; Jahnke, J. P.; Idso, M. N.; Labban, El, A.; Ngongang Ndjawa, G. O.; Heumueller, T.; Vandewal, K.; Salleo, A.; Chmelka, B. F.; Amassian, A.; Beaujuge, P. M.; McGehee, M. D. Importance of the Donor:Fullerene Intermolecular Arrangement for High-Efficiency Organic Photovoltaics. *J. Am. Chem. Soc.* **2014**, *136*, 9608–9618.

(3) Vandewal, K.; Ma, Z.; Bergqvist, J.; Tang, Z.; Wang, E.; Henriksson, P.; Tvingstedt, K.; Andersson, M. R.; Zhang, F.; Inganäs, O. Quantification of Quantum Efficiency and Energy Losses in Low Bandgap Polymer:Fullerene Solar Cells with High Open-Circuit Voltage. *Adv. Funct. Mater.* **2012**, *22*, 3480–3490.

(4) Stalder, R.; Mei, J.; Graham, K. R.; Estrada, L. A.; Reynolds, J. R. Isoindigo, a Versatile Electron-Deficient Unit for High-Performance Organic Electronics. *Chem. Mater.* **2014**, *26*, 664–678.

(5) Ma, Z.; Sun, W.; Himmelberger, S.; Vandewal, K.; Tang, Z.; Bergqvist, J.; Salleo, A.; Andreasen, J. W.; Inganäs, O.; Andersson, M. R.; Muller, C.; Zhang, F.; Wang, E. Structure–Property Relationships of Oligothiophene–Isoindigo Polymers for Efficient Bulk-Heterojunction Solar Cells. *Energy Environ. Sci.* **2014**, *7*, 361–369.

(6) Lin, Y.; Wang, J.; Zhang, Z.-G.; Bai, H.; Li, Y.; Zhu, D.; Zhan, X. An Electron Acceptor Challenging Fullerenes for Efficient Polymer Solar Cells. *Adv. Mater.* **2015**, *27*, 1170–1174.

(7) Yang, Y.; Zhang, Z.-G.; Bin, H.; Chen, S.; Gao, L.; Xue, L.; Yang, C.; Li, Y. Side-Chain Isomerization on an N-Type Organic Semiconductor ITIC Acceptor Makes 11.77% High Efficiency Polymer Solar Cells. *J. Am. Chem. Soc.* **2016**, *138*, 15011–15018.

(8) Holliday, S.; Ashraf, R. S.; Wadsworth, A.; Baran, D.; Yousaf, S. A.; Nielsen, C. B.; Tan, C.-H.; Dimitrov, S. D.; Shang, Z.; Gasparini, N.; Alamoudi, M.; Laquai, F.; Brabec, C. J.; Salleo, A.; Durrant, J. R.; McCulloch, I. High-Efficiency and Air-Stable P3HT-Based Polymer Solar Cells with a New Non-Fullerene Acceptor. *Nat. Commun.* **2016**, *7*, No. 11585.

(9) Nielsen, C. B.; Holliday, S.; Chen, H.-Y.; Cryer, S. J.; McCulloch, I. Non-Fullerene Electron Acceptors for Use in Organic Solar Cells. *Acc. Chem. Res.* **2015**, *48*, 2803–2812.

(10) Qiu, N.; Yang, X.; Zhang, H.; Wan, X.; Li, C.; Liu, F.; Zhang, H.; Russell, T. P.; Chen, Y. Nonfullerene Small Molecular Acceptors with a Three-Dimensional (3D) Structure for Organic Solar Cells. *Chem. Mater.* **2016**, *28*, 6770–6778.